Universidad de Granada

Departamento de Electrónica y Tecnología de Computadores

Desarrollo de sistemas de medida basados en sensores químicos de tipo óptico

Tesis Doctoral

Nuria López Ruiz

Editor: Editorial de la Universidad de Granada
Autor: Nuria López Ruiz
D.L.: GR 1838-2014
ISBN: 978-84-9083-021-5

Alberto J. Palma López, Catedrático de Universidad, y Antonio Martínez Olmos, Profesor Titular de Universidad, ambos del Departamento de Electrónica y Tecnología de Computadores de la Universidad de Granada y Luis Fermín Capitán Vallvey, Catedrático de Universidad del Departamento de Química Analítica de la Universidad de Granada,

CERTIFICAMOS:

Que el trabajo de investigación recogido en la presente memoria, titulada "Desarrollo de sistemas de medida basados en sensores químicos de tipo óptico", y presentada por Nuria López Ruiz para optar al grado de Doctor por la Universidad de Granada, ha sido realizado en su totalidad bajo nuestra dirección en el Departamento de Electrónica y Tecnología de Computadores y el Departamento de Química Analítica de la Universidad de Granada.

Granada, Febrero de 2014

Dr. Alberto J. Palma López	Dr. Antonio Martínez Olmos
Catedrático de Universidad	Profesor Titular de Universidad

Dr. Luis Fermín Capitán Vallvey
Catedrático de Universidad

La doctoranda Nuria López Ruiz y los directores de la tesis Alberto J. Palma López, Antonio Martínez Olmos y Luis F. Capitán Vallvey, garantizamos, al firmar esta tesis doctoral, que el trabajo ha sido realizado por el doctorando bajo la dirección de los directores de la tesis y hasta donde nuestro conocimiento alcanza, en la realización del trabajo, se han respetado los derechos de otros autores a ser citados, cuando se han utilizado sus resultados o publicaciones.

Granada, Febrero de 2014.

Director/es de la Tesis	Doctoranda
Fdo.: Alberto J. Palma López Luis F. Capitán-Vallvey Antonio Martínez Olmos	Fdo.: Nuria López Ruiz

Agradecimientos

Pensando en las personas a las que tengo que incluir en esta sección no puedo menos que sentirme afortunada. Son tantas, que podría extenderme más que para explicar el trabajo realizado en estos cuatro años.

Tengo que comenzar por mis directores Alberto, Fermín y Antonio. Si ellos no me hubiesen llamado mientras yo estaba de Erasmus en Francia para ofrecerme esta beca, nada de esto habría sido posible. Todavía recuerdo como tuve que salir corriendo hacia Bruselas para conseguir un certificado. Esa "carrera" mereció la pena, esa llamada cambió mi vida y espero que la siga cambiando. Gracias a Alberto por todo lo que me ha enseñado, por todas las charlas y por tratarme como parte de una familia de la que me siento muy orgullosa de pertenecer. Gracias a Fermín, por aportarme siempre ideas en ese campo desconocido para mí que es la química. Gracias a los dos por su atención y dedicación todos estos años. Gracias a Antonio. Si escribiese todo lo que te tengo que agradecer, no acabaría nunca. Gracias por estar conmigo al pie del cañón, por tu infinita paciencia, por tus ideas, por ayudarme en clases o midiendo, por nuestras discusiones, por nuestras risas y, en definitiva, por ser mi amigo. No uno cualquiera, sino el mejor.

Gracias al resto de mis compañeros del departamento de Electrónica: Migue, Diego, Jesús, Sofía, Didi, Pepe, Almudena, Celso,

Encarni, Antonio García, etc. No podría imaginarme un ambiente mejor en el que trabajar. Gracias por todos los ánimos, por todas las conversaciones sobre futuro que hemos tenido, por todas las tonterías y por todas las confidencias. Sé que pase lo que pase estaremos en contacto. También tengo que incluir aquí a la gente del departamento de Química, aunque muchos de ellos ya no trabajan aquí han sido y son parte importante de esto. Gracias a Isa, Miguel, María, Manuel, Carmen, Cristina, Julio, Paulina, Alfonso, Alejandro, Ismael, Anabel, Maricruz e Inma. Gracias por tratarme como a una química más sin serlo, por enseñarme y por tener paciencia conmigo cuando he intentado jugar al "Quiminova" por mi cuenta. Gracias por momentos inolvidables en ese laboratorio.

Ya que esta tesis incluye muchos temas diferentes, he tenido la suerte de compartir trabajo con mucha gente. Gracias a Luis, Mª Carmen, Manolo Melgosa, Manolo Sánchez e Ignacio. Thanks also to my lovely friends in Dublin for help me during my stay there and including me as their friend. Thanks to Dermot and Fernando for let me go there to increase my knowledge and show me how wonderful the people are there. Thanks to Vincenzo, Monika, Larisa, Michele, Bartosz, Kevin, Cormac, Thomas, Andy, Simon, Alessandra, Viviana and Giusy. Thank you so much for show me the Guinness, Taste of Emilia, Yamamori (yummy!) and help me to get over the bad weather in Ireland. Tengo que agradecer también a mis compañeros en el CITIC: compañeros de despacho, de pasillo…Curro, Oresti, Pablo, Rafa, Jose María, Joaquín, Roberto, Carlos, Santi, Alberto, Antonio, Paloma, Javi, Fran y otros muchos. Ánimo chicos, esto es duro, ¡pero es lo que nos gusta!

Gracias a mis amigos por su apoyo incondicional, por sus ánimos, y por su comprensión cuando no siempre he podido ir a las “quedadas”. Gracias a Alhambra, mi hermana. Gracias a su familia, que también es la mía. Gracias a mis Erasmus. Me alegra tener tantos amigos de verdad distribuidos por toda España y últimamente, por todo el mundo. Gracias a Boni, por enseñarme a “hacer catusilla” y reírnos tanto juntas. Gracias a todos que alguna vez me han preguntado por mi tesis y de una forma u otra me han animado a continuar en este mundo.

Gracias a toda mi familia. A mis abuelos, por presumir de lo que hace su nieta aunque no tengan muy claro lo que es. A mis tíos, a mis primos, entre los que incluyo también a la familia política. Gracias.

Gracias a mi hermano, Carlos. Siempre pendiente de mí. Espero que de verdad llegues más alto que yo. Sabes que puedes y que sólo te falta empeño.

Gracias a mis padres. Los mejores padres. Por vuestro apoyo, por vuestras ganas, que son también las mías, por darme todo lo que siempre he querido, y por ayudarme a ser como soy.

Gracias a Leo. Para ti no hay palabras. No sé como describir aquí todo lo que me has ayudado. Todo lo que significas para mí. Sólo sé que a partir de aquí se abre un futuro incierto, pero juntos, y eso hace que todo sea más fácil. Gracias infinitas.

A mis padres.

A Leo, mi otra mitad.

Resumen

En los últimos años ha existido un gran interés en el diseño y desarrollo de instrumentación portátil para el análisis de muestras en diferentes ámbitos tales como las ciencias de la salud, la industria química, ciencias medioambientales, seguridad, etc. La combinación de esta instrumentación con sensores desechables o de un solo uso ofrece una alternativa a los equipos actuales de análisis tanto por el bajo coste y portabilidad, como por la facilidad de uso que ofrecen.

En concreto, los sensores químicos de tipo óptico, de especial interés en esta Tesis Doctoral, basan su funcionamiento en la medida de las propiedades de la radiación electromagnética que son modificadas según las condiciones del entorno a las que son sometidas. Este tipo de sensores hace posible la obtención de información en tiempo real e *in situ* con un sencillo proceso de reconocimiento y procesamiento de la información. La combinación de este tipo de sensores con prototipos portátiles facilita el análisis de las muestras más allá del ámbito del laboratorio y de la instrumentación utilizada hasta hoy. De esta forma, el objetivo de esta Tesis es el desarrollo de instrumentación portátil basada en la medida de sensores químicos de tipo óptico.

El principio básico de funcionamiento de los prototipos desarrollados consiste en la medida de los cambios de color o de la

intensidad de emisión de la luminiscencia de los sensores químicos ópticos con el fin de relacionarlos con diferentes magnitudes de interés. Así, en el transcurso de esta investigación se han desarrollado diferentes prototipos utilizando para ello diferentes detectores ópticos y sensores de imagen que proporcionan la información colorimétrica requerida en cada caso.

En primer lugar, se han diseñado dos prototipos utilizando detectores digitales de color para la medida de pH en disolución y para la medida de oxígeno ambiental. Los detectores digitales de color permiten realizar la medida de coordenadas cromáticas ofreciendo para ello un componente compacto, de bajo coste y de fácil uso, que al ser combinado con un microcontrolador ofrece amplias posibilidades. Además, la mayoría de ellos permiten configurar una serie de parámetros que permiten optimizar el funcionamiento del detector para cada caso particular: tiempo de integración, área activa de detección, etc.

Teniendo en cuenta esto, se ha utilizado una matriz de sensores químicos ópticos junto con una matriz de once detectores digitales de color para la medida de pH en disolución con el fin de determinar la coordenada tonal (H del espacio de color HSV) y relacionarla con el pH correspondiente. Como fuente de iluminación de este sistema se ha utilizado un iluminante blanco que es generado por una pantalla OLED programable. Esto permite iluminar las once membranas sensoras tanto de forma secuencial como simultánea, evitando el uso de fuentes de iluminación independientes para cada membrana, con el correspondiente aumento del consumo y de tamaño final del prototipo que supondría. En este caso se han obtenido resultados de resolución de 0.02 unidades de pH con una precisión de 0.2 unidades en el rango completo de pH de 0 a 14. Además, en una segunda aproximación, se ha combinando este instrumento portátil con el uso de redes neuronales artificiales, relacionando la coordenada H con el pH de la disolución de una forma más optimizada, mejorando el valor de precisión a 0.06 unidades de pH.

En un segundo sistema portátil utilizando un detector digital de color, se ha medido la intensidad de luminiscencia emitida por una membrana sensora que es excitada ópticamente con un LED ultravioleta. La intensidad de luminiscencia, cuantificada utilizando la coordenada R del espacio de color RGB, se relaciona en este caso con la concentración de oxígeno ambiental, de forma que decrece con la concentración de este gas. En este caso, el diseño final consiste en una tarjeta RFID sobre sustrato flexible, lo que permite utilizar el diseño para empaquetado inteligente de alimentos. Además, se incluye en el prototipo un chip RFID que incorpora sensor de temperatura para corregir las derivas térmicas producidas. Los resultados obtenidos con este sistema proporcionan una resolución de 3.86 ppm al 21% de concentración de oxígeno ambiental y una precisión de 0.08%.

Siguiendo la línea principal de esta Tesis Doctoral, se han desarrollado también otros dos instrumentos portátiles utilizando un módulo que incluye una micro-cámara CMOS para la detección de color e intensidad mediante procesamiento de imágenes. La micro-cámara utiliza un sensor OmniVision CMOS VGA y permite trabajar con imágenes en formato RAW o JPEG, lo que permite el tratamiento directo de la información de color, o el procesamiento de imágenes previamente comprimidas. Las ventajas de los sensores CMOS frente a sensores CCD son, entre otras, el menor tiempo de respuesta que necesitan así como un menor consumo, lo que les hace adecuados para instrumentos portátiles como los aquí presentados. Además, se incluye en el diseño del prototipo un microcontrolador que lleva a cabo el procesamiento de imágenes, relacionando los parámetros cromáticos de interés con la medida de la concentración de oxígeno, en un primer prototipo, y con la concentración de metales pesados en disolución en un segundo equipo.

En un primer estudio, para la medida oxígeno ambiental mediante la cuantificación de la intensidad de luminiscencia, se extrae la información correspondiente a la coordenada roja (R) a partir del procesamiento de una fotografía de la membrana sensora excitada ópticamente que ha sido previamente capturada con la micro-cámara. Algunos factores, como el tamaño del área analizada de la membrana, afectan los valores finales del sistema. Así, por ejemplo, a mayor área procesada mejores valores de resolución y de límite de detección se obtienen. Sin embargo, hay que tener en cuenta también el tiempo de respuesta del equipo portátil y, por tanto, hay que llegar a un compromiso. Con este primer prototipo basado en la micro-cámara los valores de resolución y límite de detección obtenidos para la medida de oxígeno gaseoso son de 0.16% y 1.5%, respectivamente, a 21% de oxígeno ambiental.

En un segundo prototipo utilizando la micro-cámara CMOS como detector de imagen, se han obtenido las coordenadas colorimétricas de interés de una matriz de sensores químicos ópticos para ser relacionadas con la concentración de metales pesados en una disolución. En este instrumento se ha incluido una pantalla LCD táctil como interfaz de usuario, lo que además de facilitar el uso, evita la necesidad de incluir elementos externos de almacenamiento. Esto es posible ya que el microcontrolador puede obtener la información colorimétrica directamente mediante la lectura pixel a pixel de la pantalla.

Por último, en el último capítulo se aborda el uso de sensores de imagen disponibles comercialmente, tales como cámaras digitales CCD o cámaras CMOS integradas en teléfonos móviles de última generación, para el análisis colorimétrico de muestras o la determinación de intensidad de luminiscencia emitida. Con este fin, se han desarrollado tres aplicaciones diferentes para el sistema operativo Android, las cuales permiten el análisis de muestras para clasificación de suelos de acuerdo con el sistema Munsell, o, en combinación con sensores químicos ópticos, la determinación de la concentración de oxígeno gaseoso, así como el pH o la concentración de nitritos en disolución.

La primera aplicación se ha llevado a cabo utilizando un teléfono móvil de última generación, que utiliza la cámara integrada como instrumento analítico con el objetivo de medir intensidad de luminiscencia por medio del análisis colorimétrico. Se ha utilizado el mismo principio usado anteriormente para cuantificación de la intensidad emitida por la membrana sensora mediante la coordenada R ante diferentes concentraciones de oxígeno ambiental y usando una excitación ultravioleta. Con este prototipo se han obtenido resultados de resolución de 35 ppm al 21% de oxígeno con un límite de detección de 0.4%, probando así la fiabilidad de un teléfono móvil como detector de intensidad colorimétrica.

También se ha desarrollado una aplicación Android, junto con un sensor microfluídico y los sensores químicos ópticos correspondientes, que permite la medida de pH y concentración de nitritos a partir de las coordenadas colorimétricas obtenidas de una fotografía realizada sobre el sensor microfluídico. La disolución a analizar es depositada en el centro del dispositivo diseñado para este fin, y mediante capilaridad, dicha disolución alcanza las áreas sensoras donde los reactivos se han colocado previamente. Como barrera para la disolución se ha utilizado tinta indeleble que atraviesa el espesor del papel de filtro usado como soporte, impidiendo el paso de la disolución a través de ella. Una vez que se producen las diferentes reacciones colorimétricas en cada una de las áreas, y tras el análisis de la fotografía capturada utilizando el flash del móvil como iluminante, se obtienen los resultados de pH y concentración de nitritos. Con este sistema de medida se han obtenido resultados de resolución de 0.04 unidades de pH y 7% a 100 ppm de concentración de nitritos.

Una última aplicación Android ha sido desarrollada en esta Tesis Doctoral con el objetivo de realizar la clasificación de muestras de suelos mediterráneos utilizando como sistema de referencia el sistema Munsell. Así, el teléfono móvil captura una imagen de la muestra deseada, y transforma las coordenadas RGB en coordenadas XYZ y HVC a partir de modelos obtenidos de forma experimental durante el proceso de calibración. Se han comparando los resultados obtenidos utilizando la aplicación y modelos desarrollados con los resultados proporcionados por un espectrofotómetro, probando que un teléfono móvil puede ser utilizado como colorímetro para aplicaciones de clasificación. En este caso, la experimentación se ha realizado bajo condiciones controladas de iluminación, en el interior de una cabina que simula la luz día (iluminante D65). Si las diferencias CIELAB obtenidas con el método tradicional de clasificación de suelos estaban entre 4.4 y 10 unidades, con esta aplicación se mejoran estos resultados ya que se obtienen unas diferencias promedio de 3.7 ± 1.8 unidades.

Finalmente, se ha realizado el estudio y análisis de la estabilidad de salsas emulsionadas utilizando procesamiento de imágenes para extraer coordenadas cromáticas de interés a partir de una fotografía capturada con una cámara comercial digital. Tras someter las diferentes salsas mayonesas a procesos de desestabilización de temperatura y centrifugado, y procesar las imágenes en un ordenador externo para obtener las coordenadas cromáticas de interés, se pueden observar una serie de cambios en algunas de las coordenadas estudiadas (RGB, HSV, CIELAB, CMYK) entre el estado inicial y el final, lo que ofrece una idea del estado actual de desestabilización de la salsa correspondiente.

Así pues, el objetivo principal de esta Tesis Doctoral consiste en el desarrollo de sistemas de medida para sensores químicos ópticos. Este objetivo ha sido alcanzado mediante el uso de diferentes detectores ópticos o sensores de imagen para el análisis colorimétrico de muestras así como para la medida de intensidad de luminiscencia. En la mayoría de los casos estudiados, la respuesta de los prototipos y aplicaciones desarrollados se ha comparado con dispositivos comerciales ya existentes, tales como escáneres, espectrofotómetros y espectrorradiómetros, o métodos tradicionales de medida como la comparación visual de muestras o el método potenciométrico para la medida de pH.

Index

Figure index

Table index

Acronyms

ADS	Advanced Design System
AI	Artificial Intelligence
ANN	Artificial Neural Network
APS	Active Pixel Sensor
BBPA	Bis(1-butylpentyl)adipate
BSD	Berkeley Software Distribution
CA	Cellulose Acetate
CCD	Charged-Coupled Device
CIE	International Commission on Illumination
CIS	Contact Image Sensors
CMOS	Complementary Metal-Oxide-Semiconductor
CMYK	Cyan Magenta Yellow and Key (Ma *et al.* 2011)
CTAB	Hexadecyltrimethylammonium Bromide
DABCO	1,4-Diazabicyclo[2.2.2] Octane
DNA	Deoxyribonucleic Acid
DOS	Dioctyl Sebacate

EEPROM	Electrically Erasable Programmable Read-Only Memory
EG	Ethylenglycol
EPA	Environmental Protection Agency
FIT	Frame Interline Transfer
FFT	Full Frame Transfer
FT	Frame Transfer
Ge	Germanium
HF	High Frequency
HSC	Hue Saturation Chrome
HSL	Hue Saturation Lightness
HSV	Hue Saturation Value
HVC	Hue Value Chroma
IC	Integrated Circuit
InGaAs	Indium Gallium Arsenide
IT	Interline Transfer
JPEG	Joint Photographic Experts Group
LCD	Liquid Crystal Display
LED	Light-Emitting Diode
LOC	Lab On a Chip
LOD	Limit Of Detection
LZW	Lempel Ziv Welch

MAP	Modified Atmosphere Packaging
MOS	Metal-oxide Semiconductor
MSE	Mean Squared Error
NPOE	O-nitrophenyloctylether
OLED	Organic Light-Emitting Diode
OpenCV	Open Source Computer Vision Library
PAN	1-(2-pyridylazol)-2-naphthol
PbS	Lead(II) Sulfide
PDMS	Polydimethylsiloxane
PEN	Polyethylene Naphthalate
PET	Polyethylene Terephthalate
PMMA	Polymethyl Methacrylate
PNG	Portable Network Graphics
PPI	Pixels Per Inch
PS	Polystyrene
PtOEP	Platinum Octaethylporphyrin
PVC	Polyvinyl Chloride
RF	Radiofrequency
RFID	Radiofrequency Identification
RGB	Red Green Blue
RSD	Relative Standard Deviation

Si	Silicon
SPI	Serial Peripheral Interface
TBP	Tributyl Phosphate
TCPB	Tetrakis(4-chlorophenyl)borate
TDMAC	Tridodecylmethylammonium Chloride
TFT	Thin-film Transitor
THF	Tetrahydrofuran
TIFF	Tagged Image File Format
USDA	United States Department of Agriculture
UV	Ultraviolet
ZIN	Zincon
µSD	Micro Secure Digital

Chapter 1. **Motivation and objectives**

1.1 Motivation

There is a growing interest in the research and use of portable and handheld instrumentation in the last years. Although differences in size and portability exist, both types of instrumentation, handheld and portable, have been included in this work. We believe that the two of them share almost the same constraints and tradeoffs as concerns size and performance; moreover, the border between them can be blurry at times. In fact, the former is a portable device, whereas the latter is not necessarily handheld. By definition, a handheld device can be held in one's hand, indicating a high degree of compactness, and a portable one has been designed to be light and small enough to be easily carried or moved. Both have the important characteristic of being able to take them to the sample and not vice versa. This is also important for occupational safety monitoring (so-called direct reading instruments) and analyzing potentially hazardous samples such as carcinogens, highly toxic chemicals, and potentially explosive atmospheres where real-time data and remote monitoring is advisable or mandatory to enable rapid decision-making. Portable instruments are required in different fields including the chemical industry, point-of-care testing, terrorism defence, environmental protection, geochemical surveying, and occupational safety, among others (Capitan-Vallvey and Palma

2011). In Figure 1.1 it can be seen the increase in the number of publications per year related to portable instrumentation which has been accompanied by a notable industrial effort.

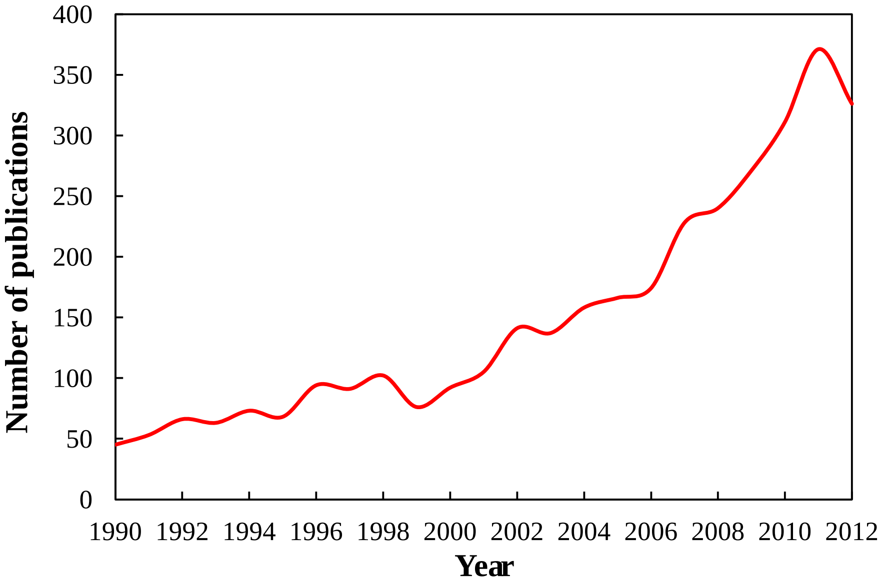

Figure 1.1 Number of publications in the field of portable instrumentation from 1990 to 2012 according to Scopus®.

The concept of chemical sensors involves a change of paradigm in analytical chemistry from general analytical systems to dedicated systems. The chemical information sought about matter is obtained in real time, possibly on site, as a result of the interaction between sensor and chemical/s in a two-step process: recognition and signal treatment. Numerous types of sensors exist, but this Ph.D. Thesis is confined to optical sensors, which are based on the measurement of electromagnetic radiation properties that are either modified or created by the recognition event and in which the sensor is included in instrumentation characterized by its portability. The concept of sensors is ubiquitous, but it is most complete when included in portable instrumentation that makes it possible to accomplish the analytical dream of moving the lab to the sample using user-friendly analytical instruments.

Moreover, in the last decades there has been a trend in analytical chemistry towards the use of fast technologies that provide real-time information through the use of simple instrumentation as the described above. With this purpose, the chemical sensors offer a wide range of possibilities (Janata 2009). In this domain, one-shot sensors, or disposable sensors, are a good alternative since they are easy-to-use and low cost devices besides they offer facility of storage, preservation and transport which satisfy the requirements for portable instrumentation. In particular, optical sensors have an increasing interest because of the advantages that they offer (Baldini *et al.* 2006), (McDonagh *et al.* 2008), (Orellana and Moreno-Bondi 2005): no electrical interferences, several possibilities of codification for the information that they provide, wide range of operation in conditions of temperature and pressure, there is no consumption of analyte and, they can be miniaturized in order to reduce the size of the final instrument. On the other hand, they have problems of chemical stability with time, they may be affected by external light and, occasionally they present short range of response needing several sensors to cover the whole range of the specie to analyze.

With the purpose of obtaining an optimal response of the instrument, different approaches have been studied with regard to the optical sensors. Diverse measurement techniques have been studied: absorption, both transmission or reflection; luminescence, both fluorescence, phosphorescence, chemiluminescence and electrochemiluminescence; and colour using various colour spaces: RGB (red, green and blue), HSV (hue, saturation and value) or HVC (hue, value and chrome) (Cantrell *et al.* 2010); and different structures of the sensors: single-analyte or multianalyte.

With this basis, this doctoral thesis presents the research works carried out in the field of the electronic portable instrumentation. Specifically, it is the product of the development of portable instrumentation for optical chemical sensors. The principle of these devices consists of the detection of the change in the colour or the intensity of emitted luminescence of these chemical sensors to measure different magnitudes either in solutions just as pH or nitrites, or ambient conditions such as the concentration of environmental oxygen.

Since for colour measurements the ambient light is an important factor, therefore all these instruments must be tested under controlled conditions of light so that a study of different illuminants has been carried out for each particular case.

The main requirements to take into account for the design of these instruments are basically small size, robustness, low cost, low maintenance and high autonomy, or low power consumption, that are advantages regarding some others available commercial instruments that can be found currently in laboratories.

With the main objective of colour detection, different available detectors have been analyzed, such as digital colour sensors or photodiodes, in order to include them in the design of the portable instrumentation. Besides, capture devices such as a CMOS micro-camera or digital cameras have been used for both colour and intensity detectors. In the last chapter, smartphones with built-in cameras have been included as handheld instruments due to their high capabilities for real-time processing. In fact, software applications have been programmed in smartphones for image processing of pictures of analytes where colour is containing the information.

1.2 Objectives

The main objective of this Ph.D. Thesis is to develop electronic platforms based on the measurements of colour properties for optical chemical sensors. Therefore, the main goal has been the design of portable/handheld battery-operated devices which provide information in real time, in situ and useful for non trained people. In order to achieve this principal purpose, several particular objectives have been addressed:

1. Design and development of portable instrumentation using digital colour detectors to measure the change of colour from optical chemical sensors. The developed compact prototypes have been tested with an array of sensing membranes for pH determination.

2. Fabrication of portable electronic prototypes using a CMOS micro-camera module as image sensor to obtain the colour information of interest from image-processing of pictures. The processing has been carried out with a microcontroller avoiding the need of external elements. This prototype has been applied to measure the concentration of heavy metals in solutions.

3. Study and analysis of the reliability of a mobile phone acting as complete analytical instrument in comparison with some commercial equipment or previous developed prototypes. The capture and the processing of the information have been made in the mobile phone, in order to obtain a self-consistent device for measuring magnitudes of interest. Two different applications for the Android operative system have been developed and implemented: for simultaneous measurement of pH and concentration of nitrites and for soil classification according to the Munsell colour system.

4. Use of optical detectors, such as digital colour detectors, CMOS or CCD image sensors, for measuring the intensity of luminescence emitted by a luminophore when it is optically excited. With this purpose, two different prototypes and one Android application have been developed and tested using a PtOEP sensing membrane for measuring oxygen concentration.

5. Study of the stability in emulsions using a commercial digital camera as capture device. In this case, the processing will be carried out in an external computer with the purpose of analyze different colour spaces and their coordinates to relate the state of stability of different mayonnaises to colorimetric parameters.

1.3 Document outline

This document has been organized in accordance with the type of optical detector or image sensor used in each measurement system as follows. In chapter 2, a very brief introduction, background and state of art to some general aspects involved in this Ph.D. Thesis is presented: the concept of colorimetry and spaces of colour, the concept of luminescence, and its applications in the different areas; a description of the optical chemical sensors and how they are being introduced in analytical procedures; and, finally, an analysis of the optical detectors and image sensors used in this work to extract information from colorimetric or luminescent sensors , including some examples of analytical applications.

In chapter 3, a description of the development and evaluation of two electronic platforms using both of them digital colour detector as optical sensor is carried out. In this chapter a portable instrument with an array of colorimetric indicators for pH determination and a Radiofrequency Identification (RFID) tag based on the colour change of a luminescent membrane for measuring gaseous oxygen concentration are presented.

In chapter 4, two different portable microcontrolled instruments using a CMOS micro-camera module as colour detector are presented: for gaseous oxygen determination from a picture of a luminescent membrane and for measuring the concentration of different heavy metals in a solution using an optical colorimetric sensor array.

Finally, in chapter 5, the use and programming of smartphones and digital cameras as analytical instruments based on processing and colorimetric determination of analytes pictures is explained. For this purpose, different studies have been carried out: development of an Android application in smartphone for measuring of gaseous oxygen; a micro-fluidic multi-sensor platform and Android application in smartphone for simultaneous determination of pH and nitrites concentration in solutions; design and development of an Android application in smartphone for soil classification according to the Munsell chart; and analysis of the stability of mayonnaises using a commercial digital camera for capturing pictures.

Chapter 2. **State of the art**

2.1 Introduction

The most common way to measure physical and chemical magnitudes is by use of sensors and transducers. A sensor is a simple element that converts a physical or chemical quantity in a signal that can be read by an observer or an instrument. Today, there are a huge number of applications for sensors, most of them even in the daily life: electrical appliances, cars, medicine, etc. But the development of a portable instrument requires to take into account the whole system and not only the sensing or the transduction part. The entire sensor system consists of transducer, sensitive layer, data-acquisition, and evaluation (Gauglitz 2005). In Figure 2.1 a general diagram block of an instrument is presented (Eren 2004) where it can be seen the need of a signal conditioner before the processing. The output must be presented to the user by showing it in a display, being internally stored or sent via wireless since a portable instrument should be self-contained (Capitan-Vallvey and Palma 2011).

Portable instrumentation design always involves trade-offs between power consumption, cost, performance, size, weight, ease of use and adaptability to different environments. All these factors have to be taken into account when the development of a handheld instrument is done by selecting and testing carefully the main parts of the electronic design.

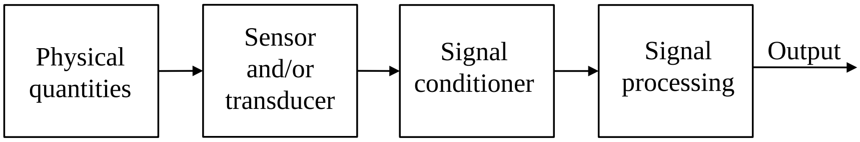

Figure 2.1 Scheme of an instrument.

Since in this work the main interest is the development of electronic instrumentation in combination with chemical sensors, in particular in handheld opto-chemical analytical instrumentation, it has been discussed the use of equipments for luminescence and colorimetric sensors which change their chemical or physical characteristics taking into account different environmental conditions. When the development of portable prototype for chemical sensing is required, it is needed to take into account the characteristics of the sample such as volume, interferents, physical properties, as well as some user limitations such as type and quality of the information, time, frequency, cost of the instrument, among others (Ligler 2009). Most of the instrumentation for optical sensors consists of a light source, devices for selecting the wavelength of interest, a detector of light or a capture device and the required electronic circuitry for carrying out the processing and the transmission of information. The main advantages that this instrumentation offer, apart from the mentioned before, are that they provide more autonomy, lower weight, lower energy consumption, and lower cost than the equipment that usually has been used for this purpose and the ease of use, even for untrained people.

In this chapter, according to the objectives of this work, a brief review of some aspects related to colorimetry, optical chemical sensors and optical and image detection devices are presented. These are three main areas of interest for the research here carried out, since the measurement of the changes of the optical properties of the chemical sensors was carried out using light intensity or colour information measured with different devices such as digital detectors, photodiodes or cameras.

2.2 Colorimetry and luminescence

Colorimetry is the science that studies all the processes related to the colour by defining methods that allow to quantify the colour information for processing and analysis with several purposes. The colour is a visual perception that is generated in the brain when nervous signals are received after the electromagnetic radiation reaches the retina. In this way, the colour is not an intrinsic feature of the matter, but it depends on how the light is reflected by an object and how it is perceived by each person (Denton *et al.* 1983). However, the colour can be determined by experimental laws of colour matching which are obtained from empirical generalizations known as trichromatic generalization (Wyszecki and Stiles 1982). The visual human system has two different kinds of photoreceptors: the rods and the cones. The cones are sensitive to colour, existing three different kinds of cone cells which are sensitive to different wavelengths: red (L, large wavelengths), green (M, medium wavelengths) and blue (S, short wavelengths) regions of the visible spectra. Therefore, any visible colour can be defined using three different parameters. On the other hand, the rods are not sensitive to colour but they are extremely sensitive in situations of low intensity of light, being responsible of the night vision. But, consequently with the visual human system, different colour spaces, which are called tristimulus spaces, have been defined in order to be able of determine numerically a colour and allow to use it as analytical parameter.

In all the applications related to colorimetry, the light source is an important feature to take into account. The International Commission on Illumination (CIE) has defined several standard illuminants identified by a letter or a number. In this way, illuminant A represents incandescent light, B direct sunlight, C an average of the daylight, D represents the phases of daylight, E is the equal-energy illuminant and F the fluorescent light sources. The D65 illuminant is the most common used in colorimetric applications which represents a phase of natural daylight with a colour temperature of 6504 K approximately (Wyszecki and Stiles 1982).

2.2.1 Colour spaces

A colour space is an abstract mathematical model, which is also represented graphically, that describes different colours as a sequence of numbers which depends on the used model. Usually, a colour is defined as a linear combination of the main colour components used in a colour space. It is possible to classify the colour spaces in four different types: linear-light tristimulus (XYZ, RGB, CMYK), xy chromaticity, perceptually uniform (CIELAB) and hue oriented (HSV, HVC) (Wyszecki and Stiles 1982). In this doctoral thesis the colour spaces mostly used are the RGB, XYZ, CIELAB, HSV, HVC and CMYK.

To be able of understanding the measurement of colour it is necessary to define several concepts related to the colorimetry. Although using a three-dimensional diagram, the colours visible by the human eye can be represented, the concept of colour can be also separated in two different parts: luminance and chromaticity. Luminance, which is related with the perception of brightness of the human visual system, is defined as the luminous intensity of light per unit area, which is the amount of light that is emitted from a particular area. Chromaticity is denoted as the proportion between the three colour stimuli that are needed to describe a colour. It provides an objective definition of the quality of colour independently of the luminance, and is usually determined by the hue and the saturation values. Hue denotes the appearance of the colour and it is associated with the dominant wavelength. Saturation is defined as the colourfulness in proportion to the brightness of the object itself or the indicative of which channel dominates (Hunt 2004).

For the measurement of colour in the field of portable instrumentation, it is usual to use only one or two colour space coordinates since the information given by the optical chemical sensors can be usually extracted by using a single component or a linear combination of two of them. In this way, it is not necessary to handle large amounts of information, simplifying the analytical procedure and, therefore, making faster the response of the instrument.

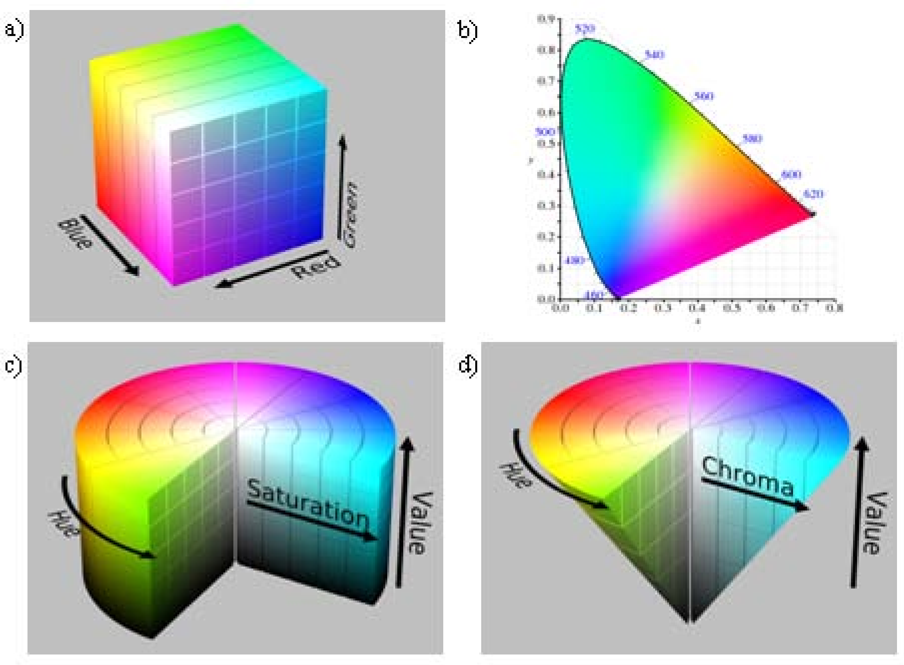

http://en.wikipedia.org/

Figure 2.2 Graphic representation of the different colour spaces: (a) RGB, (b) XYZ, (c) HSV and (d) HVC.

The RGB colour space is an additive colour space where any specific colour can be defined by the combination of the three chromaticities of red, green and blue (Hunt 2004). In Figure 2.2a it can be seen the representation of the colour gamut for this space where the values of each coordinate vary from 0 to 255. The number of colours available inside the gamut depends on the number of bits used for the system to extract the colour information, which is called the bit depth. Therefore, if 8 bits are used for each component, there are 256 levels of colour for each coordinate. The RGB colour space is device-dependent since different devices detect and reproduce a given RGB colour in a different way. The response to the red, green and blue wavelengths depends on each manufacturer. RGB is the most used colour space in capture devices since the human visual system works in a similar way, and, for this reason is used as the initial colour space from where other coordinates of other spaces are obtained. However, with the combination of the three primary colours used in this case is not enough to obtain all the colours.

The XYZ is a space derived from the RGB colour space. The X and Z coordinates are defined with cero luminance, therefore, just the Y coordinate contributes to the luminance component. For a given value of luminance, X and Z describe all the possible chromaticities. To represent this space, as shown in the chromaticity diagram of Figure 2.2b, only two coordinates are needed, xy, which are obtained using the Equations 2.1 and 2.2. To calculate the XYZ components from the RGB coordinates provided by a device, there are some standard equations which are shown in Equation 2.4. These transformations are defined for the standard illuminant D65. However, as it will be explained in the corresponding section, specific models can be obtained for a particular case, since different illuminants can be used in each application.

$$x = \frac{X}{X+Y+Z} \tag{2.1}$$

$$y = \frac{Y}{X+Y+Z} \tag{2.2}$$

$$z = \frac{Z}{X+Y+Z} = 1 - x - y \tag{2.3}$$

$$\begin{bmatrix} X \\ Y \\ Z \end{bmatrix} = \begin{bmatrix} 0.4125 & 0.3576 & 0.1804 \\ 0.2127 & 0.7156 & 0.0722 \\ 0.0193 & 0.1192 & 0.9502 \end{bmatrix} \begin{bmatrix} R \\ G \\ B \end{bmatrix} \tag{2.4}$$

In the CIELAB colour space, the L coordinate represents the luminance in a range from 0 to 100, while the a* and b* coordinates represents the change of colour from magenta to green and yellow to cyan respectively. The range for the two components varies from -60 to 60, although it can vary with the application. It is not possible to transform directly to CIELAB from RGB coordinates, so it is necessary to use a intermediate step by transforming RGB into XYZ coordinates and, using after that the Equations 2.5, 2.6 and 2.7 to get the La*b* coordinates (Wyszecki and Stiles 1982). The XYZ and the CIELAB colour spaces were designed to comprise all the colours that human visual system is able to see, but CIELAB is more perceptually uniform than XYZ, which means that a change in a colour value produce the same visual change. Therefore, since this space provides a uniform representation of the colour, it is possible to extract differences between two colours using Equation 2.8, which represents the Euclidean distance, in order to determine how different they are with respect to each other.

$$L = \begin{cases} 116 \left(\frac{Y}{Y_n}\right)^{1/3} - 16, if \ \frac{Y}{Y_n} > 0.008856 \\ 903.3 \frac{Y}{Y_n}, if \ \frac{Y}{Y_n} \leq 0.008856 \end{cases} \tag{2.5}$$

$$a^* = 500 \left[\left(\frac{X}{X_n}\right)^{1/3} - \left(\frac{Y}{Y_n}\right)^{1/3} \right] \tag{2.6}$$

$$b^* = 200 \left[\left(\frac{Y}{Y_n}\right)^{1/3} - \left(\frac{Z}{Z_n}\right)^{1/3} \right] \tag{2.7}$$

$$\Delta E_{ab}^* = \sqrt[2]{[(\Delta L)^2 + (\Delta a^*)^2 + (\Delta b^*)^2]}, \tag{2.8}$$

where X_n, Y_n and Z_n are the values for a white of reference which has to be used in the system in order to define absolute colours. Usually, the white-colour stimulus values are given by the standard illuminant used and defined by the CIE. Finally, it is worth to note that the CIELAB colour space is device-independent.

The HSV colour space is an alternative representation derived from the RGB colour space. HSV stands for hue, saturation and value respectively. The value coordinate denotes the brightness which determines the extent to which an area appears to exhibit light. The hue value varies from 0 to 360º while saturation and value coordinates vary from 0 to 1. Since most of the capture devices provide RGB information, it is needed to define the transformations between the RGB and HSV colour spaces (Smith 1978).

$$M = \max(R, G, B) \tag{2.9}$$

$$m = \min(R, G, B) \tag{2.10}$$

$$C = M - m \tag{2.11}$$

$$H = 60^{\circ} \times \begin{cases} undefined,\ if\ C = 0 \\ \left(\frac{G-B}{C}\right)/6, if\ M = R \\ \left(\frac{B-R}{C} + 2\right)/6, if\ M = G \\ \left(\frac{R-G}{C} + 4\right)/6, if\ M = R \end{cases} \tag{2.12}$$

$$S = \begin{cases} 0\ if\ C = 0 \\ \frac{C}{V}, otherwise \end{cases} \tag{2.13}$$

$$V = \max(R, G, B) \tag{2.14}$$

The main feature of this colour space is the possibility of representation of the colour in a single parameter, the hue component. In this way, previous studies of the group have shown the relevance of the hue component as a quantitative parameter (Cantrell *et al.* 2010). Since the H value determines the colour information by using just one single coordinate, it offers a good alternative to the RGB colour space where three coordinates are needed to extract and define completely the colour information. Besides, it has been proved that the hue component is more robust to lightly variations of light that could affect to the measurements. Therefore, the hue value is obtained from the RGB coordinates provided by different devices, such as digital sensors, cameras or scanners, and the statistical mode of the hue components of an image is used as analytical parameter (Cantrell *et al.* 2010).

The HVC colour space (hue, value and chroma) is denoted usually as the Munsell colour system. In this case, the hue value varies from 0 to 360º, the value from 0 to 10 and the chroma from 0 to 20, as shown in Figure 2.3. Chroma is defined as the colourfulness of an area in proportion to the brightness of a similarly illuminated area that appears to be white (Hunt 2004), or in other words, it is the purity of the colour. This kind of colour spaces based on hue and saturation are most used by artists or designers since it is more natural to think in colours such as variations of them than thinking is addition or subtraction of colours. This colour space is usually used in the natural sciences to describe the colours of soils, minerals or flowers in order to classify the different species where a set of coloured chips illustrates the colour and the corresponding hue, value and chroma coordinates to be used in visual examinations. In 1930, this colour space was adopted by the United States Department of Agriculture (USDA) as the colour system for soil researches.

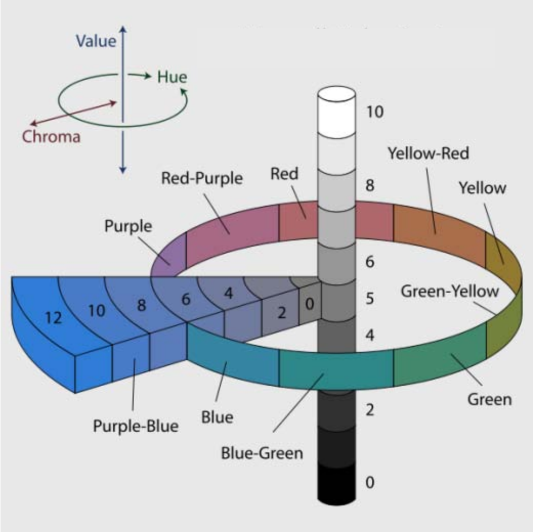

http://en.wikipedia.org/wiki/Munsell_color_system

Figure 2.3 Graphical representation of the Munsell colour system.

Finally, the CMYK is a subtractive colour space that uses cyan, magenta and yellow to represents every colour. The K represents the black colour since from only CMY is not possible to obtain a real black colour. This colour space is mostly used in colour printing where four different inks are used for obtaining the rest of colours. To transform RGB values to this space, and due to the subtraction nature of the colour space, the Equation 2.15 has to be used.

$$\begin{bmatrix} C \\ M \\ Y \end{bmatrix} = \begin{bmatrix} 1 \\ 1 \\ 1 \end{bmatrix} - \begin{bmatrix} R \\ G \\ B \end{bmatrix}, \qquad (2.15)$$

where all the colour values are normalized in the range [0, 1].

2.2.2 Luminescence

The emission of light from a solution, from the surface of powdered solid supports, or from membranes is called luminescence and occurs from molecules excited to higher energy states –some vibrational levels of the excited electronic state- by the absorption of energy. Then, it is a process of light emission non-based on the heating of an element, and therefore, it is usually produced in ambient conditions. There are different types according to the cause that produces the emission of luminescence: from chemical reactions (chemiluminescence), as a result of absorption of the incident radiation (photoluminescence: fluorescence or phosphorescence) (Figure 2.4a), from electric current passing through a substance given rise to an electrochemical reaction (electroluminescence) (Figure 2.4b), and from mechanical actions on solids (mechanoluminescence), among others.

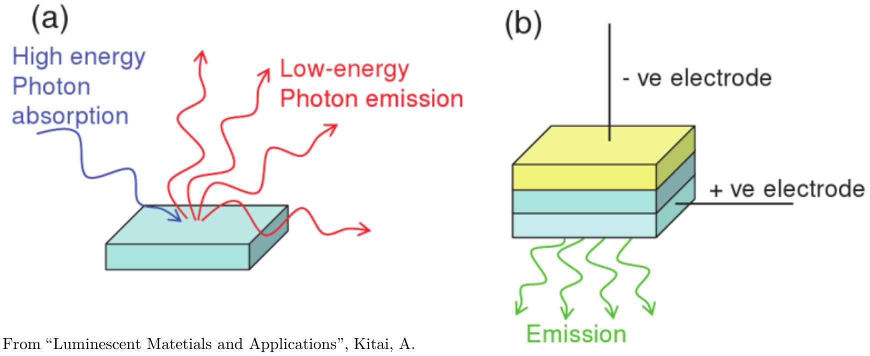

From "Luminescent Matetials and Applications", Kitai, A.

Figure 2.4 Schematic illustration of a) photoluminescence and b) electroluminescence.

A substance is luminescent, and therefore called phosphor, when if it is excited by a light source of a certain wavelength, it emits a light in a different wavelength. Usually, the wavelength of emission is higher than the wavelength of excitation, which is called Stokes' law. An important parameter of this kind of phenomenon is the lifetime of the luminescence. The lifetime is defined as the time required for the intensity of luminescence to decay from an initial state to a certain value, namely the average time that the molecule spends in the excited state prior to return to the ground state. When the excitation is removed, if the intensity of the luminescence decreases rapidly it is called fluorescence (short lifetime), while if the emission persists after the excitation it is called phosphorescence (long lifetime) (Lakowicz 2006).

Usually, the intensity of the emitted luminescence is measured by using spectrofluorometer. In this kind of devices it is possible to record both excitation and emission spectra. An emission spectrum is the wavelength distribution of an emission measured at a single constant excitation wavelength. Conversely, an excitation spectrum is the dependence of emission intensity, measured at a single emission wavelength, upon scanning the excitation wavelength (Lakowicz 2006). In the first case, emission spectra, the light passes through the sample and the intensity of the emitted light is measured by using a photomultiplier tube, photodiodes or charge-coupled devices (CCD). Other approach is the measurement of lifetime of the luminescence as analytical parameter. The lifetime is measured using spectrometers, high sensitivity CCD cameras, or similar devices. The main advantages of this method are the independence with the concentration of luminophore and the intensity of the light source, increasing in this way selectivity and sensitivity. An extended review of luminescence techniques and instrumentation has been made in (Lakowicz 2006), (Botter-Jensen, 1998). In this work the intensity of the stationary luminescence emitted by a sensing membrane has been quantified using colorimetric parameters such as the red component of the RGB colour space.

2.3 Optical chemical sensors

Although a revision of the field of chemical sensors is out of the scope of this document, a very brief introduction is given now. A chemical sensor is a device which is capable of transforms any chemical information into an analytically useful signal. Chemical sensors include two main parts: a receptor, where the chemical information is transformed into a measurable form of energy, and a transducer, which transforms that energy that carries the chemical information into useful analytical signal (Hulanicki *et al.* 1991).

Currently, one of the main objectives in Analytical Chemistry and the research in chemical sensors is the development of technologies that allow to obtain in-situ and real-time information using low cost devices that provides accuracy in the measurement of different magnitudes. Thus, in recent decades, the goal has been to reduce the response time by simplifying the analytical procedure without compromising the results. With this purpose, chemical sensors offer several possibilities that have been reported in the literature (Janata 2009). The information that can be extracted from chemical sensors is obtained in real time as result of the interaction between sensor and chemicals and this interaction implies two steps: recognition and signal treatment. A change in a physical property of the sensor as the consequence of a chemical reaction with a sample occurs or is observed in the sensor receptor.

Numerous types of chemical sensors exist (Hulanicki *et al.* 1991), (Valcarcel and Luque de Casto 1994), but this work is confined to optical chemical sensors, whose principle consists of the pass of the electromagnetic radiation through the sample, which can be solid, liquid or gas, and the interaction between both of them changes some optical parameters that can be related to the magnitude of interest (Janata 2009). The optical chemical sensors present some advantages with respect to others (Baldini *et al.* 2006), (McDonagh *et al.* 2008), (Orellana and Moreno-Bondi 2005), (Wang *et al.* 2010a): facility of use; no electrical interferences, no need of contact between the sensor and the system used for the analysis; good sensitivity and reversibility; no consumption of the analyte during the measurement; usually, they support extreme environmental conditions of humidity or temperature; they are low cost sensors; and, finally, their size can be reduced if is needed. However, they have some disadvantages such as the interference of the light source in the measurement or the photobleaching that they could suffer. The efficiency of an optical chemical sensor depends mainly on the proper choice of the recognition chemistry and the sensing platforms used to determine the analyte (Qazi *et al.* 2012). Usually, this kind of sensors is included in instrumentation characterized by its portability, which is one of the objectives of this Ph.D. Thesis.

Selectivity is one of the most important features in chemical sensing. This is the capacity of a sensor to respond only to one analyte in presence of other species (Janata 2009). Therefore, in the last years, due to the difficulty obtaining good selective sensors, the trend has become to use sensor arrays where the combination of the responses of low selective sensors with high stability and cross-sensitivity provides the information of interest (Vlasov and Legin 1998). These kinds of arrays are called electronic noses or tongues due to the similarity with the natural responses of the nose and tongue in the mammals. These systems use advanced mathematical procedures such as pattern recognition or multivariate analysis in order to processing the responses of the sensors (Vlasov *et al.* 2005).

Since the actual requirements of optical chemical sensors applications are the simplification of methods of analysis, other features that the chemical sensors should present are sensitivity and robustness, as well as having reproducible analytical characteristics. However, usually, the more robust a sensor is, the less sensitive it becomes (Janzen *et al.* 2006). To avoid this problem, a common solution is the use of disposable sensor, or one-shot sensors, which allows to provide a good robustness of the sensors in exchange for using them. To use this type of sensors, they cannot be integrated in the device, and requirements of cost and portability have to be taken into account. Furthermore, in relation with the development of portable instrumentation, a consideration of the characteristics of the sample, such as volume, concentration or physical properties, and user constraints, like the type of information needed and the accuracy, assay time or frequency, cost or power requirements, is required (Ligler 2009). Also, a trade-off between compactness and performance of the instrument has to be made. The use of one-shot sensors is extended in the last decades due to the robustness, ease-to-use, low cost and fast response that they offer besides the lower requirements of transport, preservation and storage.

Within the optical chemical sensors, it is possible to define different types of sensors according to the type of optical properties: absorbance, fluorescence, luminescence, reflectance, refractive index, optothermal effect and light scattering (Hulanicki *et al.* 1991). Absorption occurs when there is transmitted light after the incident light passed through a sample which can be a gas, liquid or a solid, and therefore, the intensity of the light is reduced. However, most of absorbance-based sensors undergo a colour change instead of a change in the intensity which means that some regions of the spectra disappear while other new appear (Baldini *et al.* 2004). For this reason, this kind of sensors is used as colorimetric sensors for applications where a system can measure the change of colour for being related to the magnitude of interest. On the other hand, fluorescent chemical sensors usually present an emission peak with longer wavelength than the absorption peak. The intensity of the emission can be related to the concentration of an analyte. This kind of sensors is widely used due to its sensitivity combined with the required selectivity. Both, absorption and fluorescence sensors require an excitation light source to modify the optical properties to determine and measure.

Luminescence sensors are based on chemical reactions which produce products in an excited state. In these sensors, the intensity of the luminescence generated as well as the luminescence lifetime depends on the concentration of a chemical involved in the reaction (Korotcenkov *et al.* 2010). The luminescence can be measured by determination of the intensity which presents some advantages such as the simplicity and low cost. However, with this approach, the measurement depends strongly on the stability of the light source, as well as the detector sensitivity or the luminophore distribution and stability (Sanchez-Barragan *et al.* 2006). The measurement of the luminescence lifetime has been also used in portable instrumentation, for example for measurement of gases in blood (Kieslinger *et al.* 1997), (Lippitsch *et al.* 1997). In recent years, a colorimetric approach is being used to determine the intensity of the luminescence (Evans and Douglas 2006), (Evans and Douglas 2009), and, therefore, besides the traditional techniques for measuring colour using some kind of detector, imaging techniques can be also used for this purpose. Absorption, fluorescence and chemiluminescence sensors are the most common optical sensors in the current researches and literature.

Many works have been carried out and reported in the literature related to optical chemical sensors: use of phosphorescent complexes of porphyrin ketones in applications for oxygen sensing (Papkovsky *et al.* 1995); organically modified silicate films for stable pH sensors (Makote and Collinson 1999); reversible chemical reactions of optical sensors for detection of amines, alcohol and humidity (Mohr *et al.* 1999); determination of oxygen, pH and carbon dioxide using luminescence lifetimes of optical sensors (Liebsch *et al.* 2000); use of several pH indicators with different pKa's to cover a wider range of pH (Lin and Liu 2000); detection of different proteins using an array of fluorescent protein surface receptors (Baldini *et al.* 2004); detection of cancer biomarkers based on pH induced colour changes (Chu *et al.* 2012), and so on. An extended review of the recent developments related to optical chemical sensors and portable instrumentation can be found in (Capitan-Vallvey and Palma 2011).

In this report, several optical sensors have been used in combination with different portable instruments which provide the information of interest for each case. In this way, an optical colorimetric sensor array was used for pH determination; another optical sensor array was used to measurement of concentration of dissolved heavy metals; and a luminescence sensing membrane was used in several prototypes for the measurement of gaseous oxygen concentration.

2.4 Optical detectors and image sensors

In this section, different types of optical detectors and image sensors are briefly revised. Their principle consists of absorbing light energy and converts it to electrical energy which has to be processed to extract information. In this way, their main objective is to convert the incident light in manageable information that could be processed to obtain a relation between that light (intensity, colour, etc.) and the magnitude of interest. They usually are able to respond to incident ultraviolet, visible or infrared electromagnetic radiation. Optical detectors convert incoming optical energy into electrical signals and image sensors convert an optical image into electronic signal. The optical detectors usually generate an electrical current which is proportional to the intensity of incident optical radiation. In the image sensor, for each element, the same process of current or voltage generation takes place.

In the case of image sensors, which are mostly used in digital cameras and today on smartphones, if the electronic signal generated is converted to digital values, any information of light can be represented at the end as a numerical sequence of zeros and ones. In digital imaging, a pixel is the smallest controllable element of an image and it is usually represented by a single optical detector or element, such as a capacity or a photogate, which captures the incident light. So for each pixel, the obtained binaries numbers characterize the corresponding intensity and the colour information.

As mentioned before, the development of portable instrumentation is a constant trade off between compactness, cost, performance and power consumption. All these features need to be taken into account to select the optical device to be included in the electronic design.

2.4.1 Photodiodes

A photodiode is a type of photodetector that transforms the received light into voltage or current, depending on the mode of operation. They are usually used to detect and determine the intensity of the light when the p-n junction that constitutes the photodiode is illuminated. There are several types of photodiodes, but all of them work under the same principle: silicon (Si) or GaAsP photodiodes, GaAsP schottky; PIN Si photodiodes, and Si avalanche photodiodes.

http://www.edmundoptics.com/ http://www.conrad.com/ http://www.digikey.com/

Figure 2.5 Different types of photodiodes.

The range of electromagnetic wavelengths of operation is determined by the material used for the fabrication of the photodiode. In this way, Si photodiodes range from 190 to 1100 nm, germanium (Ge) photodiodes from 400 to 1700 nm, indium gallium arsenide (InGaAs) from 800 to 2600 nm, and Lead(II) sulphide (PbS) from 1000 to 3500 nm. (Held 2008).

In this work, only Si photodiodes are taken into account. Some characteristics of the Si photodiodes are (Singh 2000): linear response with the intensity of light; low noise; they are mechanically durable as well as compact devices; they possess very long life; easy calibration; and, finally they offer very high quantum efficiency, about 80% at 800 nm. On the other hand, they present some disadvantages with regard to other photodetectors since they are of small area, they do not present internal gain, as well as, for some applications the response time is high.

When a Si photodiode receives an incident light with energy greater than the energy of the band gap, the electrons placed in the valence band are excited to the conduction band. As a result, they leave the corresponding holes in the valence band. In the depletion layer, the electrons are accelerated for the electric field towards the N-layer, and the holes to the P-layer. Therefore, a positive charge proportional to the incident light is generated in the P-layer and a negative charge is in the N-layer, as it can be seen in Figure 2.6. The spectral and the frequency responses of a photodiode can be controlled by modifying the thickness of the N-layer and the P-layer, as well as the dopant concentration. When an electrode is formed from the P-layer and N-layer and there is connection with an external circuit there is a flow of the electrons and holes to the opposite respective electrode. This process generates the current proportional to the incident light that characterize the behaviour of a photodiode.

The main characteristics of a photodiode are the responsivity, the dark current and the bandwidth, previously mentioned (Zeghbroeck 2004). The responsivity is the photocurrent divided by the incident light power, and the dark current is that current generated in absence of light. The dark current limits the minimum power light that can be detected by the photodiode; therefore, to maximize the sensitivity of the device, the dark current must be minimized (Tavernier and Steyaert 2011) and also it has to be taken into account for the calibration of the device. Occasionally, for some applications, the photodiodes are reverse biased in order to increase the upper limit of linearity, but, on the other hand, the dark current is increased and also the noise level. For these reasons, reverse biased photodiodes have been never used in this work.

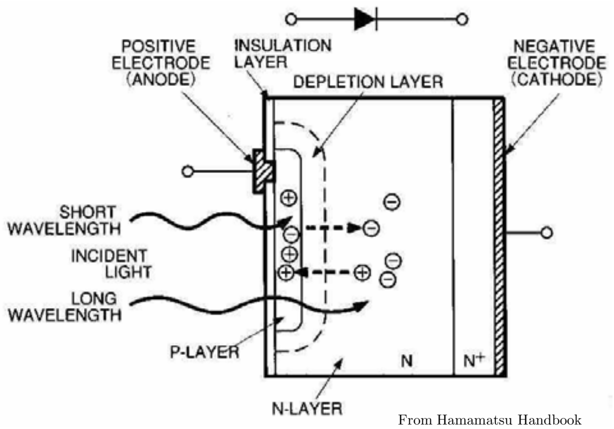

From Hamamatsu Handbook

Figure 2.6 Si photodiode cross section.

Photodiodes are utilized in a wide variety of applications, but mainly for light measurement (Figure 2.7a), as in light meters for cameras, or in consumer electronics such as smoke detectors (Figure 2.7b). Also, they are used in medicine and chemistry for computed tomography or chemical analysis respectively (Figure 2.7c) (Ma *et al.* 2011). In the researcher field, they have been employed for different purposes: oxygen determination using a sensing film to coat the photodiodes (Capitan-Vallvey *et al.* 2007), (Palma *et al.* 2007b); for determination of potassium and nitrate using disposable sensors (Palma *et al.* 2006), (Palma *et al.* 2008); as pH meter using light to frequency converters (Caldara *et al.* 2012); for fluorescent detection in a wide range of bead-based immunodiagnostic assays (Yamazaki *et al.* 2012) and in microfluidic devices (Ryu *et al.* 2011). They are also used in some applications being connected as a photodiode array in order to collects information from a wider range of wavelengths providing faster response than CCD and CMOS sensors as will be explained below. The most common use of this configuration is for spectrometers and spectrophotometers but they are also used for food analysis by determining colour additives (Ichi *et al.* 1995), (Harp *et al.* 2012). As it can be deduced, most of these mentioned applications are based on detection of light properties for determination of different species. In this way, the combination of photodiodes with filters allows to detect selected regions of the spectra, only taking into account the wavelengths of interest, and, therefore, providing colorimetric information.

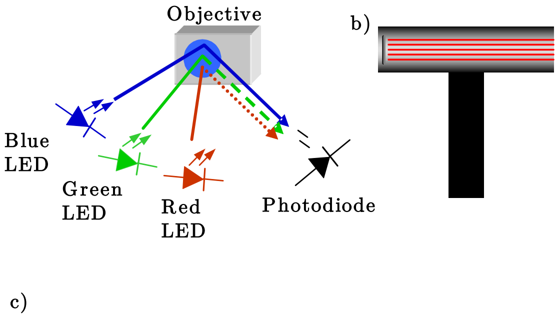

Figure 2.7 Some of the applications of photodiodes: a) Colour or light detection, b) Smoke detectors, and c) Analysis of samples.

2.4.2 Digital colour sensors

A digital colour sensor is generally a monolithic CMOS photo integrated circuit (IC) that provides the response at three different wavelengths which are red, green and blue components. A photo IC consists of a photosensitive part, usually a photodiode, and a signal processing circuit that are integrated in the same package. The photosensitive part consists of a number of elements arrayed in a mosaic pattern where each element is sensitive to a wavelength by using optical filters. The processing circuit consists of an amplifier, an analog to digital converter, and the necessary elements to convert the received power to a digital signal. There are two different types of photo integrated circuits. One of them is a monolithic photo IC including both parts, the photosensitive and the processing circuit, in the same chip, offering high-speed response and lower sensitivity to electromagnetic noise. The other type is a hybrid photo IC where each part is placed in a different chip and they are connected within one package. The main advantage of the hybrid IC is the possibility of improving some characteristics such as the sensitive area or the spectral response. The detected signals are serially output as words of digital data, depending on the number of bits on the model of digital colour sensor used. For compactness reasons, only monolithic photo ICs have been included in the developed measurement platforms in this work.

The internal circuitry of the digital sensor depends on the manufacturer, but usually each of the RGB photodiodes has an internal amplifier, as shown in Figure 2.8. This configuration allows to obtain the RGB component of the incident light simultaneously. The incident light is converted into frequency (a square digital wave) and the output is a serial word of bits, one for each measured colour.

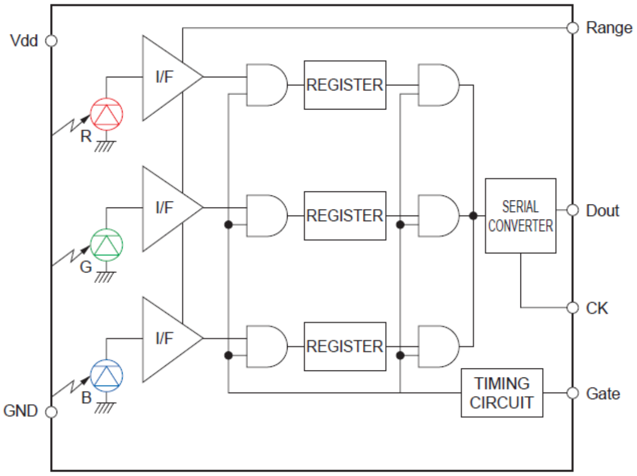

Figure 2.8 Internal block diagram of a digital colour sensor.

The response of each detector, i.e. the curve responses of the device for each wavelength, depends on the manufacturer and the selected filters. Usually, in order to detect each wavelength individually a Bayer filter is used, which consists of a series of filters arranged as shown in Figure 2.9. The filter array includes individual luminance and chrominance sensitive elements that are intermixed with luminance elements dominating the array, since the human visual system has relatively greater ability to discern luminance details (Bayer 1976). Therefore, there are filters that allow to pass the green colour, which are employed as the luminance elements, and others that allow to go through the red and blue region of the spectra, which are employed to get chrominance elements. The number of elements is not proportional for the three colours in order to imitate the human visual system which is more sensitive to green wavelengths. As an example, in Figure

2.10, the response of the S9706 digital colour sensor from Hamamatsu (Hamamatsu Photonics, Japan) to red, green and blue regions of the spectra is shown.

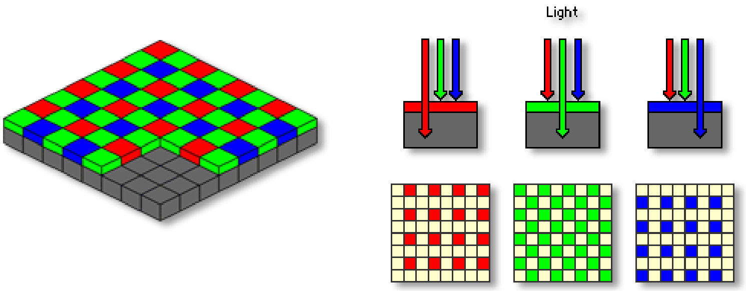

http://www.dpreview.com/glossary/camera-system/color-filter-array

Figure 2.9 Bayer filter.

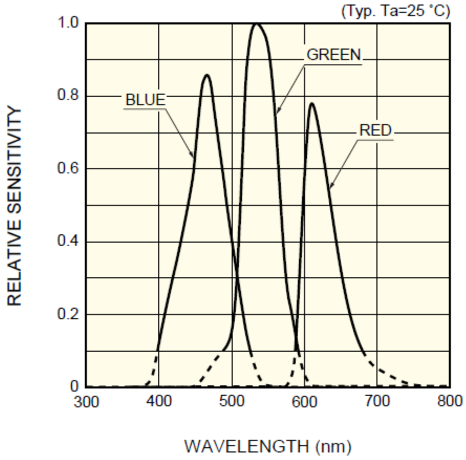

From datasheet of detectors S9706 (Hamamatsu)

Figure 2.10 Spectral response of the digital colour sensor S9706 to different wavelengths: red (•=615 nm), green (•=540 nm) and blue (•=465 nm).

This kind of sensors offers a good alternative to colorimetric detection because its compactness, small size and weight, high reliability and low power consumption. Some of the digital colour detectors allow to configure different parameters in order to improve the technical features according to the requirements of the application. In this way, the active photosensitive area can be set to high sensitivity, with all the elements activated or low sensitivity, where only a part of them contributes to the output. Other parameter is the integration time, which is the time that the incident light is being taken into account for the response. For a given value of illuminance, the higher the integration time, the higher the output.

As it can be seen in Figure 2.11, in some cases the digital colour sensors can be presented as a module in which one or several LEDs act a light source. In this way, the response of the digital colour detector is optimized with regard to these LEDs which act as light source by taking into account the response curves of the each particular sensor. The most common application of digital colour sensor is the adjustment of the backlight brightness on LCD displays: combined with a microcontroller, they allow to maintain a constant level of brightness to avoid the deterioration over time.

http://www.ams.com/eng http://www.hamamatsu.com/jp/en/index.html

Figure 2.11 Several models of digital colour sensors.

2.4.3 CCD and CMOS sensors

Charged Coupled Device (CCD) technology was invented by Boyle and Smith in 1969. They are semiconductor devices within the family of charge transfer devices that transfer charges by using potential wells. Therefore, in the CCD architecture there are three basic functions: charge collection, charge transfer and conversion of the charge into measurable voltage. The elementary block of a CCD system is called photogate and it consists of a metal-oxide semiconductor (MOS) capacitor (Yotter and Wilson 2003). The potential wells are made by supplying to the MOS structure electrodes different voltages.

The created charge in each photogate, also called pixel, is proportional to the incident light and it also depends on the integration time and the quantum efficiency of each one. When the incident light is collected during the integration time, the charge is kept in the pixel architecture, but it has to be transferred to an amplifier which is placed physically separated from the pixels. The signal charge of each pixel is collected into the potential well beneath the electrode as shown in Figure 2.12. Then, the charge is transferred pixel to pixel in a sequential way until the charge of every pixel reaches the amplifier. The way to transfer the charge to the next gate is applying a positive voltage to the CCD gates, being this process controlled by a processor included in the CCD sensor. It is important to optimize the overlapping between the different clock pulses

The main problem of this system is that if one pixel is damaged, it affects not only to its information but also to the adjacent photogates.

Therefore, there are several configurations in order to carry out the transference of the charge from the pixels to the amplifier.

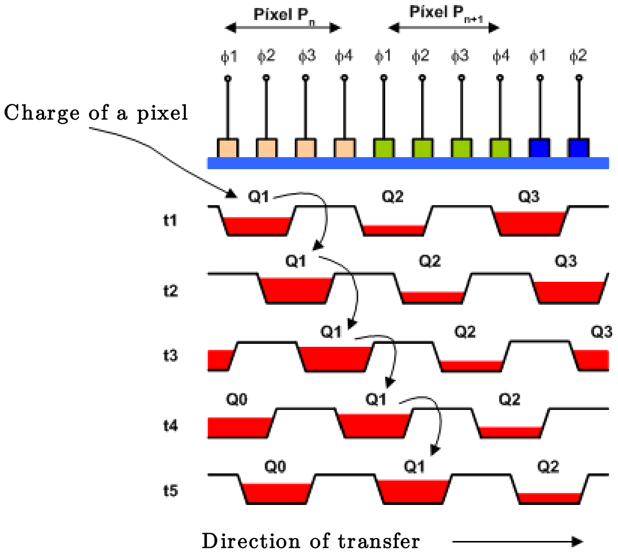

Figure 2.12 Transfer of charge through potential wells with a four phase clock.

The CCD array, called full-frame transfer (FFT), consists of a series of column registers and at the end of each column there is a horizontal register of pixels as shown in Figure 2.13. All charge must be readout of the serial register before the next line can be transferred (Holst, 2007). The full frame array is useful in applications that do not require time resolution of less than one second, approximately. This configuration allows to have a larger number of pixels, or the same number of pixels but with larger size in comparison with other types of CCDs.

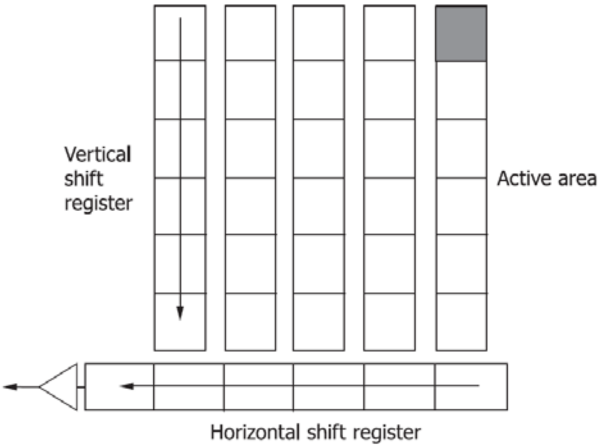

Figure 2.13 Full frame transfer CCD.

There is another kind of CCD arrays: frame transfer (FT), interline transfer (IT), frame interline transfer (FIT and one-dimensional. In the FT CCD there is a storage array between the CCD array for the image and the horizontal serial register, as shown in Figure 2.14. The storage array is identical to the light sensitive array, but covered with a mask of an opaque metal, such as aluminium, to avoid light influence. Once that the image data have been collected and converted into electrical potential by the image array, the data are transferred to the parallel storage array, and from here, they will be readout by the serial shift register which transports the charge packets to an output amplifier as a serial data stream. As it can be seen in Figure 2.14, separate clocks are required to control the CCD array: there is a clock to control the image array, another one to control the storage array and the last clock is to control the serial shift register. FT CCDs are quicker than FFT, since the time necessary to transfer the image information is shorter if it is transferred to the storage area instead of being sent directly to the serial register. For this reason, this kind of arrays is useful in applications that need a fast response like investigating rapid kinetic processes. On the other hand, only one-half of the chip is useful to obtain image information, having a bigger chip size and higher cost. However, the FT CCDs are still slow, so they are used in cameras with slow frame rate.

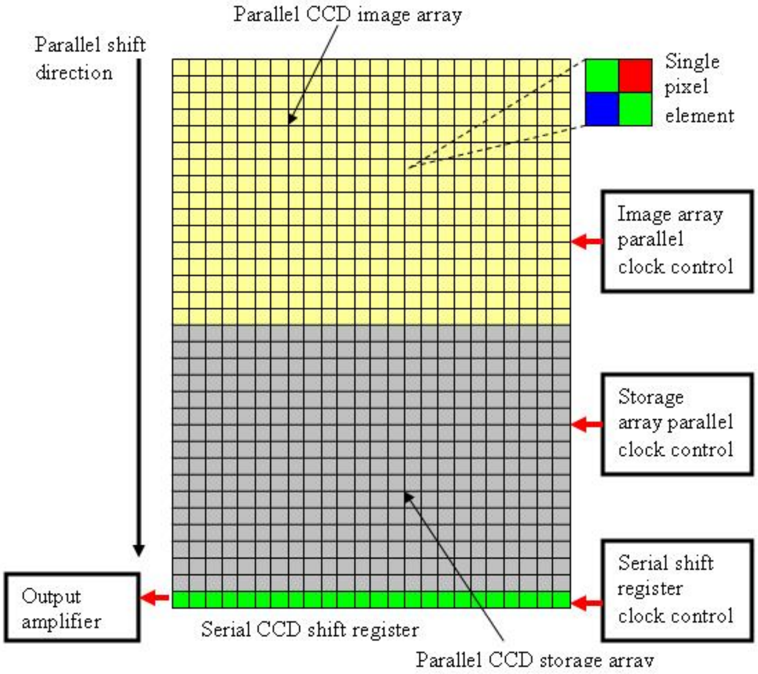

http://www.spacealliance.ro/articles/view.aspx?id=201003190321

Figure 2.14 Frame transfer CCD.

In the IT CCD array, columns of active image pixels and masked-storage-transfer pixel alternate over the entire parallel register array (Spring *et al.* 2012). In this configuration, the charge transfer from each pixel to the vertical shift register is performed simultaneously. Although the speed is higher, they have reduced dynamic range, resolution and sensitivity since 75% of the surface is occupied by storage-transfer channels.

The process to convert the charge in a measurable voltage is carried out by a floating diode and the amplifier. The diode acts like a capacitor and is precharged to a reference level. The capacitance is partially discharged by the amount of charge that has been transferred. After, the floating diode is recharged, before the next charge packet arrives, to repeat the same process. Once that the corresponding voltage for each pixel is obtained, it is transferred to an analog-to-digital signal converter which changes the voltage into digital information, that is 0 and 1 binary code, readable by a computer or other final device. It is also possible to use a MOS transistor arranged in a source-follower mode with a reset transistor in its gate as a circuit to change the charge into voltage as shown in Figure 2.15

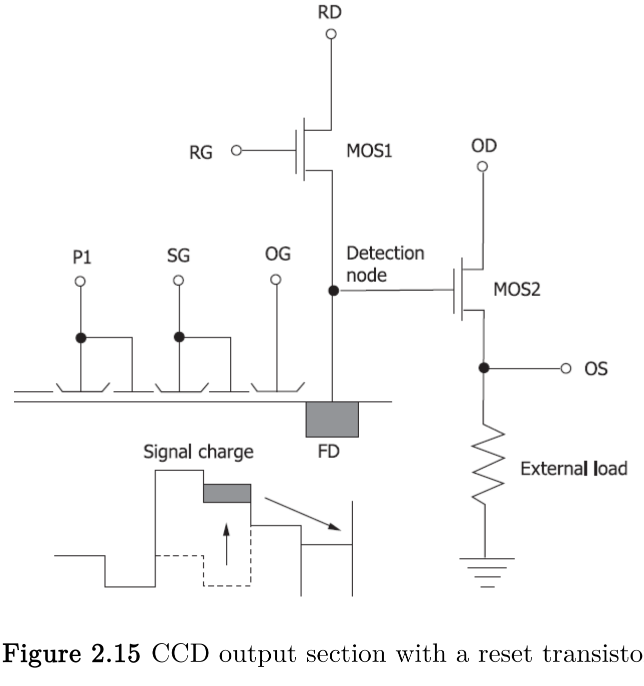

Figure 2.15 CCD output section with a reset transistor.

In the same way that for digital colour sensors, it is possible to produce colour images using CCD surfaces that detect red, green and blue colours. To get and split the colour information most of the CCD cameras use a Bayer filter, as explained in the previous section. Each pixel element contains four photogates masked with red, green and blue filters. Another approach to obtain colour images is to use a three-chip design where the image is divided using a beam-splitting prism and the corresponding colour filters. Then, the divided light is captured by three different CCDs, and, after, a recombination produces the coloured image. Finally, there is an approach that consists of switching sequentially the filters over a single CCD, capturing each component separately.

The most common uses for CCD sensor are in capture devices as scanners, professional cameras (Spring *et al.* 2012), (Sakaue *et al.* 2009) and (Hradil *et al.* 2002) or printers. Also, they are present in scientist and industrial applications, for water analysis (Lapresta-Fernandez *et al.* 2009), in environmental sciences (Jaakkola *et al.* 2010), (Tanaka *et al.* 2006), (Park, 2011), in food analysis (Knecht *et al.* 2004), (Antonelli *et al.* 2004), (March *et al.* 2005) and, finally, chemical analysis of heavy metals (Maleki *et al.* 2004), (Abbaspour *et al.* 2006).

Nowadays, the CCD image sensors are being replaced with CMOS image sensors (Yotter and Wilson 2003). It was in the 1990s when CMOS sensors emerged as an alternative to CCD arrays. The main advantage is that more than one active transistor can be integrated in each pixel. Besides, CMOS image sensors differ from CCD designs in the way the sensors are manufactured and, also, how the charge is transferred through the array. CMOS sensors are manufactured on standard semiconductor production lines instead of dedicated production lines as CCD sensors (Holst, 2007) and they allow to reduce the size of the photo-sensing system. For working with CMOS sensors and coloured images, the Bayer filter is used in the same way that for digital colour sensors and CCD image sensors.

In CMOS image sensors the charge-to-voltage process takes place for each pixel, which means that all the charges can be processed at the same time. In this way, the photodiode pixel is connected to a charge amplifier, as it can be seen in Figure 2.16 and Figure 2.17, where the feedback capacitance storages the corresponding charge of each photodiode. The output voltage of the amplifier is proportional to the incident light that is taken into account during the integration time which comprises from when the reset of the charge amplifier is turned off to when the hold pulse is input to each hold circuit. By inputting a hold pulse to each circuit of each pixel the charge of all the amplifiers is reset, keeping the charge in the respective hold circuits. Charge integration starts and ends at the same time for all the pixels. Taking into account that the readout from the hold circuits is made in a different circuit to the charge integration, this image sensors offer a high-speed response.

Other configuration is the active pixel sensor (APS) shown in Figure 2.18. Here, the voltage conversion and the amplification are carried out directly in each pixel obtaining lower limits of detection and wider dynamic range. The voltage is buffered by a source follower transistor and transferred to output buses through switches located in the pixel area. When the conversion is carried out, the voltage needed for the pixel reset is lower than for CCD's. Regarding to the consumption, it is lower for the CMOS sensors since only one row is addressed at the time during the readout, so that they are more suitable for portable devices. Since CCD sensors require an external element to perform the conversion, the equipment will be bigger than in CMOS case.

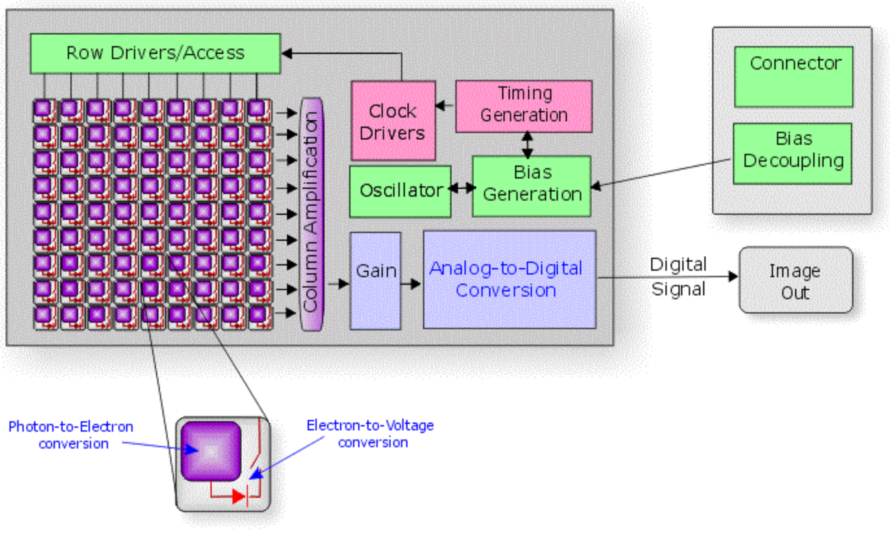

http://www.jiscdigitalmedia.ac.uk/guide/digital-cameras/

Figure 2.16 CMOS image sensor array.

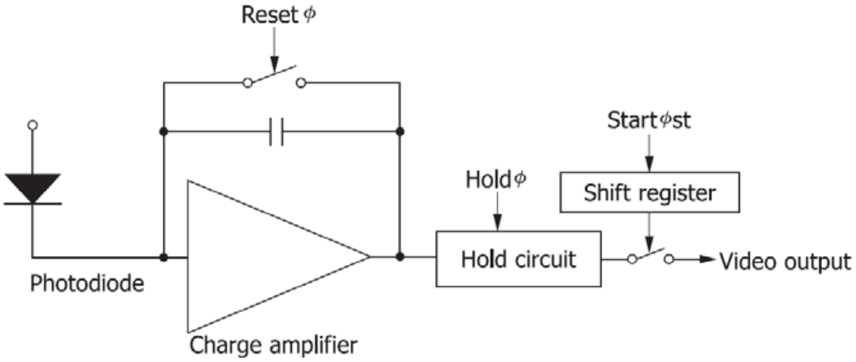

Figure 2.17 Light to voltage conversion in a CMOS image sensor.

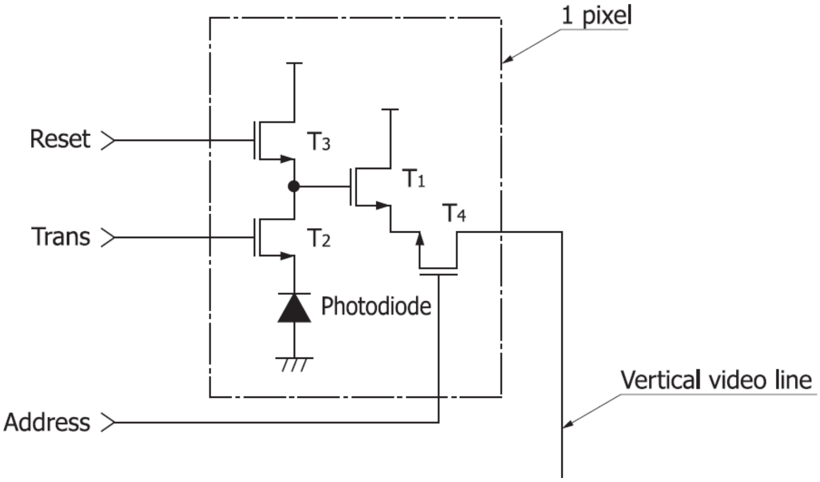

Figure 2.18 Active pixel sensor in CMOS image sensors.

On the other hand, some CCD devices present lower noise, since there is only one amplifier at the end of the process instead of having one amplifier for each pixel and, therefore, some systems can be used to reduce the noise of the signal. The fact of having different amplifiers or circuit for each pixel in CMOS image sensors produces a noise pattern in the picture since it is possible to have slightly differences with the response of each elemental unit. Besides, the light sensitivity is lower than for CCDs, due to the space occupied by the amplifiers and, consequently, more amplification is needed and more noise is produced. There are possible solutions for these problems but then the cost of the unit is then increased.

CMOS are widely used in consumer electronics, such as compact digital cameras, mobile phone cameras, handy-camcorders and digital lens reflex cameras, in automobiles, surveillance, robot vision or security (Ohta 2008). In the last decades, further applications of CMOS image sensors in biotechnology, communications and medicine have emerged, such as for optical ID tags (Yu *et al.* 2012), optical wireless communication (Ngo *et al.* 2012), fluorescence detection (Guo and Sonkusale 2012), etc.

The most common use of CMOS sensors in the last years is in mobile phone cameras, which are of special interest for this Ph.D. Thesis. More than 90% of the camera phones in the market today use CMOS image technology. Traditionally, CCD sensors were used since they produce better-looking images with less noise, but in a mobile phone the speed and the power consumption are important factors to take into account.

The main advantages of camera phones are cost and compactness. Of course, phone cameras are more limited that separate digital cameras: they have fixed focus lenses, little optical zoom and smaller sensors than produce less quality pictures and it is not possible to control all the parameters that are available in a usual camera. However, the main telephone companies, like Samsung®, Nokia®, Apple® or Toshiba®, are working on better designs for CMOS sensors, promising even 41 megapixels CMOS sensors. Even, some companies, like Apple® or Samsung®, are manufacturing accessories to add to the mobile phone camera trying to improve the capture of pictures: fish eye lenses, optical lenses with zoom, external tripod or ports to use with an external flash.

Due to this progress in built-in cameras in smartphones, they are being used in the latest years as analytical instrumentation. In this field, several studies have been carried out using a mobile phone as portable equipment for the detection and the analysis of samples, even in combination with chemical sensors. Determination of concentrations of urinary glucose and protein (Lee *et al.* 2011b), measurement of pH in test paper strips (Chang 2012), classification and analysis of liquid coloured samples (Iqbal and Eriksson 2013) or, simply, as portable chemical analyzer (Garcia *et al.* 2011) or rapid diagnosis test reader platform (Mudanyali *et al.* 2012) are some of the uses of smartphones.

2.4.4 Scanners

An optical scanner is a device which is used to turn documents or printed pictures into digital images that a computer is able to read. To determinate the quality of a scanner there are three parameters. Colour depth is the number of bits used for representing the information of each pixel to indicate the colour. Resolution, measured in pixels per inch (ppi), is the number of pixels present in an image. And, finally, density range that measures the capacity of a scanner to distinguish variations of shadows and brightness details inside the image. A higher value of colour depth implies a wider range of possible colours to be determined. Typical values of colour depth in scanners are 24 or 48 bits, which corresponds with 8 or 16 bits per channel, respectively.

There are several types of scanners: handheld scanners, flatbed scanners, sheetfed scanners, film scanners and drum scanners. In this Thesis, and only with analytical purposes, it has been used the flatbed scanner which consists of a flat glass surface where the document to scan is placed as it can be seen in Figure 2.19. Under the document there is a mobile element which contains the light source and the sensors, if it is a reflection scanner, or just the sensors, if it is a transmission scanner. In transmission mode the light source is placed over the document, using mirrors for that purpose. The light source sweeps the document while the sensors capture the reflected or transmitted light and convert into electrical signals the received intensities. Later, the signals are turned into digital information using and analog-to-digital converter. In fact, most of the scanners are composed of a CCD image sensor, previously explained, or contact image sensors (CIS). This last kind of sensors consists of a linear array of detectors covered with a lens and LEDs at red, green or blue wavelength acting as light source. They are placed in direct contact with the object to scan, providing a good quality image, which is lower than for CCD devices, but with lower power consumption.

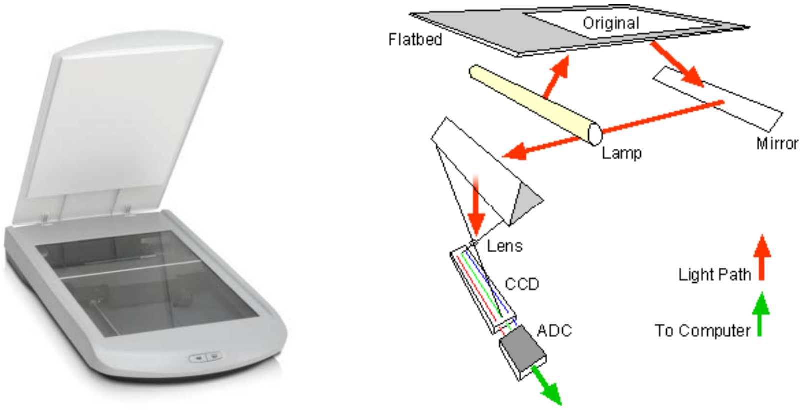

http://www.jiscdigitalmedia.ac.uk/guide/the-digital-still-image

Figure 2.19 Flatbed scanner.

The result of the scanning process is a decompressed RGB image that can be compressed in different formats. The commonest output formats are JPEG, TIFF, bitmaps or PNG:

- JPEG (Joint Photographic Experts Group): it is a method of lossy compression that allows to select the degree of compression with regarding to storage size and image quality. It is possible to reach 10:1 compression without perceptible loss in the image quality. The compression is made having into account to facts: the sensitivity of the human eye to changes in luminance or chrominance, being more sensitive to changes in brightness that in colour and the more sensitivity to changes in brightness in homogeneous areas than in areas with variations.

- TIFF (Tagged Image File Format): it is an adaptable file lossless format that allows to handle image and data within a single file. It includes header tags (size, definition, compression method, etc.) defining the image's geometry. It is allowed to use Lempel–Ziv–Welch (LZW) compression as an option to reduce the size of the file.
- Bitmap: it is a format where a picture is defined by its height and width (in pixels) and its colour depth (in bits per pixel) which represents the quality of the colour in the image. It saves the colour information of each pixel but on the other hand, it consumes more resources than other picture formats that use compression.
- PNG (Portable Network Graphics): it is a lossless format that supports palette-based images, grayscale images and full-color non palette based RGB[A] images. It does not require a patent license, unlike GIF (Graphics Interchange Format) which is called to be replaced with PNG.

The scanner is used in analytical sciences such as radiology (Schulze *et al.* 2002), soil sciences (Aydemir *et al.* 2004), biology (Davis *et al.* 2005) or food analysis (Hatcher *et al.* 2004), (Yam and Papadakis 2004). The most interesting way of use for this Ph.D. Thesis is the obtaining and processing of digital images by scanning colorimetric sensors, like pH sensors (Capel-Cuevas *et al.* 2010), iron and pH sensors (Abbaspour *et al.* 2006), or some other organic compounds (Zhang and Suslick 2005). The main objective is to extract the colour information from the picture by image-processing carried out with an external computer in order to relate it to the analyte of interest. In this Ph.D. Thesis, scanner has been used for comparison with the developed prototypes.

2.4.5 Spectroradiometers and spectrophotometers

These devices take measurement of the optical intensity with regard to the wavelength or the frequency. In particular, a spectroradiometer is an instrument designed to measure radiometric quantities as a function of the wavelength. It is an essential instrument for the measurement of spectral power distributions, chromaticity, colour rendering index and some other photometric quantities. The collected light passes through a monochromator to read it in narrow bands of wavelength. In practice, the measurement of a spectral radiometric quantity involves the comparison of the test source with a reference source of known spectral radiance (Wyszecki and Stiles 1982). There are two different types (Liu and Luo 2011): mechanical scanning type, which provides a high accuracy but with a long time of measurement, and array type which provides a faster response. Also they can be classified as basic type, with a low signal to noise ratio, low sensitivity and a narrow linear dynamic range, and high accuracy type that offers the opposite features. The output of a spectroradiometer can be expressed as spectral radiant power distribution, tristimulus values and chromaticity, correlated colour temperature or photometric quantities.

A spectrophotometer is an instrument that allows to measure the reflected colour of a sample or a surface as well as the amount of light that is absorbed by that sample. Therefore, it can take measurement of the wavelengths of the light that are absorbed, transmitted or reflected. In this case, the measurements are carried out in the visible region of the spectra, from 400 to 700 nm, although in the latter years there are spectrophotometers that can cover the range from 200 to 2500 nm. As it can be seen in Figure 2.20, the light emitted by the lamp is collected in a monochromator which separates the light in wavelengths in order to obtain the corresponding information for each one using for the purpose a photodetector, such a photodiode, a CCD image sensor or an array of photodiodes. There are two kinds of spectrophotometers: single beam or double beam. In the double beam spectrophotometer there are two different paths: one through a reference sample and the other with the sample to analyze. This offers a more stable measurement, but on the other hand the instrument is less compact than a single beam spectrophotometer. Some spectrophotometers can also measure luminescence by measuring the intensity of light emitted by a sample after optical excitation.

The light sources used depend on the requirements of the application, but there are spectrophotometers that use xenon (from 250 to 1000 nm), mercury, deuterium (ultraviolet), tungsten (Rossel and Webster 2011) or mercury lamps, x-ray tubes, or plasmas among others light sources. The required illuminant depends of the range of wavelengths that will be studied when a given surface or sample is illuminated. Also the required photodetector of the spectrophotometer is chosen according to the wavelengths of interest, as shown in Figure 2.21

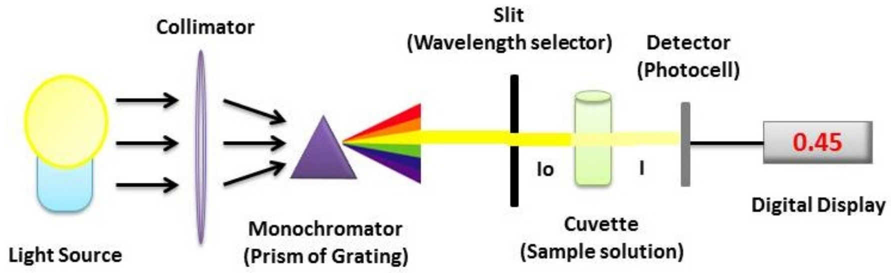

http://namratraheda.blogspot.com.es/2013/06/spectrophotometry-part-1.html

http://www.laserfocusworld.com/articles/

Figure 2.20 Single beam spectrophotometer.

.

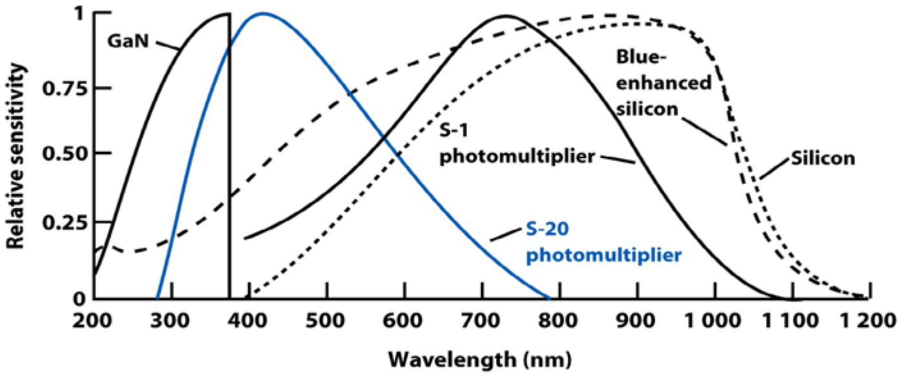

Figure 20-11
Quantitative Chemical Analysis, Seventh Edition
© 2007 W. H. Freeman and Company

Figure 2.21 Range of wavelengths for each kind of photodetector.

Both of them are used to calibrate LCD displays in laptops or televisions (Shepherd 1997), (Lopez-Alvarez *et al.* 2009). Also they are used in analytical sciences or for classification of samples since they provide spectral information that can be useful for identification of the analytes: for analysis of water properties (Wang and Gordon 1994), (Davies-Colley *et al.* 1997), for soil analysis (Campos *et al.* 2003) or for food analysis (Steinmetz *et al.* 1999), (Xiaobo *et al.* 2010) among other fields. In this Ph.D. Thesis, this instrumentation was used to obtain the colour information of soil samples in order to establish the models of transformation between different colour spaces in an experimental way instead of using the standard equations.

Chapter 3. **Digital colour sensors**

3.1 Introduction

Digital colour sensors are small devices that offer the possibility of colour detection by optimizing the resources needed by other kind of devices to measure colour. In this way, in the design of portable instrumentation for optical chemical sensors the use of digital colour sensors is an increasing field of interest. In this chapter, two different applications using digital colour sensors as detectors are presented: pH determination and measurement of the gaseous oxygen concentration. Specifically, the model of digital colour sensor used in these systems is the S9706 from Hamamatsu (Hamamatsu Photonics, Japan). This sensor allows the possibility of configuration for different parameters such as the integration time or the active area of sensing. For each application these parameters will be studied, taking into account their influence in the provided results.

Firstly, the development of a sensor array-based optical portable instrument for the measurement of pH is described. In this case, twelve digital colour sensors are used, facing each one a sensing element of the used optical colorimetric sensor array. Together with the detectors, an organic light-emitting diode (OLED) display is placed in the design acting as programmable light source for the system (Martinez-Olmos *et* *al.* 2011a). The colour information of each sensing element is provided by the detector in order to relate the hue (H) coordinate of the HSV colour space to the pH of a solution. Later, an optimization of the system is carried out, including an artificial neural network (ANN) to improve and optimize the processing algorithm, reducing computational cost, and therefore, the time of response of the system as well as reducing the uncertainty obtained with the previous algorithm.

Finally in this chapter, a radiofrequency identification (RFID) tag for determination of concentration of the gaseous oxygen is presented. Here, only one digital colour sensor S9706 is combined with an ultraviolet light-emitting diode (LED) which is used to excite the luminescence of platinum octaethylporphyrin (PtOEP) complex. The intensity of the luminescence emitted by the membrane is quantified colorimetrically using the R coordinate of the RGB space, provided by the detector, and related to the concentration of the gaseous oxygen. These components as well as the rest of the circuitry included in the design of the instrument are attached to a flexible substrate, which is suitable for smart packaging applications as explained below.

3.2 Portable instrument for pH determination

The measurement of pH is a routine analysis carried out daily in chemical laboratories. Until now, the potentiometric method has been mostly used due to its simplicity, reversibility and speed. But this method presents some drawbacks such as the electrical interference or the need of a reference electrode. Therefore, optical sensors for pH measurement may compensate some of these disadvantages (Capel-Cuevas *et al.* 2010).

In a general approach, optical pH sensors are based on reversible changes induced by pH in the structure of an acid-base indicator and translated into changes in spectroscopic phenomena such as absorption, reflectance, luminescence, energy transfer or colour (Chen *et al.* 2010), (Chu *et al.* 2012). However, there are other kind of optical sensors not based on acid-base indicators, such as that based on changes in the ionisation of unclad silica optic fibre by pH traced by methylene blue adsorption via evanescent field (Deboux *et al.* 1995), as well as those where the pH-dependent polymer suffers a change in the membrane turbidity (Shakhsher *et al.* 2004).

In this work, the first mentioned methodology is used based on membranes with acid-base indicators immobilized. It is important to realize that in acid-base indicators the change in the measured optical signal with pH results in a narrow sigmoidal shape dependence according to the Henderson-Hasselbalch equation. Thus, the dynamic working range for pH optical sensors is limited to a few pH units (2-3) (Heng *et al.* 2003) and even shorter if the linear relationship in the middle of the sigmoidal response is used. This short range is one of the main drawbacks of these optical sensors for pH, along with their non-linear response, which requires different sensing membranes to cover the whole pH range.

The simultaneous analysis of complex samples is one of the most complex challenges that can occur in Analytical Chemistry. Of the several approaches used to multianalyte systems, sensors are one of the most promising, typically through the use of array of sensors. This array technology allows the simultaneous analysis of several analytes in a single experiment. Moreover, the use of a number of distributed selective chemical sensors provides also better spatial resolution (Gopel 1998), (Rakow and Suslick 2000), (Janzen *et al.* 2006).

There are two kind of array based on the number of analytes present in the sample. Microarray technology permits up to thousand of analytes being analyzed, such as array-based gene expression analysis or protein microarrays based on antigen-antibody or ligand-receptor reactions (Roda *et al.* 2005), or microarrays that combine multi-spot immunochip technology and immunochromatography, for example for determination of drugs of abuse in urine (Taranova *et al.* 2013). On the other hand, macroarrays are used for the analysis of a small number of analytes but, due to the higher size, they can be analyzed by means of different types of imaging devices. Examples of positional two-dimensional arrays based in colour measurement include the device described for iron and full-range pH determination by immobilizing reagents on cellulosic paper and determination of RGB coordinates (Abbaspour *et al.* 2006), (Safavi *et al.* 2007); an electrochemiluminescent enzymatic biosensor screen-printed array for L-lactate and D-glucose (Corgier *et al.* 2005); and, a complementary DNA macroarray for detection of twelve potato viruses using chemiluminescence or colorimetric detection (Maoka *et al.* 2010). Some examples of encoded bead macroarrays can be found in the literature, such an optical imaging fibre for pH, O_2 and CO_2 solutions (Steemers and Walt 1999).

However, this approach where specific reagents are used offers disadvantages such as obtaining good selectivity against similar analytes or the proportional increasing of the number of sensor with the number of analytes. Because of this, an alternative paradigm based on general or differential receptors have emerged (Lavigne and Anslyn 2001): an array of non-specific or low selective sensors, called electronic tongues (for samples in solution) and noses (for gaseous samples) and that produces analytical signals, allows the analysis of multi-component samples. Using this approach different experimental works have been carried out such as reagents in microplate wells image by means of a CCD camera based on quenching fluorescence (Baldini *et al.* 2004); arrays of colorimetric membranes placed on hydrophobic silica base whose colour is studied using a scanner (Zhang and Suslick 2005), (Zhang and Suslick 2007); colorimetric optical sensor arrays were the indicators are placed in a nanoporous sol-gel matrix and analyzed with a scanner (Lim *et al.* 2008); and printed sensor arrays in PET film using also a scanner to determine the colour variation (Suslick *et al.* 2010).

For the pH measurement, it is common to work with an array that contains complementary pH indicators in order to cover the whole range of interest from 0 to 14. These indicators provide information that can be extracted by means of imaging techniques. In this way, commercial multi-colour pH paper strips have been measured with a conventional scanner (Abbaspour *et al.* 2006), (Lapresta-Fernandez and Capitan-Vallvey 2011) and pH membranes in a triacetylcellulose support have been analyzed with a CCD colour camera (Safavi *et al.* 2007). As it can be seen in the literature, most of the analysis of colorimetric optical sensor arrays have been carried out using scanners or CCD cameras.

Here, a portable instrument that makes possible the determination of pH by means of a disposable colorimetric sensor array and digital colour sensors has been developed. In a first approach, eleven membranes were used in order to cover the whole range of pH, but, after an optimization process, just four of them were enough. The acquisition of colour information is carried out using a programmable light source and a set of colour detectors that provide the RGB coordinates from each analyte in digital format. This information is used to calculate the hue parameter of the HSV colour space, which is used as analytical parameter to be related to the pH.

3.2.1 Reagents, instrumentation and software

The chemicals used to prepare the pH sensitive films were potassium tetrakis(4-chlorophenyl)borate (TCPB, CAS Nº 14680-77-4), tridodecylmethylammonium chloride (TDMAC, CAS Nº 7173-54-8), aliquat 336 (CAS Nº 5137-55-3), o-nitrophenyloctylether (NPOE, CAS Nº 37682-29-4), dioctyl sebacate (DOS, CAS Nº 122-62-3), bis(1-butylpentyl)adipate (BBPA, CAS Nº 77916-77-9), tributyl phosphate (TBP, CAS Nº 126-73-8), high molecular weight polyvinyl chloride (PVC, CAS Nº 9002-86-2), cellulose acetate (CA, CAS Nº 9004-35-7), ethylenglycol (EG, CAS Nº 107-21-1) and tetrahydrofuran (THF, CAS Nº 109-99-9) all purchased from Sigma (Sigma-Aldrich Química S.A., Madrid, Spain). Bromothymol blue (CAS Nº 76-59-5), phenol red (CAS Nº 143-74-8), thymol blue (CAS Nº 76-61-9), m-cresol purple (CAS Nº 2303-01-7) and PAN (CAS Nº 85-85-8) from Sigma, liphophilized Nile blue (CAS Nº 125829-24-5) and purpurin (CAS Nº 81-54-9) from Fluka (Fluka, Madrid, Spain), cresol red (CAS Nº 1733-12-6) from Panreac (Panreac, Barcelona, Spain), alizarine (CAS Nº 72-48-0) from TCI (TCI Europe, Belgium), and sicomet red P (CAS Nº 5281-04-9) from BASF (BASF, Ludwigshafen, Germany) were used as acid-base indicators. As support sheets, Mylar-type polyester (Goodfellow, Cambridge, UK) was used. The HCl and NaOH used were supplied by Sigma. All reagents were of analytical reagent grade and were used without any further purification. All aqueous solutions were prepared in reverse-osmosis type quality water (Milli-RO 12 plus Milli-Q station from Millipore, conductivity 18.2 mS).

For the optical characterization, the spectra for the different light sources were measured using a mini-spectrometer RC series C11007MA (Hamamatsu Photonics, Japan) with 256 pixels, spectral resolution at 9 nm half width and 16 bits of intensity resolution.

For the electrical characterization of the prototype, the following instrumentation was used: a mixed signal oscilloscope (MSO4101, Tektronix, USA), a 6½ digit multimeter (34410A, Agilent Technologies, USA), a 15 MHz waveform generator (33120A, Agilent Technologies, USA) and a DC power supply (E3630A, Agilent Technologies, USA). In the image acquisition and digitalization process in order to compare with the instrument developed, a commercial scanner ScanMaker i900 (Microtek, Taiwan) was used, with a 6400 x 3200 dpi resolution, a maximum optical density of 4.2 and 24 to 48 bits of colour. The software to manage the scanner was Silver Fast Ai provided by Microteck. The images were processed with a set of scripts and functions developed by us in Matlab r2007b (The MathWorks, Inc, Natick, MA, USA). Statistical calculations were performed with the Statgraphics software package (Manugistics Inc. and Statistical Graphics Corporation, USA, 1992), and Microsoft Excel (Microsoft Corp., Redmond, WA, USA) was used for general calculations. A Crison pH-meter (Crison Instruments, Barcelona, Spain, model Basic 20) with a combined double junction glass electrode, calibrated against two standard buffer solutions (pH 4.0 and 7.0), was used for the pH measurements. For the implementation on a computer of a configurable user interface designed only with calibration purposes, Microsoft Visual Basic 6.0 (Microsoft Corp., Redmond, WA, USA) was used.

3.2.2 Sensor array preparation

For the preparation of the sensor array a section of 5 cm × 4 cm of transparent Mylar polyester is required. The main advantage of this material is the high transparency that offers between thicknesses from 12 to 23 µm avoiding the change of wavelength of the light that goes through it. Moreover, it is highly resistant to the interaction with different chemical reagents, which makes possible the deposition of cocktails in the surface without reactions between them. Therefore, it is a common support used in colorimetric applications.

This support was covered with an adhesive black film of PVC with 12 holes (3 columns and 4 rows), 5 mm of diameter each, in order to reduce the light dispersion and prevent the cross of information between the different sensing elements, as shown in Figure 3.1.

In each hole, 8µL of the corresponding cocktail were cast and after quick evaporation the sensing membrane was prepared. The cocktails for the pH membranes were prepared by dissolving the different chemicals needed in 1 mL of distilled THF according to the composition presented in Table 3.1. As it can be seen, the sensing elements contain different types and amounts of colorimetric acid-base indicators to determinate the colour intensity; membrane polymers, plasticizers and lipophilic salts to minimize the leaching; and, if necessary, humectants added to the previous mentioned reagents in order to determine the response time of the reaction. By blending these reagents, three conditions were reached in the obtained membranes: no leaching, change of a colour coordinate in the reaction and full covering of the pH range by overlapping the different responses of each membrane.

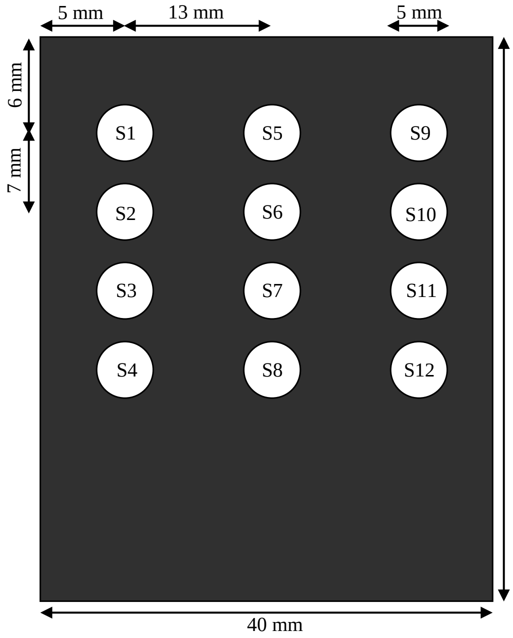

Figure 3.1 Sensor array design.

As a result, eleven different membranes, containing ten different pH indicators, were prepared to cover the whole pH range. Besides, one of the positions was kept empty to test the light source in the instrument.

Table 3.1 Membranes composition (%w/w) for the pH sensor array.

Membrane	Indicator (%)	Lipophilic salt (%)	Plasticizer (%)	Membrane polymer (%)	Humectant (%)
S1	Sicomet red P (1.41)	Aliquat 336 (5.63)	NPOE (66.20)	PVC (26.76)	--
S2	m-Cresol purple (3.00)	TDMAC (13.47)	DOS (28.00)	CA (33.00)	EG (22.57)
S3	PAN (1.43)	TDMAC (10.00)	NPOE (65.00)	PVC (23.60)	--
S5	Purpurin (1.43)	TDMAC (8.29)	NPOE (67.00)	PVC (23.29)	--
S6	Cresol red (1.43)	Aliquat 336 (4.54)	NPOE (67.00)	PVC (27.00)	--
S7	Liphophilized Nile blue (1.43)	TCPB (3.63)	TBP (67.00)	PVC (27.91)	--
S8	Bromothymol blue (3.00)	TDMAC (4.00)	DOS (28.00)	CA (37.00)	EG (19.60)
S9	Alizarin (1.43)	TDMAC (10.29)	NPOE (67.00)	PVC (21.3)	--
S10	Thymol blue (3.14)	TDMAC (11.57)	DOS (28.00)	CA (37.00)	EG (20.43)
S11	Phenol red (1.43)	TDMAC (6.93)	BBPA (26.00)	CA (30.00)	EG (35.64)
S12	Thymol blue (5.00)	TDMAC (18.40)	DOS (28.00)	CA (33.00)	EG (15.60)

Once the measurement of pH is obtained using one sensor array in the way later explained, the macroarray can be discarded. The main advantage of the use of disposable sensors is that there is no need of preservation conditions in order to avoid the damage of the sensors, what simplify the process of the use of the instrument. Furthermore, disposable sensors are inexpensive, easy-to-use and well known in the literature (Feng *et al.* 2010), (Carey *et al.* 2011), (Lapresta-Fernandez and Capitan-Vallvey 2011).

3.2.3 Description of the instrument

In Figure 3.2 a block diagram of the developed instrument is shown. As it can be seen, it is a microcontroller-based system designed to measure the colour of the membranes in the pH sensor array previously described. For that purpose, a programmable light source is included in the design and used to transmit the light through the sensing membranes. The colour information obtained as result of the processes of absorption and reflection in the optical sensor array is collected using an array of digital colour detectors.

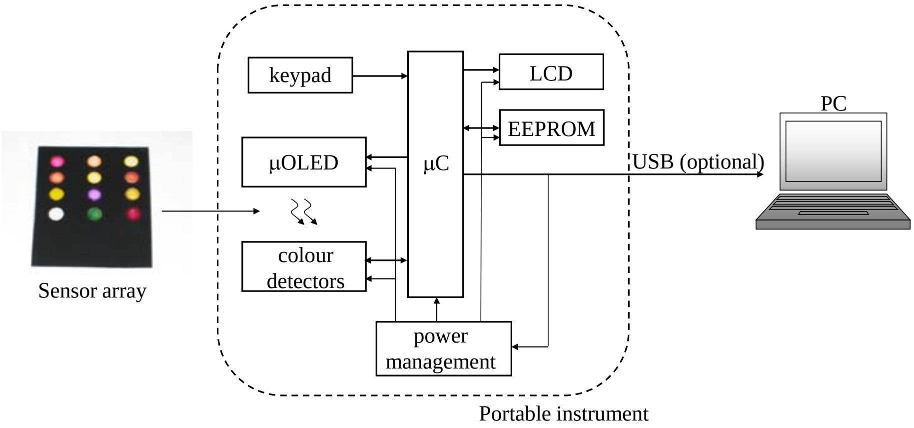

Figure 3.2 Scheme of the instrument.

The microcontroller used was model PIC18F4550 (Microchip Technology Inc., USA) and it was selected because of the integration of a USB module that allows ease of communication with an external device, such as a computer, for design and calibration purposes. Also, five input-output ports are available in this model to control all the others modules presented in the instrument, such as the USART port for communication with an OLED display. Also, the microcontroller has 24 KB of flash memory and 2 KB of SRAM. The user interface of the portable instrument consists of a keypad which lets the user select different measurement modes through a menu that is shown in a liquid crystal display (LCD) screen. This screen also shows the results obtained from the measurement process, although they can be also stored in an EEPROM memory for further processing. Also, in order to design a portable instrument, a PP3 battery was included in the final prototype, which is enough to supply the whole system. In addition, the system can be power supplied through a connection to an external computer with a USB port.

The main module of the design is the colour measuring module. In most of the colorimetric instruments based on reflection or absorption of light, one or several LEDs are used as light source (O'Toole and Diamond 2008), (Palma *et al.* 2008), (Supharoek *et al.* 2012). In this work the use of 12 different LEDs for the illumination of the sensing elements of the optical array is not an optimal solution, not only for the required area but also because of the differences of intensity of the emitted light between them as well as for the possible deviations in the alignment. Therefore, here an OLED display is used to cover the full optical sensor array. In this way, the colour measuring module consists of an OLED display, which works as a programmable light source, and twelve digital colour detectors aligned with the sensor array. For the OLED display the selected model was 160-GMD1 (4DSystems, Penrith, Australia) that makes possible a direct communication with the microcontroller via two-wire serial bus. This is a compact, cost-effective OLED display with an embedded graphics controller that allows to control the alignment with each one of the detectors and the configuration of the light source by software, which is advantageous against the use of a LED. On the other hand, the irradiance of the OLED display is lower than the generated with a LED but it is still intense enough for this purpose. The embedded commands permit to configure the background colour as well as the intensity of the light in the screen and draw shapes in 65K different colours. The main features for the OLED screen are: 160×128 pixel resolution, 1.69” diagonal with an active are of 33.6 mm ×26.9 mm, 5 pin interface to any host device, voltage supply from 3.6 V to 6.0 V and 40 mA nominal current when using a 5.0 V supply source, serial RS-323, possibility of micro-SD (µSD) memory card in order to storage illumination patterns and graphic commands.

The model of the colour detectors used is the S9706 from Hamamatsu as mentioned earlier. This digital colour sensor consists of a set of photodiodes sensitive to three different regions of the spectrum: red (• = 615 nm), green (• = 540 nm) and blue (• = 465 nm), which makes possible the simultaneous measurement of the RGB coordinates of the received light. The induced current of these photodiodes is on-chip processed to generate the colour information which is presented as a 12-bit serial output for each component. Therefore, the result of the three measurements is a 36-bit word that can be directly processed by the microcontroller without further processing. Since the output of each detector is connected to a different input port of the microcontroller, simultaneous measurement of all the membranes could be carried out providing a fast response of the instrument. However, in order to avoid the stray light interference between them, the measurement was carried out sequentially as explained below.

The colour determination of the pH membranes was made by measuring the transmitted light as follow: the sensor array was aligned in the path between the programmable OLED display and the colour detectors in order to receive the light that came from the light source and transmit the wavelengths that are not absorbed. To avoid the influence of other external lights, the instrument was enclosed in a black box with only a small opening at the bottom to insert the sensor array, as shown in Figure 3.3.

Figure 3.3 Photograph of the developed prototype during the measurement process.

When the sensor array is placed correctly in the instrument each digital colour detector is facing one of the membranes of the sensor. The illumination pattern of the OLED display consists of a black background where, sequentially, a white circle appeared aligned with each one of the element of the sensor array and the corresponding detector. Every circle acts as light source during the corresponding integration time, in order to measure the RGB coordinates of each one of the membranes by integrating the incident light. The size and the centre position of the circles can be configured by software, which allows to obtain the correct alignment of the three component needed on the measurement process. In Figure 3.4 it is shown the described structure.

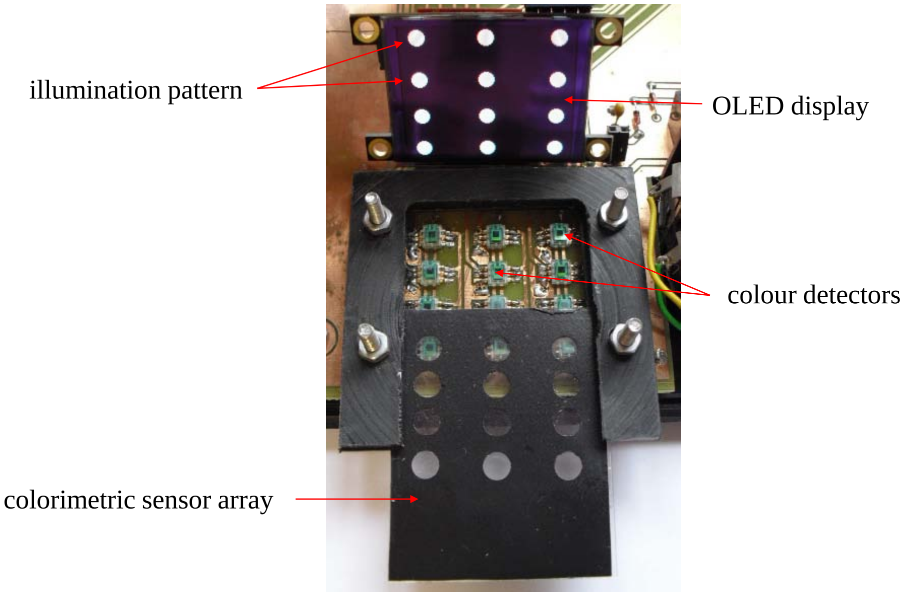

Figure 3.4 Sensing module: OLED display with white circles as illuminants, sensor array support and digital colour detectors.

The response of the completed system was evaluated for each 0.1-0.2 pH unit from 2 to 14 by adding volumes of 1.0M, 0.1; or 0.01M of

HCl or NaOH using a microburette to an aqueous solution. After each addition and magnetic stirring, the sensor array must be placed inside the solution during 5 minutes to equilibrate the reaction, and then, after drying carefully, was introduced into the instrument in order to be measured. The corresponding determined pH is shown in the LCD screen as can be shown in Figure 3.3. The pH of the solution was also measured using a potentiometric procedure in order to compare the response provided for both systems.

3.2.4 Results

In this section the results of the characterization and optimization of the system are presented. In order to have a fully characterization of the instrument, the optimal configuration of the programmable light source and digital colour sensors, the minimum number of sensing elements needed for univocal pH determination and others measurement conditions of the whole system were studied. To carry out this procedure, a user interface was designed using Visual Basic 6.0. As it can be observed in Figure 3.5, the interface allowed to change parameters of the OLED display, such as the brightness or the colour of the illuminant, as well as the integration time of the digital colour sensors. The influence of these parameters in the measured RGB coordinates and, therefore, the hue coordinates will be explained below. The programme provides an output file with all the measurements for further processing during the calibration process.

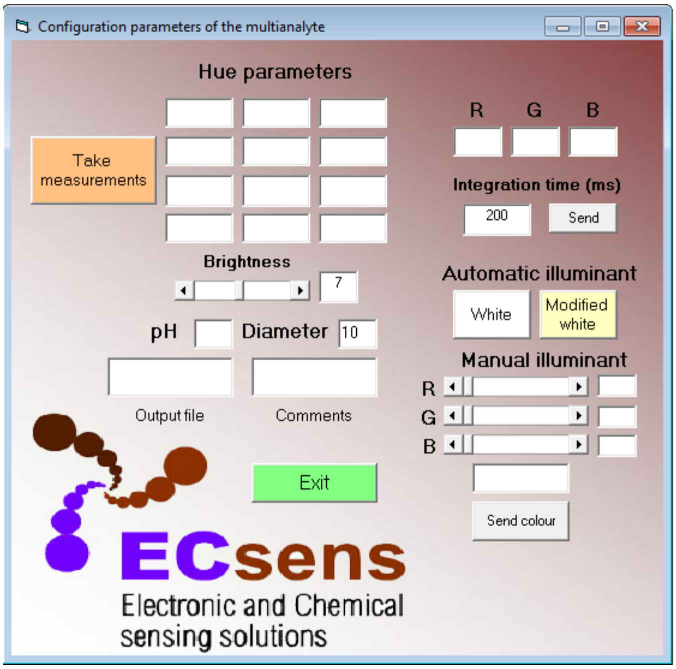

Integration time (ms) 200

Brightness 7

Diameter 10

Figure 3.5 Configurable user interface in the PC that makes possible to test different parameters of the instrument.

Finally, in this section, a comparison with a laboratory colorimetric system and a discussion of its use as pH-meter was included. With this purpose, calibration and validation of the system were carried out and, finally, the instrument was applied to real samples.

Digital colour detectors

In order to cover a wide photometric range, two parameter of the sensor can be selected. Firstly, the active area of the sensor can be configured in two modes: low sensitivity (3×3 elements) or high sensitivity (9×9 elements). The active area consists of 9×9 photodiodes in total, alternating red, green and blue sensitivity in a mosaic. In this case, instead of using the 3×3 centre area, which corresponds to low sensitivity, the full area was selected to collect the maximum incident light from the sensing elements of the sensor array. Furthermore, with a higher area, the influence of possible non homogeneities in the membranes over the measured value is reduced.

The second parameter that can be configured is the integration time. This parameter determines the period of time in which the incident light is integrated to determine the RGB coordinates, that is, the time interval in which the photodiode matrix generates a photocurrent for each optical radiation acquisition. The integration time has a possible range of configuration from 10 µs to 100 s that can be changed using a unique input pin: setting the gate pin to high the integration time started, and switching to low level the integration stopped. According to the device datasheet, under constant illumination conditions, the sensor output increases linearly with this time until reaching output saturation. Therefore, long time of acquisition means that the response is slower and the output could saturate, whereas short time of integration supposes a faster response but noisy and low intensity light collection, i.e., low sensitivity. In this point, a trade-off has to be made with this configuration parameter. In this system, 200 ms was tested as a time that provides fast response without compromising of the sensitivity. Moreover, the results show that there is no change in the H value from 150 to 500 ms (RSD • 0.8%).

Finally, the stability of the colour detector was checked, using with that purpose a white LED (NSPW300, Nichia, Japan), biased with a thermal stabilized current source, an emitting constant light over the detector. The results showed a good stability since the signal drift was lower than 0.1% in 90 min of measurements every 0.2 s.

OLED display

With respect to the OLED display, it is well known that in colorimetric applications the use of a standard illuminant is recommended. One of the most used illuminants is sunlight, defined as D65 illuminant (Wyszecki and Stiles 1982). In this case, the OLED display used as light source allows to define up to 65.536 colours in each one of the pixels of the screen by combining red and blue components, with values from 0 to 31 (5 bits), and green component, from 0 to 63 (6 bits). With the code (31, 63, 31) the screen displays its white colour, whose spectrum is shown in Figure 3.6. As it can be seen, there is an excess of the blue component in this white colour due to the internal configuration of the screen. In order to obtain an illuminant closer to the standard D65, an optimization process was carried out to reduce the blue component by modifying the three values of the components to (30, 63, 19) for red, green and blue respectively. In Figure 3.6 it is shown the spectrum obtained for the "modified white" and the D65 illuminant spectrum for comparison. Although all the depicted illuminants were tested as light source, best results were obtained using the modified white and therefore, it was used as light source during the measurement process. The main differences between both spectra are found below the 450 nm and over the 550 nm region, so lower transmittance levels will be induced in comparison with systems that use D65 illuminant.

The OLED display allows the configuration of the intensity of the emitted light. There are sixteen available levels from 0 (completely darkness) to 15 (maximum brightness). The influence of this parameter was studied, providing better results for the sensing element array in the 5-8 range, since for higher values the hue value obtained is identical to the hue value of the illuminant, that is 0.6, and for lower values the emitted light was not enough to provide response in the detector. For a given colour, measuring the RGB coordinates during ten minutes with intervals of five seconds, the relative standard deviation (RSD) in the resultant H value using the level 7 of intensity was of 2.5%. Since this is an acceptable deviation, the level 7 of intensity was the selected value.

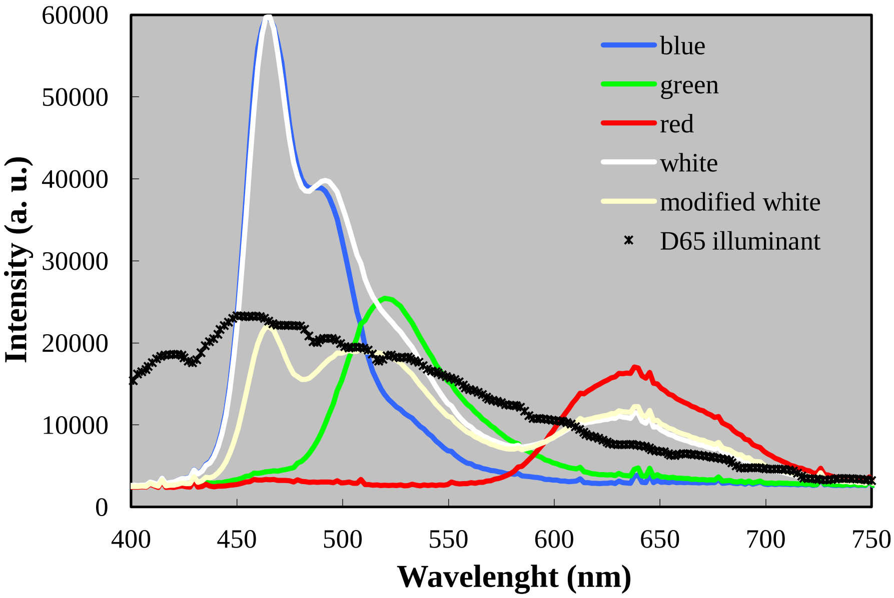

Figure 3.6 Spectra of the OLED screen and D65 standard illuminant.

After the study of the OLED display parameters, the light uniformity of the display was analyzed by sensing the emitted light with a digital colour sensor placed facing the display in different positions. This study shows that there is no variation of the captured light in the whole area of the display, generating the detector always the same output signal. Besides, the stability of the display and the velocity of the response were tested measuring the light emitted when the display is switched on and off alternately. To carry out this, the display background was changed from black to modified white in cycles, as depicted in Figure 3.7. It can be deduced from this graphic that the light emission is fast enough to avoid the need of time delays to carry out the measurements once the equipment is switched on. The RSD of the H value is 0.6% that shows that the light emitted by the display is very stable and repetitive.

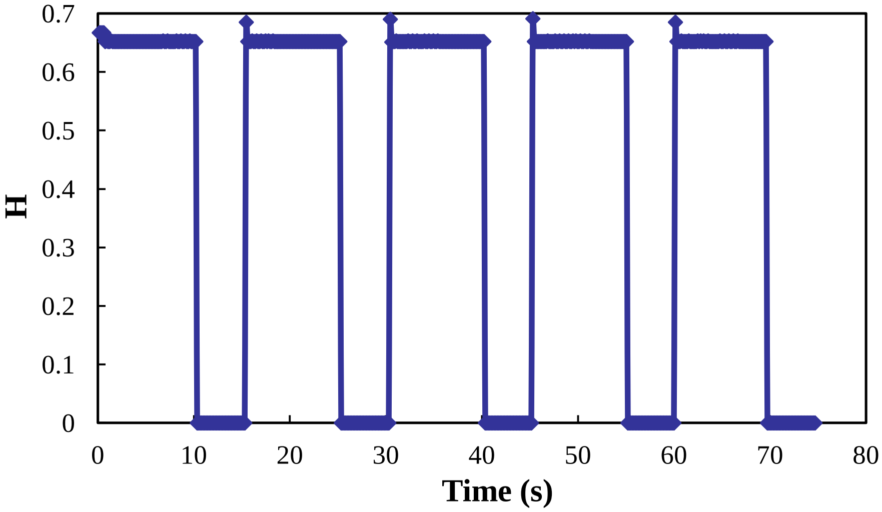

Figure 3.7 Study of stability and velocity of response of the display from black background to white modified background.

The last parameter to take into account in relation to the light source is the diameter of the circles that act as illuminant for each one of the membranes in the sensor array. Twelve circles were depicted on the display aligned with the corresponding membrane and digital colour sensor. Since the diameter of the sensing elements is 5 mm, values of diameter from 5 to 12 mm were studied in order to cover the whole area of the membrane. It has been demonstrated that there is not significant variation in the output signal and the corresponding H value with this parameter between 5.75 and 10.25 mm (less than 5% RSD). Taking this into account, the diameter of the circles was fixed to 6.35 mm for this study.

pH measurement

The process followed to measure the pH based on the colour changes of the membranes is described in this section. First, the response of each sensing element of the sensor array is obtained with the instrument. After that, a minimization of the number of elements needed to cover the full range of pH is carried out, in order to reduce the computational cost, and, therefore, increasing the velocity of response of the instrument.

The characterization of each sensing element was performed by measuring the H component for each one of them in the whole range of pH using twelve replicate arrays. For the purpose of this calibration, acid (HCl) or basic (NaOH) solutions were added to an aqueous solution. Once the solution is stabilized in a pH value, the sensor array was immersed during five minutes in order to let the reaction in the membranes completely occur (Capel-Cuevas *et al.* 2010). Figure 3.8 depicts the sigmoid responses and as it can be seen, in some cases, the sigmoid signal is double. From Figure 3.8, and also from the column of pH range shown in Table 3.2, it can be deduced that using the eleven membranes the whole range of pH, from 0 to 14, is covered. The colours of the membranes and, therefore, the hue components have a variation that allows to determine the pH in the complete interval.

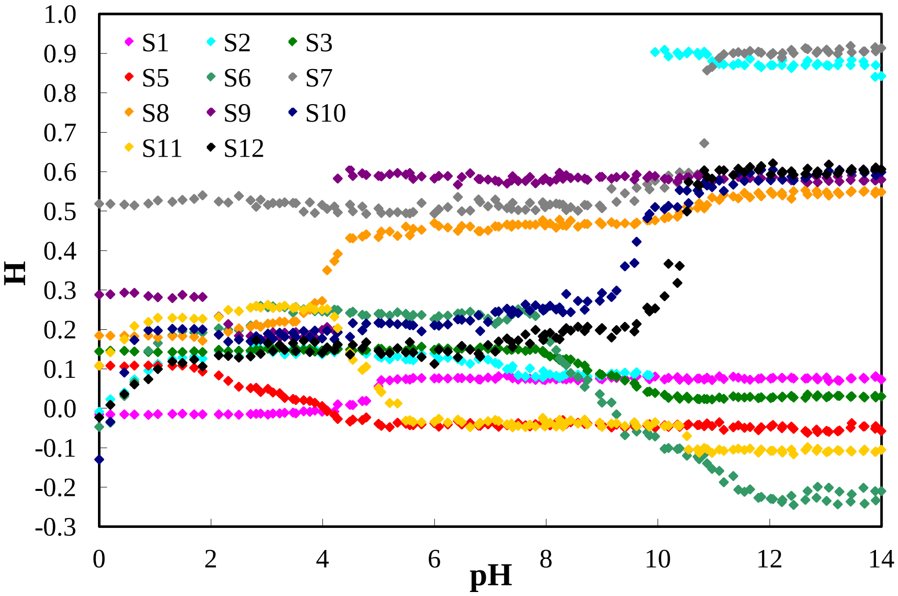

Figure 3.8 Sensor array response: relation between the H value of each membrane and the pH of a solution.

The immobilized acid-base indicators belong to neutral (HI), cationic (HI+) or anionic (HI-) types, and the reaction with acid or base in the membrane phase involves different mechanisms characterized by an equilibrium constant Ke. In case of cationic by ion-exchange mechanism between protons and alkaline ions X+ the reaction follows the Equation 3.1, where bars indicate species in the membrane phase and R- the lipophilic salt present. In the case of neutral on anionic species, both monobasic and dibasic, occurs by coextraction mechanisms (Equations 3.2 and 3.3).

$$X^+ + \overline{HI^+} + R^- \overset{K_e}{\leftrightarrow} \bar{I} + H^+ + \overline{XR} \tag{3.1}$$

$$\overline{HI} + \overline{XR} \overset{K_e}{\leftrightarrow} \overline{IR} + X^- + H^+ \tag{3.2}$$

$$\overline{HIR} + \overline{XR} \overset{K_e}{\leftrightarrow} \overline{IR_2} + X^- + H^+ \tag{3.3}$$

The proton activity in aqueous phase is related to the equilibrium constant K_e through a sigmoidal response function that includes the degree of protonation, and the analytical concentrations of indicator C_I and lipophilic salt C_R, respectively. In Table 3.2 the K_e values for each membrane using two different measurement systems are shown. As it can be observed from the K_e obtained with the portable instrument and those calculated from the scanner, there are some differences, even higher than one order of magnitude for purpurin, bromothymol blue and phenol red. In this case, these divergences can be justified since the illuminant and photodetectors used in both devices are different, and therefore, the emitted and captured lights are not the same.

Table 3.2 K_e values for each sensing element calculated from the scanner and the portable instrument for comparison.

Membrane	**Indicator**	**pH range**	**Scanner K_e**	**Portable instrument K_e**
S1	Sicomet red P	5.18-6.60	7.1×10^{-5}	2.7×10^{-5}
S2	m-Cresol purple	0-1.90	4.9×10^{0}	1.4×10^{0}
		8.65-10.77	2.8×10^{-9}	3.2×10^{-9}
S3	PAN	7.57-10.95	3.4×10^{-9}	4.3×10^{-9}
S5	Purpurin	1.90-4.56	2.0×10^{-3}	7.0×10^{-3}
		12.44-13.81	9.4×10^{-7}	2.9×10^{-8}
S6	Cresol red	7.35-13.19	4.3×10^{-9}	4.5×10^{-9}
S7	Liphophilized Nile blue	9.46-11.99	1.3×10^{-10}	3.2×10^{-10}
S8	Bromothymol blue	2.82-7.15	7.1×10^{-6}	2.5×10^{-4}
S9	Alizarin	4.56-6.35	2.2×10^{-5}	2.0×10^{-4}
S10	Thymol blue	0-0.85	3.7×10^{0}	5.5×10^{0}
		8.87-10.36	1.3×10^{-8}	4.4×10^{-9}
S11	Phenol red	5.37-6.80	1.2×10^{-8}	4.4×10^{-6}
		9.46-11.40	--	3.3×10^{-10}
S12	Thymol blue	0-1.42	1.5×10^{0}	1.8×10^{0}
		9.04-11.56	3.7×10^{-9}	8.2×10^{-10}

To compare clearly the responses of the two instruments, portable and scanner, Figure 3.9 depicts the curves for two of the membranes (S2 and S12). Despite the different ways in which the responses have been obtained, the curves are very similar. In the case of the scanner, the response was obtained by acquiring a digital image and processing the result in an external computer to calculate the corresponding H value (Cantrell *et al.* 2010). Nevertheless, the curve produced by the portable system here presented was obtained by processing of the colour detector output directly in the microcontroller with no need of external instruments, simplifying the procedure of pH measurement and providing a faster response. As mentioned before, the minor differences are caused for the discrepancies between illuminants and detectors.

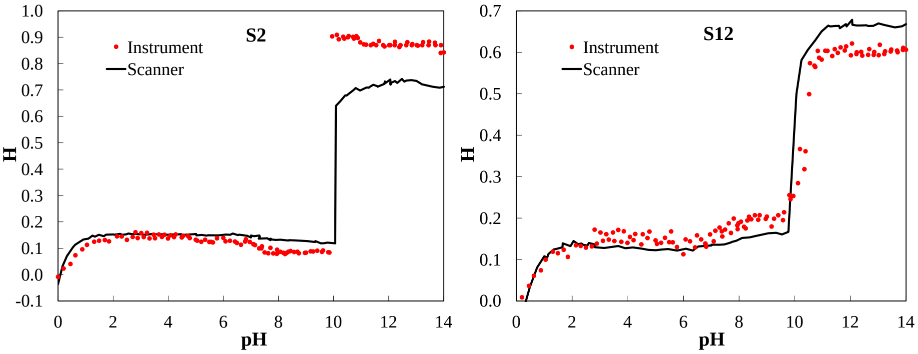

Figure 3.9 Response of two membranes (S2 and S12) measured with a commercial scanner and the portable instrument.

From Table 3.2 it can be deduced that the final number of sensing elements can be reduced, since most of them cover the same range of pH and, in consequence, there is redundant information. With the purpose of reducing the computational cost of the portable instrument, a minimization of the required membranes was done. The criteria followed for the minimization process were to select membranes with the maximum H variation to cover the maximum range of pH. Overlapping in the membranes responses should be avoided. As a result, the sensing elements selected were: S2 that covers the pH range 0-1.90 and 8.65-10.77, S5 covering 1.90-4-56 and 12.44-13.86, S6 that covers 7.35-13.19 and, finally, S8 for the range 2.82-7.15.

Once the minimum number of membranes of the sensor array was determined, a response modelling was done in order to find the relation between the H component and the pH. As it can be seen in Figure 3.10, there is no univocal pH determination since for a measured value of the hue component more than one value of pH can be obtained. To solve this, an algorithm that evaluates the response of the four selected sensing elements is proposed. This procedure involved two steps. Firstly, all the possible ranges of pH for a given value of the H component are calculated for each sensing element. In order to get those values, the response of each membrane was modelled using increasing or decreasing linear sections as the shown in Figure 3.10 for two of them (S5 and S6). As it can be seen, for a value of H there are two possible values using S6 response, and four values using S5. In this way, the microcontroller provides a list of possible ranges of pH for each one of the four sensing elements. The second step consists of the comparison of the ranges detected for each membrane, in such a way that the only range in common for all of them was the correct range of pH to have into account, as shown in Figure 3.10.

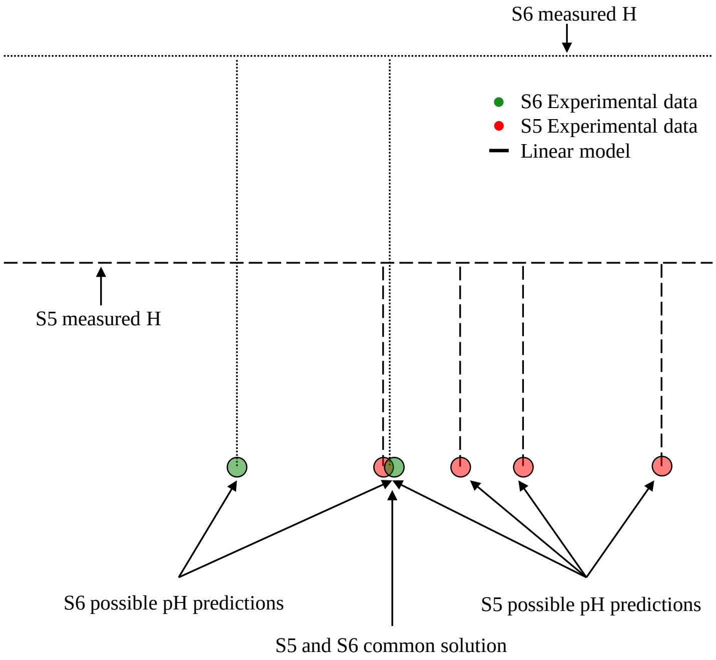

Figure 3.10 Lineal modelling for S5 and S6 sensing elements. No univocal response is observed since one H value can produced several pH values.

Since the linear fitting is not accurate enough to provide a correct value of pH, the determined range of pH is used to obtain a more precise value of pH. With this purpose a more accurate model of the corresponding sensing element response is used. A trade-off between the curves fitting and the complexity of the equations to be processed by the microcontroller was made and cubic polynomial functions were selected, as depicted in Figure 3.11. These equations are simple enough for the microcontroller which is able to calculate the pH in a short time after the colour measurements. The accurate modelling of these responses was made using a function as the shown in Equation 3.4.

$$H(pH) = A + B \cdot pH + C \cdot pH^2 + D \cdot pH^3 \qquad (3.4)$$

The coefficients obtained for the fit functions, as well as the range of pH where the equation was defined, are listed in Table 3.3. As shown, the membrane placed in S5 can cover two different ranges of pH. Finally, the pH calculation corresponding to a measured value of the H coordinate was obtained by solving the third degree equation for a particular membrane in the range of pH previously estimated.

Table 3.3 Coefficients for the cubic modelling and pH range.

Membrane	pH range	A	B	C	D	R^2
S2	0-1.90	-0.006	0.200	-0.109	0.024	0.973
S5	1.90-4.56	0.566	-0.416	0.113	-0.011	0.991
S8	2.82-7.15	0.794	-0.483	0.121	-0.008	0.991
S6	7.35-13.19	2.582	-0.459	0.020	-0.0002	0.988
S5	12.44-13.86	17.047	-3.480	0.288	-0.007	0.966

In order to prove the reliability of the reconstruction algorithm previously described, a set of 102 validation data, with 12 replicas, was prepared covering the full range of pH. The correlation coefficient R^2 was calculated obtaining a value of 0.994 and the mean squared error (MSE) has a value of 0.167. Hence, it was possible to assume that the prediction model provide a suitable performance for pH measurement. This fact can be observed in Figure 3.12a, where the pH predictions fit the original pH values in the whole range of pH, although the accuracy decreases in the range (13-14) due to the lower variation of the membrane in that region.

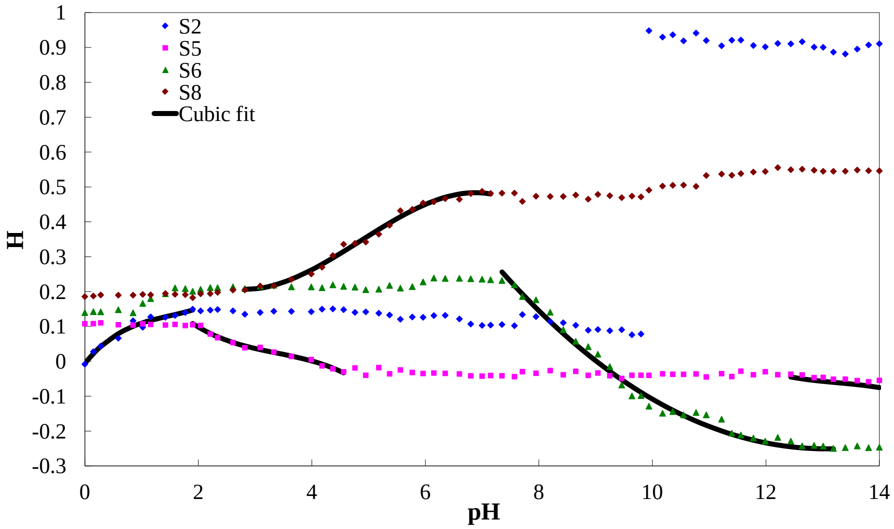

Figure 3.11 Response modelling for four membranes using cubic polynomial functions.

Eventually, the proposed measurement system was applied to 14 real water samples which consist of tap and river water from Granada (Spain) whose pH was adjusted using acid or base to cover the whole range of pH. 6 replicas were measured and the corresponding pH was calculated for each one of them, as shown in Figure 3.12b. In this case, the MSE was of 0.180. From Figure 3.12b, it can be deduced the good correlation between the two set of data, having a R^2 coefficient of 0.993, which confirms the good behaviour of the instrument acting as pH-meter.

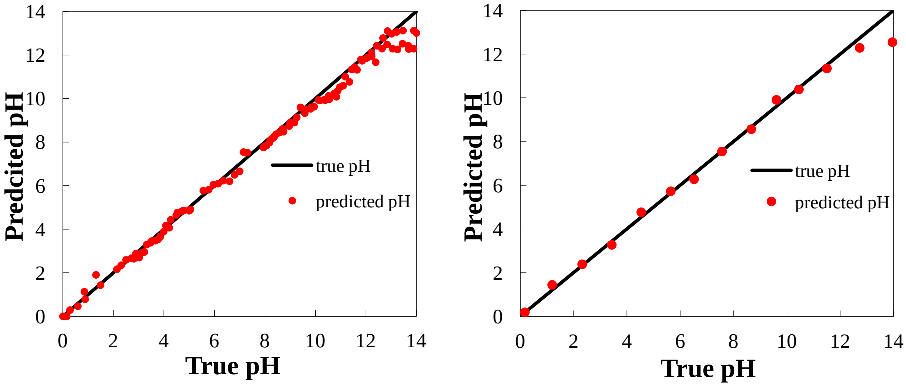

Figure 3.12 Comparison between true pH values and the predicted using the portable instrument for (a) the validation data and (b) real samples.

The portable instrument here presented has a resolution in units of pH equal to 0.02 in the whole range of pH. This value was obtained taking into account that the H parameter can be expressed as a 12-bit word since it is a linear combination from the RGB coordinates (12-bit word for each component). Assuming a worst case in which only 10 bits are significant and a range of H from -0.3 to 1, as it can be seen in Figure 3.11, the resolution of H is 0.0013. The accuracy of the system was obtained as the standard deviation of the validation data and the value from this calculation is 0.2. The response time of the instrument is 1.5 s, since as it is mentioned above, the integration time and the modelling of the responses were selected in order to improve this time. Hence, the final time response is the sum of the integration time of each detector (200 ms) and the processing time to obtain the hue value and the corresponding pH value (175 ms). A summary of these specifications, and other main features of the portable instrument, is presented in Table 3.4. Finally, the power consumption of the device is 1 W in measurement mode and 25 mW in standby, i.e. with the microcontroller in sleep mode.

Table 3.4 Technical specifications of the instrument.

Number of sensors	12 max
pH range	0-14
Response time	1.5 s
Resolution	0.02
Accuracy	0.2
Dimensions	15 cm × 17 cm × 5 cm
Weight	400 g
Connectivity	USB 2.0
Power	PP3 battery

3.2.5 Artificial neural network applied to portable systems

In this section, an improvement of the algorithm employed in the portable instrument previously described is presented. This optimization is carried out by means of the use of an artificial neural network (ANN).

Nowadays, artificial intelligence (AI) is applied to several research topics such as artificial vision, instrumentation or robotics. The artificial intelligence is defined as the capability of a computer to operate similarly to the human brain, taking into account the involved learning processes. In particular, the ANNs are a specific technique of AI. An ANN is a simplified model of the human brain that is capable of acquiring knowledge using the experience, which is represented by the available information in the network. An ANN consists of a set of artificial neurons arranged in layers which are related using weighted connections between the different neurons of the layers. Hence, the main parameters of an ANN are the number of layers, the number of neurons per layer, the connectivity degree and the kind of connections between different neurons.

One drawback of the calibration presented in the previous section is the non-linearity of the functions to describe the response of the pH membranes. Neural networks (NN) (Haykin 1999) have been proposed to solve this problem, but they have some limitations on the classic training methods that make the model calibration processes difficult (Bengio *et al.* 1994). There are several works about pH and neural networks in the literature: working with an optical fibre pH sensor in the range from 2.51 to 9.76 with errors of 0.08 and 0.07 in different configuration of the network (Taib *et al.* 1996); and using an optical pH sensor based on the immobilization of a mixture of two dyes on a membrane where the ANN is used to cover the whole range of pH providing mean square errors of 0.03 and 0.04 for test and control sets, respectively (Safavi and Bagheri 2003).

In previous works of the group using the same optical sensor array, different mathematical approaches were used. Firstly, linear, sigmoid competitions and sigmoid surface models were studied, providing MSE of 0.111, 0.075 and 0.266 respectively for tap river water (Capel-Cuevas *et al.* 2010). Then, neural network were applied as a prediction technique (Capel-Cuevas *et al.* 2011) obtaining the best results with 11 input neurons, 10 hidden neurons and one output neuron, providing a MSE of 0.043. In this work, artificial neural networks have been applied in order to provide a better optimal solution of the pH of a solution than the provided by the cubic models obtained in section 3.2.4. The hue coordinates obtained from each sensing membrane by means of digital colour detectors are used as inputs for the neural network. Then, a multi-objective algorithm produces a set of neural networks with maximum accuracy and the optimal sensing elements to be included in the sensor array.

pH determination model

A Multilayer Perceptron (Haykin 1999) with one hidden layer was designed for this purpose. With this configuration, the outputs from the first layer are the inputs for the second one, and so on. Here, the hue value obtained from each sensing element is a candidate input for the network, and the output is the predicted pH value. The activation function for all hidden neurons, which determines the output of a neuron given the set of inputs, was set to the sigmoid function and the output neuron response is computed as the weighted linear aggregation of the output value provided by the intermediate hidden neurons.

In order to optimize the system, reducing the number of elements of the optical array, the computational cost and the memory of the microcontroller, three criteria were established to be minimized using a multi-objective procedure as shown in Equation 3.5: (1) criterion $f_1(x)$ to minimise the number of sensing elements; (2) criterion $f_2(x)$ to minimise the network prediction error between the real and the predicted pH; and (3) criterion $f_3(x)$ to minimise the number of hidden neurons. The error to be reduced is the maximum absolute error between the network response and all the calibration data, and it does not depend on the number of training data.

$$x^* = min_x\{f_1(x), f_2(x), f_3(x)\} \tag{3.5}$$

$$f_1(x) = N^0(x) \tag{3.6}$$

$$f_2(x) = max_p\{|pH'_p - pH_p|\}\forall p \tag{3.7}$$

$$f_3(x) = N^1(x), \qquad (3.8)$$

where x represents the neural network parameters to be optimized, x^* is the set of optimal solutions, pH_p is the real measurement of pH, pH'_p is the value of pH predicted by the neural network, N_0 is the number of inputs and N_1 the number of hidden neurons.

A hybrid version of the NSGA-II multi-objective algorithm was designed in combination with the Levenberg-Marquardt non-linear optimisation method using the Baldwinian hybridation strategy (Cuellar *et al.* 2011). The resulting method is able to provide a set of optimal neural networks according to the Pareto optimality criterion. To achieve a NN of a set of NN satisfying the three criteria, the dominance over solutions of the multi-objective algorithm is defined in Equation 3.9. In this work, a neural network x dominates the neural network y, and it reads x<y, if the solution y is not better than x in any of the criteria to be optimised, and also x is better than y in at least one of the three criteria. If a solution x does not dominate y and also y does not dominate x, both are non-dominated solutions. The Pareto front is composed of the set of solutions that are not dominated by any other solution.

$$x < y \leftrightarrow \forall i \in \{1,2,\dots n\} f_i(x) \leq f_i(y) \land \exists j \in \{1,2,\dots n\}: f_j(x) \leq f_j(y) \quad (3.9)$$

It is necessary to optimise the network weights and biases in order to achieve a suitable pH determination, the number of sensing elements to minimise the cost and size of the prototype, and the number of hidden neurons to improve the power consumption of the instrument as well as the time of processing. As it can be seen in the equations below, W is a matrix containing the network connection weights as real numbers, B is a vector with the bias values of the neurons as real numbers, I is a vector with binary values to indicate which sensing elements in the array are used for pH determination in the network and H is a vector with binary values to indicate the network hidden neurons. Here, as an example, a maximum of five inputs and four hidden neurons are represented in the equations and in Figure 3.13. This representation is widely extended in the literature for multi-objective optimization of NN (Abbass 2001), and it has the advantage of being flexible enough to be used for the optimization of more complex NN models such as recurrent NN.

$$W = \begin{pmatrix} w_{1,1}^1 & w_{1,2}^1 & w_{1,3}^1 & w_{1,4}^1 & w_{1,5}^1 & 0 & 0 & 0 & 0 \\ w_{2,1}^1 & w_{2,2}^1 & w_{2,3}^1 & w_{2,4}^1 & w_{2,5}^1 & 0 & 0 & 0 & 0 \\ w_{3,1}^1 & w_{3,2}^1 & w_{3,3}^1 & w_{3,4}^1 & w_{3,5}^1 & 0 & 0 & 0 & 0 \\ w_{4,1}^1 & w_{4,2}^1 & w_{4,3}^1 & w_{4,4}^1 & w_{4,5}^1 & 0 & 0 & 0 & 0 \\ 0 & 0 & 0 & 0 & 0 & w_{1,1}^2 & w_{1,2}^2 & w_{1,3}^2 & w_{1,4}^2 \end{pmatrix} \tag{3.10}$$

$$B = (b_1^1 \quad b_2^1 \quad b_3^1 \quad b_4^1 \quad b_5^1) \tag{3.11}$$

$$\mathrm{I} = (1 \quad 1 \quad 0 \quad 1 \quad 0) \tag{3.12}$$

$$H = (0 \quad 1 \quad 0 \quad 1) \tag{3.13}$$

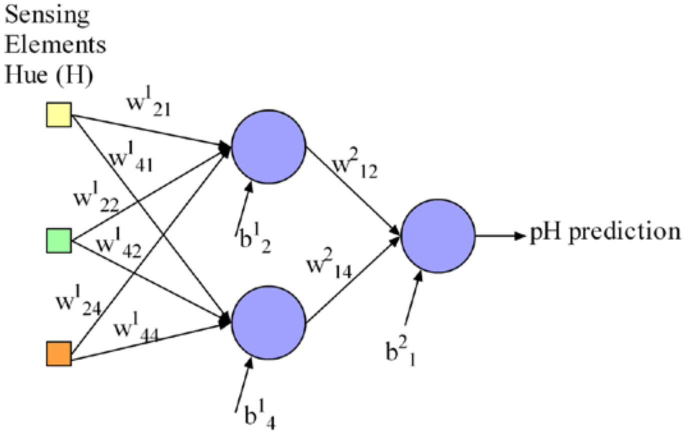

Figure 3.13 Neural network represented in Equations 3.10-3.13.

Results of the artificial neural network

As mentioned in the previous section, the hue value is stable, simple to calculate and easily obtaining from commercial devices, maintaining a superior precision with regards to variations in indicator concentration, membrane thickness, detector spectral response, and light source (Cantrell *et al.* 2010). So here, using the hue value of each sensing element as input for the neural network a value of pH is predicted. The experiment was designed sampling in uniform steps the whole range of pH from 0 to 14, using a total of 121 solutions to build the calibration data set. The hue value was extracted using the portable instrument described above in order to obtain the data to train the neural network. The multi-objective hybrid NSGA-II algorithm (Cuellar *et al.* 2011) was executed 30 times using the parameters shown in Table 3.5.

Table 3.5 Parameters of the multi-objective hybrid NSGA-II algorithm used in this case.

Bounds for the number of hidden neurons	2 (min.) – 11 (max.)
Bounds for the number of sensing elements	1 (min.) – 11 (max.)
Bounds for network biases and weights	[-10,10]
Number of layer of the NN	1 (input), 1 (hidden), 1 (output)
Crossover probability	0.7
Mutation probability	0.2 (number of sensing elements) 0.2 (number of hidden neurons) 0.2 (network weights) 0.1 (mutation per gene)
Population size	100
Number of algorithm generations	700
Number of local search iterations with Levenberg-Marquardt	10

This procedure returned 21 non-dominated solutions in the Pareto frontier meeting the three objectives established with Equations 3.5, 3.6, 3.7 and 3.8. In Table 3.6 a summary of the obtained results is shown, describing the number of inputs and hidden neurons needed, as well as the used elements of the optical sensor array and the error values for comparison with other methods. The maximum absolute error presents some high values since all the replicates of the measurements were used without removing the outliers values obtained by bad used of the portable instrument. Despite the wide range of solutions provided using different levels of accuracy, complexity or number of elements needed, only solutions 1, 10, 12 and 18 are taken into account due the low error values provided and they can be selected to be programmed in the microcontroller depending on the criterion established to be improved. Thus, solution 18 uses lower number of elements, whereas solution 1 uses lower number of hidden neurons and, therefore, it has lower complexity, and so on.

Table 3.6 Performance of the resulting networks applying hybrid NSGA-II algorithm in calibration.

Solution number	**Maximum absolute error (pH units)**	**Number of hidden neurons**	**Number of network inputs**	**Sensing elements used for pH prediction**	**MSE (Calibration data)**
1	0.873	4	7	3 4 5 6 8 9 11	0.048
2	1.098	3	3	4 5 10	0.114
3	0.864	5	7	3 4 5 6 8 9 11	0.048
4	1.656	2	2	7 9	0.508
5	1.014	3	4	4 5 10 11	0.080

6	1.279	2	3	4 5 10	0.141
7	1.079	2	5	1 4 5 10 11	0.113
8	1.099	2	4	4 5 10 11	0.118
9	0.910	8	6	4 5 6 8 9 11	0.047
10	0.766	6	11	1 2 3 4 5 6 7 8 9 10 11	0.031
11	0.883	3	7	3 4 5 6 8 9 11	0.057
12	**0.734**	**9**	**11**	**1 2 3 4 5 6 7 8 9 10 11**	**0.028**
13	0.917	5	5	1 4 5 8 9	0.064
14	0.959	3	6	1 4 5 6 9 11	0.071
15	0.757	7	9	1 2 3 4 5 6 7 9 11	0.037
16	1.428	3	2	5 7	0.116
17	3.058	2	1	7	1.026
18	0.978	5	4	4 5 9 10	0.065
19	0.980	3	5	3 4 5 9 10	0.073
20	0.924	4	6	1 2 4 5 9 10	0.061
21	0.945	4	5	1 4 5 9 10	0.066

To validate the portable instrument using ANN, the solution number 12 was selected since it improved the error values, overcoming other solutions. As pointed out in Table 3.6, the selected solution use all (11) the sensing elements. The network was implemented in C language and programmed in the microcontroller described in previous section. The code needed to implement this ANN required only 10% of the available program memory of the microcontroller which is 3 Kb.

In order to validate the obtained NN, a set of 50 equally spaced solutions in the range of pH was used, making 5 replicates of the sensor array in each case. The correlation coefficient R^2 was calculated with a result of 0.9997 and, also, the MSE was obtained for the validation data being of 0.004 in pH units. Additionally, a set of 10 samples of water equally distributed in the whole range of pH were also analyzed, taking five replicates in each case. The obtained MSE in this case has a value of 0.015. In Figure 3.14 the correlation graph between the true values and the predicted for validation data is shown, as well as for the test data where the correlation factor R^2 is higher than 0.999 in both cases.

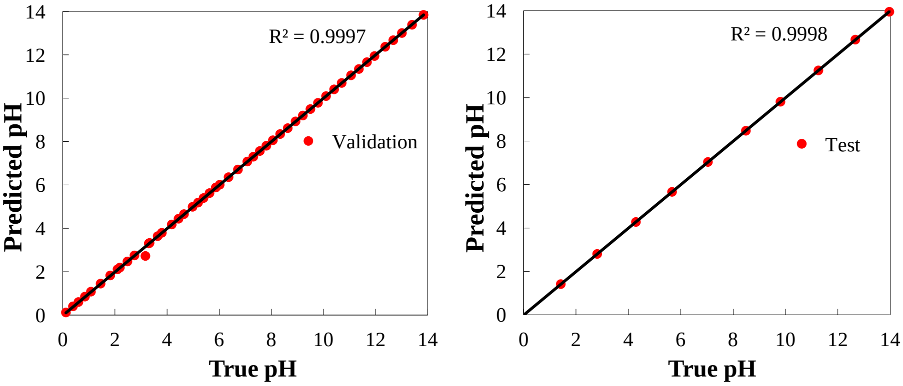

Figure 3.14 True and predicted pH values using the portable instrument with NN for (a) the validation data and (b) real samples.

Also, this method was applied to real samples such as beverages, personal care products and cleaning samples. The pH of this set of samples was validated against the produced by a pH-meter, and the results can be seen in Table 3.7. In this table are shown the errors obtained between the potentiometer and the scanner, and the potentiometer and the portable instrument. The error obtained using the neural network method here described offers, in most of the cases, better results than the provided by image processing using the scanner. The average error of the scanner in comparison with the potentiometer is of 0.13 whereas for the portable instrument is 0.1. The MSE between the scanner and the developed system is 0.024. Even though the improvement is not so significant with regard to the scanner, the portable instrument offers faster response and the possibility of obtaining the results in-situ.

Table 3.7 Comparison between the pH measured using different devices.

Sample	Potentiometer	Scanner	Error	Portable instrument	Error	P-value
Lemon dressing	2.35	2.19	0.16	2.31	0.04	0.016
Orange soft drink	2.75	2.83	0.08	2.67	0.08	0.044
Orange fizzy drink	2.91	2.98	0.07	2.92	0.01	0.035
Blackberry liqueur	2.91	3.08	0.17	2.95	0.04	0.107
Lemon fizzy drink	3.30	3.43	0.13	3.34	0.04	0.021
Cola fizzy drink 1	2.85	2.78	0.07	2.89	0.04	0.055
Vinegar	3.03	2.99	0.05	3.09	0.06	0.616
White wine	3.35	3.29	0.05	3.36	0.02	0.117
Mandarin juice	3.57	2.44	0.13	3.52	0.04	0.228
Pineapple juice	3.68	2.69	0.01	3.67	0.02	0.633
Peach juice	4.01	4.12	0.12	4.06	0.05	0.208
Tinned gherkin	2.89	2.72	0.17	2.91	0.02	0.033
Tinned artichoke	3.80	3.78	0.02	3.72	0.08	0.021

Tinned mushroom	4.96	4.86	0.10	5.02	0.06	0.296
Tinned soya	3.97	4.07	0.10	4.05	0.08	0.558
Tinned olive	4.07	4.14	0.07	4.09	0.02	0.183
Tinned carrot	3.76	3.72	0.04	3.78	0.02	0.265
Beer	4.16	4.30	0.14	4.24	0.08	0.176
Alcohol-free beer	4.50	4.25	0.25	4.38	0.12	0.116
Black tea	4.93	5.08	0.15	5.21	0.28	0.068
Decaffeinated coffee solution	5.67	5.33	0.34	5.42	0.25	0.311
Skimmed milk	6.70	6.59	0.11	6.61	0.09	0.822
Sparkling mineral water	5.30	5.29	0.01	5.36	0.06	0.292
Mineral water 1	7.17	7.19	0.02	7.14	0.03	0.149
Tap water	7.85	7.97	0.12	7.96	0.11	0.294
Toothpaste solution (1:3)	7.22	7.31	0.09	7.36	0.14	0.297
Mouthwash	7.30	7.53	0.23	7.43	0.13	0.178
Diluted washing-up liquid	7.30	6.87	0.42	7.02	0.28	0.299
Sodium bicarbonate saturated solution	8.44	8.37	0.07	8.30	0.14	0.527
Ammonia solution (1:10)	11.04	11.46	0.42	11.58	0.54	0.312

The main features of this instrument are obtained as explained in section 3.2.4, where resolution of the pH is 0.02 since it depends on the resolution of the detector and in this case, the same S9706 model has been used. The accuracy of the system was obtained as the standard deviation of the validation data and the value from this calculation is 0.06. As it can be seen regarding to the accuracy achieved without using ANN, which was of 0.2, here this factor has been improved considerably. The power consumption of the device is 450 mW in measurement mode and 25 mW in standby state. These values in the consumption prove that the neural network offers a more optimized algorithm of resolution that reduces the computational cost of the system, reducing the total time of response and, therefore, the power consumption of the instrument.

3.3 Design of a radiofrequency identification tag for oxygen sensing

Oxygen sensing is highly demanded in many different fields of research such as environmental or medical sciences or food packaging technology. Until now, electrochemical sensors have been used for many applications, but they suffer some drawbacks (Wang *et al.* 2010a). This fact has increased the interest in using optical oxygen sensors where the main principle of them consists of the change of properties in the presence of gaseous or dissolved oxygen. The most common properties monitorized to measure of oxygen are the absorption of radiation and the quenching of the luminescence.

In the case of absorption sensors the colour change can be measured to provide qualitative or semiquantitative information or the change in absorbance or reflectance to obtain fully quantitative information by means of an external detection unit (Evans and

Douglas 2006). Several works have been carried out using different chemistries such as oxyhaemoglobin (Mills 2005), myoglobin (Zhujun and Seitz 1986), or methylene blue and glucose (Lee *et al.* 2005) among others.

Luminescence-based sensors use the quenching by molecular oxygen of the emission from a luminophore immobilized in a support. This kind of sensors allows more accurate measurement than the absorption sensors, but on the other hand, they require instrumentation in order to measure the emission intensity or lifetimes (Mills 2005), (Borisov *et al.* 2006). In recent years, a new approach using luminescence sensors has appeared. It is based on the measurement of the colour of the luminescence, using the change of colour in the emission as analytical property, thus combining the advantages of luminescence and absorption sensors (Wang *et al.* 2010a).

Here, a RFID tag using this approach is presented. A colour digital detector is able to capture the colour of the emission intensity of the luminophore, using the red component of the RGB colour space in order to determine the concentration of the surrounding oxygen. The sensing membrane is made using the PtOEP complex that changes its luminescence intensity and lifetime when the oxygen concentration varies. In next sections, a similar approach will be presented as well for oxygen sensing, but in those cases, the colour determination will be made using a micro-camera module or a built-in smartphone camera. In this case, the RFID is used as transmission method to send the information of interest from the measurement system to the user or a PC for further analysis.

This RFID tag here described can be applied to the smart packaging field. The main objective of a package is the protection and preservation of food and beverage from external contamination. Besides this barrier function, in the recent years there has been more research and development in order to provide to the package new systems to improve the control over the packed food. Among these, significant new functional package systems include smart and active packaging, modified atmosphere packaging (Jaakkola *et al.* 2010) and edible films/coatings (Han 2005). With the smart packaging it is possible to sense some properties of the enclosed food or the environment in which is kept by informing to the consumer or the manufacturer about the state or the process that the food has followed (Kerry *et al.* 2006). Some examples are time-temperature, gas leakage, ripeness, toxin or biosensors indicators (Restuccia *et al.* 2010).

In this section, the smart packaging achieved with the RFID tag is applied to the determination of oxygen concentration, as mentioned before. The presence of oxygen is one of the main causes of food spoilage (Rooney 1995) since it facilitates processes like microbial growth, lipid oxidation, protein decomposition and discoloration (Mills *et al.* 2012). Usually, the food is packed in a modified atmosphere where the concentration of oxygen is reduced from 0.5 to 2% or even less (Faustman and Cassens 1990), (Blakistone 1998). Since the whole tag can be printed in flexible substrate, it is possible to use it over the package to monitor the oxygen concentration in which the food is sealed. This allows to the user to know if the package seal has been broken and, therefore, if the state of the food has changed.

3.3.1 Reagents, instrumentation and software

The chemicals used were platinum octaethylporphyrin complex (PtOEP, Porphyrin Products Inc., Logan, UT, USA), 1,4-diazabicyclo[2.2.2] octane (DABCO, 98%), tetrahydrofuran (THF) and polystyrene (PS, average MW 280,000, Tg: 100 °C, GPC grade), all three supplied by Sigma (Sigma-Aldrich Química S.A., Madrid, Spain). The gases O_2 and N_2 (>99%) were supplied in gas cylinders by Air Liquid (Air Liquid, S.A., Madrid, Spain).

A 120 threads per centimeter (T/m) Nylon thread mesh has been used to manufacture the screen printed patterns. The tags were printed with SunTronic CRSN 2442 silver ink (Sun Chemical, Parsippany, NJ, USA) and consisted of one layer printed with a Serfix III screen printing machine (Seglevint SL, Barcelona, Spain). Finally, the curing process took place at 120 ºC during 5 minutes.

The chosen substrate was polyethylene naphthalate (PEN, Kaladex® PEN Film, Dupont Teijin FilmsTM, Japan) with 125 µm of thick. Since the application of the tag required the light going through the substrate, the used material had to present high transparency for the wavelengths of interest. Polyethylene terephthalate (PET), which is widely used in packaging applications, was considered in first place. PEN polyester is chemically quite similar to PET but is more resistant to the temperature and is certified for long term electrical use. Although both materials have a high optical transmission (>85%) in the visible spectrum, PEN was finally selected due to its better adherence for the sensing membrane. On the other hand, this material is more expensive and has a lower flex life than PET.

A two-step process was developed in order to do the transfer of chips. Firstly, the H20E conductive-adhesive resin (Epoxy Technology Inc., Billerica, MA, USA) was used to make the interconnections between integrated circuits and printed silver pad. A double layer 50 µm-thick dry adhesive AR Clear 8932 (Adhesives Research, Inc. Glen Rock, PA, USA) was placed on the bottom part of the chips to fix them to the substrate. The last step was heating up in an oven at 120ºC for 20 minutes to cure the conductive resin. Since the dry film adhesion improved with temperature, the heat treatment was also useful to provide better adhesion of the chips to the substrate.

The following instrumentation was used in the process of electrical characterization of the system: a mixed signal oscilloscope (MSO4101, Tektronix, Beaverton, OR, USA), an 8½-bit Digital Multimeter 3158A (Agilent Technologies, Santa Clara, CA, USA), a 15 MHz waveform generator 33120A (Agilent Technologies, Santa Clara, CA, USA), an E5071C network analyzer, a N4431A kit (Agilent Technologies, Santa Clara, CA, USA), a Precision Impedance Analyzer 4294A and an impedance probe kit (4294A1) (Agilent Technologies, Santa Clara, CA, USA), a DC power supply E3630A (Agilent Technologies, Santa Clara, CA, USA) and a RFID reader TRF7960 (Texas Instruments, Dallas, TX, USA). A user interface made in Visual Basic© was used in a computer for calibration purposes. All chemicals were weighed with a DV215CD balance (Ohaus Co., Pine Brook, NJ, USA) with a precision of ±0.01 mg.

The standard mixtures for instrument calibration and characterization were prepared by controlling the flow rates of the different high purity gases O_2 and N_2, being the latter used as inert gas, entering in a mixing chamber using a computer-controlled mass flow controller (Air Liquid España S.A., Madrid, Spain). The total pressure of operation was 760 Torr and the flow rate 500 cm^3/min.

A thermostatic chamber, with a lateral hole for allowing the connexion to a computer and the gas tubing entrance, made it possible to maintain a controlled temperature between −50 °C and +50 °C with an accuracy of ±0.1 °C for thermal characterization of the tag response.

Advanced Design Simulator (ADS, Agilent Technologies, Santa Clara, CA, USA) based on momentum method was used for simulating the electrical behaviour of the printed antennas, including the surface roughness and the substrate influence on the RF performance.

3.3.2 Membrane preparation

The cocktail for the preparation of the oxygen-sensitive membrane was made by dissolving 0.5 mg of PtOEP and 12 mg of DABCO in 1 mL of a solution of 5% (w/v) of PS in freshly distilled THF. The sensitive membrane was cast by placing a volume of 10 µL of cocktail on a flexible substrate using spin-coating technique under ambient atmospheric conditions. After the deposition of the sensing membranes, the substrate containing them was left to dry in darkness in a THF atmosphere for 1 h. The obtained membranes were homogeneous, transparent and pink coloured. The sensing membranes containing PtOEP in PS are recommended to be cured in darkness for 9 days before their use (Vargas-Sansalvador *et al.* 2009). When they are not in use, they must be kept in darkness in order to extend their lifetime.

3.3.3 Description of the prototype

The monitoring system for intelligent packaging here presented determines the concentration of gaseous O_2. With this purpose, the system measures the intensity of the luminescent emission generated in the membrane which is quenched by the surrounding O_2. Usually, the scheme for the intensity measurement consists of a photodetector, such as photodiode, that generates a current proportional to the incident light. Nevertheless, it is possible to substitute this kind of photodetectors by colour detectors, whose output is a signal proportional to the colour of the incident light and to the intensity of this colour (Capitan-Vallvey and Palma 2011). This strategy for the quantification of light intensity has been proven to be highly sensitive and allows discarding external interferences (Schaferling *et al.* 2003), (Park *et al.* 2010). For this reason, in this work, it is used instead of the classical light measurement through photodiodes.

The incident intensity is quantified using the red coordinate (R) of the RGB colour space which is obtained directly as the output of a digital colour detector when it is reached by the light of the membrane. In the sensing module of this prototype, shown in Figure 3.15, the oxygen sensitive membrane is excited and the generated luminescence is detected using a digital colour detector. Also, there is a transmission block which consists of a RFID tag and that will be later explained.

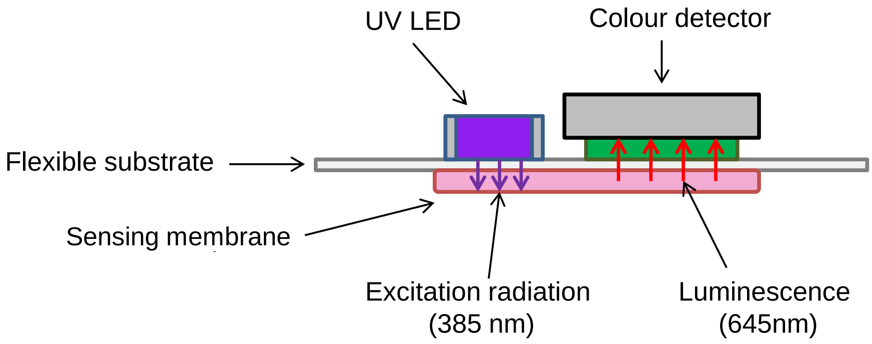

Figure 3.15 Sensing module of the RFID tag.

The optical excitation of the membrane is carried out using a surface-mount LED (OCU-400UE390, OSA Opto Light, Berlin, Germany) whose peak of emission is placed at 385 nm. The luminescence generated by the luminophore when it is excited is dynamically quenched by oxygen thus causing changes both in phosphorescence intensity and lifetime (Capitan-Vallvey *et al.* 2007). In this case, luminescence intensity is related to the concentration of the surrounding gaseous oxygen. This emission is registered by means of a colour detector model S9706, whose main features are already mentioned in sections 3.2.3 and 3.2.4. In this work, just as the previous section, a high sensitivity mode was chosen in order to cover a more extended area of the membrane surface. The integration time, which can be modified by software, has influence in the response time and resolution of the system as explained below.

Although simultaneous reading of the RGB components in the incident light is provided, only the red and blue coordinates are considered in this case, being the green value irrelevant. Since the system was optically isolated to avoid external light interference, the R value corresponded exclusively to the luminescence generated by the

PtOEP complex and its value depended on the intensity of this emission and, therefore, on the O_2 concentration (Park *et al.* 2010). In darkness conditions, the B value of the reading corresponded to the visible emission of the LED and it was used as a reference signal in order to correct fluctuations in the source illumination (Wang *et al.* 2010a).

As it can be seen in Figure 3.15, the disposition of these components was arranged as follows: on the inner surface of flexible substrate (PEN) the membrane is deposited. In this way, this is the only element of the system that is placed inside the package, whereas the full electronics was printed on the outer side of the substrate. The LED for the optical excitation was placed very close to the colour detector, and facing directly the membrane from the external side of the substrate. Although in the literature similar dispositions of the sensing elements are reported, it is common to manipulate the substrate with the intention of using it as waveguide to transport the excitation and response emissions (Mayr *et al.* 2009), (Courbat *et al.* 2011). This process for measuring of the light inevitably implies optical losses in the propagation (Courbat *et al.* 2011). In order to avoid this effect, in this work the package surface is treated merely as a substrate for the system, and both the exciting emission and the response luminescence travel directly from the LED to the membrane and from the membrane to the colour detector, as depicted in Figure 3.15.

In order to process the information provided, both the LED and the S9706 detector were connected directly to a microcontroller model PIC18F46J50 (Microchip Technology Inc., USA) which has been selected because of its low power consumption (nanoWatt XLP Technology). With the objective of avoiding thermal drifts, the LED was biased in a pulsed mode by the microcontroller, which introduced a pulse train of a high frequency (500 kHz) and 3.3 V between its terminals. This biasing configuration eliminates the use of a current source in the design and, therefore, it simplifies the system.

3.3.4 The RFID tag

The system here presented consists of two different blocks: the sensing module, above described, and the transmitting module formed by a RFID tag for the remote reading of the measurement. In Figure 3.16 it is shown the scheme of the whole system. Red lines in the picture represent the principal power lines while blue connections are secondary power lines. It is a microcontroller-based system but in this case a RFID module was included in order to add a wireless transmission of the concentration of oxygen inside the package. The measured data is transmitted using the protocol ISO15693 which operates in the high frequency (HF) band at 13.56 MHz and has a maximum reading distance of 1-1.5 meters for active RFID tags (Rida *et al.* 2009). The main feature in this work was the printing of the designed antenna and all the electronics described in the previous sections on a flexible substrate used for the package.

The RFID chip used in this work was the model SL13A from Ams (Ams International AG, Rapperswil, Switzerland) which includes, besides the RF interface, an 8 kbit EEPROM and a temperature sensor, the latter being used in the design for the compensation thermal drifts. The 10 bits temperature value is obtained through an on-chip A/D converter which uses a calibrated bandgap reference as reference voltage. Both the EEPROM and the temperature data could be reached through SPI interface using the microcontroller. The main advantage of including a memory module was the possibility of data storage for further reading using a commercial RFID reader. In addition, the chip could be supplied from either the battery or through the RF field that an external reader generates, making possible the operation of the system in passive or active mode. This is feasible since the chip has an internal regulator which is able to provide a voltage output of 3.4 V and a maximum current of 4 mA for the rest of the elements of the circuit when it is supplied in the passive mode. Therefore, it is possible to configure the RFID tag in the passive mode where the measurement of the oxygen concentration is carried out only when the user requires a reading. If the system is configured to take measurements in a continuous mode, the oxygen concentration and the temperature data are stored in the memory including a timestamp, and the inclusion of an external battery is required.

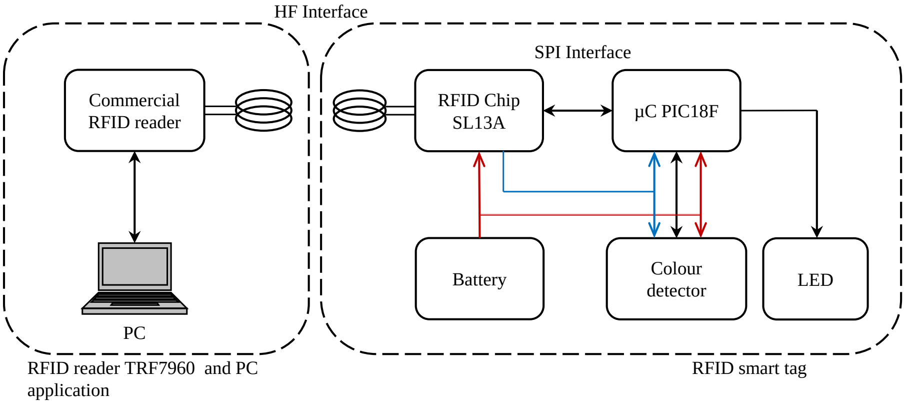

Figure 3.16 Block diagram of the design for the RFID tag.

The antenna used in this design is a custom-designed screen printed inductor. Recently, this kind of coils has been reported in literature (Rida *et al.* 2009), (Vyas *et al.* 2009) and it has been selected due to its flexibility which makes it proper to the application here presented. Since the RFID chip has a capacitance about 25 pF at the frequency of interest and the resonance occurs when $\bullet_0 = 1/\sqrt{LC}$, a value of 5.5 µH for the coil antenna must be achieved in order to resonate at the desire frequency. The start point to design and optimize the antenna has been extracted from the Wheeler model (Mohan *et al.* 1999). Using the ADS software to simulate the inductors to determine the dimensions for the specific inductance at 13.56 MHz, and taking into account the thickness of 13.37 µm (Saini *et al.* 1998) achieved with the screen printing technique, the final dimensions are 75 mm × 45 mm with 7 turns. The width of the conductor and the interspacing between the lines are each 600 µm.

In active mode, a polymer Lithium-ion battery PGEB01 from General Electronics (General Electronics Battery Co., Ltd, Shenzhen, P. R. China) was used to power on the tag. This is a rechargeable battery of 3.7 V and 40 mAh. The reading of the data supplied by the tag was carried out with a HF band commercial reader TRF7690EVM from Texas Instrument (Texas Instrument Inc., USA). This reader is fully compatible with the protocol ISO15693 used for the communication.

Antenna characterization

In order to characterize the antenna used in this work, simulation and experimental analysis were carried out. RF electrical characterization for the fabricated coils inductors was performed by measuring their inductance quality factor and equivalent circuits. The measurements were done using the four-point measurement technique. The results confirmed that the inductance value of the coil is not much affected by the substrate (Saini *et al.* 1998). With the simulation, the values obtained for the induction and quality factor are 5.62 µH and 2.676, respectively while the experimental values are 5.8 µH and 3.5 at the resonance frequency of 13.56 MHz. These values were in concordance, and the mismatch could be explained because there is a reduction of the self-resonant frequency of the inductors, 32 MHz, unlike the simulated value of 35 MHz, as it can be seen in Figure 3.17.

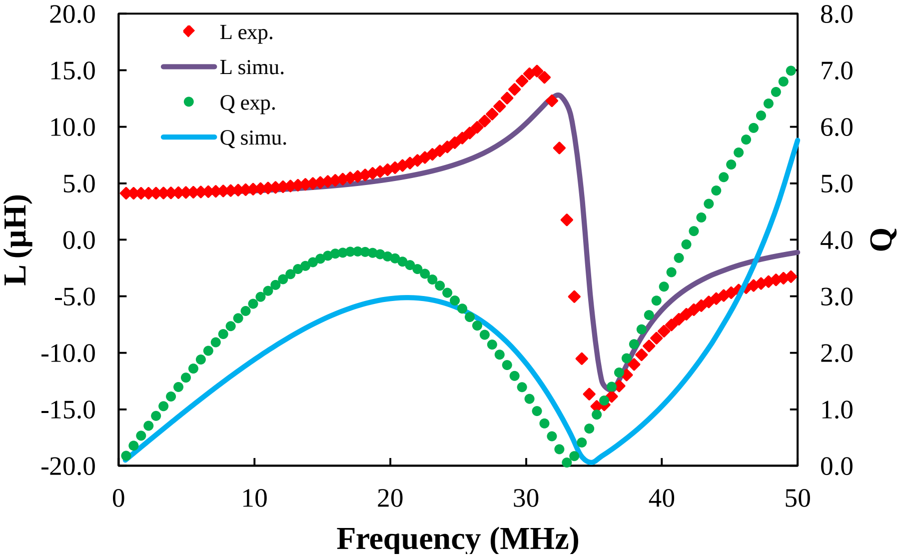

Figure 3.17 Simulated (lines) and measured (symbols) frequency response of the antenna.

The operation of the antenna was tested with a commercial RFID reader model TRF7960 which had a read range around 12 cm in vertical direction and 11.2 cm in horizontal during the operation in passive mode. Using an impedance analyzer, the resonance frequency of the full system was evaluated. As shown in Figure 3.18, the impedance of the tag reached a value of 1.6 K• at the resonance frequency. In this study, the point where the phase is null is at frequency of 13.6

MHz. Since the protocol ISO15693 specification related to anti-collision mechanism establishes a tolerant range of ±7KHz around the 13.56 MHz, this system is valid for a wireless communication.

Finally, the power consumption of the system was measured: 34.4 µA in idle mode and 3.55 mA in sensing mode. This value is low enough to be provided by the internal regulator of the RFID chip SL31A, whose maximum current value according to the datasheet is 4 mA. Therefore, the tag could operate in a passive mode without need of an external battery in the circuitry.

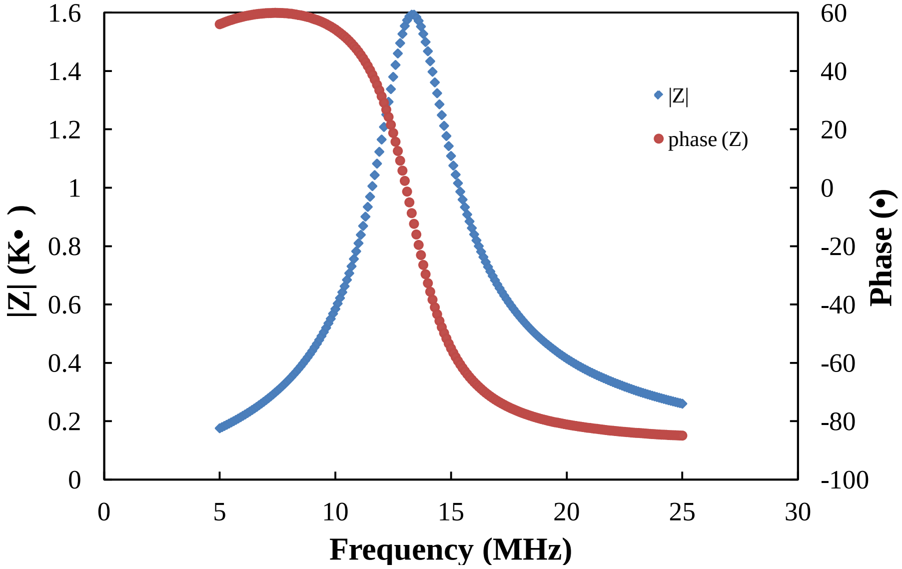

Figure 3.18 Impedance of the tag as a function of the frequency.

3.3.5 Results

In Figure 3.19 a picture of the whole system is presented. The sensing block is not covered in order to show the structure of this module, but in measurement mode must be kept in darkness to avoid the influence of the external light in the intensity measurement carried out by the detector.

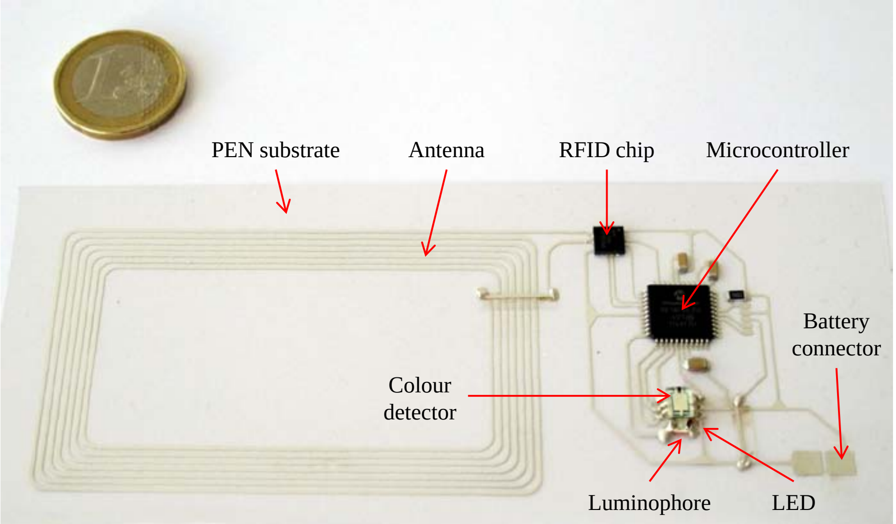

Figure 3.19 Photography of the designed system.

System calibration

The luminescence detection is carried out after the excitation of the membrane by the UV radiation emitted by the LED. The PtOEP complex presents two main peaks of absorption at 380 nm and 535 nm, as depicted in Figure 3.20 (Capitan-Vallvey *et al.* 2007). Although several works have been carried out using a green LED with a peak emission in 525 nm (Ricketts and Douglas 2008), (Vargas-Sansalvador *et al.* 2011b), here a UV LED is used. The main reason of using this wavelength for the excitation of the membrane is that the peak of emission of 380 nm of the LED are not in the visible region of the spectra and, therefore, there is no interference of the light source in the colour received by the digital colour detector.

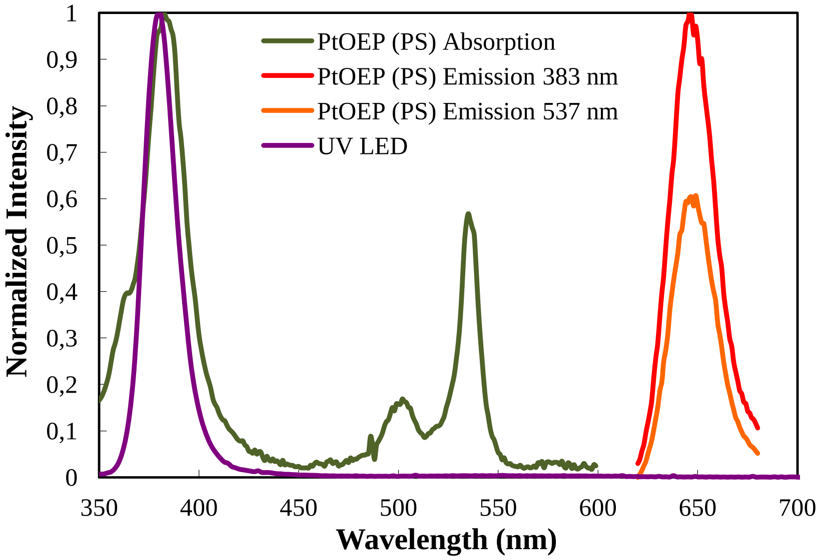

Figure 3.20 Spectra of the absorption and emission of the PtOEP complex and the UV LED.

As the UV excitation produces an increase in the temperature over time that affects to the intensity of the luminescence, the LED was biased directly through the microcontroller. The microcontroller introduces a voltage pulse train of 3.3 V at a frequency of 500 KHz reducing the number of elements for biasing the LED as well as the power consumption of the circuitry. The frequency was chosen in order to produce a period of the biasing signal much lower than the response time of the PtOEP complex, 2 µs against a range of hundreds of microseconds (Vargas-Sansalvador *et al.* 2011b), minimizing the influence of the commutation in the membrane response. After the LED is biased, a small delay of 0.5 s is elapsed before the measurement process in order to assure a stable state of the LED and consequently, of the light emitted. Moreover, the S9706 detector collects incident light during an established integration time, thus removing the influence of possible fluctuations of the luminescence in the measurement. On the other hand, if the power line of the microcontroller is not completely stable, variations of the emitted radiation of the LED could appear. In order to avoid this influence, the R coordinate of the RGB colour space given by the S9706 detector was normalized by the B coordinate (Wang *et al.* 2010b), whose value corresponded to the radiation of the LED since the emission of this takes place in the UV region. As a result, the concentration of oxygen is related to the R/B ratio.

In Figure 3.21 it is shown the relationship between the value R/B and the concentration of oxygen at room temperature (21ºC). Full range from 0 to 100% of concentration is depicted and for each point of concentration six replicas were taken, although the errors bar are too small to be appreciated in the graph (and the following ones). In this figure, the average of errors is of $6 \cdot 10^{-4}$. The integration time of the colour detector was set in 200 ms, since the influence of this parameter has been explained previously on this report.

The Figure 3.21 shows a decreasing of the R/B parameter with the increasing of environmental oxygen. The curve can be fitted to a Freundlich isotherm equiation for luminescence which models a non-linear Stern-Volmer behaviour and it can be represented as shown in Equation 3.14 (Carraway *et al.* 1991) where I represents the intensity of the emitted luminescence, I_0 the intensity in the absence of oxygen and, • and • are fitting parameters. In this case, the fitting curve for the response of the sensor, shown in Figure 3.22, has as parameters • = 0.30 and • = 0.7636 with a correlation factor $r^2 = 0.995$. The average of errors for all the points is of $3 \cdot 10^{-3}$, which are too small to appear in the graphic. The parameters R_B and R_{B0} denote the ratios

R/B and R_0/B_0, respectively, which correspond to the measurement of the intensity of luminescence in presence and absence of oxygen.

$$\frac{I_0}{I} - 1 = \alpha[O_2]^{\beta}, \tag{3.14}$$

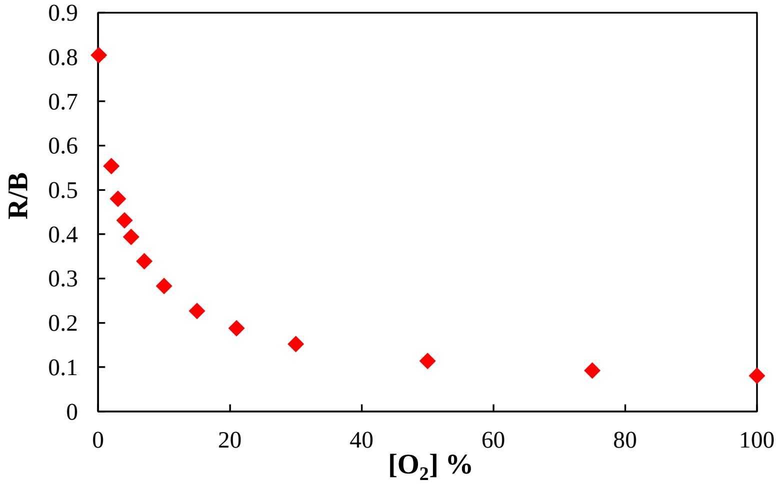

Figure 3.21 Response curve of the RFID tag at 21ºC.

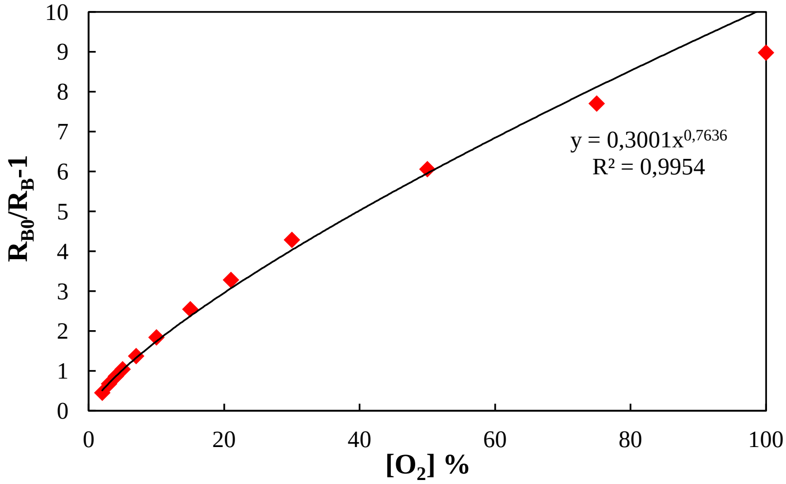

Figure 3.22 Calibration curve of the oxygen RFID tag fitted by to a non-linear Stern-Volmer model.

It is evident that the output data of the detector is higher if the selected integration time is longer. This fact can be observed in Figure 3.23: the higher the integration time, the broader the range of the R coordinate. Therefore, when the integration time is higher, the resolution of the system is also increased. In consequence, there is dependence between the technical specifications of the system, such as resolution and response time, and the integration time parameter.

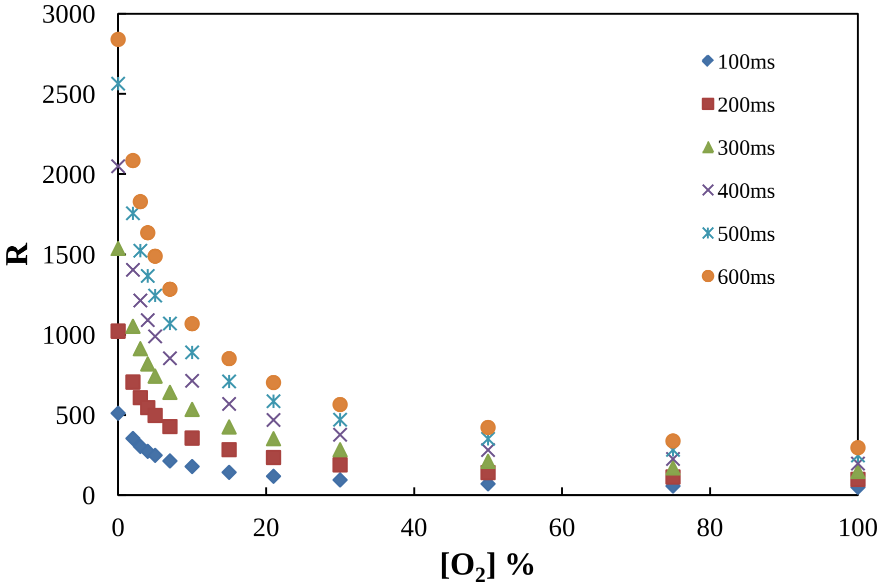

Figure 3.23 Response curves at different integration times.

Using Equation 3.14, the theoretical resolution of the system can be obtained by taking derivatives in both sides and approximating these derivatives to increments. The resolution calculated is:

$$\Delta O_2 = \frac{I_0\left(\frac{I_0 - I}{I\cdot\alpha}\right)^{1/\beta}}{I\cdot\beta(\mathrm{I} - \mathrm{I}_0)}\Delta I, \qquad (3.15)$$

where • I is the resolution in the measurement of the light and is related with the resolution of the colour detector in this way:

$$\Delta I = \partial\left(\frac{R}{B}\right) = \frac{\Delta R}{B} + \frac{R\cdot\Delta B}{B^2}, \qquad (3.16)$$

where ΔR and ΔB depend on the integration time as explained. Consequently, the resolution of the system depends on the integration time as well. It is common to take a reading error of ±2 or ±4 LSB for the internal analogue to digital converter in this kind of devices; in this case, an error of 8 LSB is considered to include variations in the concentration of the oxygen flow from the gas mixer. Therefore, if the resolution of the S9706 is 12 bits, this criterion is equivalent to take into account only 9 bits of resolution. From Equation 3.12, the values of resolution for the different integration times can be obtained at several oxygen concentrations and they are shown in Table 3.8. This table confirms that a higher integration time produces a better resolution, achieving up to 0.11 ppm of O_2, which is the lowest value that can be reached without saturation of the output of the detector. This result is much lower than resolutions obtained in previous works of the group (Palma *et al.* 2007b), (Vargas-Sansalvador *et al.* 2011b) which were of 5000 and 500 ppm, respectively.

Table 3.8 Theoretical resolution values (in ppm) for different integration times and O_2 concentrations at room temperature (21ºC).

Integration time	**2% O_2**	**10% O_2**	**21% O_2**
100	0.62	3.05	7.7
200	0.31	1.53	3.86
300	0.21	1.01	2.59
400	0.16	0.76	1.94
500	0.12	0.61	1.55
600	0.11	0.51	1.29

Table 3.8 shows the data corresponding to theoretical resolutions. In the practice, the resolution of the instrument is determined by the maximum values achieved for the red and blue components and the minimum possible variation of them taking into account that 12 bits are used by the digital colour detector to encode the RGB coordinates. Therefore, the experimental resolution is determined by the difference between the oxygen concentrations obtained using the maximum value and the immediately inferior value of the R and B coordinates. With this information, the value of resolution of the instrument at 0% of oxygen concentration is 1.1 ppm, which is still much lower than the resolution achieved in previous works.

Two more important parameters must be analyzed to complete the characterization of the system: accuracy and limit of detection (LOD). The accuracy achieved with the RFID tag, obtained as the standard deviations of the measurements, which also depends on the concentration of oxygen, is 0.01% and 0.08% at 2% and 21% of O_2 respectively with 200 ms of integration time. The LOD was obtained using the standard criteria: LOD = $y_b + 3s_b$, where y_b is the average blank signal and s_b is the standard deviation of the blank, which is determined using a minimum of ten replicas. Although there is a dependence of the LOD with the integration time it does not show a constant tendency and, therefore, the range of variation of the LOD at different integration times goes from 9 to 58 ppm of gaseous oxygen. Therefore, the LOD for 200 ms of integration time, which has been selected in this work, has a value of 55 ppm of O_2. Since this is a low limit, it is possible to affirm that the system is suitable for smart packaging where the food is preserved at very low oxygen concentrations.

Temperature dependence

The intensity of the luminescence emitted by the PtOEP complex has a thermal dependence (Schanze *et al.* 1997), (Gouin and Gouterman 2000), (Palma *et al.* 2007b) and, therefore, it must be taken into account and compensated (Vargas-Sansalvador *et al.* 2011b). In Figure 3.24 the response of the instrument at different temperatures is depicted using six replicas for each oxygen concentration at a given temperature value. At it can be seen, an increase in the temperature reduces the intensity of the membrane causing a lower red value. To take into account this effect, the fitting parameters • and • are modelled with the following equations:

$$\alpha = -1.09 \cdot 10^{-5} \cdot \mathrm{T}^3 + 5.14 \cdot 10^{-4} \cdot \mathrm{T}^2 - 4.35 \cdot 10^{-3} \cdot \mathrm{T} + 0.198 \;\; (\mathrm{r}^2 = 0.981) \tag{3.17}$$

$$\beta = 8.22 \cdot 10^{-6} \cdot \mathrm{T}^3 - 3.85 \cdot 10^{-4} \cdot \mathrm{T}^2 + 3.39 \cdot 10^{-3} \cdot \mathrm{T} + 0.797 \;\; (\mathrm{r}^2 = 0.987) \tag{3.18}$$

Since the RFID chip included in the system has an internal temperature sensor which is able to measure temperatures from -40 to 60 ºC, with an accuracy of 0.5 ºC, the thermal drift can be determined and compensated using these equations.

For each measurement, the prototype obtain the data temperature from the RFID sensor in order to determine the thermal drift for each case and correct that effect using the corresponding equations.

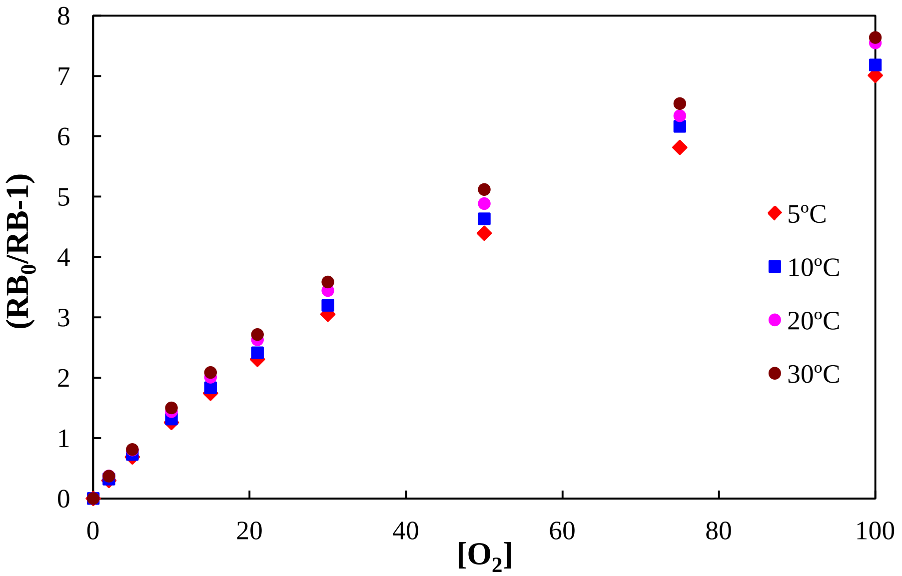

Figure 3.24 Temperature dependence of the system.

3.4 Conclusions

In this chapter, two different portable instruments have been described and studied. Firstly, a portable optical multianalyte instrument with twelve sensing modules has been presented and used for the determination of pH in a solution. The analytical procedure consisted of the determination of the colour variation of eleven sensing elements, or four elements after a minimization process, in order to relate the hue coordinate of the HSV colour space with the pH. The designed equipment had a simple but versatile electronic design where an OLED display acted as programmable light source, twelve digital colour detectors generated a digital output which quantified the incident light, and a microcontroller carried out the processing of the data in order to obtain the hue value from the RGB coordinates provided by the detector. The result is easy-to-use compact equipment, designed using simple electronics components, that provides a simple user interface and it is capable of give a reliable measurement of pH in few minutes. Here, in section 3.2.4, a complete analytical and technical characterization has been performed and it can be seen the high degree of concordance between the pH of the solution and the pH estimated by the portable instrument.

This approach was improved by the use of artificial neural networks to optimize the pH calculation to be implemented in the microcontroller. Using the hue value of each sensing element as an input for the neural network and a layer of hidden neurons, the pH of a solution was predicted. With this purpose a multi-objective NN calibration procedure using the NSGA-II algorithm was designed in order to minimize the computational cost of the prediction models applied in the microcontroller, maximising the accuracy and minimising the number of sensing elements of the array.

In section 3.3, a novel design of a RFID tag for the measurement of gaseous oxygen is presented. This system is oriented to monitor the oxygen present in smart packages for food, since the tag is printed in a flexible substrate which can be easily attached to the package envelope. The used material is PEN, where by means of screen printing and silver ink the tracks between components are printed. The sensing membrane is placed on the inner surface and the circuitry is located on the outer side. This system includes a RFID chip for data transmission that also allows the operation in active and passive mode, as an internal regulator is able to provide the current needed for the whole system obtaining the power supply from the electromagnetic field of a commercial RFID reader. In this section a fully characterization of the response of the system as well as the response of the antenna has been explained, taking into account the possible variations due to the temperature and other parameters like the integration time.

In Table 3.9, a summary of the main characteristics obtained with the described systems is presented. As it can be seen, the accuracy and the power consumption in the measurement of pH were substantially improved using ANN to optimize the algorithm. In the case of the measurement of the concentration of oxygen low values of resolution, accuracy and LOD were obtained. These results are suitable for smart packaging applications where the food is sealed in low concentrations of oxygen.

Table 3.9 Summary of the main features for the instruments using digital colour sensors.

Instrument		**Resolution**	**Accuracy**	**LOD**	**Power consumption**
pH		0.02	0.2	----	5 mA (standby mode) 200 mA (sensing mode)
pH (neural networks)		0.02	0.06	----	5 mA (standby mode) 90 mA (sensing mode)
Gaseous oxygen	2%	0.31 ppm	0.01%	55 ppm	34.4 µA (standby mode)
	21%	3.86 ppm	0.08%		3.55 mA (sensing mode)

All the results presented in this chapter confirm the possibility of employing digital colour detectors as a tool in the field of the optical chemical sensors. It has been proved the reliability of colour and luminescence detection in comparison with other traditional systems such as photodiodes, scanners, CCD cameras or potentiometric methods for the determination of pH. Here, portable instruments for the measurement of O_2 and pH have been presented, but other kind of optical sensors could be analyzed using the same principle.

The study of some parameters related with the determination of the colour coordinates has been explained, such as the integration time or the active area of the digital colour detectors or the intensity of the light source. They should be configured depending on the final purpose of the application. Thus, for example, in the case of oxygen measurement it will be necessary to increase the integration time to obtain maximum resolution, or decrease that time for applications that need faster response. Besides, in this chapter a study of stability for the different used light sources has been carried out since the illuminant must be stable enough to provide reliable results not affected by the own variations. Also, the external light conditions must be controlled in order to avoid interferences in the calculation of the coordinates.

Contributions

Martinez-Olmos A, Capel-Cuevas S, Lopez-Ruiz N, Palma AJ, de Orbe I, Capitan-Vallvey LF (2011) *Sensor array-based optical portable instrument for determination of pH.* Sensors and Actuators: B. Chemical 156, 840-848.

Capel-Cuevas S, Lopez-Ruiz N, Martinez-Olmos A, Cuellar MP, Pegalajar MC, Palma AJ, de Orbe-Paya I, Capitan-Vallvey LF (2012) *A compact Optical Instrument with Artificial Neural Network for pH Determination.* Sensors 12, 6746-6763.

Martinez-Olmos A, Fernandez-Salmeron J, Lopez-Ruiz N, Rivadeneyra-Torres A, Capitan-Vallvey LF, Palma AJ (2013) *Screen printed flexible radiofrequency identification tag for oxygen monitoring.* Analytical Chemistry 85, 11098-11105.

Capel-Cuevas S, Ariza-Avidad M, Martinez-Olmos A, Lopez-Ruiz N, de Orbe-Paya I, Palma AJ, Capitan-Vallvey LF. *Sensor array-based colorimetric portable instrument for pH determination in different matrices.* 16th European Conference on Analytical Chemistry EUROANALYSIS 2011 (Belgrade, Serbia 11-15 September 2011).

Chapter 4. **Micro-camera systems**

4.1 Introduction

In this chapter two different portable instruments using a CMOS micro-camera as colour detector are presented. This micro-camera module uses an OmniVision CMOS VGA colour sensor whose details will be explained below. The camera module allows to work either in JPEG or raw formats for the pictures. The raw format permits a direct treatment of the data provided by the CMOS colour sensor without need of decoded algorithm and, therefore, it is suitable for systems where information is required in short time.

As mentioned in the second chapter, CMOS sensors offer lower response time as well as lower consumption in less size than in the case of CCD sensors. For these reasons, the CMOS micro-camera module is suitable for the development of portable instrumentation as the prototype here presented.

The first developed system is used for determination of gaseous oxygen concentration. In this case, a UV LED excites a PtOEP sensing membrane in the same way as explained in section 3.3 but, instead of using a digital colour detector, the luminescence emitted by the sensing element is captured using the CMOS micro-camera. The final prototype is enclosed in a black box where the support with the sensing membrane is placed in order to avoid the influence of external light. After image processing of the taken picture, the concentration of the surrounding oxygen can be determined. The user interface is a touch micro-LCD that has an on-board memory card adaptor for data storage and allows to show the results of the processing as well as the picture. A complete characterization and calibration of the system is presented taking into account temperatures and time drifts.

Secondly, a portable instrument to measure the concentration of different heavy metals in solution using an optical colorimetric sensor array is presented. In this case, eight sensing membranes placed in a plastic support change their colour with regard to the concentration of certain metals contained in a sample when they are in contact. The micro-camera captures a picture of the array, and after image processing carried out by a microcontroller, the hue value is obtained and related to the corresponding metal concentration. This work is still under study as detailed in the corresponding section.

4.2 Portable system for oxygen measurement

The measurement of gaseous oxygen is a field of increasing interest in areas such as environmental and life sciences, food packaging or health care. The use of optical sensors in these areas is also a growing trend since they present some advantages over the electrochemical sensors used until now like the facility to miniaturize them, simplicity of use, as well as they are low cost sensors that provide a high sensitivity and reversibility without suffering electrical interference or oxygen consumption (Wang *et al.* 2010a).

The combination of the advantages of luminescence and absorption-based sensors has carried out to a new approach whose principle consists of the measurement of the colour or the intensity of the luminescence emitted by the optical chemical sensor. Therefore, this approach has been used for the determination of concentration of dopamine, tripropylamine and proline using a CCD camera (Lin *et al.* 2009); for the measurement of multiple optical sensors, such as temperature and carbon dioxide, using a signal separation algorithm in CCD and CMOS cameras (Stich *et al.* 2009); or for the analysis of potassium, magnesium or conventional pH strips using a conventional digital camera (Lapresta-Fernandez and Capitan-Vallvey 2011), among others. Several works have been carried out using the same approach for oxygen sensing. Most of them use CCD cameras in order to capture an image of the sensor in microfluidic environments (Ungerbock *et al.* 2013) or using a LCD as light source (Park *et al.* 2012); although CMOS sensors have been also used for the same purpose (Shen *et al.* 2011). Besides, a comparison between the measurement of luminescence intensity and decay time for determination of oxygen using a CCD camera has been reported (Liebsch *et al.* 2000).

In section 3.3, a RFID tag for determination of the concentration of oxygen applied to smart packaging was presented. Here, the detection is carried out using a CMOS micro-camera module. A picture of the emission produced after the excitation of the sensing membrane is taken and, after image processing, the red component of the intensity is related to the oxygen concentration. Therefore, the basis of this instrument is quite similar to the used in the RFID tag, changing the detection method from a digital colour detector to a CMOS micro-camera but using the same PtOEP complex.

4.2.1 Membrane preparation

The sensing membrane was prepared by casting 15 µL of the cocktail containing the PtOEP complex on a quartz crystal used as support using a spin-coating technique under ambient atmospheric conditions. The reagents used for the preparation of the sensing PtOEP cocktail were detailed in section 3.3.2. The crystal has 44 × 12.5 × 1.25 mm of dimensions which are smaller enough to be placed in front of the micro-camera with the aim of focusing the whole sensing membrane. After the membrane deposition, the quartz crystal was kept in darkness to leave dry in a THF atmosphere for one hour. The result of this procedure was a sensing membrane homogeneous, transparent and pink. As aforementioned, this kind of membranes must be cured in darkness for 9 days before their use.

4.2.2 Description of the prototype

The handheld device presented in this section provides a measurement of the concentration of gaseous oxygen by measuring the intensity of the emission generated by the sensing membrane after excitation with a UV LED. The emitted intensity is quantified using the red component of the RGB colour space which is obtained from the processing of a picture of the luminophore captured with a micro-camera module during the excitation.

The instrument uses a microcontroller model PIC18F2550 from Microchip (Microchip Technology Inc., USA). This microcontroller is a low cost device with an integrated USB module that has been used with calibration purposes to connect with an external PC and processing the information during the calibration procedure. The microcontroller has 3 input/output ports and requires a 5 V power supply that can be provided by a PP3 battery, an USB connection during calibration process or an AC/DC external adaptor.

The design of the prototype includes a touch LCD screen model µLCD-32PT (SGC) from 4DSystems (4DSystems, Australia) in order to show both the image taken by the micro-camera and the results after the measurement procedure and to act, as well, as user interface. The inclusion of this device avoids the need of using external element to handle the instrument. The module is a low cost display with 56 × 77.6 × 3.7 mm of size and 3.2' diagonal that offers 240 × 320 QVGA of resolution and allow to select up to 65.000 possibilities of colours since it integrates a 4-wire resistive touch panel. The display uses the latest thin-film transistor (TFT) technology and it also incorporates an embedded PICASO-SGC serial graphics controller. The communication with the microcontroller is carried out via serial port and, besides, an on-board micro-SD memory card adaptor allows data storage. The PICASO-SGC is a graphics controller that permits to use powerful graphics, as well as, texts, images and even animations.

The portable instrument uses a micro-camera as detector system. The selected model, shown in Figure 4.1, was a µCAM-TTL Serial JPEG Module from 4DSystems (4DSystems, Australia). This camera is a low cost and low powered module, with reduced dimensions of 28 × 32 mm, that makes it suitable for this kind of portable applications of small size. It is possible to encode the captured pictures either in raw or JPEG formats since it incorporates a JPEG compression chip, as well as selecting different colour or grey resolutions or picture sizes. In the same way that for the touch screen, there are several predefined instructions for the communication between the camera module and the microcontroller, or the micro-camera and the LCD screen, which is made via serial interface. When a raw picture is required from the micro-camera, the corresponding image information is sent in an only package. The microcontroller here used is not faster enough to receive the packet, processing the information of each pixel and send it to the LCD to show it while is receiving more data. Therefore, the picture information is then sent directly to the LCD display. Since the images are taken in raw format, there is no need of decoding algorithm over the picture and direct communication between the touch screen and the camera module can be done without using the microcontroller as intermediate. The fact of sending directly the picture taken by the micro-camera to the LCD display avoids the need of using any external element for data storage. The colour information of each pixel in the picture is written in the corresponding pixel of the LCD screen, from where the microcontroller can read the coordinates pixel to pixel for carrying out the processing.

http://www.4dsystems.com.au/downloads/microCAM/uCAM/Docs/uCAM-Product-Brief-REV1.pdf

Figure 4.1 Micro-camera TTL serial module.

The micro-camera uses an OV7640 Colour CMOS VGA (640 × 480) sensor from Omnivision (Omnivision Technologies, California). This is a low voltage CMOS image sensor that uses a proprietary sensor technology in order to reduce the electrical source of noise, such as smearing or fixed pattern noise in the picture by improving the quality of the final image. The CMOS sensor carries out process of image quality taking into account some factors like hue, colour saturation, gamma, or sharpness. For this purpose, the micro-camera was configured to provide a raw picture of 16-bit of RGB resolution, namely without compression, in order to avoid the need of decompression algorithms for obtaining the coordinates of interest. The format used by the camera module is RGB565, which means that 5, 6 and 5 bits are used for red, green and blue components respectively. In this kind of devices where the light is captured, the green coordinate is usually encoded with more bits per pixel in order to imitate the behaviour of the human eye, which is more sensitive to the green than the red or blue components. Since there is no compression of the obtained colour information, every single pixel can be written directly on the touch LCD with no need of decoding algorithms carried out by microcontroller. Although using raw format the picture information is heavier than using JPEG format, this avoids the need of using data storage for further processing of the image and, also, direct communication can be done between the components of the design. Therefore, raw format is still suitable for applications that need real-time information.

Both elements, the LCD display and the CMOS camera module, transmit and receive information to the microcontroller and between them using the serial port. To allow intercommunications between the three components, two digital multiplexors were included in the design of the prototype. The multiplexors, model CD74HCT157 from Texas Instruments (Texas Instruments Incorporated, USA), were connected as shown in Figure 4.2. Firstly, the microcontroller turns on the LCD screen, and after, it sends commands to the micro-camera to set the parameters of the picture to take. When the micro-camera is ready for the transmission of the image information, the communication with the screen is established to send directly the picture between them. Therefore, as it can be seen in Figure 4.2, the LCD screen needs to share the serial bus of reception with the microcontroller, to receive instructions for turning it on, and with the micro-camera, to receive directly the information of the taken picture (solid lines). On the other hand, the bus of reception of the microcontroller needs to receive data from the camera and the LCD screen (dotted lines). These interconnections are managed by using multiplexers which modify their control inputs to select the corresponding connection each moment.

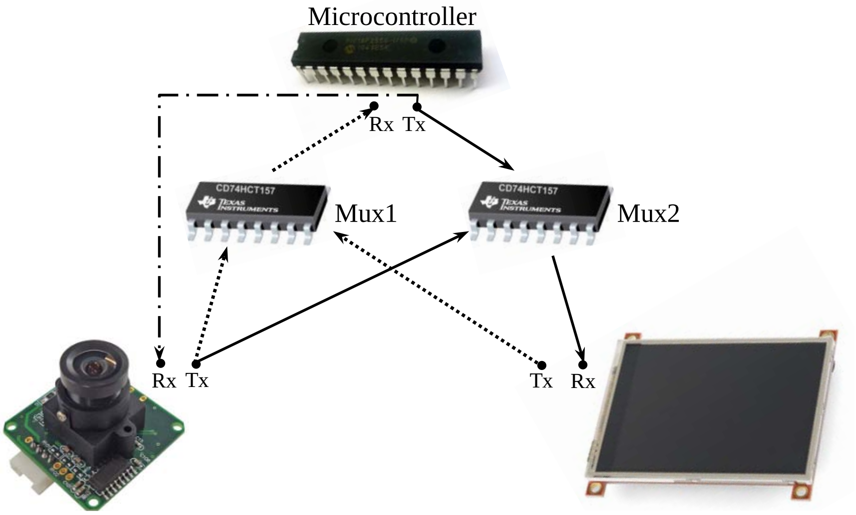

Figure 4.2 Diagram block of connections using multiplexors.

The sensing module of the instrument, shown in Figure 4.3, is composed of an UV LED to excite the luminophore and the colour micro-camera to capture the intensity of the luminescence emitted by the sensing membrane. As it can be seen in the figure, the PtOEP complex is deposited on one side of a thin crystal quartz and it is placed facing the micro-camera. This support was chosen since the crystal quartz is transparent throughout the ultraviolet, visible and near infrared regions (Skoog *et al.* 2007). The LED is situated at the short end of the crystal and very close to the edge to avoid the dispersion of the radiation before it reaches the crystal. The main objective of this configuration is that the quartz crystal acts as a waveguide and not only as support for the luminophore avoiding the direct influence of the light source, and the saturation, in the micro-camera sensor. Otherwise, if direct alignment between these three elements had been configured instead, overexposed regions in the picture could appear. When the LED is biased, the optical radiation reaches the sensing element through the crystal and the emission produced by the excited membrane is captured taking a picture with the micro-camera. The radiation that reaches the luminophore is enough to cause a steady-state excitation of the membrane that produces an emission in the red region of the spectrum with a maximum at a wavelength of 645 nm.

The distance between the luminophore and the micro-camera is not critical, since the lens of the camera can be focused in a relative extensive range of distance. In this prototype, the distance was set to 0.7 cm in order to capture a picture of the whole membrane covering the maximum number of pixels of the photograph. In this way, a higher number of pixels are available to be processed to extract the red component information, which corresponds to the intensity of luminescence as it is later explained.

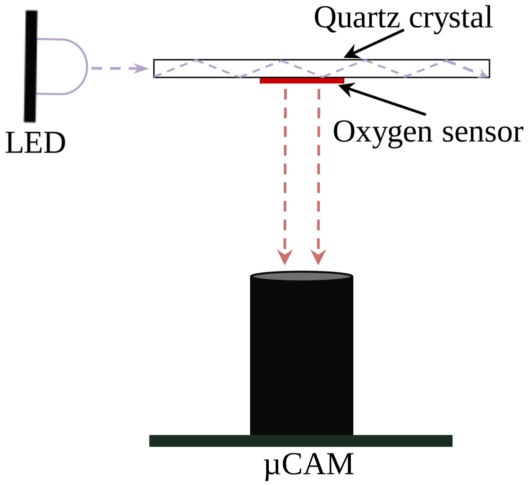

Figure 4.3 Sensing module of the portable device for determination of the oxygen concentration.

To correct the thermal drifts produced due to the dependence of the intensity of the luminescence emitted by the sensing membrane with the temperature, a DS1624 temperature sensor from Maxim (Maxim Integrated, USA) was included in the design. The temperature resolution offered by this sensor is 0.03125 ºC and it is able to measure temperatures from -55 ºC to 125 ºC. The thermometer provides a 13-bit word to indicate the temperature, which is sent to the microcontroller via two-wire serial communication.

All the connections between the elements placed in the design are shown in Figure 4.4. The connections of the microcontroller with the multiplexors, the micro-camera module, the LCD screen or the temperature sensor are indicated. Also, the USB connection is pointed out, since for calibration purposes the prototype was supplied using this port instead of a PP3 battery.

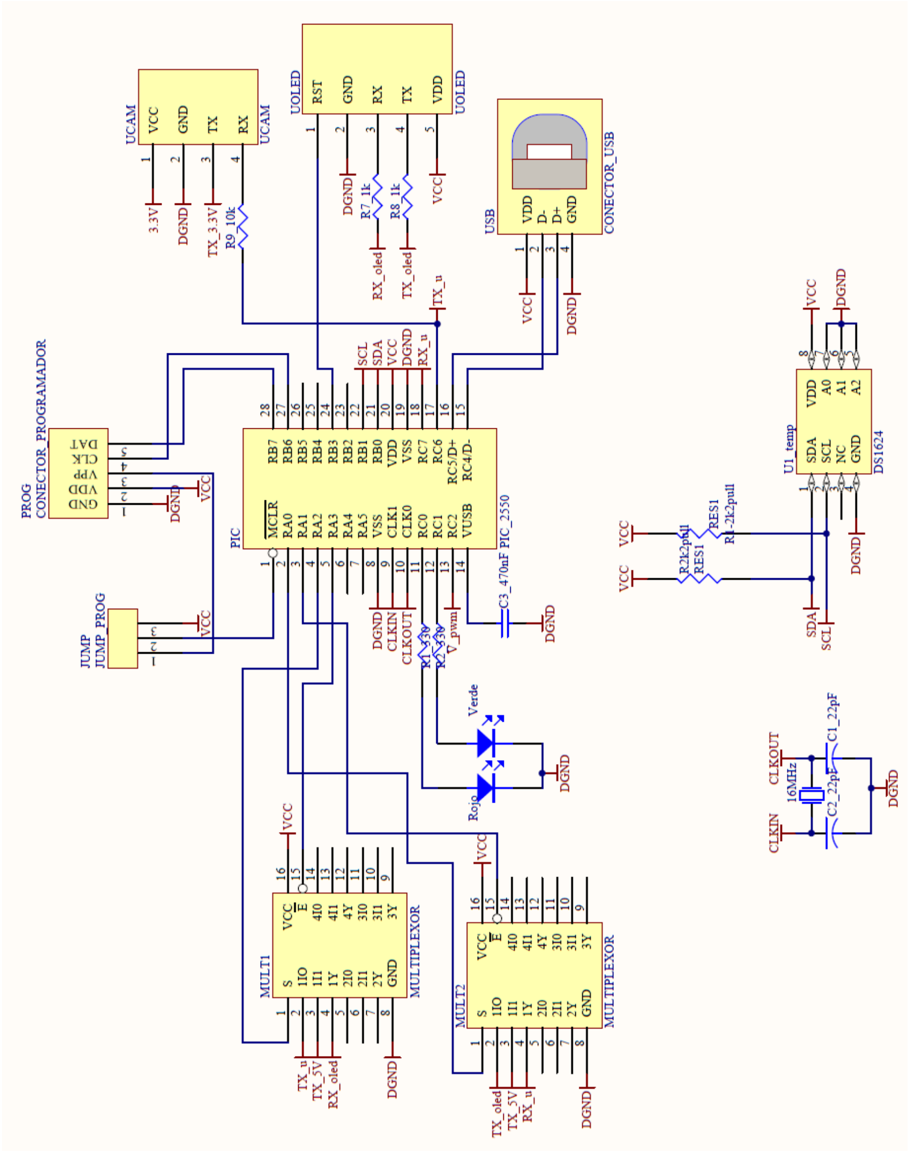

Figure 4.4 Scheme of connections in the developed prototype.

The intensity of the luminescence depends of the surrounded gaseous oxygen as a consequence of the quenching of the PtOEP complex luminescence. Since the emission of the membrane is placed at 645 nm, the information relative to the O_2 surrounding oxygen can be obtained by measuring the red component of the luminescence under stable conditions (Park *et al.* 2010). As shown in Figure 4.5, the value of the red component decreases when the concentration of gaseous oxygen is increased. To obtain a reliable measurement of the red component, before the capture of the picture, the sensing membrane must be activated at least 30 seconds, since the phosphorescence emission intensity of the PtOEP complex undergoes a transient characterized by a rise in the time from 10 to 30 seconds (Papkovsky 1993), (Vargas-Sansalvador *et al.* 2011b). After this time of delay, the membrane is in a stable state and the picture can be taken to be sent to the LCD screen where is stored pixel-by-pixel for further processing. This time must be kept constant for all the measurements, since an increasing in the time between the activation of the LED and the photograph produces an increasing of the temperature that affects to the intensity of the luminophore as it will be described below.

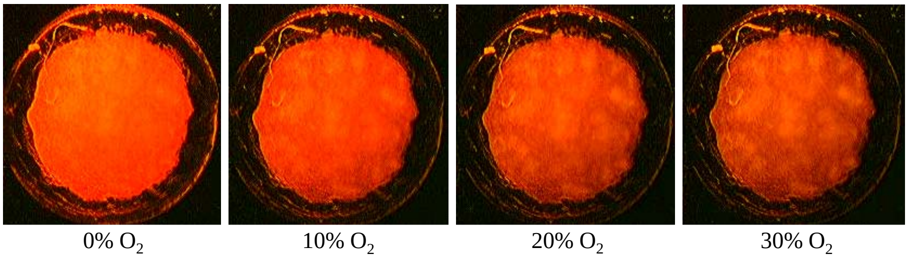
0% O_2 10% O_2 20% O_2 30% O_2

Figure 4.5 Pictures taken with the micro-camera at different concentrations of O_2.

An external picture of the developed prototype is shown in Figure 4.6. It can be observed the transparent and pink coloured sensing membrane that has been placed outside the instrument after the capture of the picture, which is shown in the LCD screen. Since the LCD acts as user interface, it allows to the user select manually the area of interest of the membrane to be processed, thus discarding the defectives regions or the edges where the membrane is not so homogeneous. Once the area is selected, the microcontroller reads the colour information of the pixels inside that region pixel by pixel directly from the LCD screen. Only the red component of the RGB coordinates is taken into account in order to calculate the statistical mode of this value (Cantrell *et al.* 2010) to be related to the concentration of oxygen. Therefore, the concentration of oxygen at ambient conditions can be determined obtaining the value of the R coordinate in the selected area of the image, which is a quantification of the intensity of the luminescence.

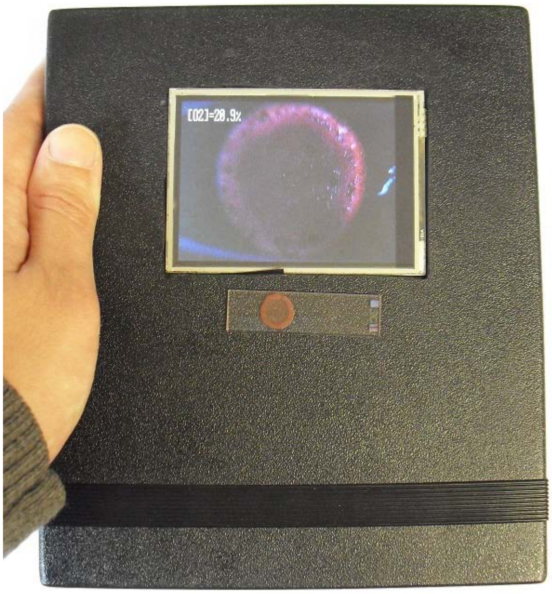

Figure 4.6 External photograph of the portable instrument at ambient oxygen concentration.

4.2.3 Results

As mentioned before in section 3.3.5, the PtOEP complex presents two peaks of absorption at 380 nm and 535 nm. Although several works have been carried out using a green light to excite the membrane (Martinez-Olmos *et al.* 2011b), (Palma *et al.* 2007a), (Vargas-Sansalvador *et al.* 2011a), here, a UV LED was chosen with maximum emission at 380 nm. As the peak of emission of the UV LED is not in the visible region of the spectra, there is no interference of the light source in the picture captured by the micro-camera. The UV LED is biased using a stable configurable current source that produces an output between 6 and 120 mA. The intensity of the radiation emitted by the LED was configured taking into account two conditions: firstly, to maximize the output range of the measured red component to improve the resolution of the system and, secondly, to avoid the saturation of the image caused by an excess of emission from the overexcited luminophore. In this case, a current of 19 mA for biasing the LED is chosen which provides the maximum value possible of 31 units for the red component in absence of oxygen, since only 5 bits are used for the R coordinate.

System calibration

When the sensing membrane is excited with the UV LED, it generates a luminescence at 645 nm, which falls within the red region of the spectrum. Hence, when the micro-camera captures pictures of the luminophore at different oxygen concentrations is the red component of the image the coordinate that varies while the others (green and blue) remain constant and practically negligible due to the arrangement of the optical components. This method is more efficient than taking into account the whole RGB colour space, because less information is required and therefore the processing is faster and more effective. Although in the previous chapter the R/B ratio was used for the measurement of the intensity of the luminescence, here due to the arrangement of the components to avoid direct influence of the ultraviolet light source in the picture, there is no need of using the blue component to correct possible variations in the light emitted. Furthermore, the possible variations of light are reduced since the emission is not in the visible region of the spectra and the UV LED is biased using a current source which makes more stable the emission that in the previous prototype. Finally, as the resolution of the micro-camera is lower than the offered by the digital colour detector the emission of the light source is almost not detected in the picture.

The response obtained with the portable instrument was tested in the full range of oxygen concentration from 0 to 100%, using six replicas for each point at room temperature (21ºC). The measurements were taken under stable atmosphere conditions, waiting 2 minutes after the gas emission of the gas blender in order to equilibrate the instrument atmosphere. The results obtained are shown in Figure 4.7, and, as it was expected, the intensity of the red component of the luminescence decreases when the oxygen concentration increases in concordance with the photographs presented in Figure 4.5. This response can be fitted to a Freundlich isotherm equation for luminescence which models a non-linear Stern-Volmer behaviour as shown in Equation 4.1.

$$\frac{R_0}{R} - 1 = \alpha[O_2]^{\beta} \qquad (4.1)$$

Where R_0 represents the intensity of the luminescence in the absence of gaseous oxygen and • and • are fitting parameters.

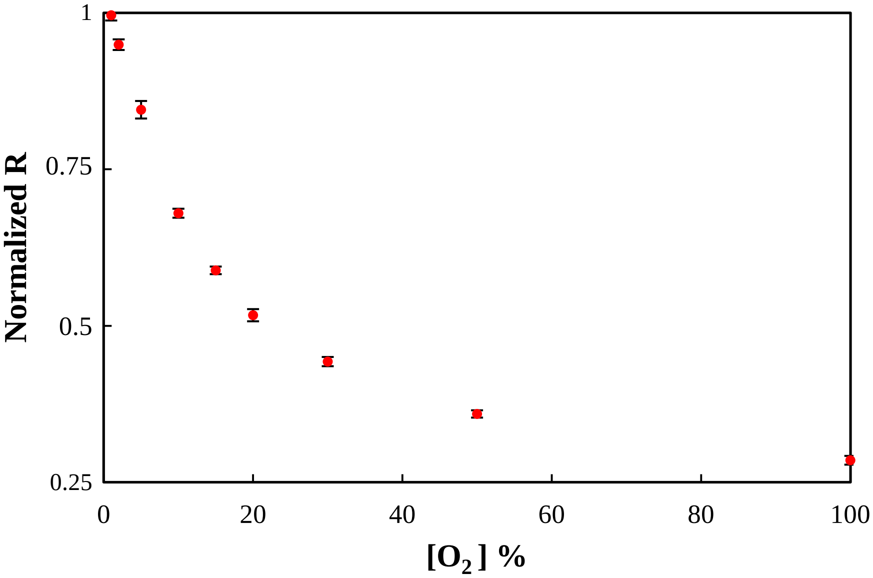

Figure 4.7 Response of the sensing membrane obtained with the red component provided by micro-camera.

The fitting parameters are considered to provide some information about the sensors. • is a measure of the heterogeneity of the system and the curvature of the Stern-Volmer curve and • is the K_{SV} of the Stern-Volmer equation (Douglas and Eaton 2002). For the response of the curve here obtained, represented in Figure 4.8 , • = 0.11 and •=0.647 with a correlation factor of $r^2 = 0.996$.

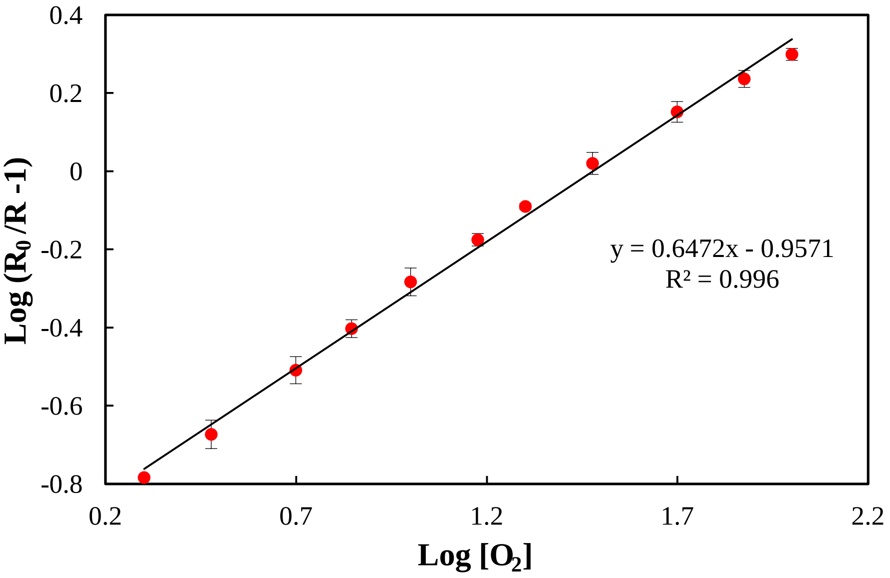

Figure 4.8 Calibration curve of the instrument.

These parameters describe the calibration curve obtained analyzing most of the area of the sensing membrane. However, a study of the influence of the analyzed area in the technical specifications of the instrument was carried out. This study allows to reach a trade-off between the time of response of the instrument and the responses obtained with different processed areas of the sensing membrane as well as study and improve the technical features of the prototype. The theoretical resolution of the portable instrument was obtained in the same way as explained in section 3.3.5 and using the Equation 3.12. In this case, I correspond to R coordinate and $\bullet I$ corresponds directly to $\bullet R$ which in this case is 1/32 since 5 bits are used for the red component by the CMOS sensor. As it can be seen in Table 4.1, the resolution has a low variation with the increasing of the analyzed area. On the other hand, the limit of detection was calculated using the criteria LOD $= y_b + 3s_b$, where y_b is the average blank signal and s_b is the standard deviation of the blank which was determined using six replicas. As observed in the table, the LOD improves with the size, and, therefore, the higher the area analyzed, the lower the limit of detection of the prototype.

Table 4.1 Theoretical resolution and LOD values for different analyzed areas of the sensing membrane.

Area (%)	Resolution (21% O_2) (ppm)	LOD (%O_2)
18%	1600	1.5
27%	1115	0.46
45%	1203	0.19
65%	941	0.20
73%	1045	0.09

Nevertheless, since the microcontroller needs a long time to processed an extensive area of the membrane due to the slow communication with the LCD screen, the processed area was reduced to a size of 40x40 pixels. This area corresponds with an 18% of the area of the membrane and it was chosen to covering the central region of the luminophore since the edges present non-homogeneities that could modify the measurement. With this configuration the resolution achieved was of 0.16% (1600 ppm) at 21 % of oxygen and the LOD was 1.5% of O_2. These values of resolution are higher than the provided by the RFID tag studied in the previous chapter: 0.31 ppm. The main reason of this variation is that the micro-camera offers 5 bits of resolution for the red component in contrast with the 12 bit used by the digital colour detector. However, the resolution reached in this case is better than in other works carried out in the group (Palma *et al.* 2007a). The accuracy was obtained as the standard deviation of the measurements also depends on the concentration oxygen, being 2.14% of variation in the measurement provided at 21% of O_2.

Finally, the stability of the system was studied taking measurements for 8 days every 3 hours at ambient oxygen. The data obtained show a time drift in the value of the red component of 0.038% per day of the full scale range which implies a drift of 0.035% per day in the measured oxygen. These values show a good stability of the sensing membrane since the response is not significantly affected by photobleaching (Papkovsky 1995).

Temperature dependence

As discussed in section 3.3.5, the temperature has an important influence on the intensity emitted by the luminophore at different oxygen concentrations (Papkovsky 1995). Therefore, this effect had to be taken into account and compensated using for this purpose the temperature sensor included in the design and previously described. A thermostatic chamber, whose main features are detailed in section 3.3.1, was used for carrying out the temperature calibration.

In Figure 4.9 the response of the instrument at different temperatures is shown. The curves were obtained using six replicas for each concentration of oxygen at a given temperature. As it can be seen, increasing in the temperature decreases the light intensity emitted by the sensing membrane causing a lower red signal. To consider this effect, a thermal dependence was included in the • parameter that can be expressed as a polynomial function of the temperature as shown below:

$$\beta = 3 \cdot 10^{-5} \cdot T^3 - 0.0023 \cdot T^2 + 0.048 \cdot T + 0.3978 \ (r^2 = 0.99), \quad (4.2)$$

where T is expressed in Celsius degrees. • parameter kept independent to the temperature, since it varies between 0.09 and 0.096 for different temperatures but with no tendency to be compensated. By including this model in the instrument the thermal drifts in the measurement were compensated by the microcontroller. Therefore, the microcontroller receives a measurement of temperature from the DS1624 sensor during the acquisition process of taking the picture of the membrane, and introduces the value in the • parameter to compensate the effect of the temperature in the emitted luminescence.

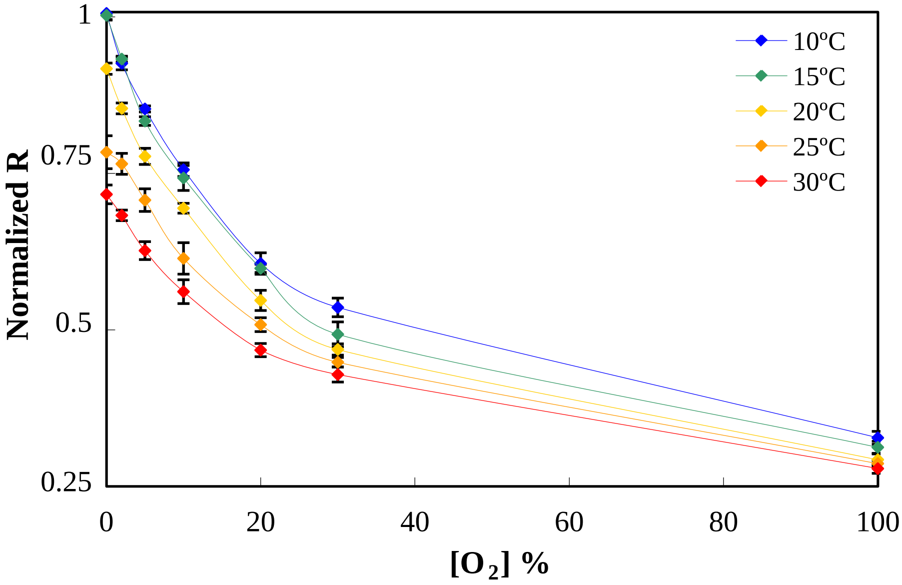

Figure 4.9 Dependence of the instrument with the temperature.

Hence, as observed during the section, the results obtained with this prototype show that poorer values of resolution and limit of detection are achieved than the provided by the RFID tag. As mentioned before, the main reason is the lower resolution offered by the micro-camera module. However, this system offers an advantage that it is worth to note. The digital colour detector was placed directly over the substrate where the sensing membrane was placed covering just a small area of the luminophore. In that case, if the sensing membrane presents any heterogeneity, such as a bad deposited region or photobleaching, in the region where the detector was placed, the measurement of oxygen could be significantly affected. Using the micro-camera module, a picture of a higher region of the surface of the PtOEP complex is taken, and since the statistical mode of the red component is used as a value of interest, the effects of the heterogeneities are removed from the final red coordinate used for determination of concentration oxygen. As it was studied, if the region of the sensing membrane analyzed increases, the LOD of the system is improved while the resolution remains constant. Therefore, if the time of response of the prototype is not a critical feature to optimize, lower values of oxygen could be determined

4.3 Handheld colorimeter for determination of heavy metal concentrations

The detection and determination of heavy metals have an increasing interest in the area of drugs analysis and control as well as in quality controls. Therefore, the employed methods have to been improved more and more in order to solve specifics problems that appear in pharmaceuticals and industrial production of medicines (Vukovic *et al.* 2007). The monitoring of heavy metal concentrations is an important field due to their effects in the environment or living organism. Particularly, the analysis in water samples of the presence of heavy metals have been an important issue in the recent years since thirteen transition metal ions have been listed by the Environmental Protection Agency (EPA) as priority pollutant (EPA, 1972).

With the purpose of analysis of water samples for determination of heavy metal concentrations, an optical sensor array has been used in this work. As explained before, the combination of non-specific or low selectivity sensors provides an analysis of several analytes using a reduced number of sensors. Since the conventional approaches for multi-analyte using specific sensors require a large number of sensor which increase proportionally to the number of analytes, this kind of non-selective or high cross sensitive arrays are suitable for portable instruments where a reduce size is a requirement. In these arrays, the combination of signals obtained from each sensing element provides qualitative or quantitative information by means of some mathematical procedures, pattern recognition and/or multivariate analysis (Vlasov *et al.* 2005), (Ciosek and Wroblewski 2007), such as artificial neural networks (Cuellar *et al.* 2011). Besides, the use of disposable sensors allows to obtain a good robustness of the sensor, as mentioned in section 2.3. Most of the chemical sensor arrays are used in the field of food, beverage, environmental and pharmaceutical analysis (Ciosek and Wroblewski 2007). The analysis of optical sensor arrays is carried out mostly with CCD cameras or scanners using different colour spaces, such as the RGB. In this work, the hue value of the HSV colour space is used since previous studies of our group have demonstrated higher stability and repeatability for this component (Cantrell *et al.* 2010).

A portable instrument for the measurement of heavy metal concentrations is presented in this section. The instrument configuration presented in this section is based on an array containing membranes with non-selective chromogenic reagents, namely two types with PAN and Zincon, as a disposable optical tongue for the identification and quantification of mixtures of Zn(II), and Cu(II). The sensing polymeric membranes work by complexation with the immobilized chromogenic reagents through a co-extraction equilibrium that produces intense changes in colour working as bitonal sensors (Vukovic *et al.* 2012). The disposable array sensor is inserted in the device facing a CMOS micro-camera that captures a picture of it after the submersion in a solution of unknown metal concentrations. The processing of the picture, which is carried out by the microcontroller, provides the colour information of interest, in this case the hue value of the sensing elements, in order to relate them with the concentration of different metals presented in a solution. This device avoids the need of external processing using a PC, simplifying the procedure of analysis and providing in-situ information of the water samples. The results of the procedure, i.e. the concentration of metals, are shown in a touch micro-LCD screen which also acts as user interface.

4.3.1 Reagents, apparatus and software

The chromogenic reagents used for the preparation of the array were 1-(2-pyridylazol)-2-naphthol (PAN) and 2-carboxy-2'-hydroxy-5'-sulfoformazyl-benzene monosodium salt (Zincon (ZIN)) from Sigma. The amounts of polymers, reagents, plasticizers and lipophilic salts were optimized in order to immobilize the reagents with the conditions of no leaching, non-selective behaviour and change of colour of the reaction. For characterization of the sensing films, individual membranes were prepared by using spin-coating technique from the cocktails containing the reagents in THF or in ethanol. Working standard solutions of Zn(II) and Cu(II) ($100\ \mu g \cdot mL^{-1}$) were prepared by diluting the standard stock solution of each metal (1000 μg · mL^{-1}) with concentrated HNO_3, all from Sigma (Ariza-Avidad *et al.* 2013). By dilution with water the lower concentrations solutions were obtained. All chemicals were of analytical-reagent grade, and reverse osmosis-purified water (Milli-RO12 plus Milli-Q station, Millipore) was used throughout.

The support to place the cocktails is similar to the explained in section 3.2.2, but in this case it counts only with 8 holes, since the micro-camera has a reduced visual field and the number of sensing elements that could be captured in the picture is lower than in the case of the pH instrument. Since only two different membranes were prepared for this purpose, 4 holes for each one were used in order to have replicates of the measurements. The Mylar support was covered by an adhesive and black PVC layer. For each sensing element, 8 μL of the corresponding cocktail were cast.

The optical spectra were measured using a mini-spectrometer RC series C11007MA (Hamamatsu Photonics, Japan) with 256 pixels, spectral resolution at 9 nm half width and 16 bits of intensity resolution. For the electrical characterization of the prototype a mixed signal oscilloscope (MSO4101, Tektronix, USA) and a 6½ digit multimeter (34410A, Agilent Technologies, USA) were used.

For comparison of the instrument designed with a commercial device a commercial scanner ScanMaker i900 (Microtek, Taiwan) was used, whose features are described in section 3.2.1. The software to manage the scanner was Silver Fast Ai provided by Microteck. The images were processed with a set of scripts and functions developed by us in Matlab r2010b (The MathWorks, Inc, USA). For general and statistical calculations Microsoft Excel (Microsoft Corp., USA) was used. And, finally, for the implementation on a computer of a configurable user interface used only with calibration purposes, Microsoft Visual Basic 6.0 (Microsoft Corp., USA) was used.

4.3.2 Description of the instrument

The portable instrument presented in this section is a microcontroller-based system that allows to calculate the hue value of the sensing elements of an array from an image captured with a camera module integrated in the design. The colour information is used to determinate the concentration of metals in a solution where the sensor array was immersed. A general scheme of the prototype is shown in Figure 4.10. As it can be seen, the design is quite similar to the used for measurement of oxygen concentration except for the arrangement of the sensing module and the temperature sensor, which is not included in this case. Also, it is worth to be noticed that in this case the sensor array has eight sensing membranes, whose processing after the reaction process has to be carried out by the microcontroller.

The system uses a microcontroller model PIC18F2550 from Microchip (Microchip Technology Inc., USA), a touch LCD screen, which shows the results and acts as user interface and data memory of the picture, and the micro-camera module responsible for the capture of the image of the sensor array. The main features and settings of these components of the design have been discussed in section 4.2.2. When the picture is taken, it is shown on the screen where the user can select manually the membranes to analyze, thus discarding defective membranes of the array. Here, due to the size of the sensor array, the distance between the camera and the array is higher than in the previous case, therefore another factor must be taken into account. The camera module includes a built-in lens that produces a distortion of 120 degrees in the final picture. The higher the distance between the array and the camera, the higher is the distortion. This factor has been tested as later explained and it does not have influence in the hue parameter studied for each sensing element of the sensor array.

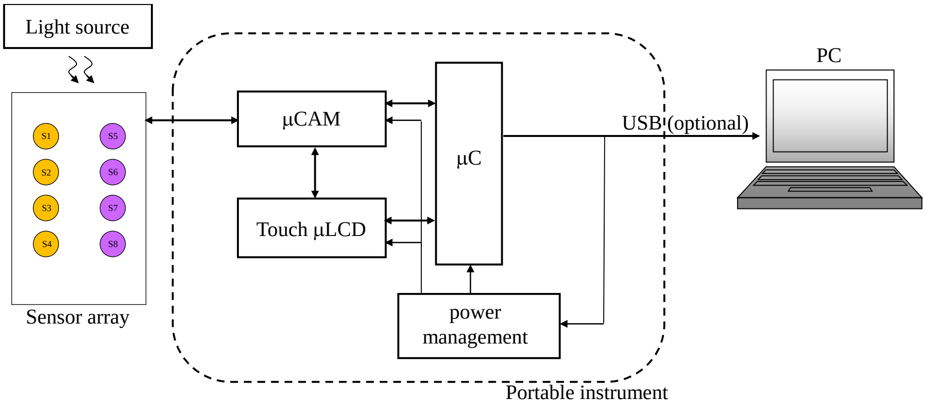

Figure 4.10 Diagram block of the instrument developed.

In Figure 4.11 an internal photograph of the final prototype is shown. In the top left of the figure, two multiplexors were placed in order to control the communication between the microcontroller, the micro-camera module and the LCD screen, since the port used by these components was the serial port. With the control inputs of the multiplexors, the connections could be selected according to the required operation, and, therefore, there were no interceptions between them. This system also permitted to send directly data from the micro-camera to the LCD screen, avoiding the need of external storage since the colour information of each pixel is saved on the corresponding pixel in the screen.

Figure 4.11 Internal view of the prototype.

At the bottom of Figure 4.11, it can be observed the micro-camera module, which is surrounded by four Moonstone ½W white diffuse LEDs from Avago (Avago Technologies, Singapore) that act as light source. The spectra of the four LEDs were measured having two main components at 450 and 550 nm as shown in Figure 4.12. The LEDs are positioned in order to have an angle of 45 degrees with respect to the sensor array positioned horizontally facing the micro-camera. In this way, the emission of light of each LED reaches the optical sensor array but do not interfere directly with the micro-camera, thus avoiding the saturation of the picture by an excess of illumination.

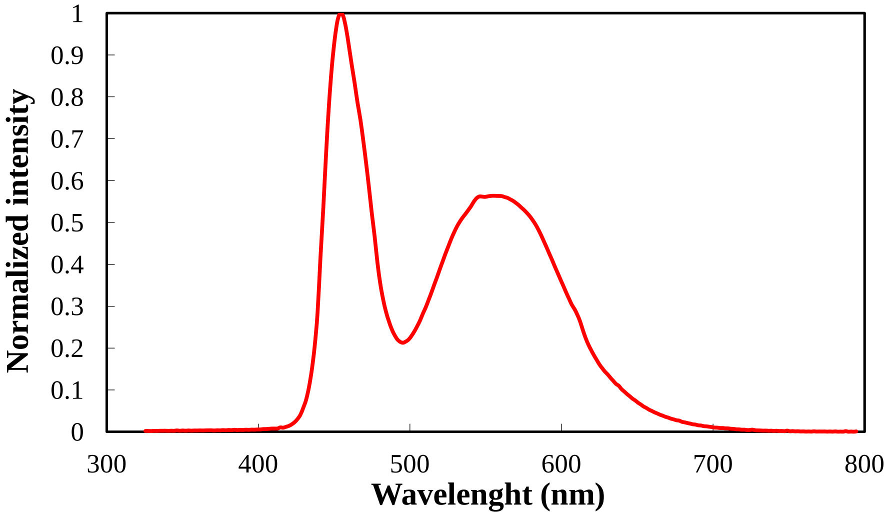

Figure 4.12 Spectrum of the white LEDs used as light source.

The determination of the heavy metal concentrations is carried out from image processing of a picture of the optical array sensor taken with the micro-camera. Since the prototype is enclosed in a black box, external illumination to take the picture is needed. The light source used to act as illuminant during the measurement process will be discussed in the section below, showing different alternatives that were tested in order to improve the results of the prototype.

To proceed with the measurement, the optical sensor array, with each one of the sensing element covered by the corresponding cocktail, is immersed in a solution with unknown concentration of metals. After 15 minutes of immersion the reaction has completely occurred (Ariza-Avidad *et al.* 2013). Then, after drying carefully the sensor array, it is placed in the instrument facing the micro-camera and the user starts the capture process by using the touch LCD screen. The captured image is shown directly on the display where the user can select the membranes of interest to be analyzed by touching on the screen and the hue value is obtained for each one. This option allows to discard defective membranes to avoid an erroneous value of concentration due to one amiss sensing element, as well as it makes the measurement independent of the position of the sensor array in the picture since the user determines the area of the sensing elements to take into account. After image-processing, the RGB coordinates of each sensing membrane are extracted from the data provided by the micro-camera and read from the LCD screen in order to obtain the hue value with a transformation between spaces as explained in section 2.2. The hue value of each kind of membrane is processed to be related with the concentration of the metals present in the solution where the sensor array was immersed. A mean value of the concentrations of every selected membrane is shown in the LCD screen as final value for the concentration of metals.

4.3.3 Results

In this section the results of different tests carried out with this prototype are exposed. Firstly, a study of the light source depending on the measurement mode, i.e. transmission or reflection mode, is performed. This determinates also the position of the optical sensor array in the device for taking the measurements. After that, the calibration of the portable instrument is presented using two metal ions for this purpose: Cu(II) and Zn(II). Here, the response of the membranes to the presence of each metal is carried out separately. Although the main objective is the study of solutions with unknown concentrations of a mixture of different metals, this final procedure of validation is currently under study since the sensing membranes are being improved by using inkjet print techniques. With this procedure the obtained optical sensor array will be smaller and more homogeneous providing a more suitable surface to be analyzed due to the lower resolution offered by the micro-camera module and removing the effects of the edges in the membranes in order to improve the results.

Light source

In a first approach, the sensor array was placed over a transparent surface situated on the cover of the portable instrument and facing the micro-camera. In that case the ambient light was used as light source as shown in Figure 4.13a. In order to avoid an excess of light, causing saturation and overexposure of the picture, a thin white film of PVC was positioned over the sensor array to act as intensity attenuator of the ambient light. The main problem here is that the pictures can be taken in many different environmental situations, which makes difficult the obtaining of similar results since the RGB coordinates can be different under different light conditions and, therefore, the hue value as well.

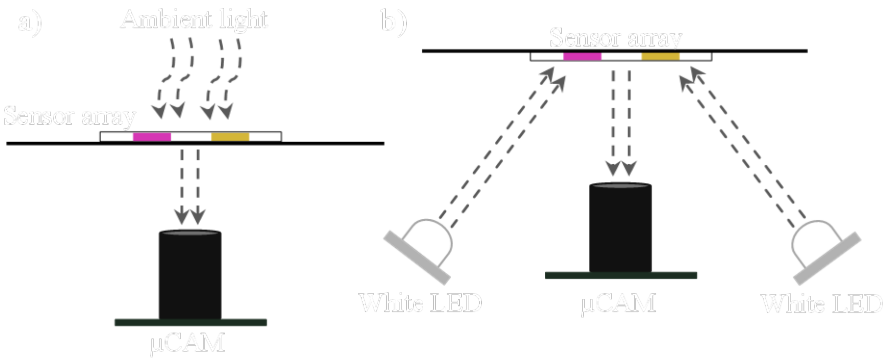

Figure 4.13 Different configurations of light source using a) ambient light and b) white LED as illuminants.

In order to avoid this effect, the second configuration shown in Figure 4.13b was tested. In this case the optical sensor array was placed inside the black box that contains the circuitry and four white diffuse LEDs were used as light sources, being positioned as shown in Figure 4.11. With this configuration the measurements were carried out under controlled conditions of illumination, simplifying the processing since there is no need of corrections due to changes in the light source.

A set of 7 plastic foils of different colours were tested to compare the hue component provided by a commercial scanner and these two described configurations. A script of instructions implemented in Matlab© was used to extract the coordinates from the scanned image (Cantrell *et al.* 2010). As it can be seen in Figure 4.14, there is higher concordance and lower variation with the results provided by the commercial scanner using the white LEDs as illuminant. The MSE obtained for the transmission mode is 0.02 while for the reflection mode is 0.001. For this reason, the second approach was used from this point to the end of the characterization of the system.

Once the configuration of the light source was determined, a set of 24 reference colour boards were used to compare the hue value of a wider range of colours using the scanner and the designed prototype. In Figure 4.15 the values of the H coordinate are shown for different colours, obtaining a MSE of 0.005 and a maximum error of 0.15 between the scanner and the prototype. As it can be observed, the colours are ordered in increasing hue value presenting the green and the purple regions higher mismatches than the others studied areas.

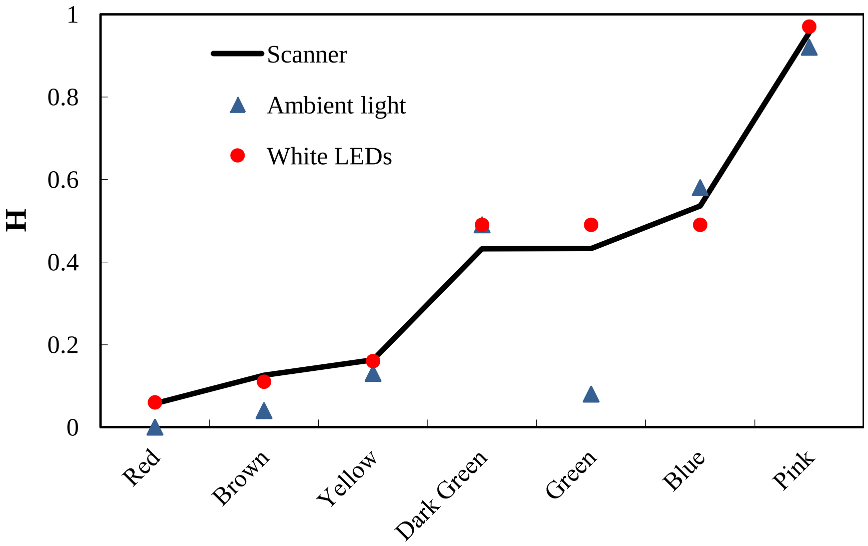

Figure 4.14 Comparison of the hue component obtained by transmission or reflection with a commercial scanner using colour plastics.

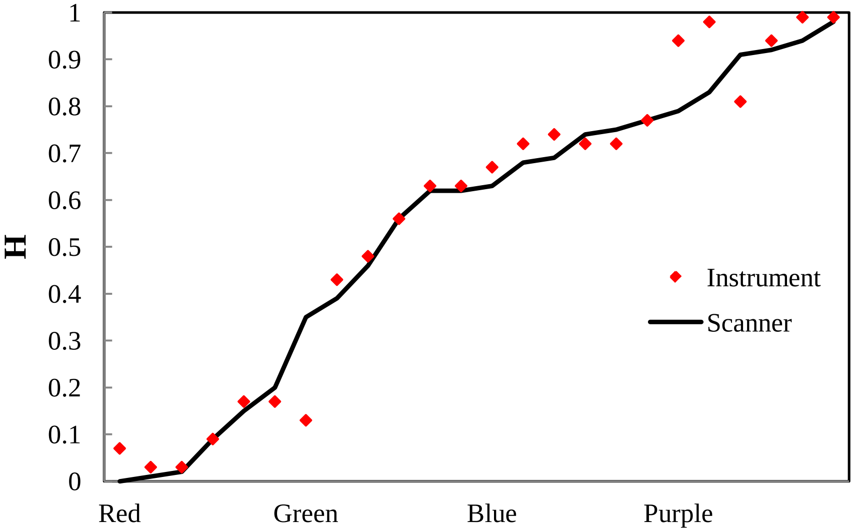

Figure 4.15 Comparison of the hue component for 24 coloured boards measured using the scanner and the prototype with white LEDs as light source.

Therefore, as it was expected, since the ambient light could have uncontrolled variations the results obtained were better for the reflection mode where four stable white LEDs were used as illuminants. The prototype then was placed inside a black box in complete darkness in order to avoid external influences of other light sources.

Heavy metals determination

The characterization of the optical sensor array for heavy metal determination was carried out with four replicates for each membrane, PAN or ZINCON, using solutions containing the metals ions in a range from 0.06 to 65 mg/l for each metal. Figure 4.16 shows the used sensor array in two different states. The solutions have a pH of 9.5, since in this range the metals present a more stable behaviour. As in previous studies, a comparison between a scanner and the response of the portable instrument was performed in order to compare the reliability of the prototype with a commercial device.

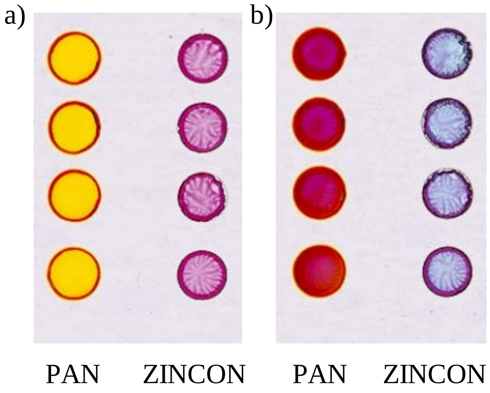

Figure 4.16 Sensor arrays used for calibration with two different sensing membranes: PAN and ZINCON, a) before reaction, b) after reaction.

In this work only the study of the response of the sensing membranes for each metal individually has been carried out. As depicted in Figure 4.17 and Figure 4.18, the response curves obtained with the scanner and the portable instrument have similar behaviour for both copper and zinc metal ions. However, there are some discrepancies caused by the different illuminants used in each device as well as the difference in the detectors. Besides, while the micro-camera offers 16 bit of resolution as much for the RGB coordinates (RGB565), the scanner provides from 24 to 48 bits of colour and, therefore, the range of possible colours detected by the scanner is wider and the determination of them is more accurate. Despite of these factors, the responses obtained with the camera module for each membrane are still acceptable, since the areas of interest of the curves vary between the same concentrations values in both equipments.

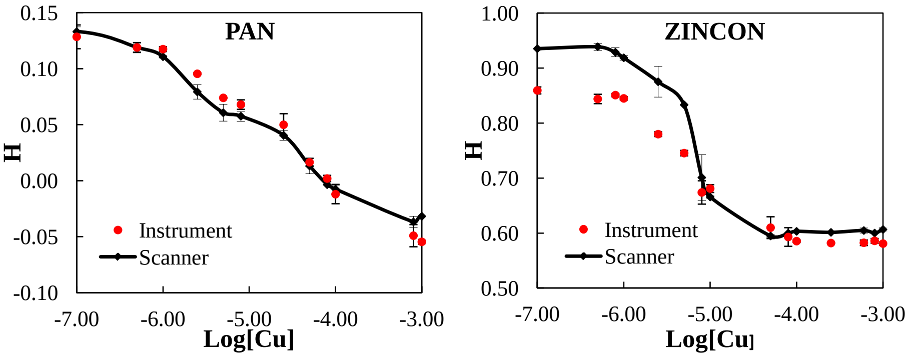

Figure 4.17 Response of the membranes in presence of copper.

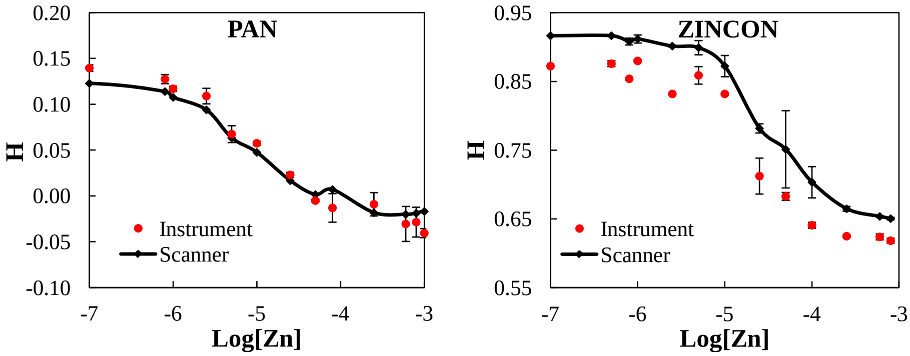

Figure 4.18 Response of the membranes in presence of zinc.

Since the lens of the camera module causes an angle distortion, the sensing elements placed in the extremes of the pictures suffer from a deformation in the photograph. Nevertheless, this loss of shape does not affect to the obtaining of the hue value, as observed in Figure 4.19.

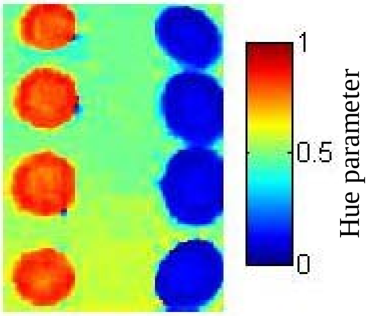

Figure 4.19 Distortion caused by the 120 degrees of the angle lens in the camera module.

With this prototype, the value of resolution achieved for the determination of heavy metal ions concentration is determined using the resolution of the hue component. For each sensing membrane and each heavy metal used, the resolution of the H component is determined by taking into account the range of variation depicted in

Figure 4.17 and Figure 4.18. Only a maximum number of 4 significant bits is used for represent the hue value and obtaining of the resolution, since the micro-camera provides a RGB565 format for the RGB coordinates. In Table 4.2, the resolution for each metal in units of molar concentration is resumed.

Table 4.2 Theoretical resolution for each heavy metal and each membrane.

	Copper resolution (M)	Zinc resolution (M)
PAN	0.0012	0.0011
ZINCON	0.0017	0.0016

The validation of the instrument as well as the research in determination of heavy metal concentrations in solutions with mixture of copper and zinc ions are currently under study. A research about the fabrication of optical sensor arrays using the inkjet printing techniques is being carried out. Nowadays there is a trend towards the use of miniaturized optical sensors as well as reduced equipment for measuring. Inkjet printing is being used as a technique for the fabrication of chemical optical sensors, since it is possible to reduce the size of them to obtain microarrays, create optical arrays with higher number of sensors, with higher reproducibility, as well as avoiding the heterogeneities produced by the spin coating method that could cause bad read-outs of the colour. Some examples of printed sensor arrays are shown in Figure 4.20, where it can be observed all the mentioned advantages. In this field several works have been published in the latter years: fabrication of microarrays for drug screening using colorimetric detection (Arrabito and Pignataro 2010); printed films for volatile organic compounds discrimination (Mensing *et al.* 2013), (Yoon *et al.* 2013); or microfluidic paper-based devices using printing techniques (Maejima *et al.* 2013).

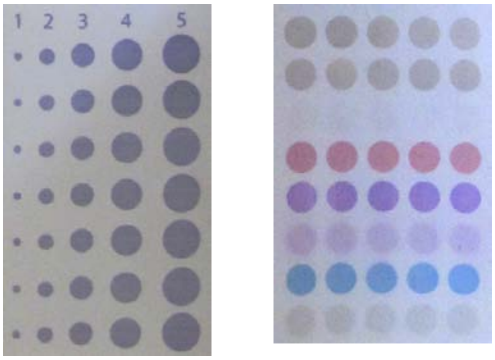

Figure 4.20 Examples of printed sensor arrays.

4.4 Conclusions

In this chapter, two different instruments using the same micro-camera module have been presented. First, a prototype for the measurement of gaseous oxygen has been described using with this purpose the same optical chemical sensor described in section 3.3 of this report. Secondly, a handheld colorimeter for determination of heavy metals concentration, such as zinc and copper ions, was presented.

In the first prototype, the sensing membrane is excited with an UV LED, which is biased using a current source, and the intensity of the luminescence emitted by the PtOEP complex is quantified by imaging techniques. In this case, a picture is taken with the CMOS micro-camera, and the microcontroller obtains the mode value of the R component of the RGB space in order to relate it to the concentration of the surrounding oxygen. The features of the developed instrument for this purpose, such as resolution or accuracy, are lower than the obtained in the previous chapter using the RFID tag. In that case, the codification of the red component was made using 12 bits of the output from the digital colour detectors, but in the case of the micro-camera only 5 bits were used for encoding of the R coordinate. However, the results have improved some previous works carried out in the group and the prototype offers some advantages: since the area of the sensing membrane which is processed and analyzed is higher than in the case of the RFID tag, it is possible to avoid bad read-outs of the instrument due to heterogeneities in the surface of the membrane. Furthermore, by increasing the area analyzed with the microcontroller, the technical specifications of the prototype can be improved, although the response time of the instrument is also increased.

With the second handheld device, the hue component of the HSV colour space is related to the concentration of metals by processing an image captured with the micro-camera. The instrument provides a user interface through a touch-LCD screen that shows the taken photograph of the optical sensor array as well as the final results of concentration after the processing. In this case, the responses of two membranes with the presence of copper and zinc ions in solutions have been studied, showing a high concordance with the results provided by a commercial scanner, despite of the different light source and detectors.

Since both systems, for determination of metals and oxygen concentration, need a light source to act as illuminant during the measurement procedure, several approaches were studied in this chapter. In the first case, an UV LED was used instead of a green

LED, in order to avoid the visible region of the spectrum and, therefore, the interference of the light in the picture. In the second prototype, transmission and reflection modes were studied as possibilities for obtaining the measurements of interest from an optical sensor array. In this case, the use of four white LEDs produce more stable measurements of the RGB components than the provided using ambient light as illuminant. As it can be deduces, the conditions of illumination in a black box are under control, which makes simpler the processing of the picture since there is no need of normalization or corrections to take into account the variations of the light.

Contributions

Lopez-Ruiz N, Martinez-Olmos A, Perez de Vargas-Sansalvador IM, Fernandez-Ramos MD, Capitan-Vallvey LF, Palma AJ (2012) *Determination of O_2 using colour sensing from image processing with mobile devices.* Sensors and Actuators: B. Chemical 171-172, 938-945.

Lopez-Ruiz N, Ariza M, Martinez-Olmos A, Vukovic J, Palma AJ, Capitan-Vallvey LF (2011) *Handheld colorimeter for determination of heavy metal concentrations.* Journal of Physics: Conference Series 307.

Lopez-Ruiz N, Ariza M, Martinez-Olmos A, Vukovic J, Palma AJ, Capitan-Vallvey LF. *Handheld colorimeter for determination of heavy metal concentrations.* Sensors and their Applications XVI (Cork, Ireland 12-14 September 2011).

Lopez-Ruiz N, Martinez-Olmos A, Perez de Vargas-Sansalvador IM, Fernandez-Ramos MD, Banqueri J, Capitan-Vallvey LF, Palma AJ. *Determination of* O_2 *with a portable instrument using color processing from sensor images.* XI Conference on optical chemical sensors and biosensors EUROPT(R)ODE XI (Barcelona, Spain 1-4 April 2012) 147.

Chapter 5. **Image processing using commercial capture devices**

5.1 Introduction

From the previous chapters it can be deduced that portable instrumentation has acquired importance in several fields such as environmental or life sciences, health care or medicine, or analysis of samples such as food, water or other different solutions. Until now, several systems have been presented, being developed and designed with the main objective of analysis of optical chemical sensors. In this chapter, commercial devices have been used as detectors for different applications such as oxygen, pH and nitrite measurement, soil classification or determination of stability in emulsions.

As mentioned in the second chapter, CCD devices are more present in digital cameras while CMOS sensors are used in mobile phones and systems where the response time need to be reduced and low power consumption is required. Here, two mobile phones with CMOS sensors and a digital camera with CCD sensor have been used.

Recently, CCD digital cameras are being used as image detectors. In this case, the pictures can be captured in the place of interest but the processing of the images has to be carried out using an external computer. Several works in different fields can be found in the literature using this kind of device: in dentistry applications for tooth colour detection (Wee *et al.* 2006); for colour measurement and detection of spots in the skin (Pladellorens *et al.* 2008); for determination of organic substances with diazotized polyurethane foams (Apyari and Dmitrienko 2008); for potassium, magnesium and pH monitoring using optical sensors (Lapresta-Fernandez and Capitan-Vallvey 2011); and, for determination of calcium concentration in water (Lopez-Molinero *et al.* 2013). In all these works the reliability of a digital camera used as a detector has been proved.

In latest years, due to the increasing in the use of mobile devices in the society, the cameras integrated in most of them, such as smartphones and tablets, are also being used as detectors. The possibility of development of applications, either in Android, iOS, Windows Phone or other operative systems, has increased the interest in mobile phone as instrumentation for analysis and classification in the researching world. With this kind of devices, the processing of the images can be performed with the internal microprocessors without need of using external elements, therefore, the information is provided in-situ and faster than using the common instrumentation in laboratories. Some of the works carried out in this field are related to chemical sensors: use of the mobile phone as portable chemical analyzer employing the hue value of the HSV colour space as parameter (Garcia *et al.* 2011); for quantifying concentrations of urinary glucose and protein (Lee *et al.* 2011b); for measurement of pH using test paper strips (Chang 2012); as UV dosimeter for monitoring the solar disinfection of water (Copperwhite *et al.* 2012); or for classification and analysis of liquid and solid coloured samples (Iqbal and Eriksson 2013), among others.

In this chapter, and for different purposes, three different image-capture devices have been used: two models of smartphone and a digital camera. They are a HTC Desire HD (HTC Corporation, Taiwan) mobile phone, a Samsung Galaxy SII (Samsung Electronics Corporation, Ltd., South Korea) mobile phone and a commercial camera Canon Powershot G12 (Canon, Japan).

Both smartphones use Android as operative system for the main reason of the open code that offers the possibilities of controlling a higher number of camera parameters or customize the applications without almost any restriction. Moreover, the community of developers is wider than for other systems and, therefore, it is easier to find solutions to the problems that can arise during the development of the application. Currently, Android leads the smartphone operative system market with almost a 75% of the terminals while iOS has only the 17% (Puder and Antebi 2013). Android can be used not only in smartphones, but also in netbooks or tablets, which are also portable devices. Java is the language used by Android, which allows to use libraries and other resources previously developed for this language, even those which are used for image-processing having available a wider range of operations and transformation on images.

5.2 Use of a smartphone for oxygen determination

As explained above, the concentration of gaseous oxygen can be determined by quantifying the intensity of the luminescence emitted by a luminophore of PtOEP complex when it is excited with an UV LED.

In previous prototypes, a digital colour detector and a micro-camera module were used for measuring the luminescence intensity. Here, a HTC Desire HD has been use as detector to quantify the intensity of the luminescence.

Several works have been carried out in recent years using smartphones as colour detectors: as decoding platform of microarrays for signal-enhanced mutation detection (Zhang *et al.* 2011); to act as a rapid-diagnosis-test reader platform (Mudanyali *et al.* 2012); for optical analysis of liquid or solid samples (Iqbal and Eriksson 2013); or for detection of biomarkers in sweat and saliva (Oncescu *et al.* 2013). In this case, the objective is to quantify the intensity of the emitted luminescence generated by the PtOEP complex when it is optically excited. In this field, there are some works in the literature that have used a mobile phone as a platform for measuring fluorescence with different purposes: for DNA detection (Lee *et al.* 2011a); using for analyzing fluorescence in paper microfluidic sensors (Delaney *et al.* 2011); or for determination of oxygen adding a external sensor module (O'Driscoll *et al.* 2013).

Here, a mobile phone was used to measure the intensity of the luminescence of a sensing membrane which was quenched by the gaseous oxygen. Measurements were carried out in a dark environment with the only influence of an UV LED that acted as excitation for the membrane. The HTC Desire HD phone was chosen since it uses the Android 2.2 as operative system and it has a built-in camera with 8 megapixel resolution, which is a high resolution for the purpose here carried out.

5.2.1 Measurement procedure

The higher resolution offered by the built-in camera of the smartphone allows to configure the pictures to have the maximum resolution with a size of 3264×2448 pixels. In this way, a higher number of pixels of the area of interest were available. This smartphone provides 8 bits for encoding each coordinate of the RGB colour space in each pixel of the picture taken. The size of the smartphone is 123×68×11.8 mm, with a LCD capacitive screen of 4.3 inches with 400×800 pixels. The HTC Desire HD phone has a 768 MB RAM and 1.5 GB of internal flash memory data storage.

The measurement of the red component (RGB colour space) of the intensity of the emission generated by the luminophore was carried out following a process similar to the explained in section 4.2. Mixtures for the preparation of the oxygen-sensitive membrane were made by dissolving 0.5 mg of PtOEP and 12 mg of DABCO in 1 mL of a solution of 5% (w/v) of PS in freshly distilled THF. The PtOEP complex was then deposited in a quartz crystal that acted not only as support of the membrane but also as waveguide for the emitted intensity of the UV LED. The arrangement of the elements of the sensing module is shown in Figure 5.1. With this configuration it was avoided the direct influence of the light source over the picture captured with the mobile phone, thus there was no saturation of the image. In this case, the membrane cannot be place inside a black box since the capture of the picture had to be started manually. For this reason, the measurement process was carried out in a dark environment with fairly controlled conditions of oxygen.

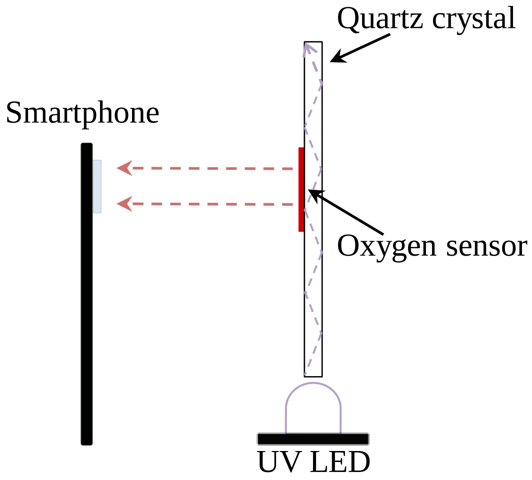

Figure 5.1 Sensing module for detection of the red component of the emitted intensity.

When the UV LED was biased with a current source, the radiation emitted excited the luminophore which generated an emission at 645 nm. The mobile phone was then placed facing the sensing membrane, and after delay time of 30 second, which is the time that the PtOEP complex needs to reach a stable state (Vargas-Sansalvador *et al.* 2011b), a picture of the luminophore was taken as it can be seen in Figure 5.2a.

Despite the distance between the luminophore and the smartphone, and due to the high resolution achieved by the camera of the mobile phone, a high number of pixels of interest, i.e. the area of the membrane, were available to be further processed directly in the phone. Once the picture was shown on the screen, the user could select the area of interest by expanding, reducing and moving the green square using the touch screen, as shown in Figure 5.2b, in order to determine the red coordinate of the intensity generated by the luminophore. This red component is related to the concentration of environmental gaseous oxygen as explained below. Besides the arrangement of the elements in this configuration, since the UV LED has the peak of emission at 380 nm, which is in the no visible region of the spectrum, there was no influence of the light source in the picture taken, as it can be appreciated in Figure 5.2. Therefore, the processing of the picture is simpler since only one coordinate is required.

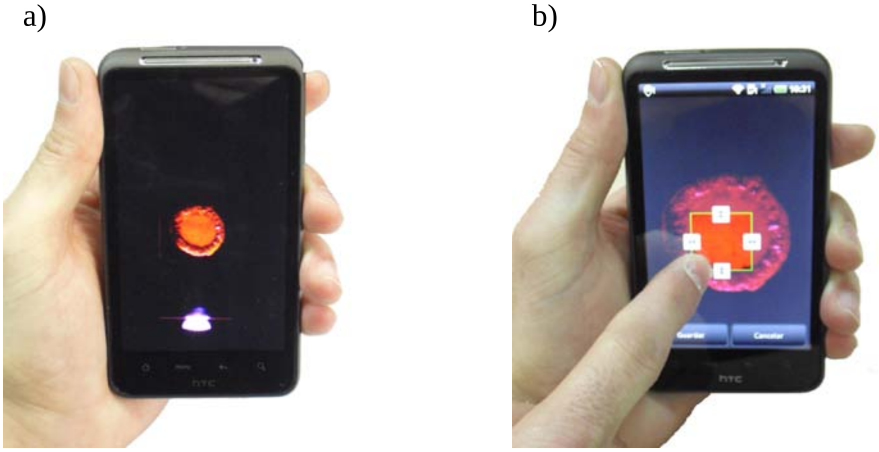

Figure 5.2 Photographs of the measurement process: a) sensing membrane and UV LED and b) selection of the area of interest.

Android application

The Android application installed in the HTC Desire HD smartphone was developed in order to extract the information about the red component from a picture of the phosphorescence emitted by the PtOEP complex. The main menu allows to take a new picture of the membrane or processing old pictures saved previously in the gallery of the phone.

To capture a new picture of a membrane, the camera of the mobile phone is activated. The camera parameters were fixed in order to avoid the uncontrolled automatic configurations and to ensure the same conditions for all the taken pictures. The parameters were set to ISO 200, white balance to daylight and the highest resolution value of 3264×2448 in order to have more pixels available in the region of interest to be processed. The ISO is the level of sensitivity that the sensor of the camera has to the available light. With low values of ISO, the sensitivity is lower, avoiding the saturation of the picture in ambient with high illumination. Besides, when the higher the sensitivity comes, the higher level of noise is present in the picture and, therefore, the information of the pixels can be modified from the real colour. Thus, since the intensity of the membrane was considered to provide enough light for the picture, there is no need of having a high ISO value. The white balance was set to daylight just to avoid the corrections carried out for the mobile phone in automatic mode. In Figure 5.2a, the result of taking a photograph of the membrane is shown. As it can be seen, the UV LED is placed at the top of the picture, and there is no influence of the light source in other areas of the image. All the pictures were stored in JPEG format, which is the most used format for this kind of capture devices.

After the capture processing, the user can select the area of interest to be analyzed by changing the size or the position of the green square displayed in Figure 5.2. When the area is selected, the application extracts the red component of every pixel inside the region by reading directly the information using some of the Java functions for image processing. With these functions it is possible to extract directly the RGB coordinates of a single pixel and separate the values of each one of them without the need of implementing any algorithm to decoding the information of the JPEG picture. In this way, only the red component is used for determination of oxygen concentration and the statistical mode of the whole set is obtained as the final value of the intensity of the luminescence. As in previous works, the statistical mode was chosen in order to avoid the heterogeneities on the membrane surface (Cantrell *et al.* 2010). The R value of the intensity generated by the sensing membrane is then related with the concentration of gaseous oxygen and shown to the user in the screen of the smartphone.

5.2.2 Results

In the same way as shown in sections 3.3.5 and 4.2.3, the red component of the intensity of the luminescence decreased with the oxygen concentration. This relationship between the R coordinate and the gaseous oxygen is depicted in Figure 5.3 where six replicas were used for each concentration of O_2 at room temperature (21ºC). Error bars are two small to be appreciated in this graphic. Due to the need of controlling the mobile phone manually inside the atmosphere where the system was placed, it was difficult to obtain stable conditions at low concentrations of oxygen and, therefore, only values higher than 10% of gaseous oxygen are shown in the curves.

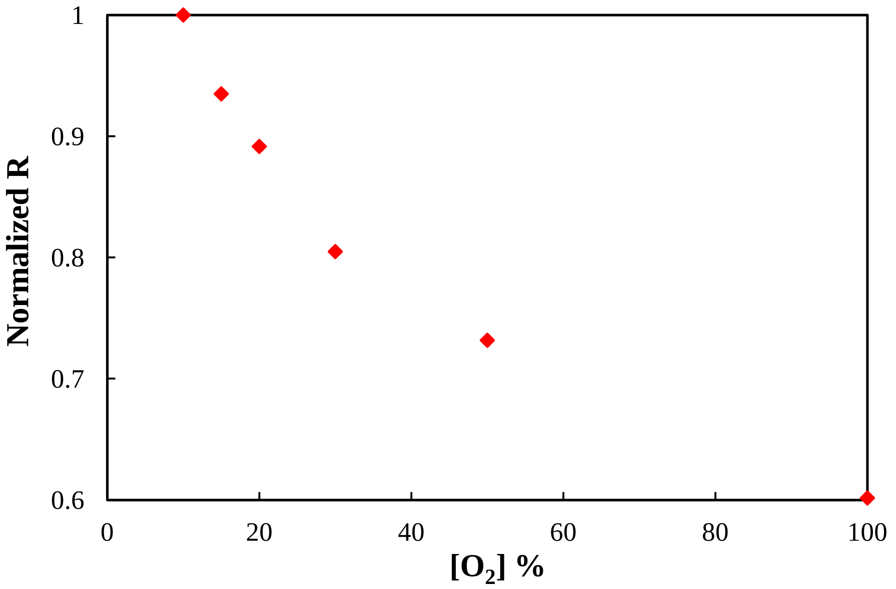

Figure 5.3 Intensity of the luminescence determined with the red component provided by the smartphone.

The response can be modelled with a non-linear Stern-Volmer function being represented with the Equation 4.1, in the same way as in previous cases (Carraway *et al.* 1991). The parameters for this response are • = 0.357 and • = 0.468 with a correlation factor of r^2=0.996.

The theoretical resolution of the portable instrument was obtained taking into account the maximum value achievable by the red component, which is 256 units corresponding to the 8 bits used by the smartphone to encode each coordinate of the RGB colour space. Then, the resolution can be determined using the Equation 5.1, where R_0 is the value of the R coordinate in absence of oxygen, as 35 ppm at 21% of O_2.

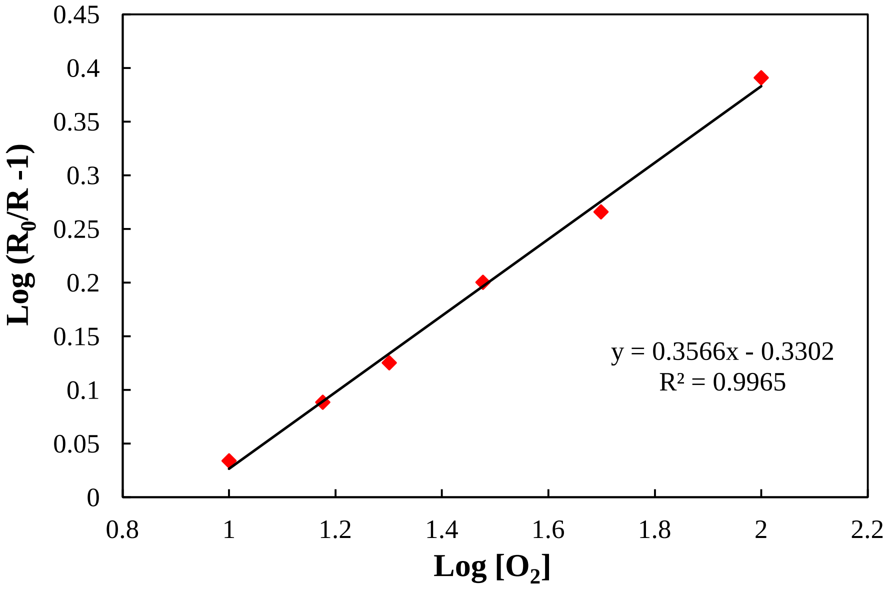

Figure 5.4 Fitting curve for the response of the system.

$$\Delta O_2 = \frac{R_0\left(\frac{R_0 - R}{R\cdot\alpha}\right)^{1/\beta}}{R\cdot\beta(R-R_0)}\Delta R \qquad (5.1)$$

The LOD for the system is 0.4% of O_2 and it was obtained following the standard procedure LOD = $y_b + 3s_b$, where y_b is the average blank signal and s_b is the standard deviation of the blank which was determined using six replicas. The maintaining of a stable atmosphere of oxygen at low values of concentrations was difficult since the smartphone had to capture a picture manually and, therefore, the environment could not be completely closed. Due to this fact, the experimental resolution of this prototype could not be obtained using experimental values. However, it can be appreciated that the theoretical resolution is better than in previous instruments, which means that with real controlled conditions and using empirical measurements the real resolution of the system could be also improved with regard to other instruments. Moreover, the achieved theoretical resolution improves the values of other equipments reported in the literature (Palma *et al.* 2007b).

The temperature dependence was not studied for this prototype, but, as shown in sections 3.3.5 and 4.2.3, an increasing in the temperature causes a reduction on the phosphorescence of the sensing membrane, therefore, the red component is lower. To take into account this factor, an external temperature sensor will be needed since the smartphone does not include this feature and consequently the design would be more complex. The effect could be modelled introducing this thermal dependence in the fitting parameters • and • as shown in previous works here presented.

5.3 Smartphone application for determination of pH and nitrite concentration using a paper-based analytical device

In this chapter a mobile phone which runs Android as operative system is also used as colour sensor. Due to the increasing interest in the use of portable instrumentation and the growing development of new smartphones, these become a solution for the analysis in real-time of different variables. The combination of smartphones with the use of disposable and low-cost sensors, such as the optical sensors studied in this work or paper-based microfluidic devices, is mainly an interest in the field of biomedical and food analysis (Martinez *et al.* 2008a), (Wang *et al.* 2011), (Chang 2012).

In particular, microfluidic devices have become an emerging technique as chemical sensors since they constitute inexpensive, simple and easy-to-produce analytical devices (Martinez *et al.* 2008a). As a general concept the microfluidic platforms pave the way for miniaturization, integration, automation and parallelization of (bio)chemical processes (Wang *et al.* 2011).

The creation of microfluidic channels on paper allows that solutions flow within the channels in a controlled manner from sampling area to detection area in which the recognition chemistry is included. It is possible to implement in the device different analytical operations such as separation, derivatization, masking, and different types of chemical reactions.

The microfluidic type devices based on paper are called as Paper-based Analytical Devices (µ-PAD). The paper-based microfluidic system is low-cost, easy-to-use, disposable, and equipment-free, and therefore, is a rising technology particularly relevant to improving the healthcare and disease screening in the developing world, especially for those areas with no- or low infrastructure (Li *et al.* 2012).

The basis of this sensors lies on the high level of compatibility that paper presents with an elevated number of chemical reagents and the capillary forces that transport liquids without external elements (Li *et al.* 2012). This fact, in combination with the hydrophobic properties that present some materials in order to delimit channels on the cellulose, makes microfluidic devices an interesting alternative for real-time applications. Several techniques of fabrication for microfluidic devices have been reported in literature: photolithography (Martinez *et al.* 2007), using layered paper (Martinez *et al.* 2008b), wax printing

(Lu *et al.* 2010), with a marker pen (Fang *et al.* 2011), or one-step plotting (Nie *et al.* 2012), among others.

In this work, a simple and faster technique is presented, where a polydimethylsiloxane (PDMS) stamp is used, together with the filter paper and indelible ink. The process implies only one step: stamping the PDMS stamp covered with the indelible ink on the filter paper. Then the ink is transferred and absorbed by the paper acting like a barrier for the sample solutions placed in the microfluidic device when it is dry. Other works have used indelible ink to create microfluidic structures (Fang *et al.* 2011), (Nie *et al.* 2012), but here the device is produced by direct contact of a stamp with the paper using commercial indelible ink.

The paper-based device here presented has been used in combination with colorimetric chemistries for measurement of pH in the range 4 to 9 and concentration of nitrites from 4 to 85 $mg \cdot L^{-1}$. The colour of detection area measured with the hue (H) and saturation (S) coordinates of the HSV colour space has been used as magnitude of interest in this case for determination of pH and nitrite concentrations respectively. These coordinates were calculated carrying out a two-dimensional analysis from pictures of the microfluidic devices captured using a smartphone Samsung Galaxy SII.

As stated during the present report, the use of portable instrumentation in combination with optical chemical sensors simplifies the analytical procedure allowing the obtaining of real-time information avoiding the need of using external elements for further processing and, therefore, reducing costs and time of processing. Here, an Android application has been developed in order to carry out the image processing of the multiple sensing areas of interest providing colour information that is related to the pH and the nitrites concentration of a solution.

5.3.1 Material and reagents

For the fabrication of the microfluidic device, standard laboratory filter paper Whatman© paper grade 1 was used. This paper is capable of absorbing the ink through the whole thickness to avoid the flow of the liquid beyond the microfluidic channels. The indelible ink used was Lumocolor© Permanent Universal Black Ink from Staedtler (Staedtler Mars CmbH & Co. KG., Germany). The viscosity of the ink was reduced using a 1:1 v/v ethanol-n-propanol and 10:1 ink-solvent mixture in order to make easier the flow through the filter paper. As a main feature of this ink, it is worth to notice the fast time of drying, in accordance with the manufacturer is few seconds, in comparison with others inks with higher times. To control the transferred ink to the stamp, a rectangular stone ink-pad of 2”×4” in size from HITT Marking (HITT Marking Devices Inc., USA) was used. According to the specifications, the ink stone is capable of providing constant flow of ink when it is in contact with a stamp. The PDMS stamp fabrication was carried out using a micromiller CAT3D from Datron (Datron Dynamics Inc., United Kingdom). The corresponding designs were performed using Solid Works© Student version 2012 and converted to the final format using AutoDesk© HSMxpress.

The chemical used to prepare the pH sensitive films were hexadecyltrimethylammonium bromide (CTAB, CAS No. 57-09-0) and phenol red (CAS No. 143-74-8) from Sigma (Sigma-Aldrich Química

S.A., Spain), clorophenol red (CAS No. 4430-20-0) from Merck (Merck Millipore, Germany) and sodium hydroxide (CAS No. 1310-73-2) from Panreac (Panreac Química S.A., Spain). For the nitrite sensitive areas, the chemical used were Nafion perfluorinated resin solution (CAS No. 31175-20-9), sulphanilamide (CAS No. 63-74-1) and N-1-napthylethylenediamine dihydrochloride (NED) (CAS No. 1465-25-4) from Sigma and polyethylene glycol (PEG) 400 (CAS No. 25322-68-3), 2-propanol, and citric acid (CAS No. 77-92-9) from Panreac. Finally, for the different pH solutions, a phosphate buffer solution made by mixing of NaH_2PO_4 (CAS No. 10049-21-5) and Na_2HPO_4 (CAS No. 7558-79-4), both from Panreac, in different proportions was used. All aqueous solutions were prepared in reverse-osmosis type quality water (Mili-RO 12 plus Milli-Q station from Millipore, conductivity 18.2 mS).

5.3.2 Fabrication of the microfluidic device

The PDMS negative molds were produced using 4 mm thick polymethyl methacrylate (PMMA) as substrate. A flat endmill was used to shave off a portion of material in order to leave flat the PMMA surface. After that, a 600 µm deep pocket was milled out and using other flat endmills of the corresponding dimensions the negative mold was milled out starting from the bottom of the pocket. After this procedure, the PDMS stamp, 10:3 w/w monomer-curing agent, was cured at 60ºC for 8 hours. The final result can be observed in Figure 5.5. The stamp was attached to a rectangular prism in order to have a plain surface to avoid irregularities during the stamping process.

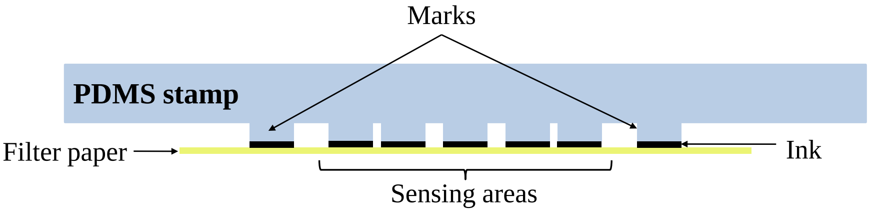

Figure 5.5 Side view of the PDMS stamp structure.

When the fabrication procedure was finished, a PDMS stamp was available for performing the stamping to obtain the microfluidic devices: the PDMS stamp was pressed three times against the stone ink-pad. The stamp loaded with the indelible ink was exposed to air for 5 seconds, in order to eliminate the bubbles on the top of the stamp caused by the pressure against the stone. Finally, the stamp was placed over the filter paper for three seconds, without need of applying any force. The obtained device as a result of this process of fabrication is shown in Figure 5.6.

As it can be seen, the final design consists of one main central area, seven sensing areas, one blank for reference and two marks: a triangle and a square. Each sensing area is a circle with an internal diameter of 5 mm and an outer diameter of 7 mm, while the diameter of the central area is of 9 mm. The entire size of the microfluidic device is 3.5 cm × 5 cm, taking into account the position of the marks. The length of the channels is of 5 mm each one with a width of 1 mm in the inner part and 4 mm taking into account the barriers. The two marks were included with the purpose of detection of positions in order to determine, from their positions, the region to process of each sensing area. Using two marks it is possible to determine the scale and the rotation factor in the different captured pictures of the microfluidic devices.

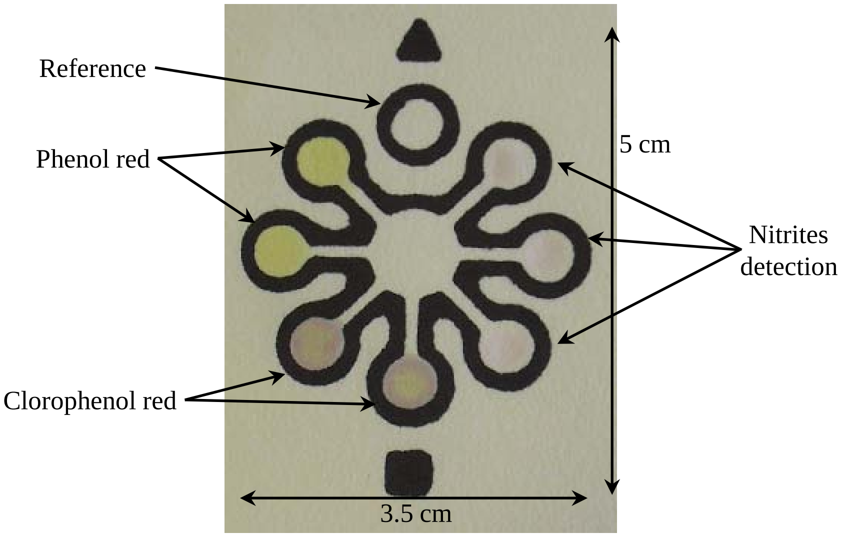

Figure 5.6 Microfluidic device with the reagents placed in each sensing area.

Once the final device is stamped and dry, the sensing areas need to be prepared with the reagents in order to have the device ready for the reactions with solutions. The pH and nitrites sensing areas were prepared taking into account three conditions: no leaching, change in a tonal colour coordinate and, for the pH sensing areas, is also necessary to cover the range [4-9] of pH using the combination of the responses for two different pH indicators which are enough to cover that range of pH. Each sensing area, as it can be seen in Figure 5.6, was prepared by casting the corresponding reagents under ambient atmospheric conditions, leaving dry between depositions the different layers to avoid the invasion of the reagents in the microfluidic channels. In order to get replicas, two sensing areas were used for each pH indicator and three sensing areas for the nitrite determination. As shown in Figure

5.6, one of the sensing areas is not connected with the centre area to use it as blank of reference during the image processing of the pictures.

The two pH indicators were made by dissolving 1.77 mg of phenol red, 8.2 mg of CTAB, and 5 µL of NaOH in 5 mL of water, and, 3.17 mg of clorophenol red with 10.93 mg of CTAB in 5 mL of water. One layer of 1.5 µL was cast for the red clorophenol cocktail while two layers of 1.5 µL were needed in the case of phenol pH indicator. For the sensing regions of nitrites three different solutions were needed. The membrane was prepared using a solution with 40% of Nafion, 33.3% of propanol and 26.7% of water and dissolving 0.013 g · mL^{-1} of PEG. Next, 33.2 mg of sulphanilamide and 126.8 mg of citric acid were dissolved in 1mL of water and were mixed in a volume ratio of 1:1 with a solution of 2.32 mg of NED in 1 mL of water. 1.5 µL of each solution were cast in the sensing areas for nitrites determination. It is important to let dry a layer before the deposition of other layer to avoid the flow of the reagents into the channel. After deposition of the sensing membranes, the support was left dry in darkness, as the NED is photosensitive, for 5 minutes. As a consequence of the described process, the obtained membranes were homogeneous, coloured for the pH areas and transparent for the nitrites regions as shown in Figure 5.6.

Measurement process

To carry out the reactions that produce the colour changes in the sensing areas, 30 µL of a solution with unknown pH and nitrites concentration were cast in the central area of the microfluidic device. Due to the capillarity of the filter paper and the barriers created by stamping the ink on it, the solution flowed towards the seven sensing areas where the corresponding reagents were placed. Fifteen minutes were needed to get the complete reaction in each one of the areas, let them dry and get a uniform colour which is readable by the Android application installed on the smartphone. The influence of the time in the colour measurement will be later explained. The whole process had to be carried out in a dark environment since the NED is photosensitive and acquires a purple colour when it is exposed to illumination. Moreover, it is important to take into account that the device must be kept in horizontal position to not favour the flow of solution in a determined direction and over a non-absorbent surface in order to avoid the transfer of reagents or sampled solution to that support.

Once the reactions have occurred, and after fifteen minutes, a picture of the microfluidic device is captured using a Samsung Galaxy SII. The picture has to be taken under controlled illumination conditions, with the only influence of the internal flash of the built-in camera. For this reason, the room must be kept in darkness.

5.3.3 Development of an Android application

For this work a Samsung Galaxy SII smartphone was chosen. This mobile phone, with a dual core processor, runs the Android version 4.1.2 and has a built-in camera of 8 megapixels that includes a LED flash, which in this case acted as light source. The dimensions of the phone are 125.3×66.1×49 mm and it has a display of 4.3” with 640x480 pixels of resolution.

The developed application set the parameters of the camera in order to avoid the automatic configuration of them by the mobile phone. For this purpose, the parameters were set as shown in Table 5.1. The ISO factor was set to 200, in a range from 100 to 800, since the built-in flash used as light source provides light enough to the ambient, avoiding the need of increase the sensitivity of the camera sensor and, therefore, decreasing the noise in the final picture. In this way the flash was set in torch mode in order to provide a constant light during the image acquisition process. Once the picture is stored on the mobile phone, the flash is turned off until the next capture. The spectrum of the emitted flash light is depicted in Figure 5.7 and it can be observed that its main component is situated at the wavelength of 440 nm.

Table 5.1 Camera parameters set in the application.

Parameter	Value
ISO	200
Flash mode	Torch
Focus Mode	Macro
White Balance	Daylight
Resolution	3264 × 2448

The focus mode was set to macro taking into account that the distance between the camera lens and the microfluidic device during the acquisition of pictures is lower than eight centimetres. Also, the application uses the autofocus option, which avoids the capture of blurred picture since before taking the picture, it is ensures the correct focus on the microfluidic device. The white balance was set to daylight mode which correspond to 5500 K of colour temperature and it is equivalent to the colour temperature of the flash light emitted by the

LED in this smartphone (5500 K – 6000 K). Finally, in order to have the maximum number of pixels of interest available, the resolution of the pictures was set to the maximum value allowed by the Samsung phone, which is of 3264 × 2448 pixels. However, the increase in the number of pixels in the picture also increases the time of processing, since the detection of the area has to be carried out using the information pixel by pixel as explained below.

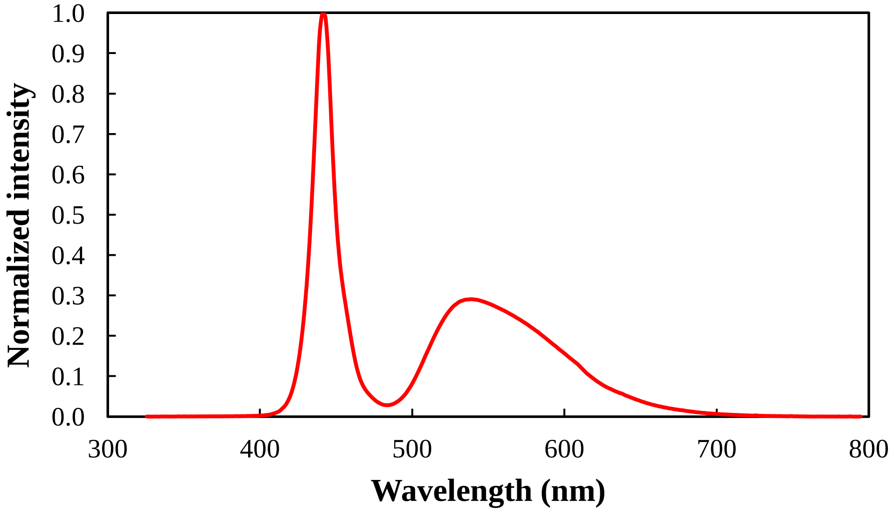

Figure 5.7 Spectrum of the flash light.

All the pictures were saved in JPEG format as it is the default format in most of the smartphones, with a resolution of 96 dots per inch (dpi) and 8-bits per RGB channel (24 bits in total). The Java language used for developing Android applications together with some own functions of the Android operative system allow to extract the colour information directly without using any decode algorithm. Nevertheless, due to the complex image-processing needed in this work to determine the position of the microfluidic devices in the picture by detection of the marks and the areas of interest and the high size of the pictures to be treated, an open source computer vision library (OpenCV) was integrated with Android to carry out the processing of the pictures.

OpenCV is a library developed by Intel (Intel Corp., USA) that is focused mainly on the real-time image processing. Since the size of the pictures obtained with this mobile phone is configured to be the maximum possible, an optimized library as OpenCV improves the time of response of the Android application. This library is an open source library under a BSD license and it can be integrated for being used with C, C++, Python or, as in this case, Java interfaces and also supports Windows, Linux, iOS and Android.

In Figure 5.8 different screen captures of the Android application are shown. The main menu, Figure 5.8a, offers the possibility of capturing a new picture of the microfluidic device or analyzing a previous stored image in the gallery. If a new picture is required, the application, using the fixed camera settings, starts the capture processing. As it can be seen in Figure 5.8b, two red marks are shown over the camera view in order to place the marks of the microfluidic device inside these areas. In this way, the picture is always in the same position, ensuring that the user does not place the sensor device in a wrong position and, furthermore, the processing of the picture is faster. When the picture is taken, and after the image processing later explained, the detection of the areas of interest is shown to the user, Figure 5.8c. It is important during the acquisition procedure to maintain the smartphone in a parallel position with respect to the microfluidic devices in order to avoid distortion of the shape in the sensing areas due to the inclination of the mobile when it is capturing the picture. If the smartphone is not placed correctly, in the image preview shown in this step the position of the sensing areas will be wrong, thus the user could discard the picture to take a new image changing the position of the phone. Once the user agrees with the sensing areas detection carried out by the application, and pressing the corresponding button, the results of the nitrites concentration and the pH of the sampled solution are shown on the screen, Figure 5.8d.

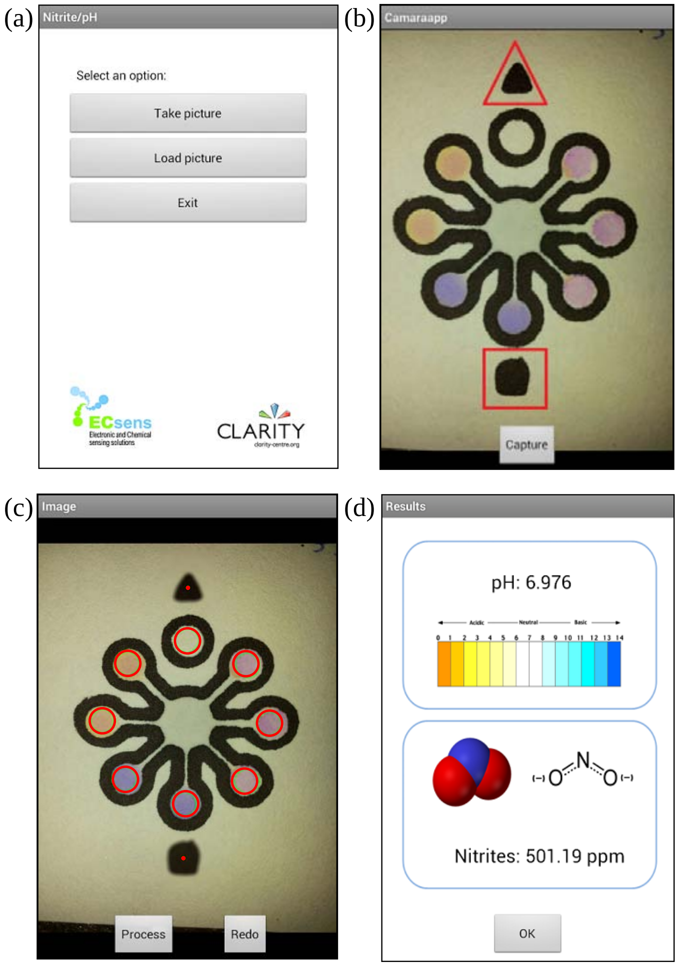

pH: 6.976

Nitrites: 501.19 ppm

Figure 5.8 Screen captures of the Android application: (a) Main menu, (b) capture of the picture, (c) marks and sensing areas detection and (d) final results obtained after image processing.

Image processing

The image processing of the pictures can be divided in three different steps: detection of the triangle and square marks, detection of the sensing areas and, finally, colour analysis of each area in order to determine the coordinates of interest. After that, the coordinates are related to the pH and the nitrites concentration of the solution placed in the centre area of the microfluidic sensor. To determine the position of the sensing areas, several steps are performed using the OpenCV library to analyze the pictures. When the picture is taken by the camera, it is saved in JPEG format, but using a predefined function of the library it can be treated channel by channel as matrices without any implementation of external algorithms to decode the colour information. Figure 5.9 shows step by step the procedures involved in the detection of the sensing areas carried out by the developed application.

For the detection of the marks, firstly, a blur filter is applied in order to attenuate the thinner dark areas in the picture, such as the edges of the microfluidic device, and keep dark the wider areas (Gonzalez and Woods 2002), such as the triangle and the square. The filter is applied pixel by pixel using the kernel described by the Equation 5.2 with a size of 40×40 for the mask.

$$\mathrm{k} = \frac{1}{40\times 40}\cdot\begin{bmatrix}1 & \cdots & 1\\ \vdots & \ddots & \vdots\\ 1 & \cdots & 1\end{bmatrix} \tag{5.2}$$

After the smoothing of the image, an inverse thresholding is applied to contrast the darker areas of the picture, which correspond to the triangle and the square, from the rest of the pixels. In that way, a black mask with the marks turned into white regions is obtained, as shown in Figure 5.9. OpenCV has implemented an option that allows to find contours in a binary picture. With that function, the position of each mark is determined, and using the vector with the contour data, the centre of the triangle and the square can be determined and pointed out with a red point.

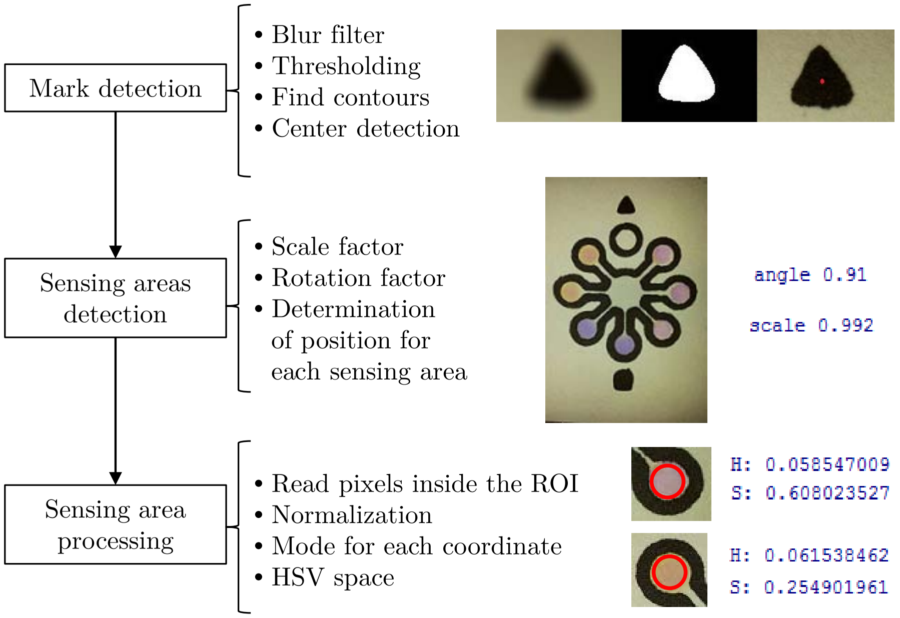

Figure 5.9 Steps of the image processing carried out in the smartphone for each picture of the microfluidic device.

Although the position of the microfluidic device is determined by the position of the square and triangle shown during the acquisition process, light variations in the angle or the scale could appear between different images as shown in Figure 5.9. In order to correct this to determine correctly the positions of the sensing areas, affine transformations are applied to the matrix of each red, green and blue channels. With the position of the marks calculated, and knowing the real distance between the two symbols, the factor or scale and rotation can be calculated over the taken picture. In Figure 5.9, an example of this factor is shown with the corresponding calculated factors of scale and rotation. To correct the factors, the matrices of rotation and scale shown in Equations 5.3 and 5.4 are applied to the matrices of each channel (Gonzalez *et al.* 2004).

$$R = \begin{bmatrix} \cos\alpha & sen\,\alpha \\ -sen\,\alpha & \cos\alpha \end{bmatrix} \quad (5.3)$$

$$S = \begin{bmatrix} s & 0 \\ 0 & s \end{bmatrix} \quad (5.4)$$

Where • represents the angle of rotation and s is the scale factor previously calculated using the real distances in the pictures.

Finally, the position of each membrane is determined taking into account the distances to the corrected position of the marks. In this way, when the centre of the sensing element is obtained, the pixels inside the area are read in order to extract their RGB coordinates. Each coordinate is normalized by the coordinates of the reference sensing area following the Equation 5.5 in order to correct light variations in the picture (Salmeron *et al.* 2012), where n=8 corresponding to the number of bits used by the mobile phone to encode each colour channel. Then, the mode of the RGB components for each sensing area is determined, and transform to the HSV colour space, which provides the information to be related to the pH and the nitrites concentration of the sample (Cantrell *et al.* 2010).

$$RGB_{normalized} = 2^{n}\, RGB_{acquired}/RGB_{white} \quad (5.5)$$

5.3.4 Results

In this section, the results of the characterization of the microfluidic device are presented. A study of the time required to starting the process of colour determination was carried out. Also, the response curves obtained for each pH indicator and the cocktail for measuring the concentration of nitrites are shown. Finally, a validation process comparing the results of the Android application with a commercial device to measure pH was performed using solutions with different concentrations of nitrites at different values of pH.

pH determination

Firstly, a study of the time needed by the pH indicators to get complete reactions in the sensing areas was carried out. That time comprises from when the sample to be analyzed is placed in the central area of the microfluidic device to the capture of the picture. This time had to be controlled as the colour in the sensing area must be uniform, and, furthermore, it must be relatively dry. The HSV coordinates take different values when the area is wet or dry, and therefore, it is critical to determine the optimum time to get the response of the two pH indicators used. For this purpose, pictures of the microfluidic device were taken from 0 to 20 minutes with 5 minutes intervals. As it can be seen in Figure 5.10, the behaviour in the clorophenol red is similar for different times, but for the phenol red 15 minutes are needed as minimum to obtain a stationary response. Therefore, 15 minutes were selected as the time needed to take the picture.

Following, the responses of each pH indicator were studied by deposition in the centre area of the microfluidic device of solutions of different pH values from 2 to 12 and taking several replicas for each value. As it can be seen in Figure 5.11, the phenol red has its transition area between 6 and 9, while the clorophenol red covers the region from 4 to 6, approximately. In this way, using these two pH indicators the range [4-9] of pH can be analyzed and determined. The curves that describe the responses are sigmoid functions, which match also with the curves described in the section 3.2.4 of this report. Error bars are too small to appear in the graphics, but the mean standard deviation values were 0.006 and 0.007 for phenol red and clorophenol red respectively.

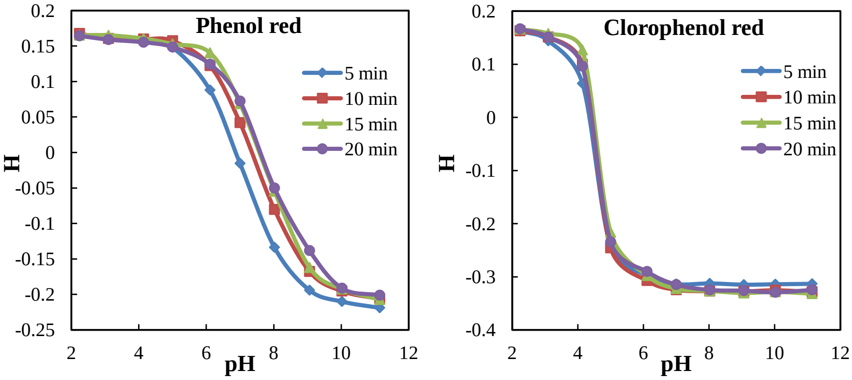

Figure 5.10 Study of the response of the pH indicators with time.

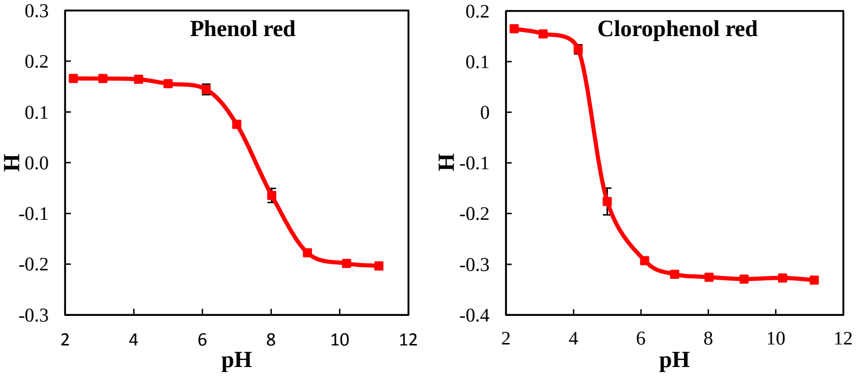

Figure 5.11 Averaged curve responses for the pH indicators at 15 minutes.

Determination of nitrites concentration

During the 15 minutes of time between the deposition of the solution sample in the centre area and the capture of the image, the microfluidic device must be kept in darkness since some of the reagents used for measuring the concentration of nitrites, such as the NED, are photosensitive. 15 minutes were determined as optimal time for pH indicators and were also checked for the reaction in these areas proving that it was also enough to get a uniform colour in the whole area.

In this case, the hue component cannot be related to the change in the concentration of nitrites since no trend was found on the corresponding curve, but the saturation coordinate of the HSV colour space provides useful information. As shown in Figure 5.12, the concentration of nitrites can be related to the saturation coordinate, although using the inverse value the tendency is clearer. For each value of concentration fifteen replicas were taken at room temperature (21ºC). The curve shows a increasing in the saturation value when the concentration of nitrites increases. The logarithm of that curve can be fitted to a linear function of the form $y=ax+b$, where a is -0.5959 and b is 2.2202 for this case, with a correlation factor R^2 equal to 0.994.

Therefore, taking into account the curves obtained for each sensing membrane used in the microfluidic devices, the pH and the nitrite concentration of a liquid sample can be determined.

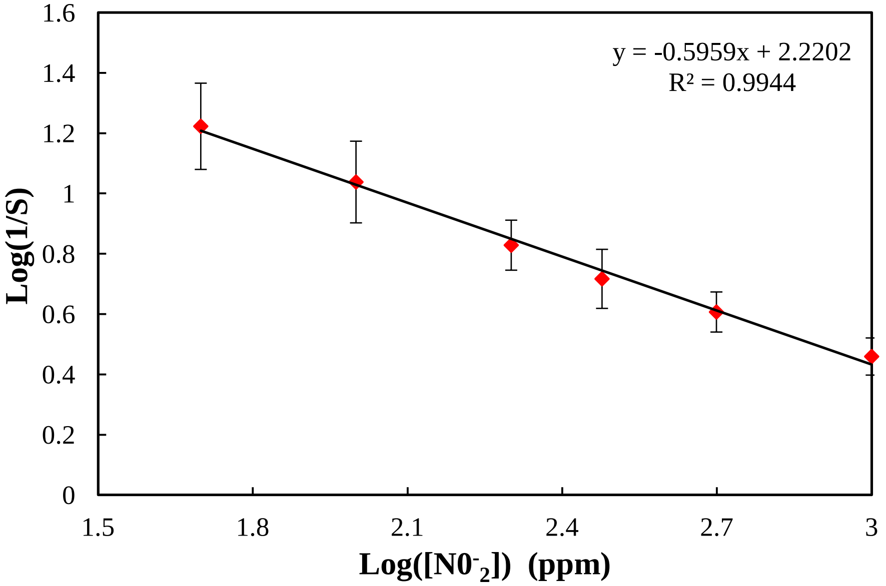

Figure 5.12 Calibration curve for nitrite concentration determination.

Validation procedure

To test the reliability of the smartphone as colour detector, nine solutions with different concentration of nitrites at different pH were prepared. The microfluidic device was prepared with two sensing areas for phenol red, other two for clorophenol red, and finally, three sensing areas for nitrite determination. Once the reagents were dry, 30 µL of each sampled solution were placed in the centre area and, after 15 minutes, a picture was taken. For each solution three replicas were taken using three different microfluidic devices. Since in the same device there are replicas for each cocktail, 18 replicas for pH were taken while for nitrites were 27 replicas in total.

To determine the concentration of nitrites, the fitting curve shown in Figure 5.12 was used. In the case of pH determination, firstly, the application must identify which indicator has to be taken into account.

For an unknown value of pH, the measured hue value of each indicator is different and only for one of them it is within the range of interest. These ranges are the region of variation of the hue coordinate determined for each pH indicator, which is from -0.3 to 0.15 for the clorophenol red and from -0.25 to 0.2 for the phenol red. Therefore, measuring the hue coordinate of the two indicators, it can be determined which one is within the range and, therefore, which indicator must be used for the pH determination. In the intervals of interest, that is from 4 to 6 for clorophenol red and 6 to 9 for phenol red, the curves were fitted to the Equations 5.6 and 5.7 for the phenol red and clorophenol red respectively in order to provide an accurate pH value, as shown in Figure 5.13.

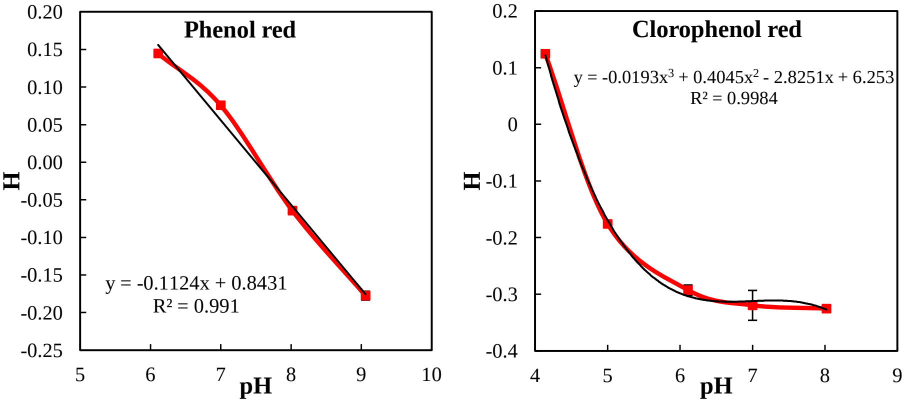

Figure 5.13 Fitting curves for the regions of interest in each pH indicator.

$$H = -0.1124 \cdot pH + 0.8431 \quad (r^2 = 0.991) \qquad (5.6)$$

$$H = -0.0193 \cdot pH^3 + 0.4045 \cdot pH^2 - 2.825 \cdot pH + 6.253 \quad (r^2 = 0.9984) \qquad (5.7)$$

For the pH determination, the MSE obtained was 0.02, which shows that the application developed and the prediction models are suitable for pH measurement. In Table 5.2 some of the obtained results are shown. In previous works described in this report, the MSE obtained was of 0.167 for the handheld instrument, and it was improved to 0.004 using artificial neural networks. In this case, the algorithm could be also improved by using ANN, lowering also this error value.

Table 5.2 Comparison between the pH of different samples using the potentiometric and the smartphone method.

Potentiometry pH value	Smartphone pH value	Error
6	6.12	0.12
6.07	6.02	0.05
7.09	7.2	0.1
8.08	8.05	0.03
8.15	8.08	0.07

The accuracy obtained as the standard deviation of the validation data was 0.09. To determine the resolution of this system, it has to be taken into account that the H parameter is a linear combination of the RGB coordinates, which are represented by 8 bits each one. Assuming the worst case with only 6 significant bits, and a range of H from 0.15 to -0.33 as shown in Figure 5.13, the resolution of pH is 0.04. This value is lower than the obtained for previous devices since in those cases the number of bits used for encode the RGB components was of 12 bits, but it is still an acceptable value of resolution.

For measuring nitrite concentration, the results obtained were less accurate than for the pH due to the lower homogeneity of the sensing areas after the reaction. When the membrane was deposited on the corresponding area, the absorption by the filter paper was not always made in the same directions due to the membrane composition, and, therefore, the reaction does not occurred in a uniform way. This fact makes difficult the detection of the HSV coordinates despite of using the mode value, since slightly variations of the S coordinate imply a higher variation of the determined concentration value. For the calculus of the technical specifications in the nitrite determination, the corresponding potential fit shown in Figure 5.12 is considered.

$$\frac{1}{S} = 166.03[NO_2^-]^{-0.596} \qquad (5.8)$$

To obtain the resolution, it is necessary to take derivatives in both sides and approximate these derivatives to increments. The resolution is then given by:

$$\Delta[NO_2^-] = \frac{\left(\frac{1/S}{166.03}\right)^{-1/0.596}}{-0.596\cdot\left(\frac{1}{S}\right)} \cdot \Delta\left(\frac{1}{S}\right) \qquad (5.9)$$

Where • *(1/S)* is related to the resolution of the smartphone, • S which in this case is 8 bits, as shown in this equation.

$$\Delta\left(\frac{1}{S}\right) = \frac{-1}{S^2} \cdot \Delta S \qquad (5.10)$$

Taking this into account, the value of resolution is dependent on the concentration, and its value is 7% at 100 mg · L^{-1} of nitrites and 2.9% at 500 mg · L^{-1}. The LOD of the system was obtained using the standard criteria LOD = $y_b + 3s_b$, where y_b is the average of the blank signal and s_b is the standard deviation of the blank determined using nine replicas. With this criterion, the value of LOD is 0.29 mg · L^{-1}.

Therefore, the determination of pH and nitrites using a smartphone provides accurate measurements as above it was proved using digital colour detectors or micro-camera modules.

5.4 Mobile phone for soil classification under controlled conditions of light

The Munsell system, explained in section 2.2.1, has been used in different fields such as natural sciences, specifically for soil science, arts or engineering to specify an existing or desired colour (ASTM 2008). Here, the work is focused on the field of the soil classification, where the measurement of samples has been carried out using mostly Munsell soil-colour charts, as well as, occasionally spectrophotometers (Torrent and Barron 1993), spectrometers (Rossel and Webster 2011) and commercial digital cameras. However, the prevalence in soil classification is the visual determination of colours by comparison which consists of determining the closest match between the soil analyzed sample and the chip contained in each one of the Munsell soil-colour charts. In these charts each chip is described by a hue value, constant for all the chips in the same chart, a value of lightness and a chroma that defines the colour intensity. Several problems of accuracy and subjectivity have been pointed out in relation with this method of colour determination (Sanchez-Maranon *et al.* 1995), (Sanchez-Maranon *et al.* 2005), (Sanchez-Maranon *et al.* 2011) since three factors can affect the decision, starting with the observer, and continuing with the illumination conditions and sample characteristics. Therefore, there is an increasing interest in using techniques that could reduce the influence of these factors.

Currently, proximal soils sensors have been used as a way of comparing soils, including evolution, degradation, pedoclimate and fertility analyses using larger amounts of data to counteract the lower accuracy of the sensors (Rossel *et al.* 2011). Also, digital cameras have been used with this purpose (Aydemir *et al.* 2004), (Rossel *et al.* 2008), (O'Donnell *et al.* 2011) to extract information of the RGB colour space from the taken pictures. Until now the information of the pixels of digital images can be extracted only as a function of the red, green and blue coordinates, and, therefore, several works have been reported to allow a transformation from this information to other colour spaces such as XYZ, CIELAB, CIELUV and others (Rossel *et al.* 2006), (Leon *et al.* 2006), (Rodriguez-Pulido *et al.* 2012).

In this section a mobile phone with a built-in camera is presented as Munsell soil-colour sensor and compared to a spectroradiometer in order to determine the reliability of the mobile phone as colorimeter. The phone captures a picture of a soil, and after image-processing, it provides an objective evaluation of soil colour. In this way, the result of this work is an Android application installed on a smartphone that takes a picture, allowing the user to select the area of interest to analyze and, by applying polynomial transformations between the RGB colour space and the others used for this purpose, the Munsell coordinates are shown on the screen. This experiment has been carried out under controlled conditions of light since the main objective of this study is to assess the viability of using a mobile phone as a colour sensor, and, therefore, it is necessary to perform the experiment under controlled illumination conditions to avoid other factors such as the daylight conditions (Sanchez-Maranon *et al.* 2011).

As mentioned in the previous section, smartphones are increasing in the market of portable instrumentation since they usually offer a good alternative to expensive techniques employed, such as colorimeters or spectrometers. Besides, the image-processing for soil classification requires the use of external computers and software for carry out the calculations, while using a smartphone the information can be obtained in-situ. For the purpose of soil classification, the smartphone should distinguish between different reddish, brownish and yellowish hues, from dark to light and of variable intensity. Thus, the colour gamut is wider than in other applications performed using colorimetry and mobile phones as sensors (Garcia *et al.* 2011), (Chang 2012).

5.4.1 Material and samples

In the same way as in the previous sections, Android was chosen as operative system for the application here developed because all the advantages mentioned. In this case, the smartphone used was a HTC Desire HD which uses Android 2.2. The model has a built-in camera that will be used as colour sensor for the purpose here presented. The camera has a CMOS autofocus sensor of up to 8 megapixels. Also, to test the functionality of the developed application in a different smartphone, a Samsung Galaxy SII was used. In this case the Android version is 4.1.2. As it can be deduced, since the manufacturers of both smartphones are different, the sensors used for each camera are different too, causing some discrepancies in the measurements and, therefore, in the results as it will be show below.

For validation purpose, a spectroradiometer and a spectrophotometer were used. The spectroradiometer model CS2000 from Konica Minolta (Konica Minolta, Japan) was used for registering of the reflected spectral-power distribution between 380 and 780 nm with 2 nm steps. For calculating the tristimulus values XYZ from the spectroradiometer measurements, the CIE 1964 Standard observer was used (CIE 2004). These coordinates were compared to the provided by the mobile phone after transformations between RGB and XYZ as later mentioned. Also, a spectrophotometer model 2600d from Konica Minolta as well was used to measure the light reflected by the studied surface between 360 and 740 nm with 10 nm steps. This instrument provides directly the Munsell colour parameters HVC for each sample using two Xenon lamps as light source.

This experiment was carried out under controlled light source conditions. With this objective, all the measurements were carried out in a dark environment with the only influence of the light provided by the GretagMacbeth Spectralight III lighting booth (X-Rite, Switzerland). All the samples were placed inside the booth during the measurement procedure, which has configured a D65 illuminant in accordance with the standard ASTM (ASTM 2008) for the Munsell colour determination.

During calibration process, 238 chips from a recent edition of Munsell soil-colour charts from year 2000 (from Munsell Colour Company, USA) were used in order to obtaining empirical values for the transformation equations from RGB to HVC. For these charts, and with calculations purposes, 10R was set to 10, 2.5YR to 12.5, 2.5Y to 22.5 and 5Y to 25.

To test the application, samples from the Natural Colour System (NCS, Sweden) Atlas were used as well as real soil samples. The initial 100 NCS samples were selected visually, among 1950 NCS available samples, in order to test the colour gamut covered by the Munsell soil-colour charts. These samples consist of pieces of artificially plain coloured papers that were measured with the spectrophotometer in order to register their HVC values. After that a final selection of 40 NCS samples were selected with a colour parameters ranged from 0.1YR and 5.5Y for hue, 2.8 and 8.2 for value and 0.5 and 8 in chroma.

Also real soil samples were used to test the reliability of the mobile phone as colour sensor for soil classification. The collected soils were textured and heterogeneous coloured samples which suppose a higher challenge than the previous NCS samples. 45 samples were chosen, all of them from Mediterranean soils with different degrees of development such as Entisols, Inceptisols, Vertisols and Alfisols. Entisols are soils that have no evidence of horizon development, inceptisols are soils with moderate degrees of soil weathering and development, vertisols have pronounced changes in volume with changes in moisture and, finally, alfisols are present in moist and semiarid areas. The four kinds of soils represent the 45% of the ice-free surface in the world. It is usual in laboratories soil studies (Torrent and Barron 1993) to prepare air-dried samples of fine earth with particles less of 2 mm in size, Figure 5.14a, and samples of the same group but homogenizing them to obtain powder with particles less than 50 µm in size, Figure 5.14b. For this work 45 samples of the first kind and 15 of the second were used. The results obtained with the spectrophotometer show colour parameters from 2.9YR to 2.3Y for hue, 3.8 to 7 in value and 1.9 to 5.6 in chroma.

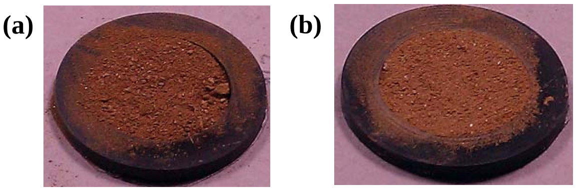

Figure 5.14 Example of soil simple with (a) particles less than 2 mm of size and (b) less than 50 µm of size.

5.4.2 Android application and method

The main objective in this work is to develop an Android application being able to classify soils by obtaining the Munsell coordinates. Also, and in order to compare the behaviour of the mobile phone as colour sensor, the XYZ coordinates are needed to compare with those provided by a spectroradiometer.

With regard to the mobile phone software and to avoid the automatic configuration of the camera parameters by the mobile phone, the developed application fixed some of them. The ISO parameter, which determines the sensitivity of the sensor to light, was set to 100 according to the daylight light source used in the booth. The white balance was fix to daylight option for high luminance (1580 lx), and finally, the flash was set to off. The smartphone saved pictures in JPEG format with a resolution of 72 dots per inch, using 24 bits for colour codification, i.e. 8 bits per channel, with a size of 1952×3264 pixels. The Samsung Galaxy SII allows to save the picture with a higher size up to 3264×2448 pixels that provides more pixels with colour information for the same region of interest.

The application was installed in the smartphone, and the different functionalities offered for the application are depicted in Figure 5.15. Initially, a main menu is shown to the user where four options are available Figure 5.15a. The first and the second options are related to the processing of a new picture captured with the camera or a previous saved photograph. The third option is for the calibration procedure which allows to normalize any colour to a white according to the colorimetry (CIE 2004). A picture of a reference white Konica Minolta PTFE (Konica Minolta, Japan) is taken under the light conditions set by the booth in order to determine its RGB coordinates, Figure 5.15c. The green square shown in the figure can be moved, expanded or contracted in order to select the area of interest of the photograph to be processed. After the selection of the region, the colour information for each pixel inside that area is obtained being read directly from the phone. The statistical mode of the red, green and blue coordinates of the white are provided and saved for normalization of soil coordinates as explained below, Figure 5.15c. The statistical mode was chosen as representative value for the reasons previously explained in this work, that is, to avoid undesirable effect of noisy pixels or non homogeneities in the soil samples (Cantrell *et al.* 2010). The same procedure is used for determination of the coordinates for the Munsell soil-colour charts during the calibration process, Figure 5.15d, and for real soil-samples in the validation procedure, Figure 5.15e. These coordinates provided by the application are normalized pixel by pixel using the white reference components following the Equation 5.11 (Salmeron *et al.* 2012) before being shown on the screen of the smartphone Figure 5.15f.

In this case, n = 8 which corresponds to the number of bits that the mobile phone uses for encoding each channel. As it can be seen, also the XYZ and HVC coordinates shown are being calculated as explained below from the RGB coordinates provided by the application.

$$RGB_{normalized} = 2^{n}\, RGB_{acquired}/RGB_{white} \quad (5.11)$$

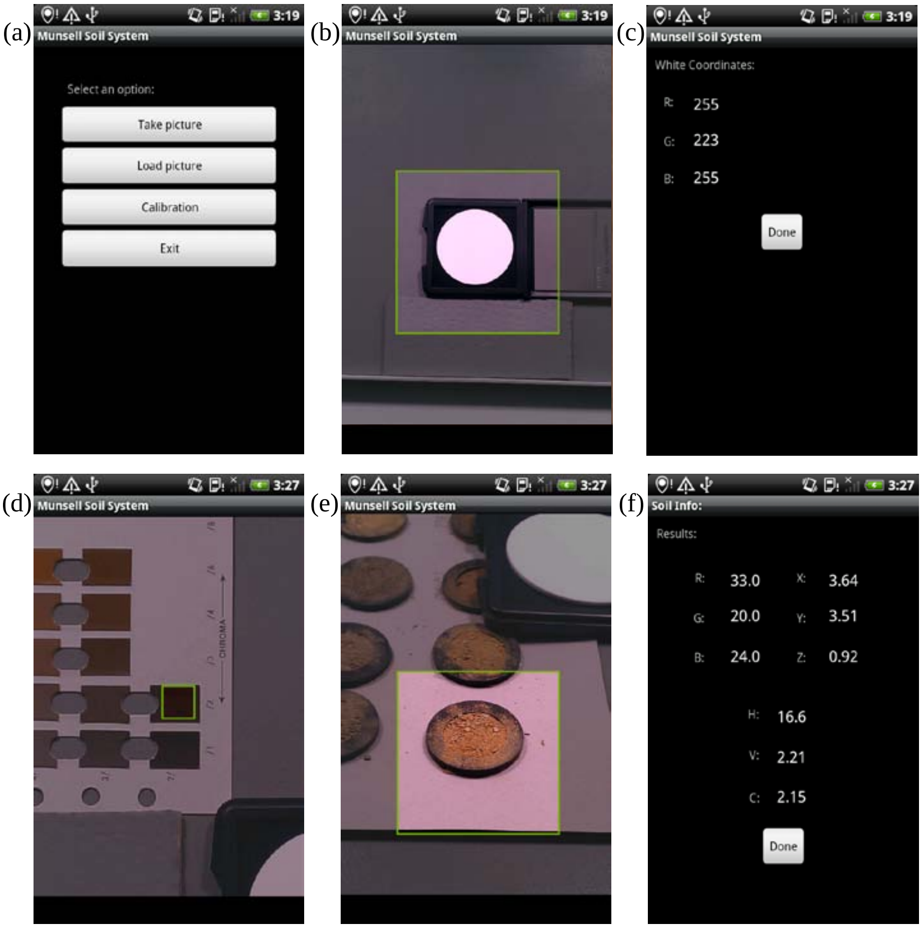

White Coordinates:

R: 255
G: 223
B: 255

Results:

R:	33.0	X:	3.64
G:	20.0	Y:	3.51
B:	24.0	Z:	0.92

H: 16.6
V: 2.21
C: 2.15

Figure 5.15 Captions of the different screens shown by the Android application during the measurement process.

Here the main objective is to obtain the Munsell as well as the XYZ coordinates from the RGB for soil classification and comparison with instrumentation, respectively. The equations used to transform the coordinates from one space to another can be extracted from literature (Rossel *et al.* 2006) or from the empirical results obtained from the colour measurements carried out in this work. Rossel uses standard transformation equations processed using the ColoSol software, while in this experimental case, the colour measurements of the 238 chips of the Munsell soil-colour charts obtained with the developed Android application were used.

All the measurements carried out for obtaining the empirical equations were taken under controlled conditions of light as shown in Figure 5.16. The samples were placed inside a booth with a fixed distance to the spectroradiometer and the mobile phone, which is placed under the instrument to avoid interference capturing the pictures and the light respectively. Three replicas were taken for each measurement.

Figure 5.16 Assembly of the instruments and samples during measurement process.

Once that the RGB and XYZ values are calculated from the smartphone and the spectroradiometer data respectively, and using the

HVC values established by the Munsell soil-colour charts, the polynomial transformation equations can be determined by the pseudo inverse method (Johnson 1996), (Penrose 1955). With this method, that follow the $i = Td$ relation, where i is the XYZ or HVC (3×1 matrix) from independent device colour and d is an RGB n×1 matrix from dependent device colour, the objective is to find out the T matrix that provides the more accurate relation between vectors i and d. The transformations were carried out using Matlab 2009b (The MathWorks, Inc, Natick, MA, USA) and using the process determined by literature (Westland and Ripamonti 2004).

5.4.3 Results and discussion

In this section the equations for the colour space transformation are presented. These equations are used for transforming the coordinates from RGB colour space obtained from the JPEG pictures to XYZ and HVC coordinates for comparison to the spectroradiometer and the Munsell charts respectively. Finally, a procedure of validation is described, using for this purpose NCS samples and real soil samples with the Android application here developed.

Transformation equations from RGB to XYZ and HVC

Three replicas were taken for each measurement which show a negligible value of standard deviation for RGB (<0.01) and XYZ (<0.03) due to the stability of the light source and the homogeneity of the chips. Table 5.3 shows the statistical Pearson's correlation coefficient r for each model. Besides, $\bullet E^{*}_{ab}$ and $\bullet E^{*}_{M}$ represents the CIELAB colour difference (CIE 2004) and the Munsell colour difference (Godlove 1951), respectively, between the measured and the predicted values. They were determined in order to study the accuracy of the models presented. As it can be seen in Table 5.3, several options were studied from a model of order one to a complex polynomial of order three. However, despite the high number of terms tested, a model of order three with just eight coefficients was enough to optimize the work performed by the mobile phone providing good results of correlation coefficients and colour differences. Therefore, the chosen model is the shown in the last row of the table.

Table 5.3 Transformation equations from RGB to XYZ and HVC obtained with the measurement of 238 chips of the Munsell soil-colour charts.

Terms of the polynomial	r for XYZ models	r for HVC models	ΔE^*_{ab}	ΔE^*_{M}
[1,R,G,B]	0.9811	0.9090	9.65	2.03
[1,R,G,B,RGB]	0.9943	0.9101	6.03	1.53
[1,R,G,B,RG,RB,GB]	0.9965	0.9246	3.44	1.12
[1,R,G,B,RG,RB,GB,RGB]	0.9965	0.9259	3.39	1.12
[1,R,G,B,RG,RB,GB,R^2,G^2,B^2]	0.9973	0.9547	2.14	1.03
[1,R,G,B,RG,RB,GB,R^2,G^2,B^2,RGB]	0.9973	0.9562	2.07	1.02
[1,R,G,B,RG,RB,GB,1.38R^2,G^2,B^2,RGB,R^3,G^3,B^3]	0.9974	0.9568	1.85	1.02
[1,R,G,B,RG,RB,GB,R^2,G^2,B^2,RGB, R^2G,G^2B,B^2R,R^2B,G^2R,B^2G,R^3,G^3,B^3 ,R^2GB,RG^2B,RGB^2]	0.9980	0.9695	1.75	0,97
[1,G,B,RG,R^2,G^2,RGB,B^3]	**0.9972**	**0.9407**	**2.03**	**1,08**

The corresponding coefficients of the selected model are shown in Table 5.4, where the complete equation that describes the transformation between colour spaces for each component is described in Equation 5.12.

$$\emptyset(RGB) = a + bG + cB + dRG + eR^2 + fG^2 + gRGB + hB^3 \tag{5.12}$$

Table 5.4 Coefficients for the polynomial model built to determine the XYZ and HVC values from the RGB coordinates.

	a	b	c	d	e	f	g	h
X	1.3502	0.0759	-0.0082	1.05E-04	0.000381	0.000124	2.79E-06	-1.31E-06
Y	0.7246	0.1146	-0.0172	-3.20E-04	3.06E-04	0.000604	3.08E-06	-1.54E-06
Z	-2.1291	0.1028	0.0879	-4.80E-04	1.04E-04	0.000174	2.41E-06	2.13E-06
H	10.5649	0.4622	-0.2192	-2.54E-03	1.92E-05	6.09E-04	7.98E-06	-4.64E-06
V	2.3252	0.0303	-0.0069	-5.36E-05	4.33E-05	-1.61E-05	2.40E-07	-2.96E-08
C	1.8311	0.0157	-0.0351	-3.80E-04	2.89E-04	0.000163	-3.00E-07	2.25E-07

In comparison to the RGB coordinates obtained with ColoSol software that uses standard equations, better results are obtained with the transformations presented in this work as it can be seen in Table 5.5. The differences in both methods can be justified because the RGB colour space is device dependent (Hong *et al.* 2001), (Westland and Ripamonti 2004), as well as the conditions of the measurements were also different during the acquisition of the colour information (Wyszecki and Stiles 1982).

As it can be deduced from Table 5.5, the transformation carried out using the smartphone from RGB to XYZ is more accurate than the provided for the HVC coordinates. This can be explained due to the same geometry of the RGB and XYZ colour spaces, while the HVC has a cylindrical structure (Wyszecki and Stiles 1982). The lower the C coordinate is, the higher the uncertainty of the H value since with a null value of C the H coordinate cannot be determined. For this reason, from the 35 chips that were estimated with a ΔH>4 units, 72% had a chroma value lower than 2 units, 8% had C=3. The other 20% had a chroma value of 7/8 and 8/8, which are extremely light and chromatic. Therefore, the equation obtained for the H coordinate fits worst to the chips with low and high values of chroma.

Table 5.5 Comparison between the data obtained in this work and the data obtained using the equations by Rossel.

	Polynomial transformation			**ColoSol software**		
	X	**Y**	**Z**	**X**	**Y**	**Z**
r	0.9971	0.9972	0.9973	0.9942	0.9945	0.9904
Mean ΔE_{ab}		2.0			14.0	
SD ΔE_{ab}		1.1			4.5	
	H	**V**	**C**	**H**	**V**	**C**
r	0.8313	0.9977	0.9708	0.8795	0.9965	0.9764
Mean ΔH/ΔV/ΔC	2.1	0.1	0.4	4.7	0.5	1.8
SD ΔH/ΔV/ΔC	1.7	0.1	0.3	2.6	0.3	0.9
Mean ΔE_M		1.1			3.2	
SD ΔE_M		0.5			1.1	

With the polynomial transformation deduced from the experimental data the difference between the real Munsell coordinates and the predicted was 2.0 ± 1.1 CIELAB units. As shown in Figure 5.17, using this equations over the 238 chips of the Munsell soil-colour charts used in the acquisition process of data, more than 90% of samples were measured with the smartphone with a colour difference • E^{*}_{ab} lower than 4 CIELAB units.

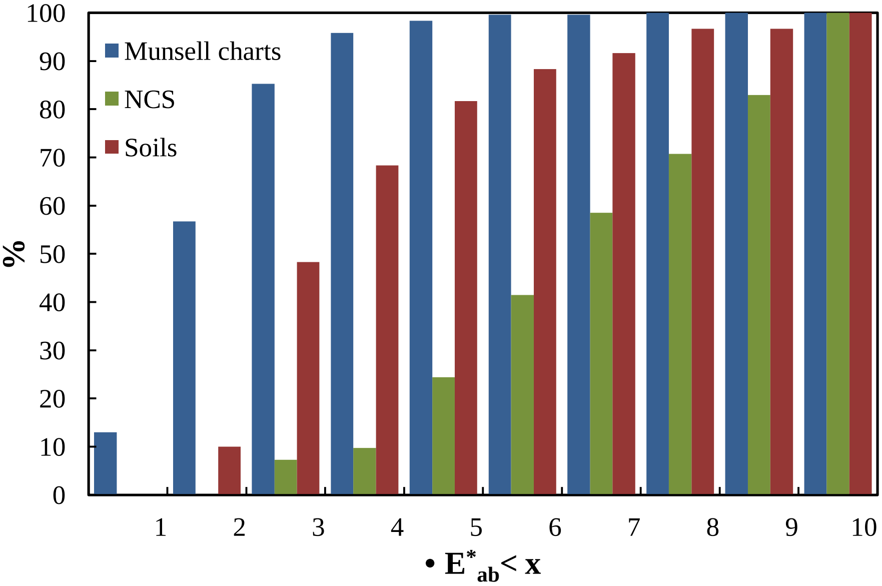

Figure 5.17 Percentage of samples with a CIELAB difference lower than a x-axis value between spectroradiometer and the HTC measurements.

Validation with NCS and real soils samples

In a first approach to real samples, 40 NCS samples were selected in order to test the models determined from real measurements with the smartphone and the spectroradiometer. These samples are also homogeneous and have plain surface and were analyzed in the same controlled conditions of illumination. For this reason, the three replicas carried out for each sample showed a negligible standard deviation for RGB ($<$0.06) with the smartphone and for XYZ ($<$0.98) with the spectroradiometer.

Applying the RGB to XYZ transformation equations over the NCS samples, it can be deduced from Figure 5.17, that, as expected, the CIELAB differences are greater than in the previous case. The higher differences were obtained for those whose hue value was higher than 22.5, that is yellowish samples, and with very low or very high chroma values. As explained before, those are the samples that cause higher discrepancies due to the difficulty in determine the H coordinate with low chromatic samples. In this way, around 50% of NCS samples were measured with the mobile phone with an error lower than 6 CIELAB units.

With regard to HVC coordinates, in Figure 5.18, the differences obtained between the measurements carried out using the smartphone and the equations here developed and those provided by the spectrophotometer are shown. As it can be seen, for NCS samples, 80% of the samples were measured with a difference lower than 3 units in the hue value, while for the value and chroma the 100% of the samples were under 3 units.

In case of real soils samples, as mentioned before, 60 samples were used in total. In Figure 5.17 it can be deduced that around the 90% of the samples were classified with a CIELAB difference lower than 6 units. In particular, the mean CIELAB difference was of 3.7±1.8 units. These results are better than the obtained from the NCS samples due to the fact that the gamut covered with the real soil samples does not include high values of chroma for the samples. However, as shown in Figure 5.18, worst results are provided by the mobile phone with regard to the HVC coordinates of real soil than those calculated from the spectrophotometer. In this case, around 80% of the soils were measured with a difference in the hue component lower than 4 units and lower than 2 units for chroma and value. Since between different Munsell charts the difference in the hue value is from 5 units, the smartphone carries out a good classification of the soil in the correct chart. Besides, as previously described, these differences can be explained due to the different light sources used for the spectrophotometer and the mobile phone, as well as for the cylindrical geometry of the Munsell system.

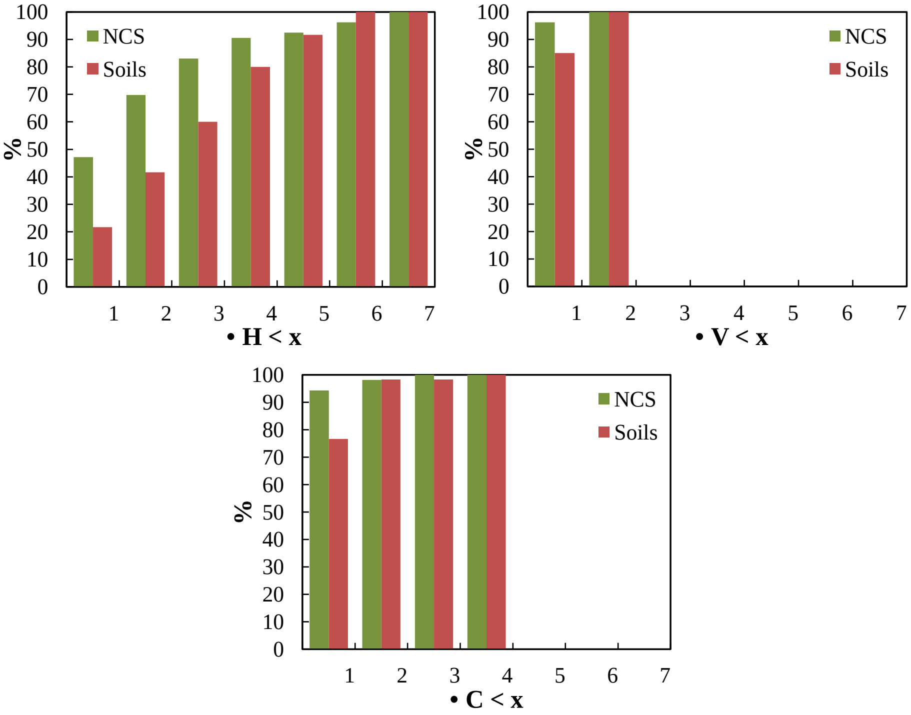

Figure 5.18 Hue, value and chroma differences between the smartphone and the spectrophotometer measurements for NCS and real soil samples.

In Table 5.6, a summary of the measurements carried out with the HTC Desire phone is shown. The mean values of the differences for the HVC colour spaces as well as for the XYZ are listed. As explained in this section, the CIELAB differences were lower for the real soil samples than for the NCS, which is reflected in the mean values of

• E^*_{ab} shown in the table. Furthermore, it is worth to be noticed the better results obtained for the ground samples than for those treated to be more homogeneous. As remarked throughout this report, the use of the statistical mode as value for the coordinates removes the influence of non heterogeneous surfaces, as in the case of the ground samples.

In addition, the measurements over the soil samples were also carried out using a Samsung Galaxy SII in order to test the developed models and equations in a different device. Due to the different manufacturer of the smartphone, the camera sensor is also different and, therefore, some discrepancies in the measurements could appear. However, as shown in the data of the table, the results are still optimal and acceptable, and the differences are not so far from those obtained with the HTC smartphone. Therefore, the application can be interchangeable for different mobile phones that run Android operative system providing good results for soil classification under the same controlled conditions of light.

Table 5.6 Summary of the differences obtained using the HTC Desire HD and the Samsung Galaxy SII smartphones with the different set of samples.

Group of samples	**Colour parameter**	**Mean value**	**Standard deviation**
NCS samples HTC smartphone	ΔH	1.69	1.69
	ΔV	0.66	0.22
	ΔC	0.36	0.34
	ΔE^*_{ab}	6.45	2.05
Ground soil samples HTC smartphone	ΔH	2.05	1.23
	ΔV	0.57	0.31
	ΔC	0.32	0.20
	ΔE^*_{ab}	5.04	2.47
Fine soil samples	ΔH	2.72	1.70
	ΔV	0.57	0.36

HTC smartphone	ΔC	0.81	0.60
	ΔE^*_{ab}	3.31	1.59
Soil samples Samsung smartphone	ΔH	3.38	1.55
	ΔV	0.63	0.26
	ΔC	0.25	0.17
	ΔE^*_{ab}	5.46	2.46

To conclude this work, a comparison with the results obtained for visual methods was made. In particular a group of ten soil scientists classifying soil colour under controlled illumination had a mean error of 4.4 and 10.2 CIELAB units for ground samples and aggregated soil samples respectively, with respect to instrumental measurements. The inter-observer variability regarding the Munsell notation of a given sample was 5.1 CIELAB units (Sanchez-Maranon *et al.* 1995). In other studies using different Munsell charts edition from different manufactures and different degrees of use, the differences were from 5.5 CIELAB units (Sanchez-Maranon *et al.* 2005). Therefore, it is possible to conclude that use the smartphone as colour sensor for soil classification reduces the inter-observer variability as well as improves the results obtained using traditional visual techniques.

5.5 Study of stability in emulsions using a commercial camera

An emulsion is a mix of two or more liquids that are usually non-mixable and, hence, it tends to be unstable. The stability of an emulsion is the capacity to remain the properties unalterable with the time, temperature or other external agents. To avoid the separation of the components and the instability, several emulsifiers are added into the mixture. For example, in the sauce industry most of the emulsions are composed of oil-water or water-oil mixtures that need other components to remain together. In the food industry the study of this parameter is fundamental to extend the useful life of different kind of food.

For analyzing and studying the stability in emulsions different processes of destabilization can be applied to the samples. Thus, the process to achieve instability can be accelerated using centrifugation methods as well as increasing the temperature of storage of the samples. With these processes of destabilization different phenomena can take place. The phenomena relating to the aggregation of particles are flocculation and coalescence, while the separation of the emulsion in different layers occurs due to the creaming or the sedimentation of particles. With the flocculation the particles of the emulsion are together but they do not lose their own identity, while in the coalescence process they mix together to form bigger droplets. The higher the size of the droplets, the lower the stability of the emulsion is. In the creaming and the sedimentation there is a separation of oil and aqueous phases (Fernandez Arteaga 2006). Similar procedures for destabilization have been used in different works for different kind of foods: for determination of emulsion stability of sesame pastes blended with pine honey (Akbulut *et al.* 2012); to study the effects of protein level and fat on emulsion stability of meat batters (Youssef and Barbut 2009); or for determination of the rheological properties and stability in low-cholesterol mayonnaises (Laca *et al.* 2010).

Generally, light scattering techniques have been used for the determination of instability of the samples, since the separation or aggregation of particles or droplets can modify the behaviour of the light through the sample (McClements *et al.* 1998). If the analyzed region of the sample is well mixed then the light has difficulties to pass through, while in separated and, therefore, no stable samples, the light can penetrate better and more light is transmitted. Some of these methods are spectroscopy, microscopy or turbidimetry (Buron *et al.* 2004), (Cretu *et al.* 2009), (Pedro and Ferreira 2009). Other methods are based on the determination of the influence of the particle size in the stability of food (McClements 2005), (McClements 2002), (Chanamai and McClements 2001). Here, a colorimetric method was used to determine the optical properties of oil-water emulsions from pictures of the emulsions and relate them to the stability. The cost of this technique is lower than the produced by other techniques and, besides, due to the opacity of some samples the use of light scattering methods is limited for this case.

Until now, the CIELAB colour space has been used mostly in the literature for determination of stability in emulsions of different origins. In particular, the colour of the emulsions is used to be related with the size or the concentration of the droplets (Chantrapornchai *et al.* 1998), (Chantrapornchai *et al.* 1999). Some of the works carried out in this field are: use of the L parameter for the stability measurement of meat emulsions using an optic fibre (Barbut 1998); use of a chromameter for measuring of the La*b* coordinates in meat emulsions to determine the stability (Alvarez *et al.* 2007), (Alvarez *et al.* 2009); or the study of the colour evolution of emulsions with sodium caseinate using the XYZ and CIELAB colour spaces (Cretu *et al.* 2009) among others. Here, different colour spaces have been used instead of find the relation between the colour of the emulsion and the stability just using CIELAB. In this way, RGB, HSV and CMYK were also studied.

The main objective of this work was to analyze different colour parameters of the acquired images of the emulsions in different phases of destabilization in order to find a relation between them and the process of destabilization. In particular, three different mayonnaises were studied with the intention of predicting the point of stability by colour determination. For the purpose, two different techniques were used to make unstable the studied sauces: the increasing of the temperature and the centrifugation of the samples in order to separate the components of the emulsions.

Destabilization procedures

With the objective of analyzing the optical properties of emulsions to determine the relation between the colour parameters and the stability, three different mayonnaises were used: light sauce and soft sauce Hacendado (Mercadona, Spain) and Calve Balance sauce (Calvé, Spain). Both, the light sauce Hacendado and the Calve Balance have a 60% less of fat content than the soft mayonnaise. These samples were destabilized with two different processes: increasing of temperature and centrifugation of the emulsions.

For the destabilization with temperature, two different processes were used. In a first approach, the samples of mayonnaises were placed in Petri dishes in order to be warmed up in an Venticell 55 oven from MMM Group (MMM MedCenter GmbH, Germany) at 50 ºC during different intervals of time. Secondly, the samples were placed in tubes of 30 mL of polyvinyl chloride (PVC) from Orto Alresa (Orto Alresa, Spain) and heated in a water bath at different temperatures from 25 to 100 ºC.

In the case of the centrifugation technique, the same tubes mentioned before were used and placed in a spinner model DIGICEN 20 with a RT153 rotor that allows to select different speeds of spinning up to 13500 rpm, which is equivalent to a maximum acceleration of 18750g. The tubes were sampled taking pictures at different intervals of time to study the influence of the spin in the stability of the three mayonnaises.

During the process of destabilization, a picture of each sample was taken with a commercial camera and analyzed further in a computer using a script with a set of instructions in Matlab R2010b (The MathWorks, Inc, Natick, MA, USA). The picture was taken under controlled conditions of light in a dark environment. As it can be seen in Figure 5.19, two energy-efficient light bulbs (8W - 6400K) were used as light source. In order to carry out a correction of the light, a white sample of reference was included in every picture, to normalize the coordinates of the sample taking into account the RGB coordinates of the reference white, following the same principle explained for soil classification in previous section (Salmeron *et al.* 2012).

The camera used was a Canon Powershot G12. This camera has a CCD sensor with up to 10 megapixels available. The settings were configured to provide a picture of 2504 × 3326 of size with 24 bits for encoded the coordinates of the RGB colour space in JPEG format. To study the change in the properties of the mayonnaises four different colour spaces were used: RGB, HSV, CMYK and CIELAB. The transformation between spaces was carried out using Matlab© and the standard equations (Wyszecki and Stiles 1982), (McConnell 2006). For all the cases, the statistical mode of each colour coordinate has been used as analytical parameter since, as mentioned in this report, it offers good stability (Cantrell *et al.* 2010) to light variations of light despite the controlled conditions of the experiment.

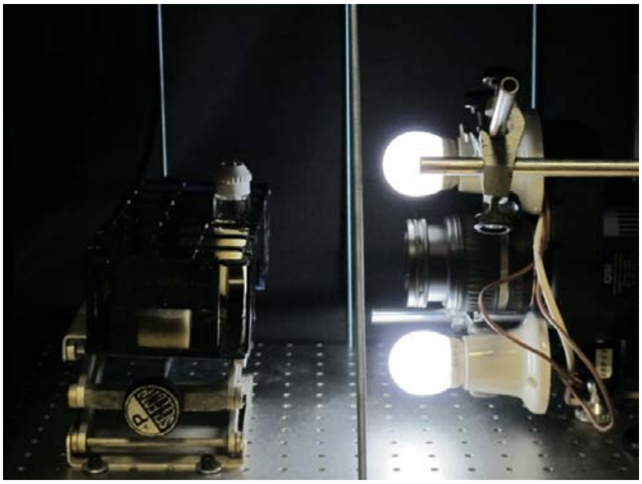

Figure 5.19 Photograph of the controlled light environment.

Destabilization by temperature

Firstly, the study of the temperature influence on the stability of the sauces was carried out. In an initial approach the samples were placed in Petri dishes and introduced in an oven in order to increase the temperature of the samples up to 50ºC. After every ten minutes of interval, until two hours, pictures of the sauces were taken for image-processing. The evolution of the colour on the surface of the mayonnaises can be observed in Figure 5.20, Figure 5.21 and Figure 5.22, where the samples changed their hue with the increasing of time of exposition to the 50ºC of temperature in the oven.

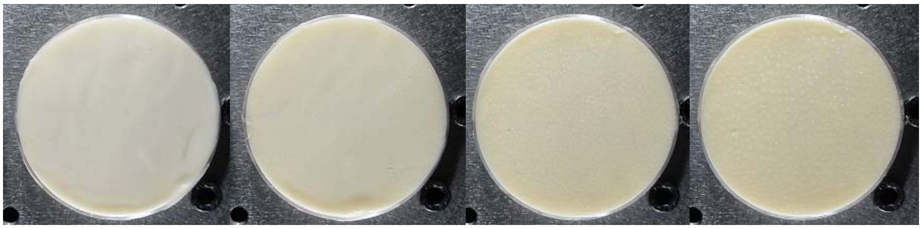

(a) (b) (c) (d)

Figure 5.20 Photograph of Calve mayonnaise at 50ºC after (a) 0, (b) 40, (c) 80 and (d) 120 minutes.

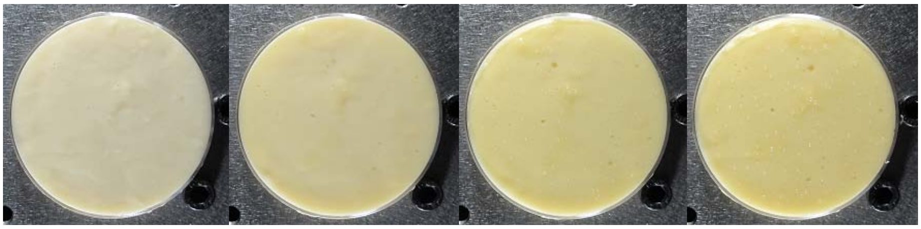

(a) (b) (c) (d)

Figure 5.21 Photograph of Hacendado light mayonnaise at 50ºC after (a) 0, (b) 40, (c) 80 and (d) 120 minutes.

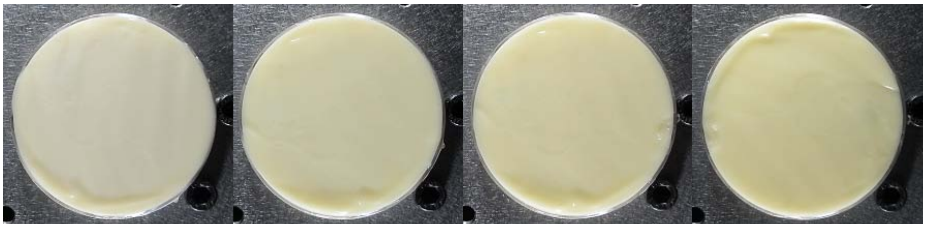

(a) (b) (c) (d)

Figure 5.22 Photograph of Hacendado soft mayonnaise at 50ºC after (a) 0, (b) 40, (c) 80 and (d) 120 minutes.

In the case of the Calve mayonnaise, Figure 5.20, the appearance of droplets on the surface of the sauce as a result of the creaming can be observed when the time of exposition is higher of 40 minutes. Also, it can be seen the higher change of colour in the light mayonnaise, Figure 5.21, than in the other cases. In order to analyze the colour behaviour of the different sauces, several colour spaces were studied to find a relationship between the parameters and the state of destabilization. It is important to indicate that using this arrangement of the samples in the Petri dishes only the surface of the sauce could be analyzed without taking into account the changes in the rest of the mayonnaise.

For the Calve Balance emulsion, the Y coordinate of the CMYK space and the B of the RGB space showed a tendency that can be used to prediction of the instability of the sauce. In this case, the fitting can be made using logarithmical or polynomial functions as shown in Figure 5.23.

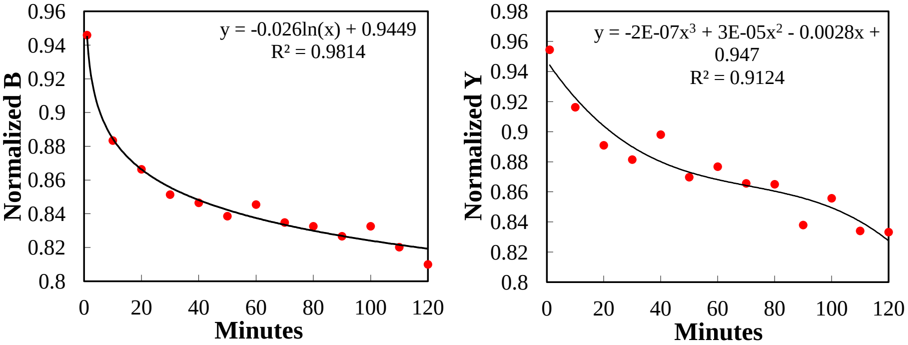

Figure 5.23 Curves of the B and Y coordinates at 50ºC for the Calve Balance mayonnaise.

The light sauce Hacendado presents a more evident change than the other two sauces. This fact is reflected in the fitting curves, which present a higher R^2 coefficient for all the selected components, as it can be seen in Figure 5.24. In this case, using the combination of two coordinates of the RGB space, red and blue, a better prediction of the stability could be made. That means that the green component of the mayonnaise remains stable, but the red and the blue provides a greenish yellow. Also, the Y and S component of the CMYK and HSV colour spaces respectively could be used with similar results.

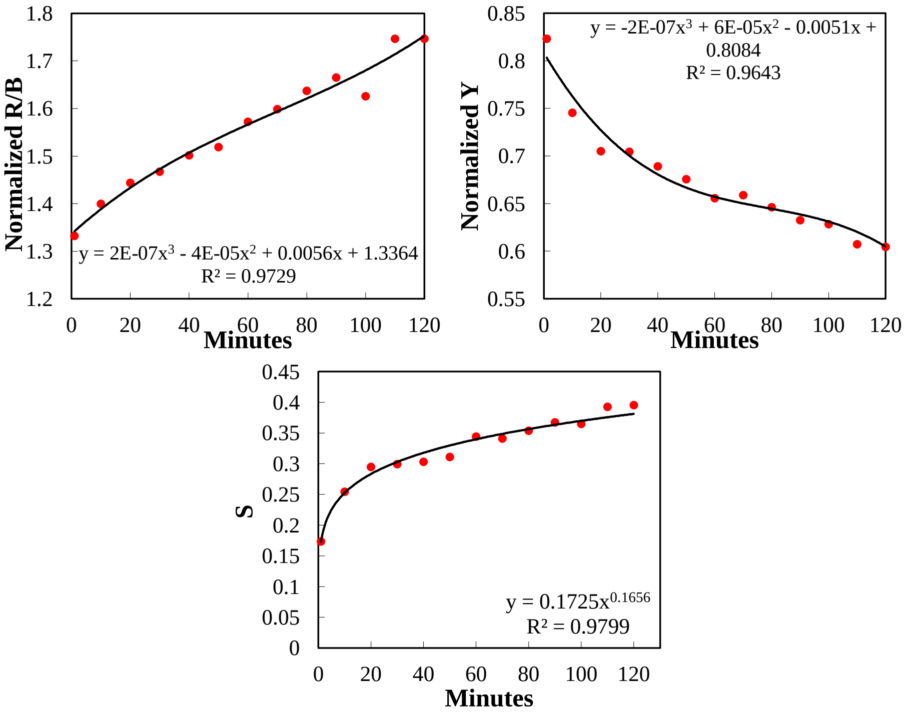

Figure 5.24 Fitting curves of the R/B, Y and S coordinates at 50ºC for the light Hacendado mayonnaise.

Finally, the soft Hacendado emulsion was studied using the same technique. In this case, the saturation and the R/B ratio are used to describe the behaviour of the mayonnaise with regard to the time of exposure at 50ºC of temperature. The results are presented in Figure 5.25.

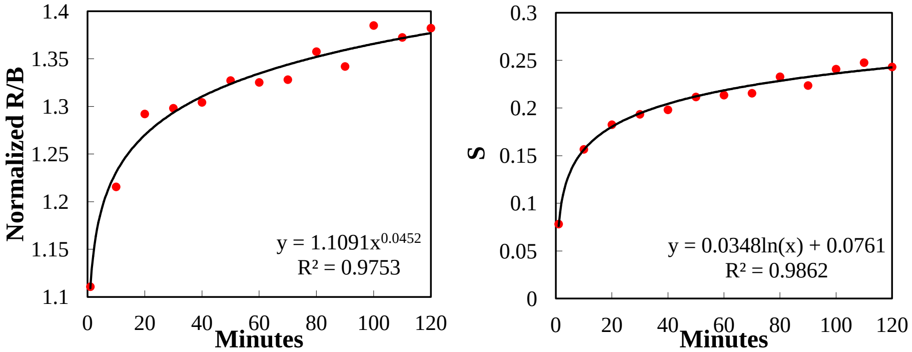

Figure 5.25 Response of the R/B and S coordinates at 50ºC for the soft Hacendado mayonnaise.

As it can be seen, for all the studied samples, the coordinates followed the same tendency, which means that the process of destabilization produces the same effect in these emulsions. As it can be deduced, using the Petri dishes, only the surface of the mayonnaise was analyzed. In order to study the influence of the temperature in the whole sample and not only in the exterior, the sauces were placed in tubes as explained in the section above. For this purpose, they were immersed in water at 95 ºC of temperature during three hours to find any sign of decomposition or instability. In Figure 5.26, the initial and final states for each emulsion are shown. The red rectangle denotes the area of the picture that was processed by the computer to extract the colour coordinates of interest and, as mentioned before, the statistical mode was obtained for each case. Each graphic represents the difference between the initial value of the colour coordinate and the obtained after the destabilization procedure.

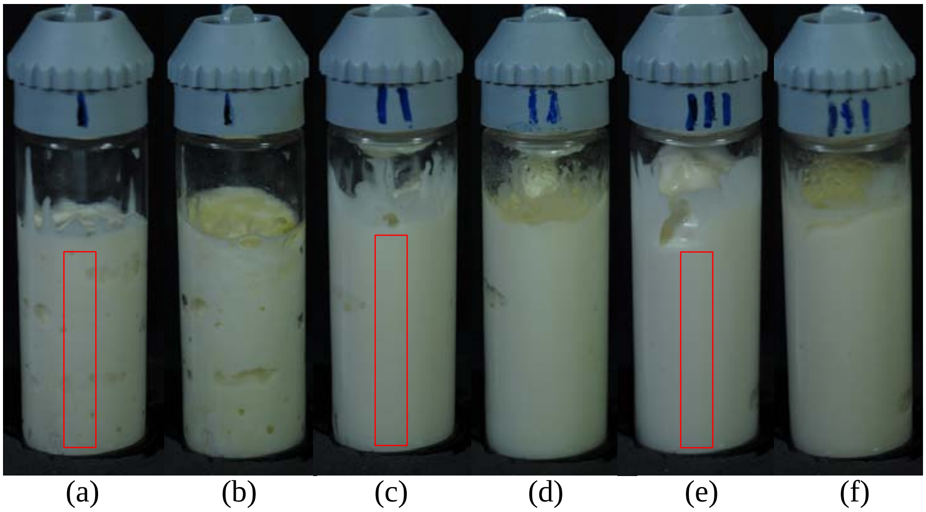

Figure 5.26 Initial and final states for the three mayonnaises after warm water bath at 95ºC for three hours: (a) and (b) light Hacendado; (c) and (d) soft Hacendado; and (e) and (f) Calve Balance.

In the first case, the light Hacendado mayonnaise shows a decreasing of the B and H components of colour, as well as an increasing in the b* coordinate of the CIELAB as depicted in Figure 5.27. The x axis represents the height in the tube going from the bottom to the top in order to study the change in the sauce during the heating process. The peaks observed in the graphics correspond to the air bubbles in the tubes of mayonnaises since the sauces where not compacted before the temperature bath.

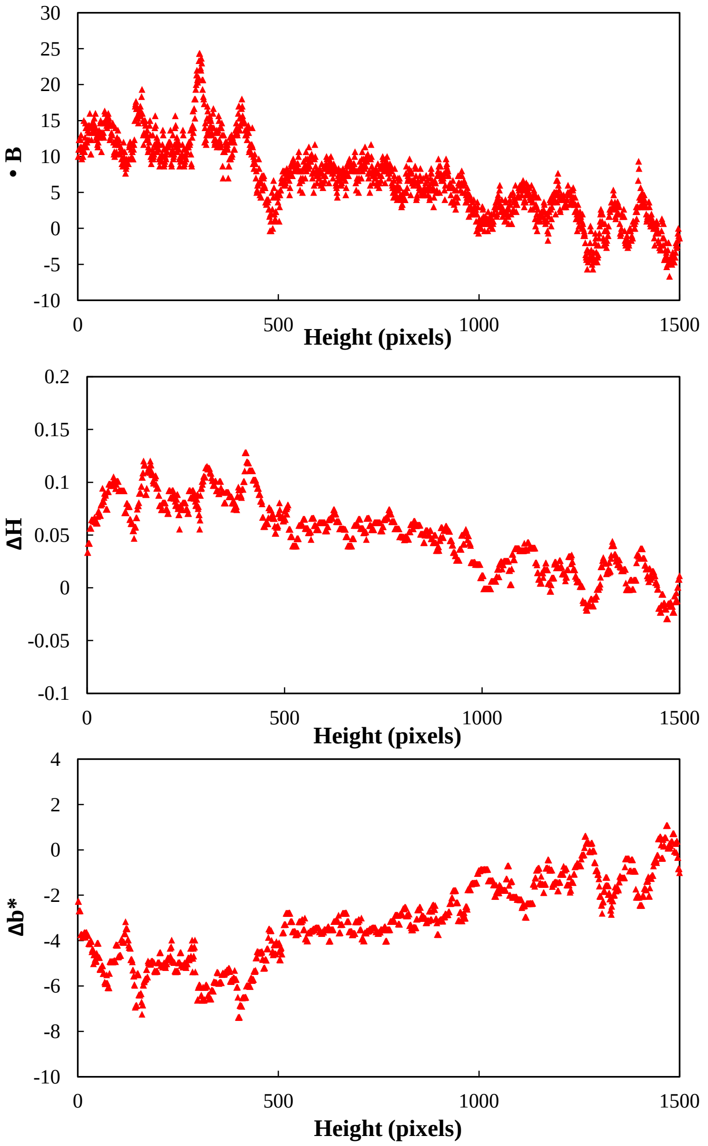

Figure 5.27 Changes in the colour components B, H and b* after heating for the light Hacendado mayonnaise.

For the second mayonnaise, soft Hacendado, only changes in the hue component are observed, as it can be seen in Figure 5.28, although the change is less pronounced than in the previous case.

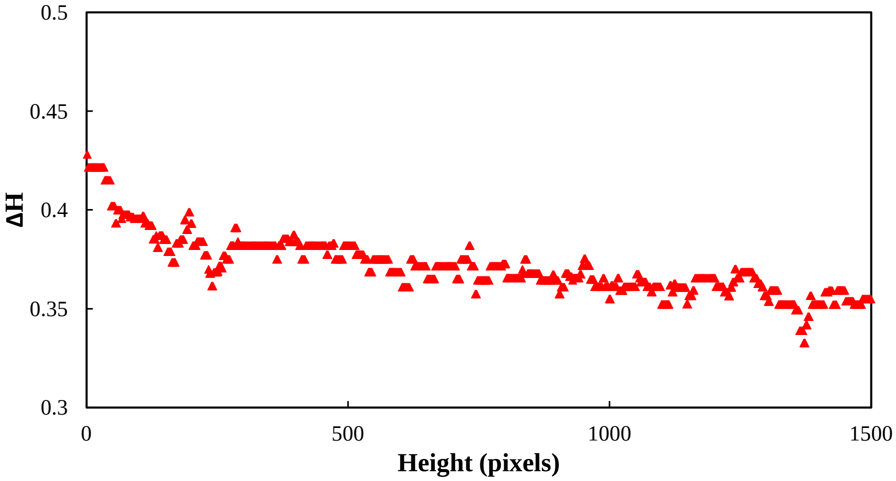

Figure 5.28 Hue component response after the temperature bath for the soft Hacendado mayonnaise.

The Calve Balance sauce does not show any variation in the colour coordinates with this kind of technique for destabilization. Therefore, the stability of this emulsion against temperature increase is higher than in the case of the Hacendado mayonnaises.

As deduced from the results shown in this section, the influence of the temperature is more visible on the surface when the sample is directly exposed to the temperature than in the second experiment carried out.

Destabilization by centrifugation

After the temperature study, spin techniques were used in order to destabilize the sauces. With this process, a separation in oily and aqueous layers was obtained for each case as observed in Figure 5.29. The samples were subjected to 12000 rpm of speed, which is equivalent to 14800 g, during 30 and 60 minutes. Due to the inclination of the tubes inside the spinner, the mayonnaise is not uniformly distributed inside the tube and, therefore, two pictures for each tube were taken in order to take into account the different layers observed from different angles. For each picture, the complete available height, pixel by pixel, was analyzed using the computer. In the same way as for the previous studies, the difference between the initial value of each colour coordinate and the final value after the destabilization procedure is shown in the corresponding figures, in order to extract any tendency to describe the behaviour of the mayonnaise.

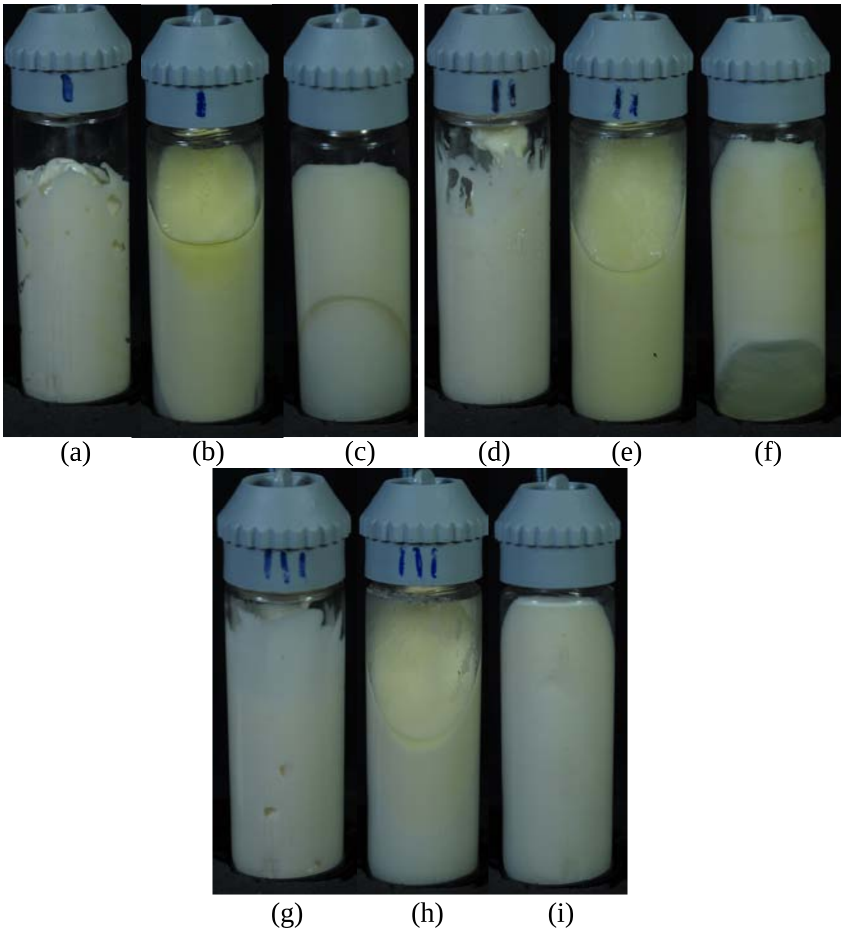
(a) (b) (c) (d) (e) (f)

(g) (h) (i)

Figure 5.29 Initial and final states for three mayonnaises after spin at 12000 rpm: (a), (b) and (c) light Hacendado; (d), (e) and (f) soft Hacendado; (g), (h) and (i) Calve Balance.

In the case of the light sauce Hacendado, an oily layer can be observed from the front while a starch layer is visible from the rear. These changes are observable in the B component of the RGB colour space, Figure 5.30, as well as in the b* coordinate of the CIELAB space, Figure 5.31, where the changes of phases are denoted in the graphics.

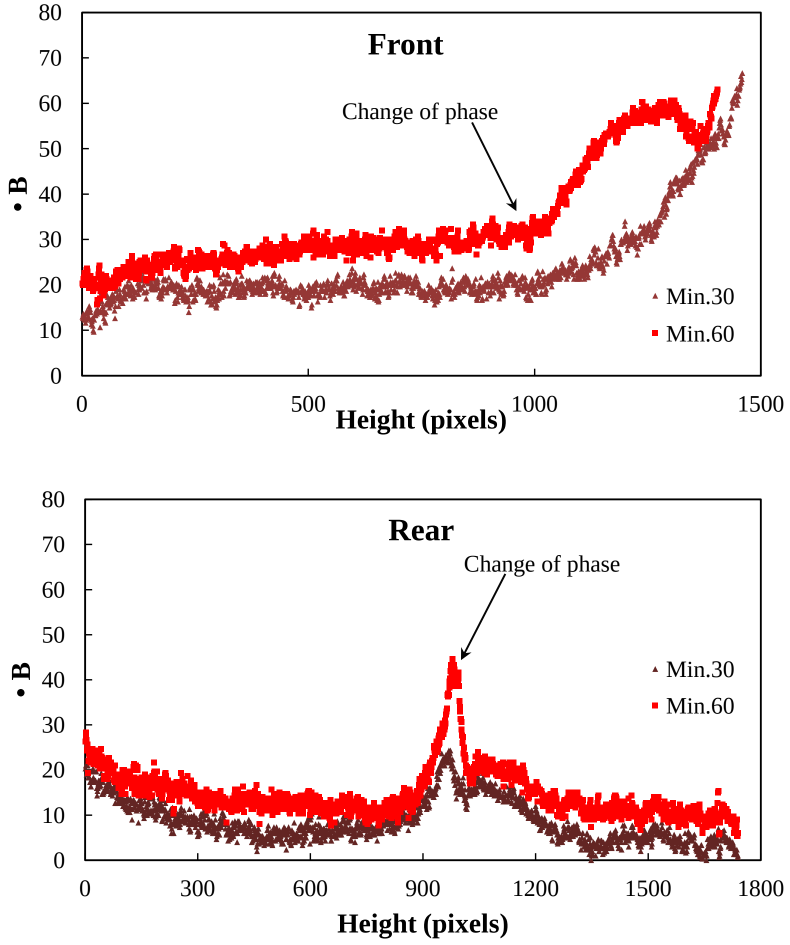

Figure 5.30 B component after 30 and 60 minutes of centrifugation for light Hacendado mayonnaise.

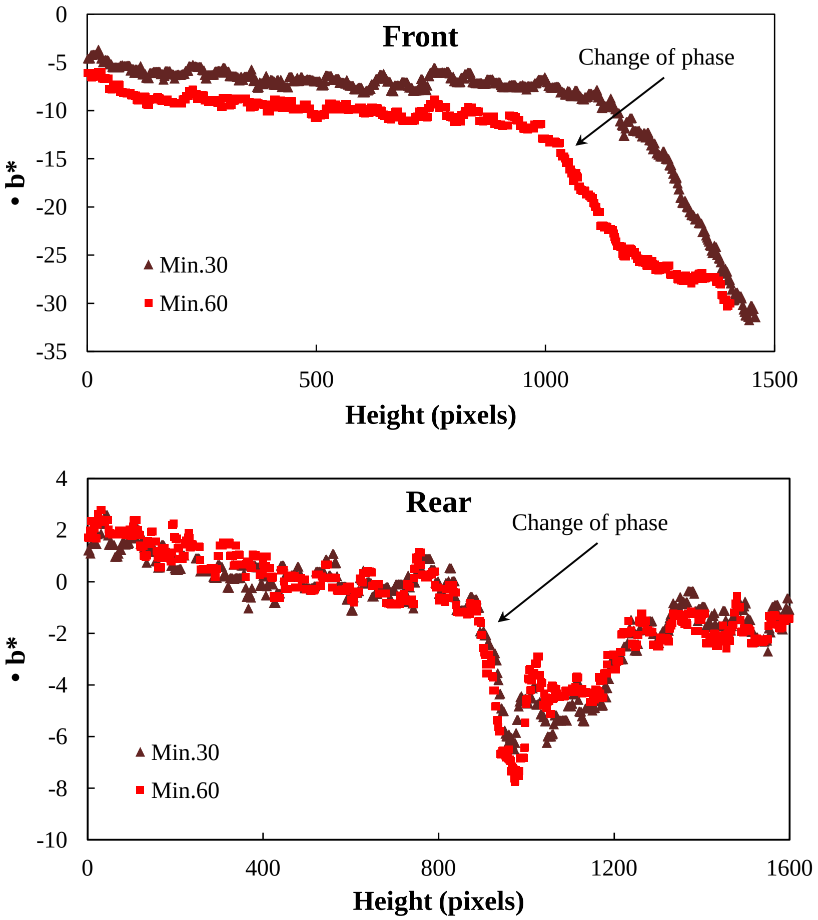

Figure 5.31 b* coordinate after 30 and 60 minutes of centrifugation for light Hacendado mayonnaise.

The centrifugation of soft Hacendado mayonnaise leads to a destabilized state where an aqueous phase can be observed at the bottom of the tube in the front picture, while in the upper layer there is a presence of oil. In this case, the components of interest to study the decomposition of the mayonnaise are the B component of the RGB space and the L coordinate of the CIELAB colour space. As it can be seen in Figure 5.32 and Figure 5.33, the changes of phase either in the front or the rear of the sample are clearly determined by the change in these coordinates.

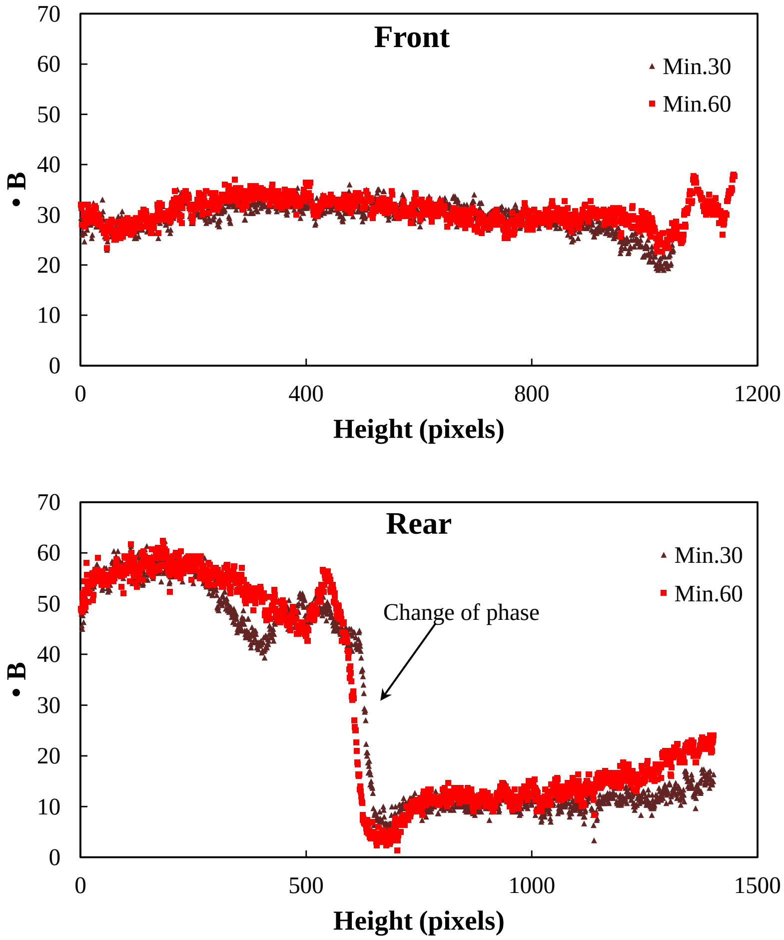

Figure 5.32 B component after 30 and 60 minutes of centrifugation for soft Hacendado sauce.

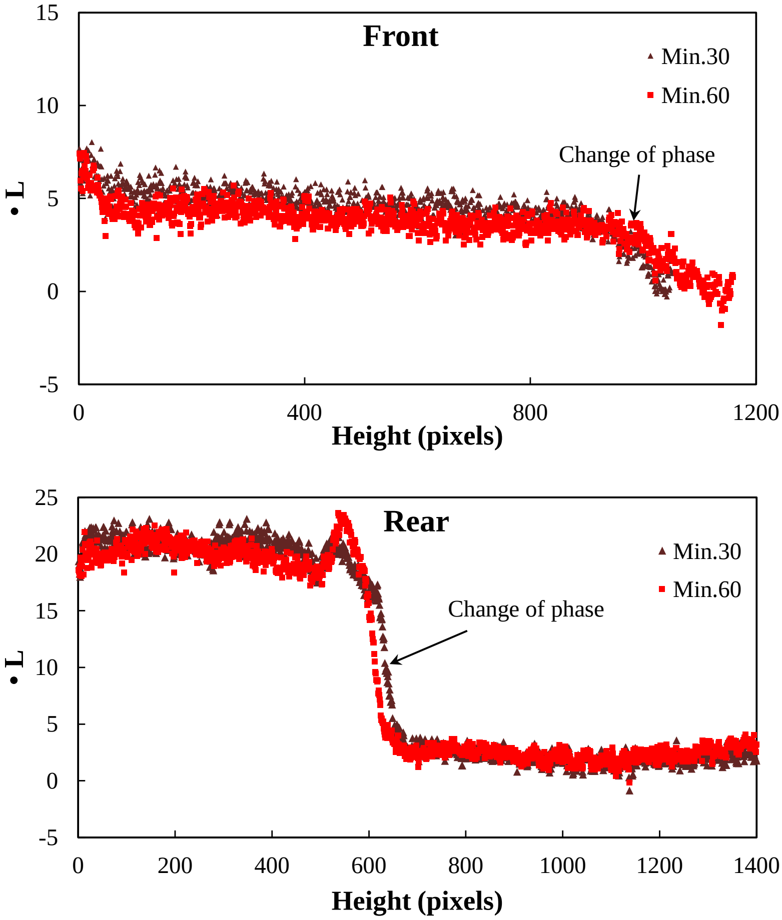

Figure 5.33 L component after 30 and 60 minutes of centrifugation for soft Hacendado mayonnaise.

For the Calve Balance mayonnaise the destabilization is less evident since the change of colour is not quite visible, as observed in Figure 5.29h and Figure 5.29i. However, when the pictures are processed the component H of the HSV colour space, as well as the b* of the CIELAB space, show a change corresponding to two different phases. In this way, from the front of the tube a separation in an aqueous phase, a main part and an oily layer is observed, while the oily phase is not observable from the rear.

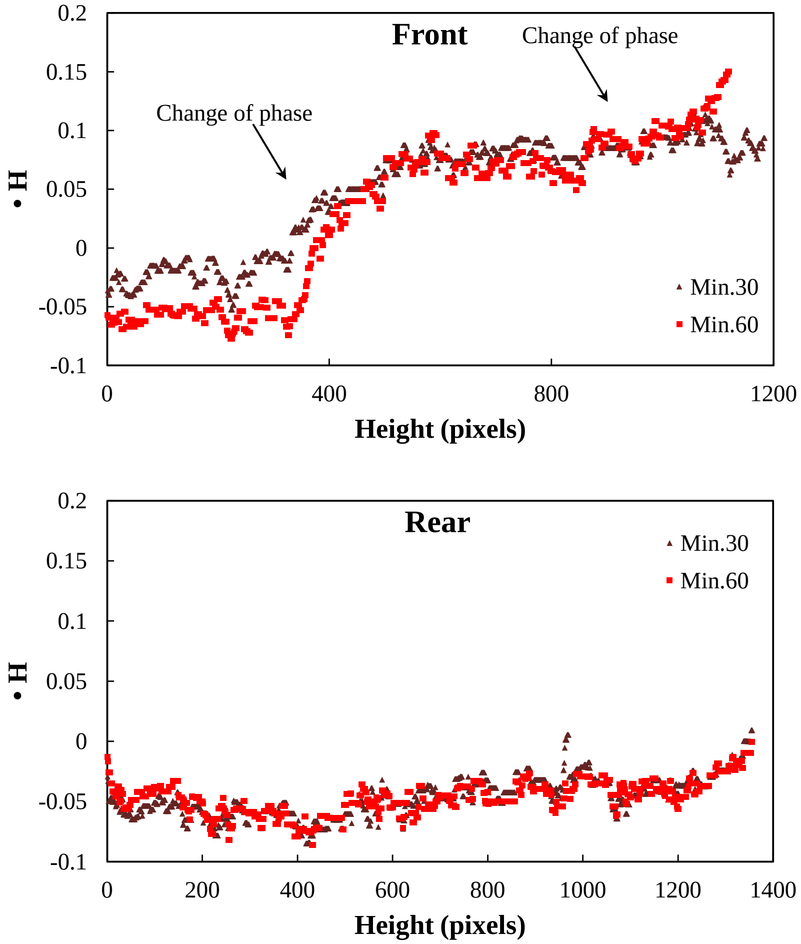

Figure 5.34 H component after 30 and 60 minutes of centrifugation for Calve Balance mayonnaise.

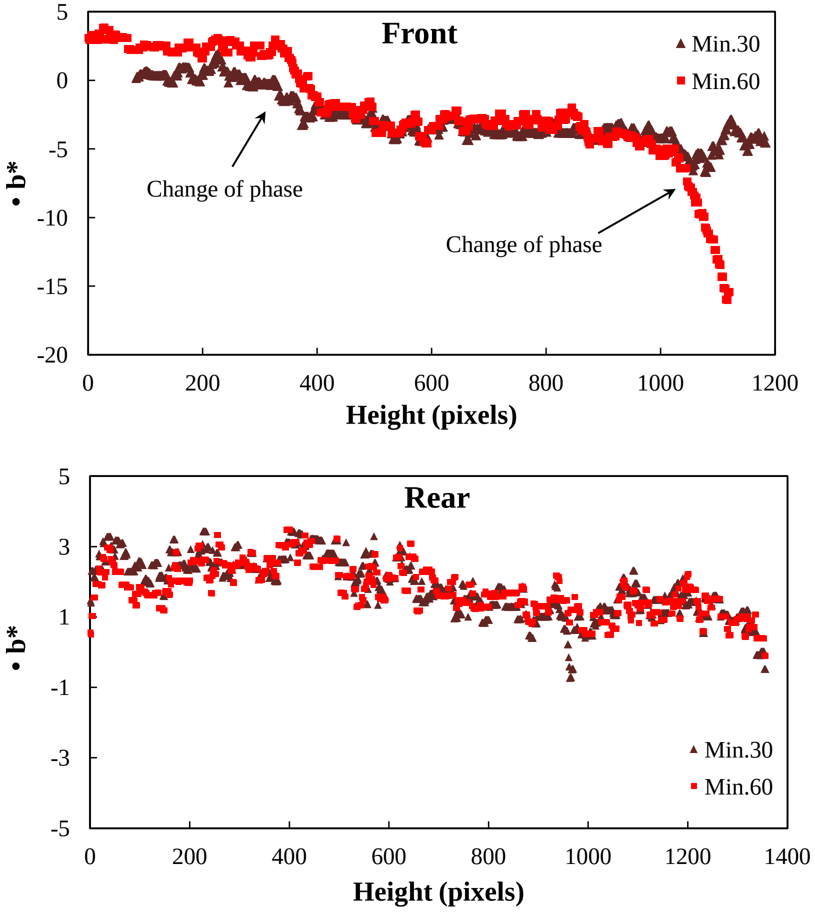

Figure 5.35 b* component after 30 and 60 minutes of centrifugation for Calve Balance emulsion.

The results here shown can be matched with the tests provided by the group of Applied Rheology from the University of Sevilla. To study the stability of emulsions this group used a commercial TurbiScan MA2000 from Formulaction (Formulaction, Toulouse, France) in order to study the backscattering produced by the samples before and after the centrifuge procedure (Mengual *et al.* 1999). The spinner used was a Medifriger BL-S from Selecta (Selecta, Barcelona, Spain) during 30 minutes at different speeds of rotation. As it can be observed in Figure 5.36 and Figure 5.37, in the tests carried out by our group the velocities were chosen faster, in order to study the extreme cases of destabilization showing the complete separation of the mayonnaises in the different components.

The graphics presented show the back scattering light from a sample without centrifugation and the same sample after 30 minutes of centrifugation at the specified velocity of revolution. In this first figure of the light sauce Hacendado, Figure 5.36, anticipation in the back scattering of the centrifuged sample can be observed. This denotes the presence of a starch layer at the bottom of the tube as a result of the destabilization procedure as shown as well in Figure 5.29b and Figure 5.29c. Besides, in that figures an oily phase can be observed at the top of the tube, since a yellowish layer appears, whose effect is not observed in the rheological test here exposed since the speed of rotation was not high enough to separate those components. The starch layer was also shown in Figure 5.30 and Figure 5.31, where the effect was more pronounced due to the higher rotation speed.

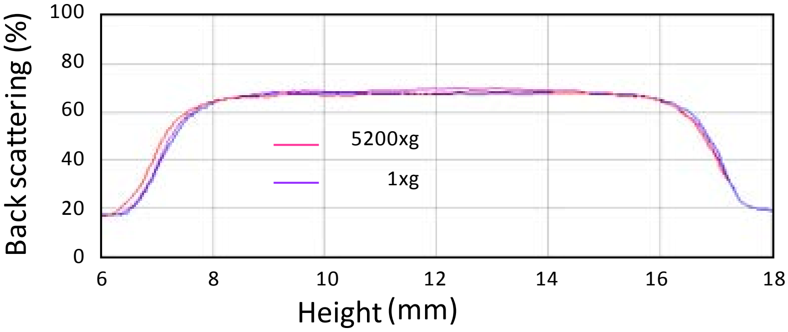

Figure 5.36 Back scattering graphics for the soft mayonnaise from Hacendado.

In the case of the soft Hacendado mayonnaise, from 1300g, which correspond with red line in Figure 5.37, signals of destabilization appear and three phases can be distinguished. This correspond with the effects previously analyzed from Figure 5.29e and Figure 5.29f. At the bottom of the tube an aqueous layer appears which allows the pass of the light, and at the top of the tube an oily phase is present. This matches with the results presented in the study with the spinner and the corresponding colorimetric coordinates presented in Figure 5.32 and Figure 5.33.

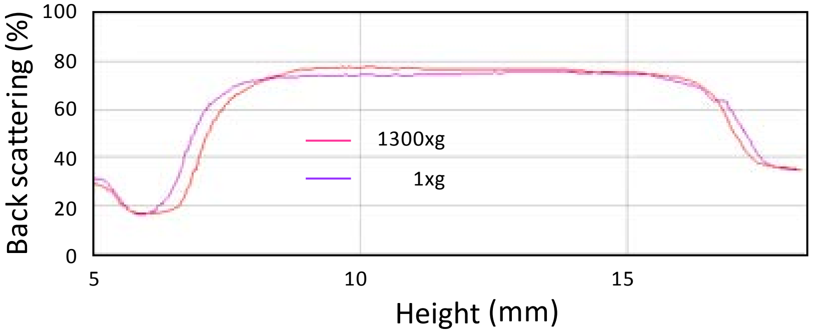

Figure 5.37 Response of the soft mayonnaise of Hacendado to the back scattering technique.

From the results here presented it can be deduced that the beginning of a destabilization state in an emulsion can be determined by studying the chromatic coordinates of the sample. It has been demonstrated that centrifuged processes cause higher destabilization of the mayonnaises in different phases than the produced by increasing of temperature of storage. Also, in particular, the Calve Balance emulsion shows a more stable behaviour than the Hacendado mayonnaises.

5.6 Conclusions

In this chapter, two different smartphones have been used as colour sensors for three different purposes: measurement of oxygen concentration by determination of the intensity of the luminescence emitted by a sensing membrane when it is optically excited; pH determination and measurement of concentration of nitrites by analyzing the change of colour in sensing areas of a microfluidic device; and finally, soil classification by removing subjective factors in the visualization of the soils and the Munsell soil-colour charts.

The determination of the oxygen concentration was measured with a resolution of 35 ppm at 21% of O_2. This value is higher than in other previous prototypes shown in this work since the number of bits used for encoding the coordinates in the smartphone is lower. The limit of detection was of 0.4% of gaseous oxygen. These values prove that using a smartphone as a detector to determine the intensity of the luminescence is suitable and provides real-time measurement of the oxygen concentration.

In the measurement of pH using the smartphone to capture and analyze a picture of the microfluidic device the results show a good behaviour of the smartphone under controlled conditions of light. The MSE was 0.167, the accuracy 0.09 and the resolution 0.04. With respect to the nitrites concentration determination, despite the non-homogeneity of the sensing membranes, the values of resolution and LOD are 7% at 100 ppm of nitrite concentration and 0.29 ppm respectively.

Finally, two smartphones were used to soil classification providing the RGB, XYZ and HVC coordinates of NCS and real soils samples.

New models for transformation between colour spaces were used instead of using those provide by literature, in order to adjust the models to the conditions of light where the experiment was carried out and to the sensor of the built-in camera used in this case. The mean CIELAB difference was of 3.7 ± 1.8 units which is better than the 4.4 and 10.2 units of difference obtained by visual classification carried out in different experiments. Although the improvement is not quite significant, the use of the Android application removes the inter-observer variability.

Also, in this chapter a commercial camera has been used as capture device to extract colour information that allows to study the stability of emulsions such as mayonnaises. The main objective was to be able to predict the initial state of destabilization of an emulsion by analyzing the chromatic coordinates. Several colour spaces were used, showing most of them a change that matches with the change of phase after destabilization procedures, either with temperature or using a centrifuge. Therefore, it is possible to determine when a mayonnaise is not stable by processing of a picture under controlled conditions of light.

In the same way as in previous chapters, the light source had high importance in the measurement of colour coordinates. Therefore, all the works here carried out, were performed under controlled conditions of illumination, either inside a booth with D65 illuminant, with an UV LED or the flash light of the mobile phone as light source or using two bulbs with stable spectra of emission.

Contributions

Lopez-Ruiz N, Martinez-Olmos A, Perez de Vargas-Sansalvador IM, Fernandez-Ramos MD, Capitan-Vallvey LF, Palma AJ (2012) *Determination of O_2 using colour sensing from image processing with mobile devices.* Sensors and Actuators: B. Chemical 171-172, 938-945.

Curto VF, Lopez-Ruiz N, Capitan-Vallvey LF, Palma AJ, Benito-Lopez F, Diamond D (2013) *Fast prototyping of paper-based microfluidic devices by contact stamping using indelible ink.* RSC Advances 3, 18811-18816.

Gomez-Robledo L, Lopez-Ruiz N, Melgosa M, Palma AJ, Capitan-Vallvey LF, Sanchez-Marañon M (2013) *Using the mobile phone as Munsell soil-colour sensor: an experiment under controlled illumination conditions.* Computer and Electronics in Agriculture 99, 200-208.

Lopez-Ruiz N, Martinez-Olmos A, Perez de Vargas-Sansalvador IM, Fernandez-Ramos MD, Banqueri J, Capitan-Vallvey LF, Palma AJ. *Determination of O2 with a portable instrument using color processing from sensor images.* XI Conference on optical chemical sensors and biosensors EUROPT(R)ODE XI (Barcelona, Spain 1-4 April 2012) 147.

Lopez-Ruiz N, Curto VF, Fay C, Diamond D, Benito-Lopez F, Capitan-Vallvey LF, Palma AJ. *Multianalyte colourimetric water analysis, using a mobile phone, in a paper microfluidic.* 3rd International Conference on Bio-sensing Technology (Sitges, Spain 12-15 May 2013).

Gomez-Robledo L, Lopez-Ruiz N, Melgosa M, Palma AJ, Capitan-Vallvey LF, Sanchez-Marañon M. *Mobile phone camera* *characterization for soil colour measurements under controlled illumination conditions.* 12th Congress of the International Colour Association AIC Colour 2013 (Newcastle upon Tyne, United Kingdom 8-12 July 2013).

Curto VF, Lopez-Ruiz N, Capitan-Vallvey LF, Palma AJ, Benito-Lopez F, Diamond D. *Fast prototyping of paper-based microfluidic devices by contact stamping.* 17th International Conference on Miniaturized Systems for Chemistry and Life Sciences MicroTAS 2013 (Freiburg, Germany 27-31 October 2013).

Chapter 6. **Conclusions**

The work here carried out consists of the development of portable instrumentation based on optical chemical sensors. The main conclusions of the work here developed are:

1. The use of digital colour detectors for measuring colour in portable instrumentation offer a good alternative to other techniques, such as CCD image sensors or spectrophotometers, since they are compact and easy to use in combination with a microcontroller for carrying out the processing of the information. The developed prototype was tested for measurement of pH in solutions using an optical sensor array and eleven digital colour detectors to determine the hue component of each sensing membrane. The results obtained offer a resolution of 0.02 units of pH and accuracy of 0.2. The accuracy value was later improved by using ANN to an accuracy of 0.06 units of pH.

2. Digital colour detectors have been also used for measuring the intensity of the luminescence emitted by an optically excited sensing membrane. The red coordinate of the RGB colour space extracted from the digital output was related to the magnitude of interest. Programmable parameters, such as the

integration time of the digital colour detectors, affect the values of resolution of the system. Measurement of gaseous oxygen using a RFID tag for smart packaging applications has been carried out offering a resolution of 3.86 ppm at 21% of O_2 and accuracy of 0.08%.

3. A CMOS micro-camera module was also used for measuring of luminescence intensity. The red component of the colour information extracted from the picture of the sensing membrane captured with the micro-camera determines the environmental oxygen concentration. The size of the processed area in the picture, modify the value of resolution: the higher the analyzed area of the membrane, the better the values of resolution and LOD. But, on the other hand, the time response of the instrument is increased. Despite the lower resolution offered by the micro-camera the results are better than for other works, providing resolution of 0.16% at 21% of O_2 and LOD of 1.5%.

4. A CMOS micro-camera module has been tested for measuring of colour in optical chemical sensors. The microcontroller included in the prototype carried out the processing of the image captured with the micro-camera. In this prototype the inclusion on the circuitry of a touch LCD screen avoid the need of using external elements for storage since the microcontroller can take the data directly from the pixels of the screen. The prototype was applied to determination of heavy metals concentration by using an optical sensor array offering lower values of resolution in non-mixed solutions.

5. The light source is an important factor to take into account in the different measurement processes here carried out. According to the CIE, the D65 standard illuminant (daylight) must be used in colorimetric applications. In the developed instrumentation here presented several illuminants have been included in the designs: four white LEDs, a programmable OLED display, and an UV LED in order to excite a luminophore. With regard to the light conditions using commercial devices as analytical instrumentation, different illuminants were used: a booth which simulates daylight, the LED flash of a smartphone, and two energy-efficient light bulbs. Therefore, in this Ph.D. Thesis all the experiments have been performed under controlled conditions of illumination in order to avoid external influences that could produce erroneous measurement of the colour components due to the variations of light.

6. The built-in camera of a smartphone has been used as portable instrument in order to measure the intensity of the emitted luminescence. Using the same sensing membrane as in previous prototypes for measurement of gaseous oxygen, it has been proved the potential of a mobile phone for this purpose. The resolution achieved was 35 ppm at 21% of O_2 with a LOD of 0.4%.

7. A mobile phone was also tested as colour detector, by capturing a picture of the sensor array or the sample to analyze. In this way, it has been demonstrated, by comparing

with a spectrophotometer, that under controlled conditions of illumination the smartphone can act as colour sensor for chemical analysis or classification. In particular the measurement of pH and the analysis of nitrites concentration was carried out obtaining a resolution of 0.04 units of pH and 7% at 100 ppm of nitrites concentration. Also, the classification of soil samples using the Munsell Colour System as reference has been performed. If the classification by visual methods carried out for experienced observer had a CIELAB difference from 4.4 to 10.2 units, the use of the smartphone as colour sensor reduces the difference to 3.7 ± 1.8 units.

8. With regard to the colorimetric analysis of samples, the stability in emulsions has been studied using a commercial digital camera as colour detector. The taken pictures were processed in an external PC to determine the influence of destabilization procedures in the colorimetric parameters of mayonnaises. After several tests of destabilization with spinning and temperature, it could be observed the change in some of the colour coordinates, which offer an idea of the current state of stability of the emulsions.

Therefore, the use of different optical detector and image sensors for colorimetric analysis or for measurement of the intensity of luminescence has been proved. In most of the cases, the response of the developed portable instruments has been compared with commercial devices, such as scanners, spectrophotometers and spectroradiometer, or traditional ways of measurement such as visual comparison or potentiometric method for pH measurement. The behaviour of the designed prototypes and the developed smartphone applications show similar responses with the advantages of the portability, low cost, autonomy and ease-of-use.

6.1 Future work

New technologies are constantly appearing improving preceding prototypes or components previously launched to the market. In this way, since the characteristics of some microcontrollers have been improved with regard to the used in this doctoral thesis, designs of new prototypes using advantages of new microcontrollers could be developed. Thus, some microcontrollers of the family PIC24 from Microchip (Microchip Technology Inc., USA) allow to reduce the power consumption, as well as reducing the size of the final design to achieve more compact instruments. This family also includes integrated EEPROM which allow to store the colour information of interest, such as the coordinates of the used colour space, while is being carried out the processing, avoiding the need of using any external element of storage and, therefore, reducing he response time of the instrument. Also, using the family dsPIC30F it is possible to improve the processing of digital images since they integrate the functionalities of a digital signal processor.

With regard to the prototypes and applications developed in this work, some studies need to be still carried out. In this report, the determination of heavy metals concentrations such as copper and zinc has been researched in non-mixed solutions. The characterization of the sensing membranes in solutions with mixtures of different concentrations of each metal will be performed, in order to analyze samples where there is presence of more than one heavy metal. For that purpose, and to apply this also for other optical chemical sensors, the preparation of sensing membranes using inkjet printing techniques is currently under study. The advantages of using this procedure are: minimization of the size of the sensor arrays in order to minimize the design of the prototype; increasing in the number of sensing elements in the same space to obtain more information using one single array; more homogeneity in the surface of the sensors avoiding bad read-outs values of the colour detectors because of the non-homogeneities; and higher reproducibility of the sensors arrays.

Also, as it has been deduced from the work here presented, the light source is an important factor in the measurement procedures where the colour, that is the different coordinates of colour spaces, is the analytical parameter. Until now the experiments have been carried out under controlled conditions of illumination, but in order to extend the use of the prototypes and the Android applications to other environmental conditions of light, a normalization procedure must be studied. Using some algorithm to maintain the results provided by the equipments independent of the light source will increase considerably the fields of applications. In this way, the soil classification carried out with a controlled light source could be moved to open environments.

6.2 Contributions

Published articles

1. Martinez-Olmos A, Capel-Cuevas S, Lopez-Ruiz N, Palma AJ, de Orbe I, Capitan-Vallvey LF (2011) *Sensor array-based*

optical portable instrument for determination of pH. Sensors and Actuators: B. Chemical 156, 840-848.

2. Lopez-Ruiz N, Ariza M, Martinez-Olmos A, Vukovic J, Palma AJ, Capitan-Vallvey LF (2011) *Handheld colorimeter for determination of heavy metal concentrations.* Journal of Physics: Conference Series 307.

3. Capel-Cuevas S, Lopez-Ruiz N, Martinez-Olmos A, Cuellar MP, Pegalajar MC, Palma AJ, de Orbe-Paya I, Capitan-Vallvey LF (2012) *A compact Optical Instrument with Artificial Neural Network for pH Determination.* Sensors 12, 6746-6763.

4. Lopez-Ruiz N, Martinez-Olmos A, Perez de Vargas-Sansalvador IM, Fernandez-Ramos MD, Capitan-Vallvey LF, Palma AJ (2012) *Determination of O_2 using colour sensing from image processing with mobile devices.* Sensors and Actuators: B. Chemical 171-172, 938-945.

5. Curto VF, Lopez-Ruiz N, Capitan-Vallvey LF, Palma AJ, Benito-Lopez F, Diamond D (2013) *Fast prototyping of paper-based microfluidic devices by contact stamping using indelible ink*. RSC Advances 3, 18811-18816.

6. Gomez-Robledo L, Lopez-Ruiz N, Melgosa M, Palma AJ, Capitan-Vallvey LF, Sanchez-Marañon M (2013) *Using the mobile phone as Munsell soil-colour sensor: an experiment*

under controlled illumination conditions. Computers and Electronics in Agriculture 99, 200-208.

7. Martinez Olmos A, Fernandez Salmeron J, Lopez Ruiz N, Rivadeneyra Torres A, Capitan-Vallvey LF, Palma AJ (2013) *Screen printed flexible radiofrequency identification tag for oxygen monitoring*. Analytical Chemistry 85, 11098-11105.

8. Morales DP, Castillo E, García A, Parilla L, Lopez-Ruiz N, Palma AJ (2013) *Efficient wavelet-based technique for simultaneous wandering and noise suppression in ECG signals.* Accepted for publication.

International conferences

1. Palma AJ, Carvajal MA, Lopez-Ruiz N, Ballesta-Claver J, Valencia-Miron MC, Capitan-Vallvey LF. *Portable instrumentation platform for ECL-based sensors and biosensors.* International Conference on Biomedical Electronics and Devices BIODEVICES 2011 (Rome, Italy 26-29 January 2011) 319-322.

2. Capel-Cuevas S, Ariza-Avidad M, Martinez-Olmos A, Lopez-Ruiz N, de Orbe-Paya I, Palma AJ, Capitan-Vallvey LF. *Sensor array-based colorimetric portable instrument for pH determination in different matrices.* 16th European Conference on Analytical Chemistry EUROANALYSIS 2011 (Belgrade, Serbia 11-15 September 2011).

3. Lopez-Ruiz N, Ariza M, Martinez-Olmos A, Vukovic J, Palma AJ, Capitan-Vallvey LF. *Handheld colorimeter for*

determination of heavy metal concentrations. Sensors and their Applications XVI (Cork, Ireland 12-14 September 2011).

4. Lopez-Ruiz N, Martinez-Olmos A, Perez de Vargas-Sansalvador IM, Fernandez-Ramos MD, Banqueri J, Capitan-Vallvey LF, Palma AJ. *Determination of O2 with a portable instrument using color processing from sensor images.* XI Conference on optical chemical sensors and biosensors EUROPT(R)ODE XI (Barcelona, Spain 1-4 April 2012) 147.

5. Castillo E, Morales DP, Garcia A, Parrilla L, Lopez-Ruiz N, Palma AJ. *One-step wavelet-based processing for wandering and noise removing in ECG signals.* International Work-Conference on Bioinformatics and Biomedical Engineering IWBBIO 2013 (Granada, Spain 18-20 March 2013).

6. Lopez-Ruiz N, Curto VF, Fay C, Diamond D, Benito-Lopez F, Capitan-Vallvey LF, Palma AJ. *Multianalyte colourimetric water analysis, using a mobile phone, in a paper microfluidic.* 3rd International Conference on Bio-sensing Technology (Sitges, Spain 12-15 May 2013).

7. Morales DP, Salinas-Castillo A, Martinez-Olmos A, Ariza-Avidad M, Lopez-Ruiz N, Palma AJ, Capitan-Vallvey LF. *Evaluation of a reconfigurable portable instrument for copper determination based on luminescent carbon dots.* 3rd International Conference on Bio-sensing Technology (Sitges, Spain 12-15 May 2013).

8. Gomez-Robledo L, Lopez-Ruiz N, Melgosa M, Palma AJ, Capitan-Vallvey LF, Sanchez-Marañon M. *Mobile phone camera characterization for soil colour measurements under controlled illumination conditions.* 12th Congress of the International Colour Association AIC Colour 2013 (Newcastle upon Tyne, United Kingdom 8-12 July 2013).

9. Curto VF, Lopez-Ruiz N, Capitan-Vallvey LF, Palma AJ, Benito-Lopez F, Diamond D. *Fast prototyping of paper-based microfluidic devices by contact stamping.* 17th International Conference on Miniaturized Systems for Chemistry and Life Sciences MicroTAS 2013 (Freiburg, Germany 27-31 October 2013).

National conferences

10. Capel-Cuevas S, Martinez-Olmos A, Lopez-Ruiz N, de Orbe-Paya I, Palma AJ, Capitan-Vallvey LF. *Sensor array-based portable optical instrument for pH determination.* VII Simposio Investigadores Jóvenes RSEQ-Sigma Aldrich (Valencia, Spain 10-12 November, 2010) 38-50.

11. Capel-Cuevas S, Martinez-Olmos A, Lopez-Ruiz N, de Orbe-Paya I, Palma AJ, Capitan-Vallvey LF. *Determinación de pH en muestras alimentarias, biológicas y de uso cotidiano mediante un instrumento óptico portátil basado en un array sensor colorimétrico.* I Simposio de Jóvenes Investigadores en Espectroscopia Aplicada (Madrid, Spain 6-9 July 2011).

12. Ariza Avidad M, Lopez-Ruiz N, Martinez-Olmos A, Vukovic J, Banqueri J, Capitan-Vallvey LF. *Handheld CCD micro-camera instrument for in-situ determination of heavy metals.* 13as Jornadas de Análisis Instrumental JAI 2011 (Barcelona, Spain 14-16 November 2011).

13. Capel-Cuevas S, Lopez-Ruiz N, Martinez-Olmos A, Cuellar MP, Pegalajar MC, de Orbe-Paya I, Palma AJ, Capitan-Vallvey LF. *pH determination using a sensor array-based colorimetric portable instrument.* 13as Jornadas de Análisis Instrumental JAI 2011 (Barcelona, Spain 14-16 November 2011).

14. Lopez-Ruiz N, Fernandez-Salmeron J, Martinez-Olmos A, Capitan-Vallvey LF, Palma AJ. *Monitorización de oxígeno mediante RFID en empaquetado inteligente.* XVIII Reunión de la Sociedad Española de Química Analítica SEQA 2013. (Úbeda, Spain 16-18 June 2013).

Conclusiones

La investigación llevada a cabo en este trabajo consiste en el diseño y desarrollo de instrumentación portátil basada en sensores químicos de tipo óptico. Las principales conclusiones que se pueden extraer son:

1. Los detectores digitales de color son una buena alternativa a otras técnicas de detección colorimétrica, tales como sensores CCD o espectrómetros, ya que ofrecen una solución compacta y sencilla de utilizar en combinación con el uso de microcontroladores que realicen el procesamiento necesario de la información obtenida. Uno de los prototipos que se ha desarrollado utilizando dichos detectores digitales se ha aplicado a la medida de pH en disoluciones. Se ha utilizado para ello una matriz de sensores ópticos y once detectores digitales de color con el objetivo de determinar la coordenada tonal (H) de cada membrana sensora y relacionarlo con el pH correspondiente. Los resultados obtenidos proporcionan una resolución de 0.02 unidades de pH con una precisión de 0.2 unidades. Combinando este prototipo, con el uso de redes neuronales artificiales, se mejoró el valor de precisión a 0.06 unidades de pH.

2. Los detectores digitales de color se han empleado también en la medida de intensidad de luminiscencia emitida por una membrana excitada ópticamente. En este caso, la coordenada roja (R) del espacio RGB extraída de la información

proporcionada por el detector digital se relaciona con la magnitud de interés. Se ha desarrollado un prototipo aplicado a la medida de oxígeno gaseoso incluyendo el detector en una tarjeta RFID impresa sobre sustrato flexible adecuado para empaquetado inteligente. Los resultados obtenidos proporcionan una resolución de 3.86 ppm al 21% de concentración de oxígeno ambiental y una precisión de 0.08%. Además, se ha estudiado la influencia de los parámetros programables de los detectores digitales, tales como el tiempo de integración, sobre los valores de resolución ofrecidos por el sistema.

3. Para medir intensidad de luminiscencia se ha empleado también una micro-cámara CMOS. La coordenada roja (R) extraída del procesamiento de una fotografía de la membrana sensora excitada ópticamente que ha sido capturada con la micro-cámara se relaciona con la concentración de oxígeno ambiental. El tamaño del área analizada de la membrana afecta las características finales del sistema: a mayor área mejores valores de resolución y de límite de detección. Sin embargo, el tiempo de respuesta del equipo portátil se incrementa también y, por tanto, hay que llegar a un compromiso. Los valores de resolución y límite de detección obtenidos son de 0.16% a 21% de oxígeno ambiental y 1.5%, respectivamente.

4. Otro prototipo utilizando la micro-cámara CMOS en su diseño ha sido testado en la medida de color en sensores químicos ópticos. En este caso el procesamiento llevado a cabo por el

sistema proporciona las coordenadas colorimétricas de interés y las relaciona con la concentración de metales pesados en disolución. En este instrumento se ha incluido una pantalla LCD táctil, lo que evita la necesidad de incluir elementos externos de almacenamiento al posibilitar la lectura pixel a pixel por parte del microcontrolador. Las características del instrumento portátil proporcionan valores de resolución aceptables en disoluciones con un único metal determinado.

5. En todos estos estudios, la fuente de iluminación es un factor importante a tener en cuenta durante el proceso de medida. De acuerdo con la CIE, el iluminante D65 (luz día) es el recomendado para realizar mediciones en aplicaciones colorimétricas. En esta Tesis Doctoral se han utilizado diversas fuentes de iluminación que se han incluido en el correspondiente prototipo: LED blancos, pantalla OLED programable o LED ultravioleta. Con respecto a los iluminantes utilizados en procesos analíticos de medida realizados con dispositivos comerciales, se han utilizado diferentes configuraciones: cabina con luz día simulada y controlada, flash LED de un teléfono móvil o dos bombillas con 6400K de temperatura de color. Por tanto, en esta Tesis Doctoral, todas las mediciones se han llevado a cabo bajo condiciones controladas de iluminación con el objetivo de evitar variaciones y medidas erróneas en las medidas colorimétricas realizadas.

6. La cámara integrada de un teléfono móvil de última generación ha sido probada como instrumento analítico con el objetivo de

medir intensidad de luminiscencia por medio del análisis colorimétrico. Utilizando la misma membrana sensora aplicada sobre prototipos previos para la medida de oxígeno ambiental, se ha probado la fiabilidad de un teléfono móvil como detector de intensidad colorimétrica obteniendo resultados de resolución de 35 ppm a 21% de oxígeno con un límite de detección de 0.4%.

7. Se ha utilizado también la cámara de un teléfono móvil como detector de color capturando para ello una fotografía de una matriz de sensores o de una muestra simple. Comparando los resultados obtenidos utilizando el teléfono móvil con los obtenidos por un espectrofotómetro, bajo condiciones controladas de iluminación, se ha probado que un teléfono móvil puede ser utilizado como colorímetro para aplicaciones de clasificación o análisis químico de muestras. Se ha desarrollado y utilizado para este fin una aplicación Android propia que permite llevar a cabo la medida de pH y determinación de concentración de nitritos en disolución, obteniendo resultados de resolución de 0.04 unidades de pH y 7% a 100 ppm de concentración de nitritos. Con este instrumento portátil, y desarrollando una nueva aplicación, se ha realizado también la clasificación de suelos de origen mediterráneo utilizando el sistema Munsell como referencia. Las diferencias CIELAB obtenidas con respecto a los valores originales son de 3.7 ± 1.8 unidades, mientras que con el método tradicional de clasificación de suelos se obtenían diferencias entre 4.4 y 10 unidades.

8. Finalmente, se ha estudiado la estabilidad en salsas emulsionadas utilizando una cámara digital comercial como instrumento analítico. Las fotografías obtenidas de cada salsa tras ser sometida a procesos de desestabilización son procesadas en un ordenador externo para obtener las coordenadas cromáticas de interés. Tras desestabilización por temperatura y por centrifugado de tres salsas mayonesas diferentes, se puede observar un cambio en algunas de las coordenadas estudiadas entre el estado inicial y el final, lo que ofrece una idea del estado actual de desestabilización de la salsa correspondiente.

Por tanto, el uso de diferentes detectores ópticos o sensores de imagen para el análisis colorimétrico de muestras así como para la medida de intensidad de luminiscencia ha sido probado a lo largo del presente trabajo. En la mayoría de los casos, la respuesta de los prototipos y equipos desarrollados se ha comparado con dispositivos comerciales para la medida de color ya existentes como escáneres, espectrofotómetros y espectrorradiómetros, o métodos tradicionales de medida como la comparación visual de muestras o el método potenciométrico para la medida de pH. Las respuestas obtenidas de los prototipos y aplicaciones Android desarrolladas son similares a las de estos equipos comerciales, añadiendo las ventajas de la portabilidad, facilidad de uso, bajo coste y autonomía que ofrecen.

Trabajo futuro

Nuevas tecnologías aparecen constantemente en el mercado mejorando componentes y prototipos previamente desarrollados. Por este motivo, y puesto que las características de algunos de los microcontroladores utilizados en esta Tesis Doctoral han sido ya mejoradas, se pretende llevar a cabo el desarrollo y diseño de prototipos utilizando estos nuevos componentes. Así, algunos microcontroladores de la familia PIC24 de Microchip (Microchip Technology Inc., USA) permiten reducir el consumo final del instrumento portátil, así como reducir el tamaño final del diseño para conseguir equipos más compactos. Esta familia incluye también memorias EEPROM que permiten almacenar información de interés, tales como las coordenadas cromáticas del espacio de color utilizado o algunas condiciones de medida como temperatura. De esta forma, se evita la necesidad de incluir elementos externos de almacenamiento, reduciendo también en consecuencia, el tiempo de respuesta del prototipo. Utilizando otra familia como la dsPIC30F es posible mejorar también el procesamiento de imágenes, ya que estos microcontroladores incluyen funcionalidades propias de un procesador digital de señales.

Con respecto al trabajo concreto que se ha realizado en esta Tesis Doctoral, algunas aplicaciones deben ser estudiadas más a fondo. Es el caso de la determinación de concentración de metales pesados en disolución, donde hasta ahora sólo se ha tratado de analizar disoluciones con una muestra única de un metal determinado (cobre o cinc). El objetivo final es la caracterización de la respuesta de cada una de las membranas sensoras ante la mezcla de metales en una misma disolución, pudiendo identificar diferentes concentraciones de metales pesados en un único proceso de medida.

Para este fin, así como para su aplicación en otro tipo de sensores químicos ópticos, se está trabajando en la preparación y fabricación de matrices de sensores químicos utilizando técnicas de impresión de inyección de tinta. Entre las ventajas que ofrece este procedimiento están la minimización del tamaño final de las matrices de sensores, lo que permite optimizar el prototipo; el incremento del número de sensores en el mismo tamaño de matriz para obtener un mayor número de medidas en un único proceso analítico; mayor homogeneidad en el área de la membrana sensora, evitando errores en la medida debido a heterogeneidades en la superficie; y una mayor reproducibilidad de las matrices de sensores.

Finalmente, y como se ha podido deducir del trabajo aquí presentado, hay que destacar la importancia de la fuente de luz utilizada durante el procedimiento analítico en aplicaciones colorimétricas. Hasta ahora, los experimentos han sido realizados bajo condiciones controladas de iluminación, pero con el objetivo de ampliar el uso de los prototipos y aplicaciones desarrollados a otras condiciones ambientales, se debe estudiar un proceso de normalización más complejo que permita corregir las variaciones de luz. De este modo, los prototipos ofrecerán medidas de forma independiente a las condiciones de iluminación, lo que incrementará considerablemente los ámbitos de aplicación.

Bibliography

Abbaspour A, Mehrgardi MA, Noori A, Kamyabi MA, Khalafi-Nezhad A, Rad MNS (2006) Speciation of iron(II), iron(III) and full-range pH monitoring using paptode: A simple colorimetric method as an appropriate alternative for optodes. *Sensors and Actuators B-Chemical* 113, 857-865.

Abbass HA (2001) A Memetic Pareto Evolutionary Approach to Artificial Neural Networks. In 'Advances in Artificial Intelligence. Lecture Notes in Computer Science.'. pp. 1-12.

Akbulut M, Saricoban C, Musa M (2012) Determination of Rheological Behavior, Emulsion Stability, Color, and Sensory of Sesame Pastes (Tahin) Blended with Pine Honey. *Food and Bioprocess Technology* 5, 1832-1839.

Alvarez D, Castillo M, Payne FA, Garrido MD, Banon S, Xiong YL (2007) Prediction of meat emulsion stability using reflection photometry. *Journal of Food Engineering* 82, 310-315.

Alvarez D, Castillo M, Payne FA, Xiong YL (2009) A novel fiber optic sensor to monitor beef meat emulsion stability using visible light scattering. *Meat Science* 81, 456-466.

Antonelli A, Cocchi M, Fava P, Foca G, Franchini CG, Manzini D, Ulrici A (2004) Automated evaluation of food colour by means of multivariate image analysis coupled to a wavelet-based classification algorithm. *Analytica Chimica Acta* 515, 3-13.

Apyari VV, Dmitrienko SG (2008) Using a digital camera and computer data processing for the determination of organic substances with diazotized polyurethane foams. *Journal of Analytical Chemistry* 63, 530-537.

Ariza-Avidad M, Cuellar MP, Salinas-Castillo A, Pegalajar MC, Vukovic J, Capitan-Vallvey LF (2013) Feasibility of the use of disposable optical tongue based on neural networks for heavy metal identification and determination. *Analytica Chimica Acta* 783, 56-64.

Arrabito G, Pignataro B (2010) Inkjet Printing Methodologies for Drug Screening. *Analytical Chemistry* 82, 3104-3107.

ASTM. Standard Practice for Specifying Colour by the Munsell System. D 1535-08. 2008. ASTM International.

Aydemir S, Keskin S, Drees LR (2004) Quantification of soil features using digital image processing (DIP) techniques. *Geoderma* 119, 1-8.
Baldini F, Chester AN, Homola J, Martellucci S (2006) 'Optical Chemical Sensors.' Springer.

Baldini L, Wilson AJ, Hong J, Hamilton AD (2004) Pattern-based detection of different proteins using an array of fluorescent protein surface receptors. *Journal of the American Chemical Society* 126, 5656-5657.

Barbut S (1998) Use of a fiber optic probe to predict meat emulsion breakdown. *Italian Journal of Food Science* 10, 253-259.

Bayer, B. E. Color Imaging Array. Ed. Eastman Kodak Company. 555477[3971065]. 20-7-1976. Rochester, N.Y.

Bengio Y, Simard P, Frasconi P (1994) Learning Long-Term Dependencies with Gradient Descent Is Difficult. *Ieee Transactions on Neural Networks* 5, 157-166.

Blakistone BA (1998) 'Principles and Applications of Modified Atmosphere Packaging of Foods.' Aspen.

Borisov SM, Krause C, Arain S, Wolfbeis OS (2006) Composite material for simultaneous and contactless luminescent sensing and imaging of oxygen and carbon dioxide. *Advanced Materials* 18, 1511.

Buron H, Mengual O, Meunier G, Cayre I, Snabre P (2004) Optical characterization of concentrated dispersions: applications to laboratory analyses and on-line process monitoring and control. *Polymer International* 53, 1205-1209.

Caldara M, Colleoni C, Guido E, Re V, Rosace G (2012) Development of a textile-optoelectronic pH meter based on hybrid xerogel doped with Methyl Red. *Sensors and Actuators B-Chemical* 171, 1013-1021.

Campos RC, Dematte JAM, Quartaroli CF (2003) Indirect determination of hematite content in soil from colorimetric and radiometric data. *Pesquisa Agropecuaria Brasileira* 38, 521-528.

Cantrell K, Erenas MM, Orbe-Paya I, Capitan-Vallvey LF (2010) Use of the Hue Parameter of the Hue, Saturation, Value Color Space As a Quantitative Analytical Parameter for Bitonal Optical Sensors. *Analytical Chemistry* 82, 531-542.

Capel-Cuevas S, Cuellar MP, Orbe-Paya I, Pegalajar MC, Capitan-Vallvey LF (2010) Full-range optical pH sensor based on imaging techniques. *Analytica Chimica Acta* 681, 71-81.

Capel-Cuevas S, Cuellar MP, Orbe-Paya I, Pegalajar MC, Capitan-Vallvey LF (2011) Full-range optical pH sensor array based on neural networks. *Microchemical Journal* 97, 225-233.

Capitan-Vallvey LF, Asensio LJ, Lopez-Gonzalez J, Fernandez-Ramos MD, Palma AJ (2007) Oxygen-sensing film coated photodetectors for portable instrumentation. *Analytica Chimica Acta* 583, 166-173.

Capitan-Vallvey LF, Palma AJ (2011) Recent developments in handheld and portable optosensing-A review. *Analytica Chimica Acta* 696, 27-46.

Carey JR, Susick KS, Hulkower KI, Imlay JA, Imlay KRC, Ingison CK, Ponder JB, Sen A, Wittrig AE (2011) Rapid Identification of Bacteria with a Disposable Colorimetric Sensing Array. *Journal of the American Chemical Society* 133, 7571-7576.

Carraway ER, Demas JN, Degraff BA, Bacon JR (1991) Photophysics and Photochemistry of Oxygen Sensors Based on Luminescent Transition-Metal Complexes. *Analytical Chemistry* 63, 337-342.

Chanamai R, McClements DJ (2001) Prediction of emulsion color from droplet characteristics: dilute monodisperse oil-in-water emulsions. *Food Hydrocolloids* 15, 83-91.

Chang BY (2012) Smartphone-based Chemistry Instrumentation: Digitization of Colorimetric Measurements. *Bulletin of the Korean Chemical Society* 33, 549-552.

Chantrapornchai W, Clydesdale F, McClements DJ (1998) Influence of droplet size and concentration on the color of oil-in-water emulsions. *Journal of Agricultural and Food Chemistry* 46, 2914-2920.

Chantrapornchai W, Clydesdale F, McClements DJ (1999) Influence of droplet characteristics on the optical properties of colored oil-in-water emulsions. *Colloids and Surfaces A-Physicochemical and Engineering Aspects* 155, 373-382.

Chen HX, Wang XD, Song XH, Zhou TY, Jiang YQ, Chen X (2010) Colorimetric optical pH sensor production using a dual-color system. *Sensors and Actuators B-Chemical* 146, 278-282.

Chu BY, Qi TT, Liao JF, Peng JR, Li WT, Fu SZ, Luo F, Qian ZY (2012) Colorimetric detection of cancer biomarker based on pH induced color change. *Sensors and Actuators B-Chemical* 166, 56-60.

CIE 15: Technical Report: Colorimetry 3rd Edition (2004) Internation Commission on Illumination.

Ciosek P, Wroblewski W (2007) Sensor arrays for liquid sensing - electronic tongue systems. *Analyst* 132, 963-978.

Copperwhite R, McDonagh C, O'Driscoll S (2012) A Camera Phone-Based UV-Dosimeter for Monitoring the Solar Disinfection (SODIS) of Water. *Ieee Sensors Journal* 12, 1425-1426.

Corgier BP, Marquette CA, Blum LJ (2005) Screen-printed electrode microarray for electrochemiluminescent measurements. *Analytica Chimica Acta* 538, 1-7.

Courbat J, Briand D, Wollenstein J, de Rooij NF (2011) Polymeric foil optical waveguide with inkjet printed gas sensitive film for colorimetric sensing. *Sensors and Actuators B-Chemical* 160, 910-915.

Cretu R, Dima S, Olteanu M (2009) Stability and Colour Evolution of Emulsions with Sodium Caseinate. *Revista de Chimie* 60, 683-688.

Cuellar MP, Capel-Cuevas S, Pegalajar MC, Orbe-Paya I, Capitan-Vallvey LF (2011) Minimization of sensing elements for full-range optical pH device formulation. *New Journal of Chemistry* 35, 1042-1053.

Dasgupta PK, Bellamy HS, Liu HH, Lopez JL, Loree EL, Morris K, Petersen K, Mir KA (1993) Light-Emitting Diode Based Flow-Through Optical-Absorption Detectors. *Talanta* 40, 53-74.

Davies-Colley RJ, Smith DG, Speed DJ, Nagels JW (1997) Matching natural water colors to Munsell standards. *Journal of the American Water Resources Association* 33, 1351-1361.

Davis AK, Farrey BD, Altizer S (2005) Variation in thermally induced melanism in monarch butterflies (Lepidoptera : Nymphalidae) from three North American populations. *Journal of Thermal Biology* 30, 410-421.

Deboux BJC, Lewis E, Scully PJ, Edwards R (1995) A Novel Technique for Optical-Fiber Ph Sensing Based on Methylene-Blue Adsorption. *Journal of Lightwave Technology* 13, 1407-1414.

Delaney JL, Hogan CF, Tian JF, Shen W (2011) Electrogenerated Chemiluminescence Detection in Paper-Based Microfluidic Sensors. *Analytical Chemistry* 83, 1300-1306.

Denton MB, Lewis HA, Sims GR (1983) Charge-Injection and Charge-Coupled-Devices in Practical Chemical-Analysis - Operation Characteristics and Considerations. *Acs Symposium Series* 236, 133-154.

Douglas P, Eaton K (2002) Response characteristics of thin film oxygen sensors, Pt and Pd octaethylporphyrins in polymer films. *Sensors and Actuators B-Chemical* 82, 200-208.

EPA Clean Water Act. 1972.

Eren H (2004) 'Electronic Portable Instruments: Design and Applications.' CRC Press.

Evans RC, Douglas P (2006) Controlling the color space response of colorimetric luminescent oxygen sensors. *Analytical Chemistry* 78, 5645-5652.

Evans RC, Douglas P (2009) Design and Color Response of Colorimetric Multilumophore Oxygen Sensors. *Acs Applied Materials & Interfaces* 1, 1023-1030.

Fang XE, Chen H, Jiang XY, Kong JL (2011) Microfluidic Devices Constructed by a Marker Pen on a Silica Gel Plate for Multiplex Assays. *Analytical Chemistry* 83, 3596-3599.

Faustman C, Cassens RG (1990) Influence of Aerobic Metmyoglobin Reducing Capacity on Color Stability of Beef. *Journal of Food Science* 55, 1278-1279.

Feng LA, Musto CJ, Kemling JW, Lim SH, Zhong WX, Suslick KS (2010) Colorimetric Sensor Array for Determination and Identification of Toxic Industrial Chemicals. *Analytical Chemistry* 82, 9433-9440.

Fernandez Arteaga A (2006) Preparación, caracterización y estabilidad de emulsiones y microemulsiones O/W. University of Granada.

Garcia A, Erenas MM, Marinetto ED, Abad CA, Orbe-Paya I, Palma AJ, Capitan-Vallvey LF (2011) Mobile phone platform as portable chemical analyzer. *Sensors and Actuators B-Chemical* 156, 350-359.

Gauglitz G (2005) Direct optical sensors: principles and selected applications. *Analytical and Bioanalytical Chemistry* 381, 141-155.

Godlove IH (1951) Improved Color-Difference Formula, with Applications to the Perceptibility and Acceptability of Fadings. *Journal of the Optical Society of America* 41, 760-772.

Gonzalez RC, Woods RE (2002) 'Digital Image Processing.' (Pearson: Gonzalez RC, Woods RE, Eddins SL (2004) 'Digital Image Processing using Matlab.' Pearson.

Gopel W (1998) Chemical imaging: I. Concepts and visions for electronic and bioelectronic noses. *Sensors and Actuators B-Chemical* 52, 125-142.

Gouin S, Gouterman M (2000) Ideality of pressure-sensitive paint. II. Effect of annealing on the temperature dependence of the luminescence. *Journal of Applied Polymer Science* 77, 2805-2814.

Guo J, Sonkusale S (2012) A 65 nm CMOS Digital Phase Imager for Time-Resolved Fluorescence Imaging. *Ieee Journal of Solid-State Circuits* 47, 1731-1742.

Han JH (2005) 'Innovations in Food Packaging.' Elsevier.

Harp BP, Miranda-Bermudez E, Baron CI, Richard GI (2012) Qualitative identification of permitted and non-permitted colour additives in food products. *Food Additives and Contaminants Part A-Chemistry Analysis Control Exposure & Risk Assessment* 29, 886-896.

Hatcher DW, Symons SJ, Manivannan U (2004) Developments in the use of image analysis for the assessment of oriental noodle appearance and colour. *Journal of Food Engineering* 61, 109-117.

Haykin S (1999) 'Neural Networks: A Comprehensive Foundation.' Pearson Education.

Held G (2008) 'Introduction to Light Emitting Diode Technology and Applications.' CRC Press.

Heng LY, Fang TH, Chern LH, Ahmad M (2003) Influence of methacrylic-acrylic copolymer composition on plasticiser-free optode films for pH sensors. *Sensors* 3, 83-90.

Holst, GC, Lomheim TS (2007) 'CMOS/CCD Sensors and Camera Systems.' SPIE Press.

Hong GW, Luo MR, Rhodes PA (2001) A study of digital camera colorimetric characterization based on polynomial modeling. *Color Research and Application* 26, 76-84.

Hradil J, Davis C, Mongey K, McDonagh C, MacCraith BD (2002) Temperature-corrected pressure-sensitive paint measurements using a single camera and a dual-lifetime approach. *Measurement Science & Technology* 13, 1552-1557.

Hulanicki A, Glab S, Ingman F (1991) Chemical Sensors Definitions and Classification. *Pure and Applied Chemistry* 63, 1247-1250.

Hunt RWG (2004) 'The Reproduction of Colour.' John Wiley and Sons.

Ichi T, Higashimura Y, Katayama T, Koda T, Tada M (1995) Determination of A Food Colorant, Cardenia Yellow Pigment, in Processed Foods with A High-Performance Liquid Chromatograph Photodiode-Array Detector Mass-Spectrometer System. *Journal of the Food Hygienic Society of Japan* 36, 482-489.

Iqbal Z, Eriksson M (2013) Classification and quantitative optical analysis of liquid and solid samples using a mobile phone as illumination source and detector. *Sensors and Actuators B-Chemical* 185, 354-362.

Jaakkola A, Hyyppa J, Kukko A, Yu XW, Kaartinen H, Lehtomaki M, Lin Y (2010) A low-cost multi-sensoral mobile mapping system and its feasibility for tree measurements. *Isprs Journal of Photogrammetry and Remote Sensing* 65, 514-522.

Janata J (2009) 'Principles of Chemical Sensors.' Springer.

Janzen MC, Ponder JB, Bailey DP, Ingison CK, Suslick KS (2006) Colorimetric sensor Arrays for volatile organic compounds. *Analytical Chemistry* 78, 3591-3600.

Johnson T (1996) Methods for characterizing colour scanners and digital cameras. *Displays* 16, 183-191.

Kerry JP, O'Grady MN, Hogan SA (2006) Past, current and potential utilisation of active and intelligent packaging systems for meat and muscle-based products: A review. *Meat Science* 74, 113-130.

Kieslinger D, Draxler S, Trznadel K, Lippitsch ME (1997) Lifetime-based capillary waveguide sensor instrumentation. *Sensors and Actuators B-Chemical* 39, 300-304.

Knecht BG, Strasser A, Dietrich R, Martlbauer E, Niessner R, Weller MG (2004) Automated microarray system for the simultaneous detection of antibiotics in milk. *Analytical Chemistry* 76, 646-654.

Korotcenkov G, Cho BK, Nazarov M, Noh DY, Kolesnikova EV (2010) Cathodoluminescence studies of un-doped and (Cu, Fe, and Co)-doped tin dioxide films deposited by spray pyrolysis. *Current Applied Physics* 10, 1123-1131.

Laca A, Saenz MC, Paredes B, Diaz M (2010) Rheological properties, stability and sensory evaluation of low-cholesterol mayonnaises prepared using egg yolk granules as emulsifying agent. *Journal of Food Engineering* 97, 243-252.

Lakowicz JR (2006) Plasmonics in biology and plasmon-controlled fluorescence. *Plasmonics* 1, 5-33.

Lapresta-Fernandez A, Capitan-Vallvey LF (2011) Environmental monitoring using a conventional photographic digital camera for multianalyte disposable optical sensors. *Analytica Chimica Acta* 706, 328-337.

Lapresta-Fernandez A, Huertas R, Melgosa M, Capitan-Vallvey LF (2009) Multianalyte imaging in one-shot format sensors for natural waters. *Analytica Chimica Acta* 636, 210-217.

Lavigne JJ, Anslyn EV (2001) Sensing a paradigm shift in the field of molecular recognition: From selective to differential receptors. *Angewandte Chemie-International Edition* 40, 3119-3130.

Lee DS, Chou WP, Yeh SH, Chen PJ, Chen PH (2011a) DNA detection using commercial mobile phones. *Biosensors & Bioelectronics* 26, 4349-4354.

Lee DS, Jeon BG, Ihm C, Park JK, Jung MY (2011b) A simple and smart telemedicine device for developing regions: a pocket-sized colorimetric reader. *Lab on A Chip* 11, 120-126.

Lee SK, Sheridan M, Mills A (2005) Novel UV-activated colorimetric oxygen indicator. *Chemistry of Materials* 17, 2744-2751.

Leon K, Mery D, Pedreschi F, Leon J (2006) Color measurement in L*a*b* units from RGB digital images. *Food Research International* 39, 1084-1091.

Li X, Ballerini DR, Shen W (2012) A perspective on paper-based microfluidics: Current status and future trends. *Biomicrofluidics* 6.

Liebsch G, Klimant I, Frank B, Holst G, Wolfbeis OS (2000) Luminescence lifetime imaging of oxygen, pH, and carbon dioxide distribution using optical sensors. *Applied Spectroscopy* 54, 548-559.

Ligler FS (2009) Perspective on Optical Biosensors and Integrated Sensor Systems. *Analytical Chemistry* 81, 519-526.

Lim SH, Musto CJ, Park E, Zhong WX, Suslick KS (2008) A Colorimetric Sensor Array for Detection and Identification of Sugars. *Organic Letters* 10, 4405-4408.

Lin J, Liu D (2000) An optical pH sensor with a linear response over a broad range. *Analytica Chimica Acta* 408, 49-55.

Lin ZJ, Chen XM, Jia TT, Wang XD, Xie ZX, Oyama M, Chen X (2009) Fabrication of a Colorimetric Electrochemiluminescence Sensor. *Analytical Chemistry* 81, 830-833.

Lippitsch ME, Draxler S, Kieslinger D (1997) Luminescence lifetime-based sensing: new materials, new devices. *Sensors and Actuators B-Chemical* 38, 96-102.

Liu S, Luo X (2011) 'LED Packaging for Lighting Applications: Design, Manufacturing and Testing.' Wiley.

Lopez-Alvarez MA, Hernandez-Andres J, Romero J, Campos J, Pons A (2009) Calibrating the Elements of a Multispectral Imaging System. *Journal of Imaging Science and Technology* 53.

Lopez-Molinero A, Cubero VT, Irigoyen RD, Piazuelo DS (2013) Feasibility of digital image colorimetry-Application for water calcium hardness determination. *Talanta* 103, 236-244.

Lu Y, Shi WW, Qin JH, Lin BC (2010) Fabrication and Characterization of Paper-Based Microfluidics Prepared in Nitrocellulose Membrane By Wax Printing. *Analytical Chemistry* 82, 329-335.

Ma J, Ohira SI, Mishra SK, Puanngam M, Dasgupta PK, Mahon SB, Brenner M, Blackledge W, Boss GR (2011) Rapid Point of Care Analyzer for the Measurement of Cyanide in Blood. *Analytical Chemistry* 83, 4319-4324.

Maejima K, Tomikawa S, Suzuki K, Citterio D (2013) Inkjet printing: an integrated and green chemical approach to microfluidic paper-based analytical devices. *Rsc Advances* 3, 9258-9263.

Makote R, Collinson MM (1999) Organically modified silicate films for stable pH sensors. *Analytica Chimica Acta* 394, 195-200.

Maleki N, Safavi A, Sedaghatpour F (2004) Single-step calibration, prediction and real samples data acquisition for artificial neural network using a CCD camera. *Talanta* 64, 830-835.

Maoka T, Sugiyama S, Maruta Y, Hataya T (2010) Application of cDNA Macroarray for Simultaneous Detection of 12 Potato Viruses. *Plant Disease* 94, 1248-1254.

March C, Manclus JJ, Abad A, Navarro A, Montoya A (2005) Rapid detection and counting of viable beer-spoilage lactic acid bacteria using a monoclonal chemiluminescence enzyme immunoassay and a CCD camera. *Journal of Immunological Methods* 303, 92-104.

Martinez AW, Phillips ST, Butte MJ, Whitesides GM (2007) Patterned paper as a platform for inexpensive, low-volume, portable bioassays. *Angewandte Chemie-International Edition* 46, 1318-1320.

Martinez AW, Phillips ST, Carrilho E, Thomas SW, Sindi H, Whitesides GM (2008a) Simple telemedicine for developing regions: Camera phones and paper-based microfluidic devices for real-time, off-site diagnosis. *Analytical Chemistry* 80, 3699-3707.

Martinez AW, Phillips ST, Whitesides GM (2008b) Three-dimensional microfluidic devices fabricated in layered paper and tape. *Proceedings of the National Academy of Sciences of the United States of America* 105, 19606-19611.

Martinez-Olmos A, Capel-Cuevas S, Lopez-Ruiz N, Palma AJ, de Orbe I, Capitan-Vallvey LF (2011a) Sensor array-based optical portable instrument for determination of pH. *Sensors and Actuators B-Chemical* 156, 840-848.

Martinez-Olmos A, Vargas-Sansalvador IMP, Palma AJ, Banqueri J, Fernandez-Ramos MD, Capitan-Vallvey LF (2011b) Multisensor probe for soil monitoring. *Sensors and Actuators B-Chemical* 160, 52-58.

Mayr T, Abel T, Enko B, Borisov S, Konrad C, Kostler S, Lamprecht B, Sax S, List EJW, Klimant I (2009) A planar waveguide optical sensor employing simple light coupling. *Analyst* 134, 1544-1547.

McClements DJ (2002) Theoretical prediction of emulsion color. *Advances in Colloid and Interface Science* 97, 63-89.

McClements DJ (2005) 'Food Emulsions: Principles, Practices and Techniques.' CRC Press.

McClements DJ, Chantrapornchai W, Clydesdale F (1998) Prediction of Food Emulsion Color Using Light Scattering Theory. *Journal of Food Science* 63, 935-939.

McConnell JJ (2006) 'Computer Graphics: Theory into Practice.' Jones and Bartlett.

McDonagh C, Burke CS, MacCraith BD (2008) Optical chemical sensors. *Chemical Reviews* 108, 400-422.

Mengual O, Meunier G, Cayre I, Puech K, Snabre P (1999) TURBISCAN MA 2000: multiple light scattering measurement for concentrated emulsion and suspension instability analysis. *Talanta* 50, 445-456.

Mensing JP, Wisitsoraat A, Tuantranont A, Kerdcharoen T (2013) Inkjet-printed sol-gel films containing metal phthalocyanines/ porphyrins for opto-electronic nose applications. *Sensors and Actuators B-Chemical* 176, 428-436.

Mills A (2005) Oxygen indicators and intelligent inks for packaging food. *Chemical Society Reviews* 34, 1003-1011.

Mills A, Lawrie K, Bardin J, Apedaile A, Skinner GA, O'Rourke C (2012) An O-2 smart plastic film for packaging. *Analyst* 137, 106-112.

Mohan SS, Hershenson MD, Boyd SP, Lee TH (1999) Simple accurate expressions for planar spiral inductances. *Ieee Journal of Solid-State Circuits* 34, 1419-1424.

Mohr GJ, Citterio D, Demuth C, Fehlmann M, Jenny L, Lohse C, Moradian A, Nezel T, Rothmaier M, Spichiger UE (1999) Reversible chemical reactions as the basis for optical sensors used to detect amines, alcohols and humidity. *Journal of Materials Chemistry* 9, 2259-2264.

Mudanyali O, Dimitrov S, Sikora U, Padmanabhan S, Navruz I, Ozcan A (2012) Integrated rapid-diagnostic-test reader platform on a cellphone. *Lab on A Chip* 12, 2678-2686.

Ngo H, Lee TW, Park HH (2012) A novel, low-complexity, high-speed envelope detector and its applications. *International Journal of Circuit Theory and Applications* 40, 627-634.

Nie JF, Zhang Y, Lin LW, Zhou CB, Li SH, Zhang LM, Li JP (2012) Low-Cost Fabrication of Paper-Based Microfluidic Devices by One-Step Plotting. *Analytical Chemistry* 84, 6331-6335.

O'Donnell TK, Goyne KW, Miles RJ, Baffaut C, Anderson SH, Sudduth KA (2011) Determination of representative elementary areas for soil redoximorphic features identified by digital image processing. *Geoderma* 161, 138-146.

O'Driscoll S, MacCraith BD, Burke CS (2013) A novel camera phone-based platform for quantitative fluorescence sensing. *Analytical Methods* 5, 1904-1908.

O'Toole M, Diamond D (2008) Absorbance based light emitting diode optical sensors and sensing devices. *Sensors* 8, 2453-2479.

Ohta J (2008) 'Smart CMOS Image Sensors And Apllications.' Northwest.

Oncescu V, O'Dell D, Erickson D (2013) Smartphone based health accessory for colorimetric detection of biomarkers in sweat and saliva. *Lab on A Chip* 13, 3232-3238.

Orellana G, Moreno-Bondi MC (2005) 'Frontiers in Chemical Sensors: Novel Principles and Techniques.' Springer.

Palma A, Lapresta-Fernandez A, Ortigosa-Moreno JM, Fernandez-Ramos MD, Carvajal MA, Capitan-Vallvey LF (2006) A simplified measurement procedure and portable electronic photometer for disposable sensors based on ionophore-chromoionophore chemistry for potassium determination. *Analytical and Bioanalytical Chemistry* 386, 1215-1224.

Palma AJ, Lopez-Gonzalez J, Asensio LJ, Fernandez-Ramos MD, Capitan-Vallvey LF (2007a) Microcontroller-based portable instrument for stabilised optical oxygen sensor. *Sensors and Actuators B-Chemical* 121, 629-638.

Palma AJ, Lopez-Gonzalez J, Asensio LJ, Fernandez-Ramos MD, Capitan-Vallvey LF (2007b) Open air calibration with temperature compensation of a luminescence quenching-based oxygen sensor for portable instrumentation. *Analytical Chemistry* 79, 3173-3179.

Palma AJ, Ortigosa JM, Lapresta-Fernandez A, Fernandez-Ramos MD, Carvajal MA, Capitan-Vallvey LF (2008) Portable light-emitting diode-based photometer with one-shot optochemical sensors for measurement in the field. *Review of Scientific Instruments* 79.

Papkovsky DB (1993) Luminescent Porphyrins As Probes for Optical (Bio)Sensors. *Sensors and Actuators B-Chemical* 11, 293-300.

Papkovsky DB (1995) New Oxygen Sensors and Their Application to Biosensing. *Sensors and Actuators B-Chemical* 29, 213-218.

Papkovsky DB, Ponomarev GV, Trettnak W, Oleary P (1995) Phosphorescent Complexes of Porphyrin Ketones - Optical-Properties and Application to Oxygen Sensing. *Analytical Chemistry* 67, 4112-4117.

Park J, Hong W, Kim CS (2010) Color Intensity Method for Hydrogel Oxygen Sensor Array. *Ieee Sensors Journal* 10, 1855-1862.

Park J, Kim CS (2011) A Simple Oxygen Sensor Imaging Method with White Light-Emittind Diode and Colour Charge-Coupled Device Camera. *Sensors Letters* 9, 118-123.

Park S, Achanta SG, Yang J, Kim CS (2012) Intensity-based oxygen imaging with a display screen and a color camera. *Sensors and Actuators B-Chemical* 164, 101-108.

Pedro AMK, Ferreira MMC (2009) The Use of Near-Infrared Spectroscopy and Chemometrics for Determining the Shelf-Life of Products. *Applied Spectroscopy* 63, 1308-1314.

Penrose R (1955) A generalized inverse for matrices. p. 51. Mathematical Proceedings of the Cambridge Philosophical Society.

Pladellorens J, Pinto A, Segura J, Cadevall C, Anto J, Pujol J, Vilaseca M, Coll J (2008) A device for the color measurement and detection of spots on the skin. *Skin Research and Technology* 14, 65-70.

Puder A, Antebi O (2013) Cross-Compiling Android Applications to iOS and Windows Phone 7. *Mobile Networks & Applications* 18, 3-21.

Qazi HH, bin Mohammad A, Akram M (2012) Recent Progress in Optical Chemical Sensors. *Sensors* 12, 16522-16556.

Rakow NA, Suslick KS (2000) A colorimetric sensor array for odour visualization. *Nature* 406, 710-713.

Restuccia D, Spizzirri UG, Parisi OI, Cirillo G, Curcio M, Iemma F, Puoci F, Vinci G, Picci N (2010) New EU regulation aspects and global market of active and intelligent packaging for food industry applications. *Food Control* 21, 1425-1435.

Ricketts SR, Douglas P (2008) A simple colorimetric luminescent oxygen sensor using a green LED with Pt octaethylporphyrin in ethyl cellulose as the oxygen-responsive element. *Sensors and Actuators B-Chemical* 135, 46-51.

Rida A, Yang L, Vyas R, Tentzeris MM (2009) Conductive Inkjet-Printed Antennas on Flexible Low-Cost Paper-Based Substrates for RFID and WSN Applications. *Ieee Antennas and Propagation Magazine* 51, 13-23.

Roda A, Guardigli M, Pasini P, Mirasoli M, Michelini E, Musiani M (2005) Bio- and chemiluminescence imaging in analytical chemistry. *Analytica Chimica Acta* 541, 25-36.

Rodriguez-Pulido FJ, Gomez-Robledo L, Melgosa M, Gordillo B, Gonzalez-Miret ML, Heredia FJ (2012) Ripeness estimation of grape berries and seeds by image analysis. *Computers and Electronics in Agriculture* 82, 128-133.

Rooney ML (1995) 'Active Food Packaging.' Blackie Academic & Professional.

Rossel RAV, Adamchuk VI, Sudduth KA, McKenzie NJ, Lobsey C (2011) Proximal Soil Sensing: An effective Approach for Soil Measurement in Space and Time. *Advances in Agronomy* 113, 243-231.

Rossel RAV, Fouad Y, Walter C (2008) Using a digital camera to measure soil organic carbon and iron contents. *Biosystems Engineering* 100, 149-159.

Rossel RAV, Minasny B, Roudier P, McBratney AB (2006) Colour space models for soil science. *Geoderma* 133, 320-337.

Rossel RAV, Webster R (2011) Discrimination of Australian soil horizons and classes from their visible-near infrared spectra. *European Journal of Soil Science* 62, 637-647.

Ryu G, Huang JS, Hofmann O, Walshe CA, Sze JYY, McClean GD, Mosley A, Rattle SJ, deMello JC, deMello AJ, Bradley DDC (2011) Highly sensitive fluorescence detection system for microfluidic lab-on-a-chip. *Lab on A Chip* 11, 1664-1670.

Safavi A, Bagheri M (2003) Novel optical pH sensor for high and low pH values. *Sensors and Actuators B-Chemical* 90, 143-150.

Safavi A, Maleki N, Rostamzadeh A, Maesum S (2007) CCD camera full range pH sensor array. *Talanta* 71, 498-501.

Saini, D. P., Klainer, S. M., and Coulter, S. L. Chip level waveguide sensor. [5,737,457]. 4-4-1998. United States.

Sakaue H, Ozaki T, Ishikawa H (2009) Global Oxygen Detection in Water Using Luminescent Probe on Anodized Aluminum. *Sensors* 9, 4151-4163.

Salmeron JF, Gomez-Robledo L, Carvajal MA, Huertas R, Moyano MJ, Gordillo B, Palma AJ, Heredia FJ, Melgosa M (2012) Measuring the colour of virgin olive oils in a new colour scale using a low-cost portable electronic device. *Journal of Food Engineering* 111, 247-254.

Sanchez-Barragan I, Costa-Fernandez JM, Valledor M, Campo JC, Sanz-Medel A (2006) Room-temperature phosphorescence (RTP) for optical sensing. *Trac-Trends in Analytical Chemistry* 25, 958-967.

Sanchez-Maranon M, Garcia PA, Huertas R, Hernandez-Andres J, Melgosa M (2011) Influence of Natural Daylight on Soil Color Description: Assessment Using a Color-Appearance Model. *Soil Science Society of America Journal* 75, 984-993.

Sanchez-Maranon M, Huertas R, Melgosa M (2005) Colour variation in standard soil-colour charts. *Australian Journal of Soil Research* 43, 827-837.

SanchezMaranon M, Delgado G, Delgado R, Perez MM, Melgosa M (1995) Spectroradiometric and Visual Color Measurements of Disturbed and Undisturbed Soil Samples. *Soil Science* 160, 291-303.

Schaferling M, Wu M, Enderlein J, Bauer H, Wolfbeis OS (2003) Time-resolved luminescence imaging of hydrogen peroxide using sensor membranes in a microwell format. *Applied Spectroscopy* 57, 1386-1392.

Schanze KS, Carroll BF, Korotkevitch S, Morris MJ (1997) Temperature dependence of pressure sensitive paints. *Aiaa Journal* 35, 306-310.

Schulze RKW, Rosing STR, d'Hoedt B (2002) Contrast perception in digitized panoramic radiographs compared with their film-based origin. *Oral Surgery Oral Medicine Oral Pathology Oral Radiology and Endodontics* 94, 388-394.

Shakhsher ZM, Odeh I, Jabr S, Seitz WR (2004) An optical chemical sensor based on swellable dicarboxylate functionalized polymer microspheres for pH copper and calcium determination. *Microchimica Acta* 144, 147-153.

Shen L, Ratterman M, Klotzkin D, Papautsky I (2011) A CMOS optical detection system for point-of-use luminescent oxygen sensing. *Sensors and Actuators B-Chemical* 155, 430-435.

Shepherd AJ (1997) Calibrating screens for continuous colour displays. *Spatial Vision* 11, 57-74.

Singh J (2000) 'Semiconductor Devices: Basic Principles.' Wiley.

Skoog DA, Holler FJ, Crouch SR (2007) 'Principles of Instrumental Analysis.' Thomson Brooks/Cole.

Smith AR (1978) Proceedings of the 5th Annual Conference on Computer Graphics and Interactive Techniques. pp. 12-19.

Spring, K. R., Fellers, T. J., and Davidson, M. W. Introduction to Charge-Coupled Devices (CCDs). Nikon MicroscopyU . 2012.

Steemers FJ, Walt DR (1999) Multi-analyte sensing: From site-selective deposition to randomly-ordered addressable optical fiber sensors. *Mikrochimica Acta* 131, 99-105.

Steinmetz V, Roger JM, Molto E, Blasco J (1999) On-line fusion of colour camera and spectrophotometer for sugar content prediction of apples. *Journal of Agricultural Engineering Research* 73, 207-216.

Stich MIJ, Borisov SM, Henne U, Schaferling M (2009) Read-out of multiple optical chemical sensors by means of digital color cameras. *Sensors and Actuators B-Chemical* 139, 204-207.

Supharoek SA, Youngvises N, Jakmunee J (2012) A Simple Microfluidic Integrated with an Optical Sensor for Micro Flow Injection Colorimetric Determination of Glutathione. *Analytical Sciences* 28, 651-656.

Suslick BA, Feng L, Suslick KS (2010) Discrimination of Complex Mixtures by a Colorimetric Sensor Array: Coffee Aromas. *Analytical Chemistry* 82, 2067-2073.

Taib MN, Andres R, Narayanaswamy R (1996) Extending the response range of an optical fibre pH sensor using an artificial neural network. *Analytica Chimica Acta* 330, 31-40.

Tanaka Y, Nakamoto T, Moriizumi T (2006) Study of highly sensitive smell sensing system using gas detector tube combined with optical sensor. *Sensors and Actuators B-Chemical* 119, 84-88.

Taranova NA, Byzova NA, Zaiko VV, Starovoitova TA, Vengerov YY, Zherdev AV, Dzantiev BB (2013) Integration of lateral flow and microarray technologies for multiplex immunoassay: application to the determination of drugs of abuse. *Microchimica Acta* 180, 1165-1172.

Tavernier F, Steyaert M (2011) 'High-Speed Optical Receivers with Integrated Photodiode in Nanoscale CMOS.' Springer.

Torrent J, Barron V (1993) Laboratory measurement of soil color: Theory and practice. In 'Soil Color, Special publication'. (Eds JM Bigham and EJ Ciolkosz) pp. 21-33. Soil Science Society of America.

Ungerbock B, Charwat V, Ertl P, Mayr T (2013) Microfluidic oxygen imaging using integrated optical sensor layers and a color camera. *Lab on A Chip* 13, 1593-1601.

Valcarcel M, Luque de Casto MD (1994) 'Flow-Through (Bio)Chemical Sensors.' Elsevier Science B.V.

Vargas-Sansalvador IMP, Carvajal MA, Roldan-Munoz OM, Banqueri J, Fernandez-Ramos MD, Capitan-Vallvey LF (2009) Phosphorescent sensing of carbon dioxide based on secondary inner-filter quenching. *Analytica Chimica Acta* 655, 66-74.

Vargas-Sansalvador IMP, Fay C, Phelan T, Fernandez-Ramos MD, Capitan-Vallvey LF, Diamond D, Benito-Lopez F (2011a) A new light emitting diode-light emitting diode portable carbon dioxide gas sensor based on an interchangeable membrane system for industrial applications. *Analytica Chimica Acta* 699, 216-222.

Vargas-Sansalvador IMP, Martinez-Olmos A, Palma AJ, Fernandez-Ramos MD, Capitan-Vallvey LF (2011b) Compact optical instrument for simultaneous determination of oxygen and carbon dioxide. *Microchimica Acta* 172, 455-464.

Vlasov Y, Legin A (1998) Non-selective chemical sensors in analytical chemistry: from "electronic nose" to "electronic tongue". *Fresenius Journal of Analytical Chemistry* 361, 255-260.

Vlasov Y, Legin A, Rudnitskaya A, Di Natale C, D'Amico A (2005) Nonspecific sensor arrays ("electronic tongue") for chemical analysis of liquids (IUPAC Technical Report). *Pure and Applied Chemistry* 77, 1965-1983.

Vukovic J, Avidad MA, Capitan-Vallvey LF (2012) Characterization of disposable optical sensors for heavy metal determination. *Talanta* 94, 123-132.

Vukovic J, Matsuoka S, Yoshimura K, Grdinic V, Grubesic RJ, Zupanic O (2007) Simultaneous determination of traces of heavy metals by solid-phase spectrophotometry. *Talanta* 71, 2085-2091.

Vyas R, Lakafosis V, Rida A, Chaisilwattana N, Travis S, Pan J, Tentzeris MM (2009) Paper-Based RFID-Enabled Wireless Platforms for Sensing Applications. *Ieee Transactions on Microwave Theory and Techniques* 57, 1370-1382.

Wang MH, Gordon HR (1994) Estimating Aerosol Optical-Properties Over the Oceans with the Multiangle Imaging Spectroradiometer - Some Preliminary Studies. *Applied Optics* 33, 4042-4057.

Wang SQ, Zhao XH, Khimji I, Akbas R, Qiu WL, Edwards D, Cramer DW, Ye B, Demirci U (2011) Integration of cell phone imaging with microchip ELISA to detect ovarian cancer HE4 biomarker in urine at the point-of-care. *Lab on A Chip* 11, 3411-3418.

Wang XD, Chen HX, Zhao Y, Chen X, Wang XR (2010a) Optical oxygen sensors move towards colorimetric determination. *Trac-Trends in Analytical Chemistry* 29, 319-338.

Wang XD, Meier RJ, Link M, Wolfbeis OS (2010b) Photographing Oxygen Distribution. *Angewandte Chemie-International Edition* 49, 4907-4909.

Wee AG, Lindsey DT, Kuo SL, Johnston WM (2006) Color accuracy of commercial digital cameras for use in dentistry. *Dental Materials* 22, 553-559.

Westland S, Ripamonti C (2004) 'Computational Colour Science using Matlab.' Wiley.

Wyszecki G, Stiles WS (1982) 'Color Science: Concepts and Methods, Quantitative Data and Formulae.' Wiley Classics Library.

Xiaobo Z, Jiewen Z, Yanxiao L (2010) Objective Quality Assessment of Apples Using Machine Vision, Nir Spectrophotometer, and Electronic Nose. *Transactions of the Asabe* 53, 1351-1358.

Yam KL, Papadakis SE (2004) A simple digital imaging method for measuring and analyzing color of food surfaces. *Journal of Food Engineering* 61, 137-142.

Yamazaki M, Krishnadasan S, deMello AJ, deMello JC (2012) Non-emissive plastic colour filters for fluorescence detection. *Lab on A Chip* 12, 4313-4320.

Yoon B, Park IS, Shin H, Park HJ, Lee CW, Kim JM (2013) A Litmus-Type Colorimetric and Fluorometric Volatile Organic Compound Sensor Based on Inkjet-Printed Polydiacetylenes on Paper Substrates. *Macromolecular Rapid Communications* 34, 731-735.

Yotter RA, Wilson DM (2003) A review of photodetectors for sensing light-emitting reporters in biological systems. *Ieee Sensors Journal* 3, 288-303.

Youssef MK, Barbut S (2009) Effects of protein level and fat/oil on emulsion stability, texture, microstructure and color of meat batters. *Meat Science* 82, 228-233.

Yu H, Li Y, Jiang L, Ji Z (2012) A wide range, low power clock and data recovery scheme for RFID tags. *Analog Integrated Circuits and Signal Processing* 71, 101-106.

Zeghbroeck BV (2004) 'Principles of Semiconductor Devices.'

Zhang C, Suslick KS (2005) A colorimetric sensor array for organics in water. *Journal of the American Chemical Society* 127, 11548-11549.

Zhang C, Suslick KS (2007) Colorimetric sensor array for soft drink analysis. *Journal of Agricultural and Food Chemistry* 55, 237-242.

Zhang GB, Li CX, Lu Y, Hu H, Xiang GX, Liang ZQ, Liao P, Dai P, Xing WL, Cheng J (2011) Validation of a mobile phone-assisted microarray decoding platform for signal-enhanced mutation detection. *Biosensors & Bioelectronics* 26, 4708-4714.

Zhujun Z, Seitz WR (1986) Optical Sensor for Oxygen Based on Immobilized Hemoglobin. *Analytical Chemistry* 58, 220-222.